Amphibian Antimicrobial Peptides: Their Structures and Mechanisms of Action.

A Thesis Presented for the
Degree of
Doctor of Philosophy.

by

Brian Cheng San Chia
B.Sc. (Hons.)

Department of Chemistry
THE UNIVERSITY OF ADELAIDE

March 2000

Contents

Chapter 1 - Biologically Active Peptides: An Introduction

Chapter 2 - Antibacterial Peptides and their Mechanisms of Action

Chapter 3 - Three-Dimensional Structural Studies

Chapter 4 - Orientation Studies

Chapter 5 - Maculatin 1.1 and Analogues

Chapter 6 - Uperin 3.6 and Analogues

Chapter 7 - The Caerin 4 Antimicrobial Peptides

Chapter 8 - Future Directions and Conclusions

Chapter 9 - Experimental

References

Appendix

Publications

Corrections in pencil (by JHB for BC) in answer to Examiners Comments.

Abstract

In the last decade or so, there has been an alarming increase worldwide in the number of antibiotic-resistant strains of pathogens. Efforts to find new drugs to combat this scourge have so far been of limited success. Amphibian skin is a rich source of potent antimicrobial peptides that has the potential to be developed into a new class of antibiotics. Most are specific only to pathogens and are found to exert their effects by disrupting their cytoplasmic membranes. The mechanisms by which they exert their biological effects are still a subject of controversy. Currently, two mechanisms have been proposed: (i) the channel mechanism where the peptides aggregate on the membrane surface to from a transmembrane pore. This disrupts the cell's osmoregulatory capability and results in osmolysis, and (ii) the carpet mechanism where the peptides orient themselves parallel to the membrane surface, forming a 'carpet' layer(s) before immersing themselves into the bacterial membrane, causing cell lysis.

Recently, three antimicrobial peptides, maculatin 1.1, uperin 3.6, caerin 4.1 were isolated from the respective skin glands of the Australian amphibians *Litoria genimaculata, Uperoleia mjobergii* and *Litoria caerulea*. To gain a deeper insight in their mechanism of action, three-dimensional structural studies have been conducted using circular dichroism, two-dimensional nuclear magnetic resonance and computer modelling techniques.

Experimental results reveal that all three peptides adopt an overall amphipathic α-helical conformation in membrane-mimetic environments. One of the peptides (maculatin 1.1) forms a helical structure with a 'kink' in the central region due to Pro15. Orientation studies using solid-state NMR studies suggest that ^{15}N-labelled Ala7 maculatin 1.1 interacts with bacterial membranes *via* the carpet mechanism. Further investigations involving structure-activity relationship studies and the solution structures of synthetic variants were also conducted and compared. Results suggest that: (i) the bactericidal mechanism did not involve stereospecific binding sites or enzymes and (ii) the synthetic Ala15 analogue of maculatin 1.1 has markedly reduced activity, suggesting that the kink is important for biological activity. A

comparison was also made between using trifluoroethanol (TFE), a membrane-mimicking solvent and dodecylphosphocholine (DPC) micelles in water to investigate the reliability of TFE as a membrane-mimicking solvent. Results indicate that the three-dimensional structures produced in both systems are very similar, suggesting that membrane-interacting peptides in trifluoroethanol/water mixtures are representative of those adopted in a membrane environment. The role of central flexibility within antibiotic peptides in their interaction with bacterial membranes is also discussed.

Like maculatin 1.1, uperin 3.6 and caerin 4.1 also adopt overall α-helical conformations in TFE/water mixtures. Substituting the cationic residues in uperin 3.6 for neutral amino acid residues result in the loss of bioactivity, suggesting that electrostatic interactions are involved in the mechanism of bactericidal action. Caerin 4.1 is shown to possess narrow-spectrum antibiotic activities. Although it does not contain a central proline kink along the length of the helix like maculatin 1.1, it was found to have a central flexible region between Gly11 to Gly16. It is believed that its relatively rigid helical backbone conformation can only undergo limited conformational changes and thereby loses its wide-spectrum antibiotic capability.

Litora chloris

Outline of Thesis Presentation

This thesis is presented in the following manner:

Chapter 1 gives a brief introduction to naturally-occurring bioactive peptides and their potential for development into therapeutics. Particular attention will be paid to antimicrobial peptides isolated from the skin of amphibians.

Chapter 2 reviews the mechanisms of action of a number of membrane-disrupting peptides. A summary of different experimental techniques will also be mentioned briefly.

Chapter 3 serves not only as an introduction to the experimental techniques (particularly nuclear magnetic resonance spectroscopy and molecular modelling) used to elucidate the three-dimensional structures of peptides in solution, it also explains in detail how the 'quality' and 'realism' of calculated structures are gauged using putative protocols. These protocols will be employed for all the peptides studied in this thesis (Chapters 5 to 7) and hence, will only be mentioned briefly in these chapters.

Chapter 4 explains how solid-state NMR techniques are used to probe the mechanism of action of membrane-lytic peptides by studying their interactions with lipids.

Chapters 5 to 7 contain the detailed structure-activity relationship study of selected amphibian peptides and their synthetic analogues using circular dichroism and nuclear magnetic resonance spectroscopy (discussed in Chapter 3).

Finally, Chapter 8 points out some future directions that can be undertaken: (i) to gain a deeper insight to the mechanisms of bactericidal action of these peptides and (ii) as a rationale to future drug design.

Statement

This thesis contains no material which has been accepted for the award of any other degree or diploma in any university or other tertiary institution and, to the best of my knowledge and belief, contains no materials previously published or written by another person, except where due reference has been made in the text.

I give consent to this copy of my thesis, when deposited in the university library, being available for loan and photocopying.

Brian Cheng San Chia
3/3/2000

Acknowledgements

My sincere thanks to my supervisor, Professor John H. Bowie, for his guidance and advice in all aspects of my work in The University of Adelaide.

I would also like to thank Associate Professor John Carver at the University of Wollongong for his tremendous help in teaching me the aspects of NMR and Dr Robyn Lindner for her assistance with the acquisition of the CD spectra.

Also my heartfelt appreciation to Associate Professor Frances Separovic, Tracy Lam and Dr. Terrence Mulhern from the University of Melbourne for teaching me the aspects of solid-state NMR and the computational aspects of the work presented in this thesis.

Thanks must also go to Dr Simon Pyke for useful discussions and Mr. Phil Clements for his help and advice on the operation of the NMR spectrometer.

I would like to thank The University of Adelaide for awarding me an Overseas Postgraduate Research Scholarship.

Last but not least, to my father, mother and Kent for their support and encouragement without which all this would not have been possible.
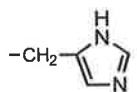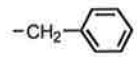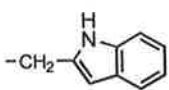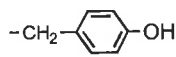
Dendrobates reticulatus

Abbreviations used in this thesis

1D	one-dimensional
2D	two-dimensional
3D	three-dimensional
CD	circular dichroism
COSY	correlation spectroscopy
DHPC	1,2-dihexanoyl-sn-glycero-3-phosphocholine
DMPC	1,2-dimyristoyl-sn-glycero-3-phosphocholine
DPC	dodecylphosphocholine
DQF	double-quantum filter
DSS	2,2-dimethyl-2-silapentane-5-sulphonate
FID	free induction decay
Fig.	figure
FT	Fourier transform
HSQC	heteronuclear single-quantum coherence
IR	infra-red
LPS	lipopolysaccharide
NMR	nuclear magnetic resonance
NOESY	nuclear Overhauser effect spectroscopy
MD	molecular dynamics
MIC	minimum inhibitory concentration
PES	potential energy surface
ppm	parts per million
RMD	restrained molecular dynamics
RMSD	root-mean-square deviation
SA	simulated annealing
SAR	structure-activity relationship
SDS	sodium dodecyl sulphate
TFE	2,2,2-trifluoroethanol
TOCSY	total correlation spectroscopy
TPPI	time proportional phase incrementation

Abbreviations used to represent amino acids
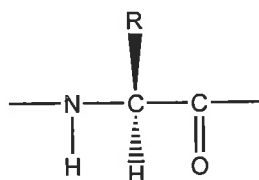
Amino Acid	R	Abbreviation
Alanine	$-CH_3$	Ala (A)
Asparagine	$-CH_2CONH_2$	Asn (N)
Aspartic Acid	$-CH_2COOH$	Asp (D)
Glutamic Acid	$-C_2H_4COOH$	Glu (E)
Glycine	-H	Gly (G)
Histidine		His (H)
Isoleucine	$-CH(CH_3)(C_2H_5)$	Ile (I)
Leucine	$-CH_2CH(CH_3)_2$	Leu (L)
Lysine	$-(CH_2)_4NH_3^+$	Lys (K)
Phenylalanine		Phe (F)
Proline	*	Pro (P)
Serine	$-CH_2OH$	Ser (S)
Threonine	$-CH(CH_3)OH$	Thr (T)
Tryptophan		Trp (W)
Tyrosine		Tyr (Y)
Valine	$-CH(CH_3)_2$	Val (V)

* The proline residue has the stucture :
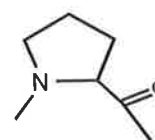
Nomenclature of amino acids in a peptide sequence

The nomenclature used for the naming of individual amino acid residues in a peptide sequence is described as follows: taking a tripeptide as an example, the naming procedure begins at the N-terminal end of the peptide sequence. In this case, the first amino acid is glycine, so it would be named Gly 1. The adjacent alanine residue will be named Ala 2 etc. In summary, the tripeptide shown below can be represented as: Gly Ala Phe or GAF.
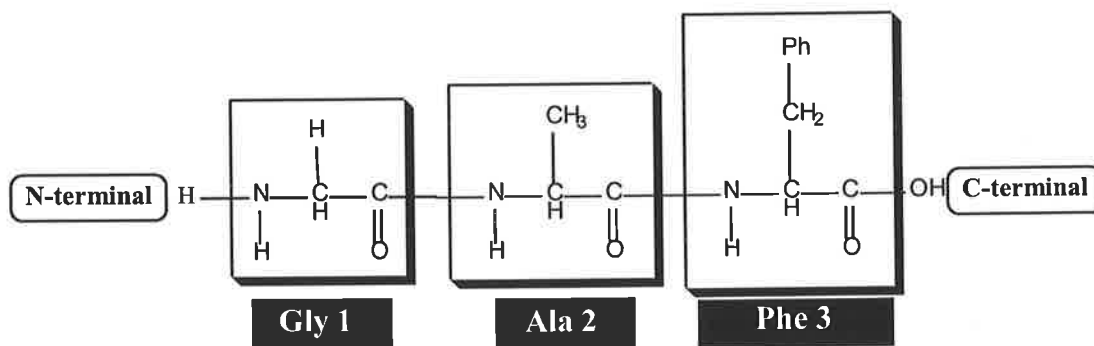
Nomenclature of individual amino acids in a tripeptide.

Chapter 1
Biologically Active Peptides:
An Introduction
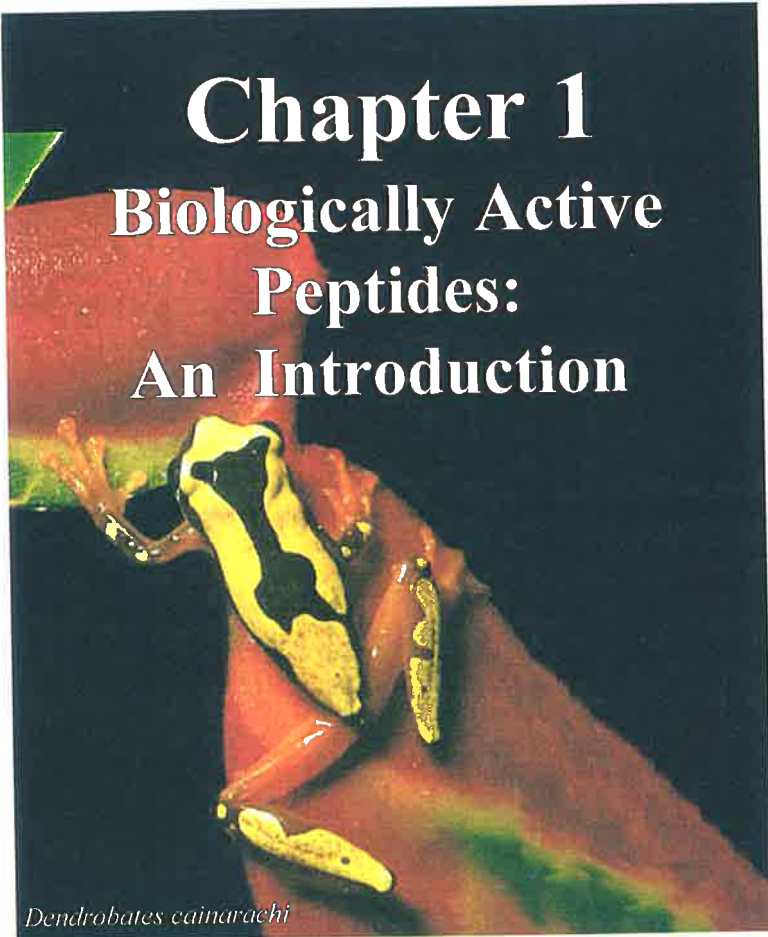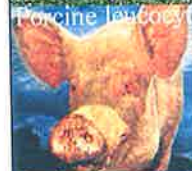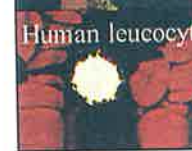
Dendrobates cainarachi

1.1 Amphibian Skin - A Chemical Arsenal

To increase their chances of survival in the wild, many organisms employ noxious chemicals (e.g., amines, steroid derivatives, alkaloids and peptides) to defend themselves against predators and pathogenic microorganisms (Bevins and Zasloff, 1990; Ganz, 1994; Boman, 1991 and 1995; Barra and Maurizio, 1995; Hancock *et al.*, 1995; Epand and Vogel, 1999). Many are membrane-disrupting peptides and can be found in a wide variety of organisms including bacteria, fungi, plants, insects, fish, amphibians and mammals. Some examples are shown in Table 1.1:

Table 1.1 Some cytotoxic peptides found in nature.

Organism	Amino acid sequence	Reference
Bacteria	VGAlAvVvWlWlWlW **gramicidin A** Lowercase residues are *D* isomers.	Andersen, 1983 Andersen, 1984 Arseniev *et al.*, 1985
Fungi	B*PBABABEVBGLBPVBBEQF **alamethicin** * B = aminoisobutyric acid	Beven *et al.*, 1999 Ducloheir *et al.*, 1998 Esposito *et al.*, 1987
Barley	KSCCKDTLARNCYNTCRFAG **thionin**	Bohlmann, 1994 Garcia *et al.*, 1998 Büssing *et al.*, 1999
Silkworm	AKIPIKAIKTVGKAVGKGLRAINIASTANDVFNFL KPKKRKH **moricin**	Hara and Yamakawa, 1995
Moth	KWKLFKKIEKVGQNIRDGIIKAGPAVAVVGQAT QIAK **cecropin A**	Boman and Hultmark, 1981 Gudmundsson, 1991
Honey Bee	GIGAVLKVLTTGLPALISWIKRKRQQ **melittin**	Tosteson and Tosteson, 1984
Flesh Fly	ATCDLLSGTGINHSACAAHCLLRGNRGGYCNGK AVCVCRN **sepacin**	Hanzawa *et al.*, 1990
Horseshoe Crab	KWCFRVCYRGICYRRCR **tachyplesin**	Nakamura *et al.*, 1988

Scorpion	RSVCRQIKICRRRGGCYYKCTNRPY **androctonin**	Ehret-Sabatier *et al.*, 1996
Sole Fish	GFFALIPKIISSPLFKTLLSAVGSALSSGGQE **pardaxin**	Lazarovic *et al.*, 1986 Shai, 1994 Oren and Shai, 1996
Frog	GIGKFLHSAGKFGKAFVGEIMK **magainin 1**	Zasloff, 1987
	GIGKFLHSAKKFGKAFVGEIMN **magainin 2**	Terry *et al.*, 1988
Mouse intestine	LRDLVCYCRSRGCKGRERMNGTCRKGHLLYTL CCR **cryptdin**	Selsted *et al.*, 1992
Porcine leucocyte	RGGRLCYCRRRFCVCVGR **protegrin 1**	Kokryakov *et al.*, 1993
	RGGRLCYCRRRFCICV **protegrin 2**	Sokolov *et al.*, 1999
Bovine leucocyte	RLCRIVVIRVCR **bactenesin**	Romeo *et al.*, 1988 Gennaro *et al.*, 1989
	ILPWKWPWWPWRR **indolicidin**	Selsted *et al.*, 1992
Human leucocyte	ACYCRIPACIAGERRYGTCIYQGRLWAFCC **defensin HNP 1**	Lehrer *et al.*, 1991 Lehrer *et al.*, 1993 Ganz and Lehrer, 1997

It is also interesting to note that bacteria are also a source of cytotoxic peptides such as bacteriocins (Jack *et al.*, 1995), gramicidin A and S (Katz and Demain, 1977; Ovchinnikov and Ivanov, 1982; Crease, 1989; Prenner *et al.*, 1999), α-toxin (Bhakdi *et al.*, 1981) and δ-lysin (Fitton *et al.*, 1980; Lee *et al.*, 1987; Tappin *et al.*, 1988), some which are now commercially available as pesticides (Thomas and Ellar, 1983). However, none of the above mentioned organisms can compare with amphibian skin with regards to the variety of these biologically active compounds (Erspamer *et al.*, 1984, Simmaco *et al.*, 1998).

Chapter 1

Amphibians evolved from fish that emerged from Devonian lakes and streams some 370 million years ago, and they and their chemistry have been evolving since then. Their remarkable ability to survive from predators (both large and small) and changing climatic conditions is due, in part, to their arsenal of host defence chemicals. These include toxins, analgesics, neuropeptides, antimicrobial and antifungal agents (Lazarus and Attila, 1993).

Man has used the medicinal and therapeutic properties of amphibian skin for more than two thousand years (Tyler, 1987). For example, the skin secretions of the Giant Monkey Frog *Phyllomedusa bicolor* (Fig. 1.1a) were used by Peruvian natives to increase their physical strength, awareness and resistance to hunger (Erspamer *et al.*, 1993) while the skin secretions of the toad *Bufo gargarizans* (Fig. 1.1b) has been used as a wound-healing agent in traditional Chinese and Korean medicine (Park *et al.*, 1995).
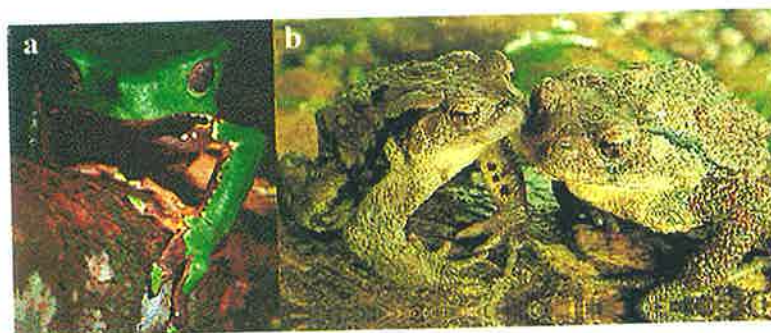
Fig. 1.1   (a) *Phyllomedusa bicolor* **(b)** *Bufo gargarizans.*

Amphibian skin secretions are not only used as therapeutic agents; the highly toxic skin secretions of poison dart frogs (Fig. 1.2) are traditionally employed by the native Indians of Central and South America to tip their blowgun darts for hunting (Fig. 1.3) (Carraway and Cochrane, 1987). Such toxins are lethal in the microgram

concentrations and each frog is known to store over two hundred micrograms of

toxin in their skin (Labler *et al.*, 1968).
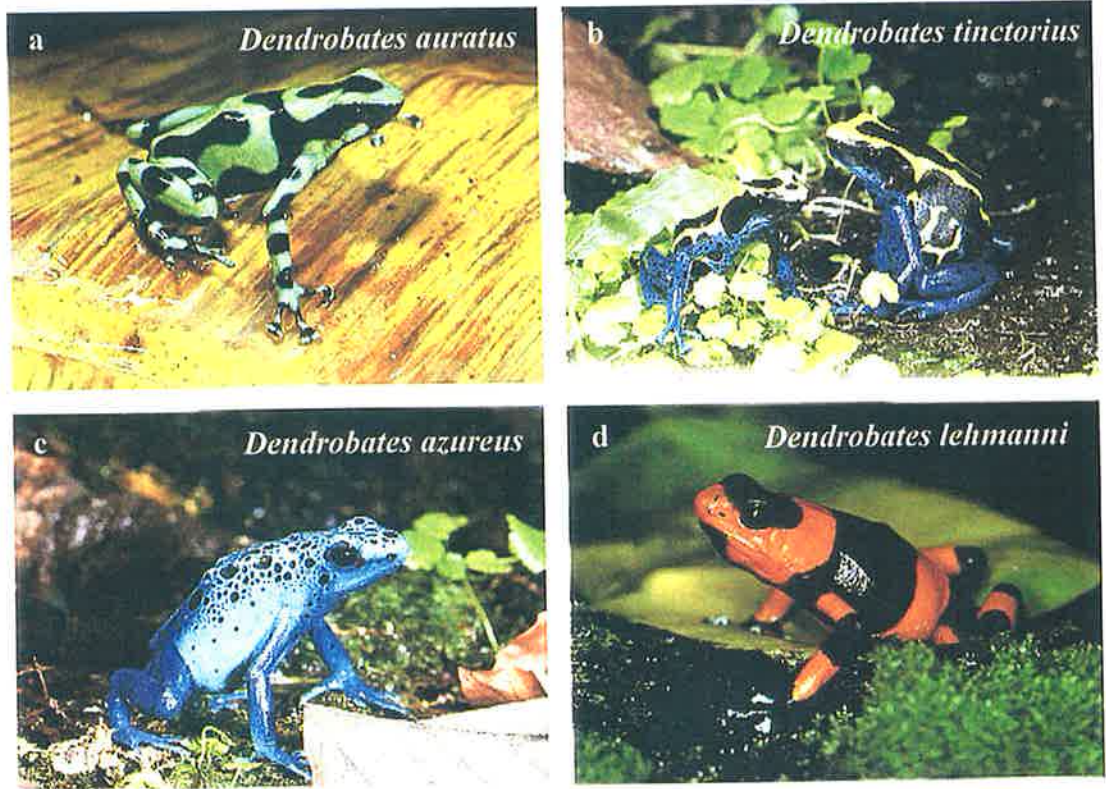
Fig. 1.2   Four species of poison dart frogs.

Fig. 1.3 (a) Coating a dart with poisonous skin secretions of *Phyllobates terribilis*, (b) a South American native with a blowgun.

Chapter 1

During the last three decades, a number of biologically active peptides from amphibian skin have been isolated and identified. Some are neuropeptides and have been shown to be analogues of hormones present in neurosecretory cells of mammalian gut and brain (Erspamer and Melchiorri, 1973; Erspamer and Melchiorri, 1980a). A few other examples are listed in Table 1.2.

Table 1.2   **Physiological functions of some peptides from amphibian skin.**

Peptide	Amphibian	Function	Reference
Angiotesin	*Crinia georgiana*	Vasodilator	Erspamer *et al.*, 1979
Bombesin	*Bombina bombina*	Muscle stimulant	Erspamer *et al.*, 1972
Bombinin	*Bombina variegata*	Antibacterial	Simmaco *et al.*, 1991
Buforin 1	*Bombina gargarizans*	Antibacterial	Park *et al.*, 1996
Bradykinin	*Rana temporaria*	Vasodilator	Anastasi *et al.*, 1991
Caerulein	*Hyla caerula*	Hypotensive	Gibson *et al.*, 1986
Dermorphin	*Phyllomedusa bicolor*	Analgesic	Negri *et al.*, 1995
Dermaseptin	*Phyllomedusa sauvagii*	Antibacterial	Mor *et al.*, 1991
			Mor and Nicolas, 1994
Magainin	*Xenopus laevis*	Antibacterial	Soravia *et al.*, 1988
		Antitumour	Berkowitz *et al.*, 1990
			Cruciani *et al.*, 1991
Ranalexin	*Rana catesbeiana*	Antibacterial	Clark *et al.*, 1994
Ranatensin	*Rana pipiens*	Muscle stimulant	Erspamer and Melchiorri, 1973
Rugosin	*Rana rugosa*	Antibacterial	Suzuki *et al.*, 1995
Sauvagine	*Phyllomedusa sauvagii*	Vasodilator	Erspamer and Melchiorri, 1980a
Tachykinin	*Phyllomedusa bicolor*	Hypotensive	Erspamer *et al*, 1993

These biologically active compounds are secreted from granular glands located on the dorsal skin surface of the animal in response to a variety of stimuli (Erspamer, 1994). For example, the South African Clawed Frog *Xenopus laevis* (Fig 1.4a) secretes chemicals that induce a yawning reflex on snakes, allowing the frog to escape unharmed (Barthalmus and Zielinski, 1988).

Not surprisingly, some of these peptides have attracted pharmaceutical interest. For example, medical researchers are currently developing muscle relaxants and anaesthetics from the neurotoxins of poison dart frogs (Negri *et al.*, 1995) while an analogue of magainin has been shown to possess anticancer activities and is currently undergoing clinical trials (Baker *et al.*, 1993).

Besides protecting the host from large predators, many of these compounds also serve as *antimicrobial agents*. Consisting mainly of peptides, they are discharged onto the skin either by adrenergic stimulation, as a response to infection or as a result of physical injury (Giovannini *et al.*, 1987). Many possess broad-spectrum antimicrobial activities, killing most strains of bacteria, fungi and protozoans. Experiments have shown that some of these peptides are specific only to micro-organisms, making them good candidates for the development of antimicrobial agents (Maloy and Kari, 1995). For example, a magainin analogue (MSI-78) is now commercially available as a topical antibiotic for the treatment of impetigo and foot ulcers, common infections caused by *Staphylococcus aureus* of which many strains are now drug-resistant (Fig. 1.4) (Marshall *et al.*, 1991; Jacob and Zasloff, 1994; Lipsky *et al.*, 1997; Fuchs *et al.*, 1998). Thus, by acting as sterilising agents for the skin, these compounds are responsible for the extraordinary freedom from infection

experienced by amphibians, even though they live and breed in bacteria-infested environments (Zasloff, 1987).
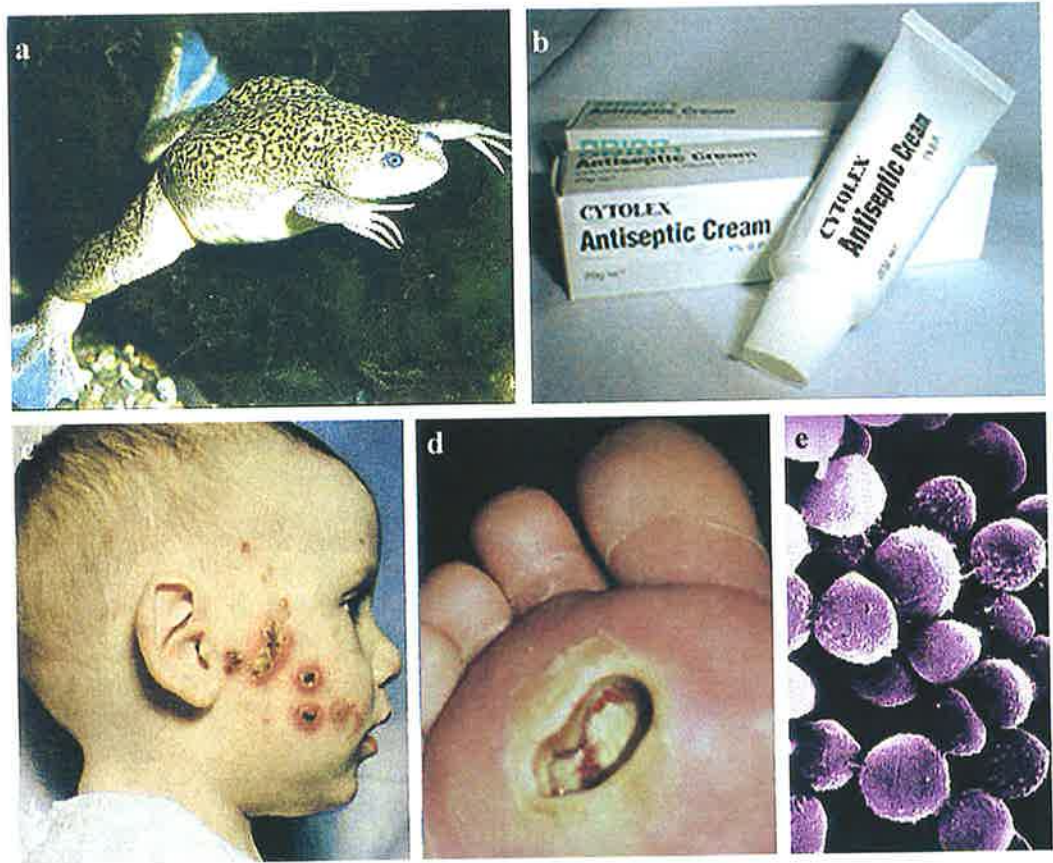
Fig. 1.4 (a) The African Clawed Frog *Xenopus laevis*. (b) Magainin analogue MSI-78 antibiotic sold under the trade name Cytolex™. (c) Impetigo, a form of skin infection (d) a foot ulcer (e) *Staphylococcus aureus*.

These host defence peptides can be promptly synthesised at a low metabolic cost due to their relatively small sizes (as compared to antibodies or macrophages) and are stored as inactive, processed peptides in large granules within the granular glands of the skin (Moore *et al.*, 1991). Fig. 1.5 illustrates a magnified view of the granular glands of a frog. In some amphibian species such as the Magnificent Tree Frog *Litoria splendida*, these glands are enlarged and localised in the head and neck regions of the body while species like *Limnodynastes terraereginae* have glands on their legs (Fig. 1.6).
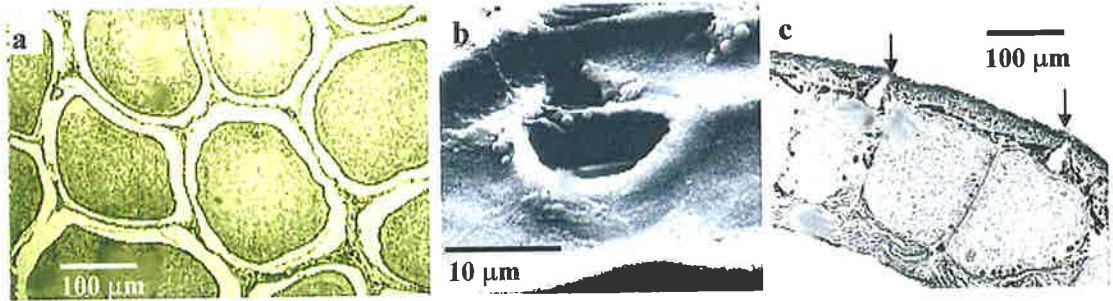
Fig. 1.5 (a) Magnified view of amphibian dermal granular glands showing secretory cells (Crook and Tyler, 1981) (b) scanning electron micrograph of a skin duct (Green, 1979) and (c) transverse view of granular glands with ducts opening onto the skin surface (arrowed).
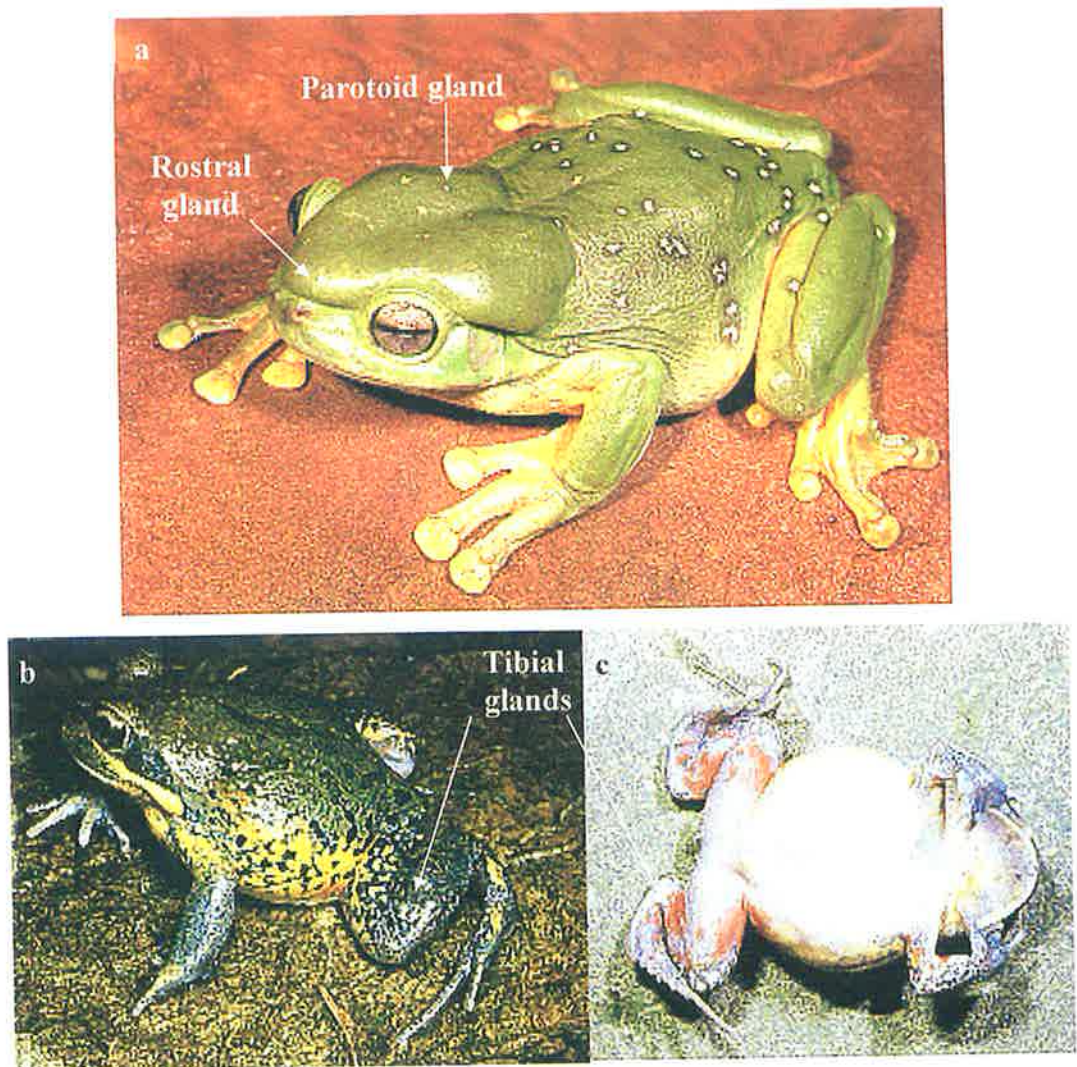
Fig. 1.6 (a) *Litoria splendida* and (b) *Limnodynastes terraereginae* dorsal and (c) ventral view showing hypertrophied glands.

1.2 Peptide Biosynthesis and Production

All active peptides are encoded and synthesised by the animal as part of larger parent peptides. These generally consist of three components: a signal peptide, a spacer peptide and the bioactive peptide (Nicolas and Mor, 1995; Amiche *et al.*, 1999). Following biosynthesis in endocrine glands, an endoprotease enzyme cleaves the signal peptide off and the remaining spacer-active peptide is transported and stored in the skin glands. At the appropriate time, another endoprotease removes the spacer peptide, releasing the active peptide onto the skin surface (Fig. 1.7) (Gibson *et al.*, 1986; Giovannini *et al.*, 1987; Terry *et al.*, 1988; Ketchum *et al.*, 1993; Ganz, 1994).
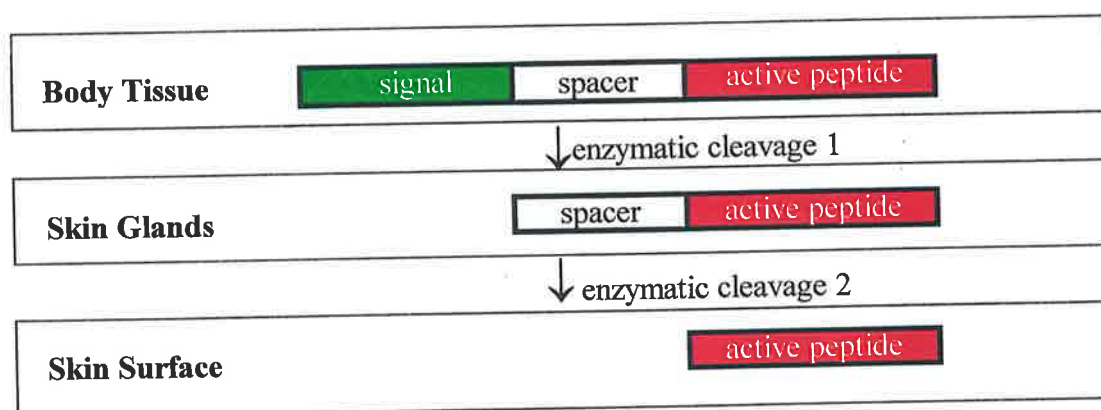
Fig. 1.7 Schematic diagram showing the biosynthetic route of active peptide formation. The active peptide is represented by the red box.

1.3 Bioactive Peptides from Australian Amphibians

To date, more than two hundred species of frogs have been identified in Australia since testing of their dermal secretions for pharmacological activity commenced in the 1960s (Erspamer *et al.*, 1966a and 1966b; Tyler, 1991). This has led to the isolation of the hypotensive peptide *caerulein* from the Australian Green Tree Frog *Litoria caerulea* (Fig. 1.8) (Anastasi *et al.*, 1968). Caerulein was also found to be an
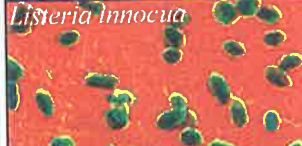
analgesic several thousand times more potent than morphine and has been used clinically (Lazarus and Attila, 1993).

The skin secretions from a number of native Australian *Litoria* species of frogs (illustrated in Fig. 1.8): *L. caerulea* (Stone *et al.*, 1993), *L. chloris* (Steinborner *et al.*, 1998), *L. ewingi* (Steinborner *et al.*, 1997a), *L. gilleni* (Waugh *et al.*, 1993), *L. splendida* (Stone *et al.*, 1992a; Stone *et al.*, 1992b) and *L. xanthomera* (Steinborner *et al.*, 1997b) contain two different families of peptides which have been named *caerins* and *caeridins* (Waugh *et al.*, 1995; Bowie *et al.*, 1999). Certain caerins were found to have appreciable biological activity. For example, caerin 1.1 has been shown to be active against a wide range of pathogens (Table 1.3) (Wong *et al.*, 1997). Caerin 1.1 is also active against *herpes simplex* I and II and the human immunodeficiency virus (HIV) [Unpublished communications with Prof. J.H. Bowie]. Caeridins, on the other hand, do not show any antibiotic activity and their function in amphibian skin is unknown at this time. New families of biologically active peptides have been recently isolated from other *Litoria* species, including two families of broad-spectrum bactericidal peptides from *L. aurea* and *L. citropa* (Wegener *et al.*, 1999; Wegener *et al.*, 2000).

It is also interesting to know that some *Litoria* species like *L. rubella* and *L. electrica* secrete peptides that have quite similar structures to human brain endomorphins (e.g. YPWF-NH$_2$ and YPWG-NH$_2$) (Zadina, 1997). These peptides have been named the tryptophyllins and are suspected to function as neurotransmitters or neuromodulators (Steinborner *et al.*, 1996; Wabnitz *et al.*,

Table 1.3   **Antimicrobial activities of caerin 1.1 against some pathogens.**
(MIC* values in brackets).

Bacterium	Pathogenicity and MIC (μg/L)
Bacillus cereus	Related to *Bacillus anthracis*, it is usually found in soil and livestock. Produces enterotoxins that causes food poisoning in meat and dairy products and cytotoxic enzymes such as heamolysins and phospholipase. (50)
Escherichia coli	A common bacteria found in our gastrointestinal and urinary tracts. Virulent stains produce enterotoxins which leads to diarrhoea, blood poisoning and kidney failure. Some strains are now drug-resistant. (100)
Leuconostoc lactis	Commonly found in the soil and can be transmitted to livestock. It produces toxins that contaminate meat, dairy and poultry products. (3)
Listeria Innocua	A food-borne pathogen commonly found in 'ready-to-eat' meat and dairy products. Causes food poisoning, septicaemia and listeriosis - a fatal form of meningitis. (100)
Micrococcus luteus	Primarily found in mammalian skin but also found in dairy products, soil and water. Causes meningitis, pneumonia and urinary tract infections. Many strains produce blood toxins that can lead to septicaemia. (12.5)
Pasteurella multocida	Found in domestic pets and household pests. It is transmitted to humans *via* rat and animal bites which can lead to septicaemia. (50)
Staphylococcus aureus	A common culprit that causes wound infections, pneumonia and blood poisoning. In 1996, 60% of the strains found in U.S. hospitals were antibiotic resistant, accounting for numerous human fatalities annually. (6)
Staphylococcus epidermidis	Present on human skin and is harmless in most circumstances. However, virulent strains can cause sore-eyes, impetigo, severe wound infections and endocarditis. (12.5)
Streptococcus faecalis	A common cause of wound and post-surgery infections leading to blood poisoning and endocarditis. They produce cytotoxins and haemolysins. Some strains are now drug-resistant and untreatable. (25)
Streptococcus uberis	Found commonly mammalian skin. Causes post-surgery infections that leads to blood poisoning and endocarditis. Some strains produce haemolysins that kill red blood cells. (3)

* MIC stands for *minimum inhibitory concentration*, the minimum concentration (in μg/L) of an antibiotic needed to inhibit the growth of a particular organism.

Fig. 1.8 Australian tree frogs of the genus *Litoria*.
(Pictures obtained from Barker *et al.*, 1995)

Table 1.4 Sequences of some peptides isolated from Australian amphibians.

Peptide	Organism	Amino acid sequence
aurein 3.1	*L. aurea*	GLFDI VKKLA GHIAG ST-NH$_2$
caerulein	*L. caerulea*	pEQDYP(SO$_3$H) TGWMD F-NH$_2$
caerin 1.1	*L. caerulea*	GLLSV LGSVA KHVLP HVVPV IAEHL-NH$_2$
	L. ewingi	
	L. gilleni	
	L. splendida	
caeridin 1.1	*L. gilleni*	GLLDG LLGTG L-NH$_2$
	L. splendida	
	L. xanthomera	
citropin 1.1	*L. citropa*	GLFDV IKKVA SVIGG L-NH$_2$
tryptophyllin 1.1	*L. rubella*	PWL-NH$_2$
tryptophyllin 1.2	*L. electrica*	FPWL-NH$_2$

1.4 Collection and Purification of Skin Secretions

Methods of collecting frog dermal secretions has evolved over the years. In the 1960s, dermal secretions were obtained *via* methanol extraction from sun-dried skins. For some species, this has resulted in the sacrifice of more than 700 specimens to obtain sufficient quantities of secretions for analysis (Roseghini *et al.*, 1976; Erspamer *et al.*, 1984; Erspamer *et al.*, 1986). Another method involved injecting noradrenalin into the amphibian to induce dermal secretion, followed by immersing it in ammonium acetate solution before scraping the precipitated material from the body (Nakajima, 1981; Gibson *et al.*, 1986; Giovanni *et al.*, 1987).

The above methods involved killing the amphibian being studied and there is increasing evidence that frog populations in many countries are in serious decline, including Australia (Tyler, 1991a). This has led to the development of a benign collection technique known as *surface electrical stimulation*. This technique involves mild electrical stimulation of the skin whereby the dermal sympathetic nerves of the frog are stimulated to induce secretions (Fig. 1.9).
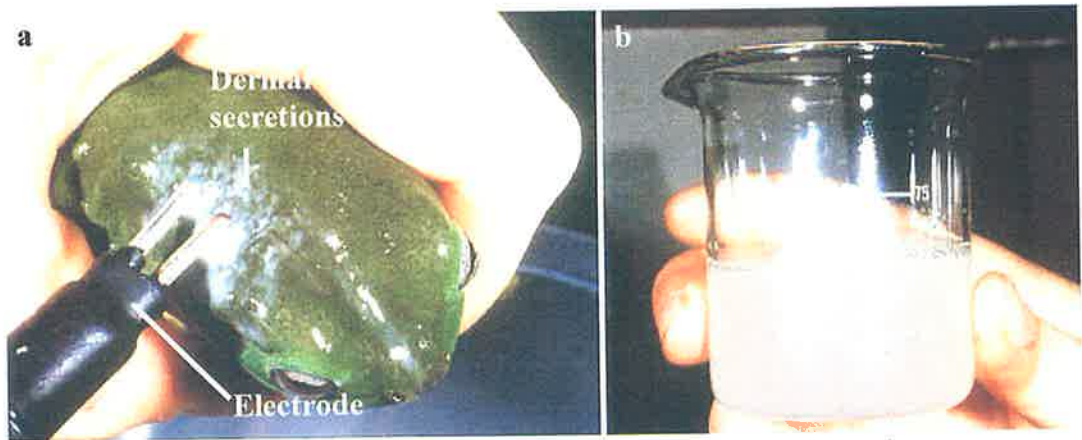
Fig. 1.9 **(a) Surface electrical stimulation on *L. caerulea* followed by (b) collection of dermal secretions.**

The secretions are washed from the skin with water, enzymes removed and the peptides separated using reverse phase high-performance liquid chromatography. Next, the primary amino acid sequences are analysed using the complementary methods of electrospray mass spectrometry and Edman sequencing. This technique can be repeated at monthly intervals as required (Tyler *et al.*, 1992). During the last decade, about 140 peptides from the skin glands of Australian frogs and toads have been isolated and characterised. No animals were sacrificed during these studies (Bowie *et al.*, 1998).

1.5 Antimicrobial Testing

Once a suspected antimicrobial peptide is isolated, purified and its primary sequence confirmed, it is commercially synthesised by Chiron Mimotopes, Clayton, Victoria. The synthetic peptide is sent to the Institute of Medical and Veterinary Science (IMVS), South Australia, for the testing of antimicrobial activities. The procedure involves introducing varying concentrations of peptide into cultures of bacteria colonies in a petri dish (Fig. 1.10) (Shafer, 1997). The results are reported as *minimum inhibitory concentrations* (MICs); the minimum concentration of an antibiotic needed to inhibit the growth of a particular organism (μg/L).
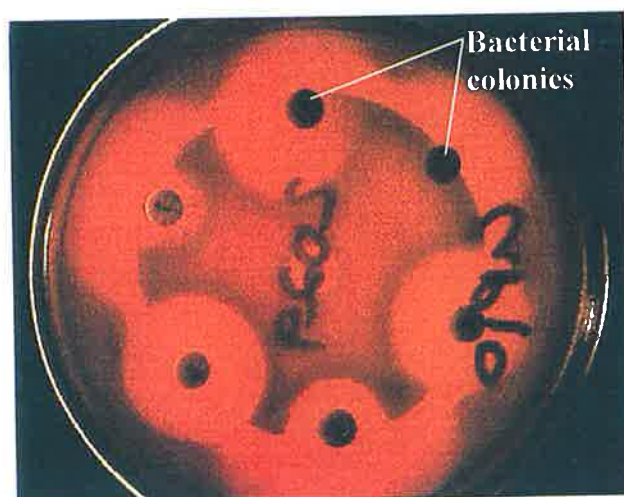
Fig. 1.10 Bacterial colonies in a petri dish.

1.6 Chapter Conclusion

Amphibian skin contains some of the most diverse yet simple biologically active compounds in the animal kingdom. These include neuro- and antimicrobial peptides. Studying all of them in detail is beyond the scope of this thesis. Instead, only selected antimicrobial peptides will be studied in detail in order to learn more about their mechanism of bactericidal action.

Chapter 2
Antibacterial Peptides and their Mechanisms of Action.

Agalychnis callidryas

2.1 Host Defence Peptides - A New Class of Antibiotics

Conventional antibiotics kill bacteria in a number of ways, generally interacting chemically with their vital biochemical functions and components. For example, many antibiotics inhibit cell wall, protein or nucleic acid synthesis by targeting specific bacterial enzymes and proteins (Tortora *et al.*, 1982). Such antibiotics are *stereospecific*, i.e., they have one or more chiral functional groups that are specific to a target binding-site(s) found on the bacteria.

In the last few decades, the blatant over-use of antibiotics has caused many of these 'magic-bullets' to lose their bactericidal capabilities. Antibiotic-resistant strains of *Staphylococcus aureus* ('Golden Staph') and *Enterococcus faecium* are reportedly discovered world-wide, claiming numerous human lives (Frieden *et al.*, 1993; Hiramatsu *et al.*, 1997; Ewald and Cochran, 1999). How do these pathogens become drug-resistant? The answer lies primarily in their capability to mutate each time they replicate, each new generation of bacteria is likely to be genetically different from the parent. Hence, essential bacterial enzymes and proteins that were once targets for antibiotics no longer have the same structural conformations, rendering conventional antibiotics useless. For example, penicillin, the first antibiotic to be used commercially on a wide scale during the second world war is now virtually ineffective against many pathogens (Neu, 1992; Sanders and Sanders, 1992). Thus it is imperative to develop a new class of antibiotics that exert their actions *via* a non-stereospecific mechanism.

The recent discovery of antimicrobial peptides from amphibian skin opens a new dimension for antibiotic development and a understanding how these peptides exert

their biological action will allow for the rationale design of new antibiotics (Coghlan, 1997). These peptides were shown to be non-stereospecific; studies comparing synthetic *D*-enantiomers to their natural *L* counterparts revealed both to have similar antimicrobial activities (Bessalle *et al.*, 1990; Wade *et al.*, 1990; Juvvadi *et al.*, 1996; Oren *et al.*, 1997; Vunnam *et al.*, 1997). How then, do these peptides exert their bactericidal action?

A number of experiments have been utilised to study the mechanisms of action of these peptides [see Blondelle *et al.*(1999) for a review]. Conductance experiments have revealed that such peptides disrupt bacterial cytoplasmic membrane potentials at micromolar concentrations (Ducloheir *et al.*, 1989; Westerhoff *et al.*, 1989; Kagan *et al.*, 1990; Cruciani *et al.*, 1992; Cociancich *et al.*, 1993; Juvvadi *et al.*, 1996; Silberstein *et al.*, 1999) while polarised attenuated reflection (Frey and Tamm, 1991; Goormaghtigh *et al.*, 1999) and Fourier-transform infrared (FTIR) spectroscopy revealed that such peptides interact with the lipid chains of synthetic phospholipid bilayers (Rana *et al.*, 1990; Rana and Blazyk, 1991). In addition, fluorescence labelling studies have shown that magainin perturbs artificial bilayers (Matsuzaki *et al.*, 1996). Such evidence suggests that these peptides interact directly with the bacterial membrane. As a result, the membrane's osmotic regulation capabilities and transport functions are disrupted which ultimately leads to cell lysis (de Waal *et al.*, 1991).

However, such experiments do not provide us with the complete picture of the bactericidal mechanism of action. Hence, three-dimensional (3D) structural studies are used to give us a better insight to their mechanism of action.

2.2 Solution Conformations of Antimicrobial Peptides

Structural studies involving circular dichroism (CD) and nuclear magnetic resonance (NMR) spectroscopy have shown that antimicrobial peptides generally adopt α-helical conformations in membrane mimicking solvents (e.g., trifluoroethanol) or when dissolved in solvents containing detergent micelles (Brown, 1979; Brown *et al.*, 1982; Lee *et al.*, 1987; Marion *et al.*, 1988; Hirsch *et al.*, 1996; Matsuzaki *et al.*, 1989a, 1997, 1998). Closer examination of these structures revealed that these helices possess a distinct segregation of hydrophobic and hydrophilic residues along the length of the helix, i.e., hydrophobic residues are along one side of the helix with hydrophilic residues on the other. A diagrammatic representation is shown in Fig. 2.1. Such helices were termed *amphipathic* helices. [This is synonymous with the term '*amphiphilic*' which is also found in some literature (Eisenberg, 1984; Segrest *et al.*, 1990)].
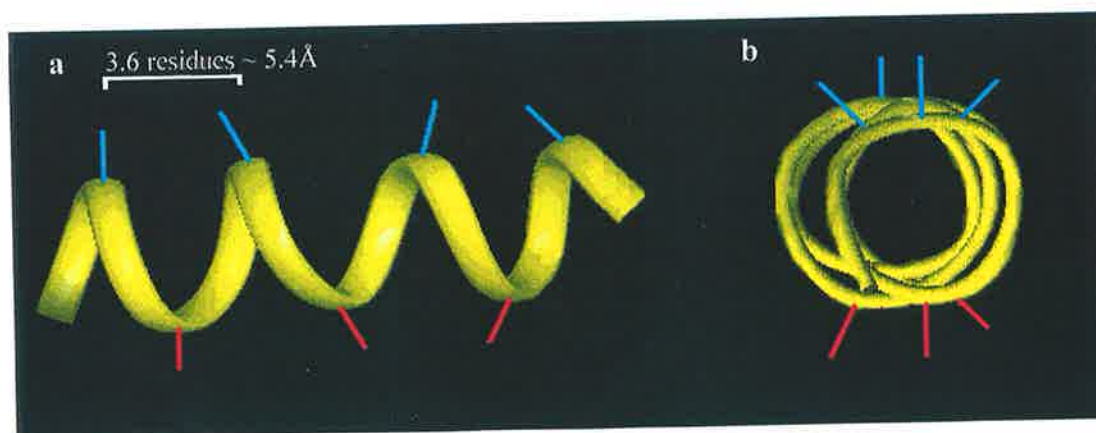
Fig. 2.1 (a) Side and (b) axial view of an amphipathic α-helix. Hydrophilic and hydrophobic residue side chains are represented by red and blue lines respectively.

2.3 The Edmundson Helical Wheel

The possibility of a peptide adopting an amphipathic helical conformation can be assessed by the use of the *Edmundson helical wheel* (Schiffer and Edmundson, 1967). This is a two-dimensional representation of the 3D structure of an α-helix with the perimeter of the wheel corresponding to the backbone of the polypeptide chain. Since one complete turn of an α-helix consists of approximately 3.6 residues, each residue can be plotted every $360/3.6 = 100°$ around a circle consecutively as shown in Fig. 2.2. Such plots show the projection of the residues onto a plane perpendicular to the helical axis.
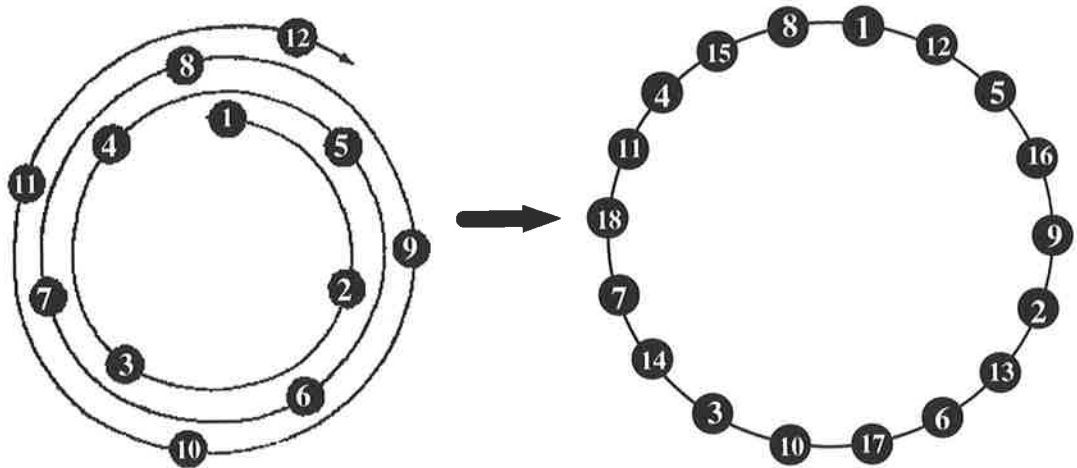
Fig. 2.2 The Edmundson helical wheel representation. Numbers represent amino acid sequence starting from the N-terminus.

If a amphipathic peptide is projected onto the wheel, amino acids with similar biochemical properties (such as hydrophobicity and charged groups) will be found clustered in an arc on the helical surface facing one direction while those possessing different properties will cluster on the opposite surface (Fig. 2.1b). This results in a clear separation of hydrophobic and hydrophilic faces. It has been postulated that the amphipathic nature of these peptides is a prerequisite for their bactericidal properties.

The formation of such a helix is thought to facilitate electrostatic attraction between cationic residues of the peptide and the anionic surface of the bacterial membrane (Westerhoff *et al.*, 1989). A simplified diagram of a typical membrane is shown in Fig. 2.3.

Hydrophilic head
Hydrophobic tail

Phospholipid
bilayer ~30Å
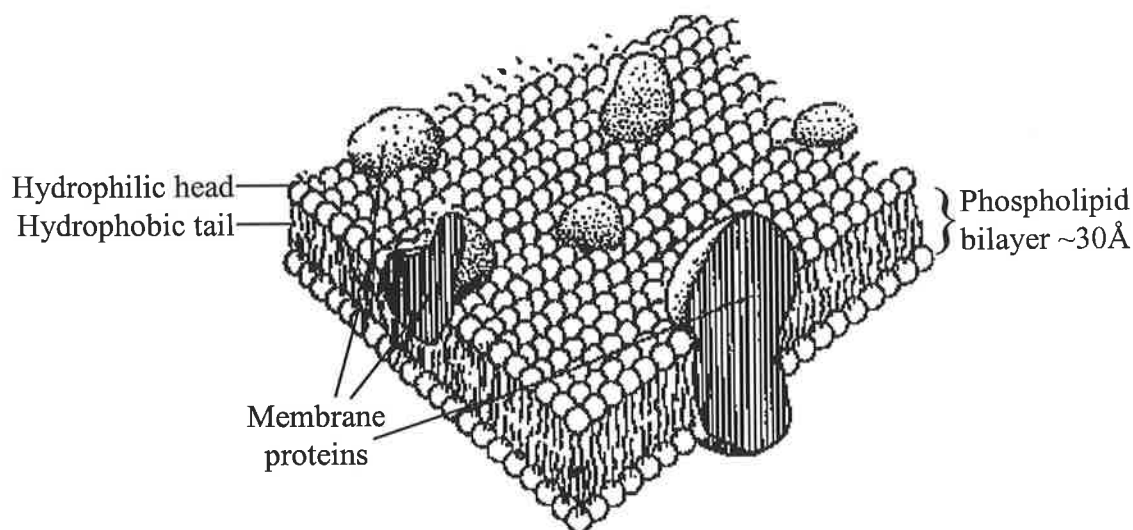
Membrane
proteins

Fig. 2.3 General structure of a bacterial membrane.
(Modified from Singer and Nicolson, 1972).

A bacterial membrane is basically made up of a phospholipid bilayer which provides a natural barrier to the flow of ions and other solutes between the bacterial cell and its environment; any disruption to the bilayer will cause cell lysis and death. Antibacterial peptides are thought to cause such a disruption.

2.4 Membrane Specificity

To develop these peptides into commercial pharmaceuticals, an important consideration has to be taken into account: are they selective only towards bacteria? Since eukaryotic cell membranes are also made up of a phospholipid bilayer, it is possible that such peptides will also lyse them.

Experimental evidence has shown that the cecropin and magainin families of antimicrobial peptides are selective only towards bacteria and protozoa (Zasloff, 1987; Chen *et al.*, 1988). This has been attributed to profound differences between mammalian and bacterial membrane designs. Bacteria, for reasons that are unclear, possess a much higher concentration of anionic phospholipids such as phosphatidylglycerol in their outer membranes (Duckworth *et al.*, 1974; Rothman and Kennedy, 1977; Voelker, 1985; Ratledge and Wilkinson, 1988). In addition, Gram-positive bacteria have acidic polysaccharides (teichoic acids) in their cell wall (Brock, 1984) while Gram-negative bacteria have acidic lipolysaccharides (LPS) located exclusively on the outer leaflet of the membrane (Lugtenberg and van Alpen, 1983; Nikaido and Vaard, 1985). This increased concentration of anionic molecules is thought to enhance the electrostatic affinity between the bacterial membrane and the highly cationic antimicrobial peptides (Miteva *et al.*, 1999). Indeed, conductance experiments have shown that cecropins (Gazit *et al.*, 1994; Gazit *et al.*, 1995) and magainins (Vaz Gomes *et al.*, 1993; Matsuzaki *et al.*, 1995) have higher affinities towards negatively charged membranes compared to uncharged ones while fluorescence, X-ray and scanning calorimetric studies have shown that antimicrobial peptides interact more strongly with anionic than zwitterionic (electrically neutral) lipid bilayers (Polozov *et al.*, 1997; Lohner and Prenner, 1999; Prenner *et al.*, 1999). Furthermore, *Staphylococcus aureus* mutants possessing a higher concentration of anionic phospholipids on their cytoplasmic membranes showed greater sensitivity towards cationic bactericidal peptides (Pescher *et al.*, 1999). In contrast, the outer bilayer surface of human cell membranes are exclusively composed of zwitterionic phospholipids, mainly phosphatidylcholine, phosphatidylethanolamine and sphingomyelin (Castano *et al.*, 1999). Anionic phospholipids, such as

phosphatidylserine, are exclusively localized in the inner bilayer surface, oriented towards the cytoplasm (Verkleij *et al.*, 1973). Furthermore, bacterial membranes lack cholesterol, a steroid which not only reduces the affinity of antimicrobial peptides for a phospholipid bilayer, but is also known to stabilize synthetic membranes (Nakajima, *et al.*, 1987; Christensen *et al.*, 1988; Tytler *et al.*, 1995). Vertebrate cell membranes, on the other hand, contain a considerable proportion of cholesterol (Fig. 2.4) which makes them less susceptible to cell lysis (Turner and Rouser, 1970; Lange and Ramos, 1983; Bloch, 1991). Indeed, conductance experiments have shown that cholesterol reduced the bioactivity of membrane-disrupting peptides while there was a significant enhancement in their potency when introduced to human erythrocytes lacking cholesterol (Nakajima *et al.*, 1987; Christensen *et al.*, 1988; Matsuzaki *et al.*, 1995).

Cholesterol

Phospholipid bilayer
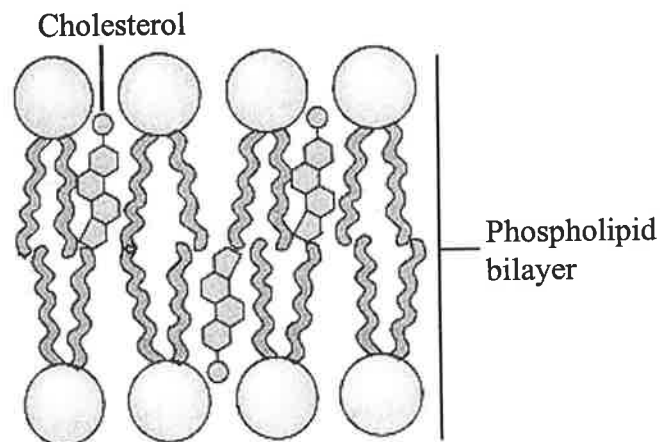
Fig. 2.4   Cholesterol stabilise phospholipid bilayers.

Circular dichroism studies have revealed that magainin adopts an amphipathic helical structure in aqueous solution containing anionic phosphatidylserine vesicles but was unstructured when exposed to zwitterionic phosphatidylcholine vesicles (Matsuzaki *et al.*, 1989b; Matsuzaki *et al.*, 1997; Matsuzaki *et al.*, 1998). The preferential binding of these basic peptides to negatively charged phospholipids may also explain their ability to selectively lyse cancerous cells, which have three to eight-fold more anionic phospholipids (typically phosphatidylserine) on their membrane surface compared to normal cells (Conner *et al.*, 1989; Utsugi *et al.*, 1991; Tytler *et al.*, 1995).

The difference in transmembrane potentials between prokaryotic and eukaryotic cells has also been suggested to play a part in cell selectivity of these peptides. Respiring prokaryotes are found to have a 'negative-inside' transmembrane potential while eukaryotic cells have no or insignificant transmembrane potential (Blondelle *et al.*, 1992; Matsuzaki *et al.*, 1995). This profound difference in the overall charge of the cell may be another reason for the preferential interaction of cationic membrane-lytic peptides with prokaryotes over eukaryotic cells.

Over the past two decades, a number of experimental techniques have been employed to gain a better insight to the mechanisms of bactericidal action of these peptides [see reviews by Bechinger (1999) and Shai (1998 and 1999)]. The next few sections will discuss the possible modes of action in greater detail.

2.5 The Channel Mechanism

Initially, all antimicrobial peptides were thought to undergo a transmembrane channel-forming mechanism, also known as the *barrel-stave mechanism* (Ojcius and Young, 1991; Shai, 1995). The process starts off with the unstructured (random coil) peptide in solution. Once in close proximity to the bacterial membrane, the cationic residues of the peptide are electrostatically attracted to the anionic headgroups of the membrane. This proposal is supported by experiments showing that adding sodium chloride inhibits the bactericidal activity of such peptides (Skerlavaj *et al.*, 1990; Sekharam *et al.*, 1991). Upon interacting with the membrane surface, the peptides adopt amphipathic α-helical structures (Inagaki *et al.*, 1989; Matsuzaki *et al.*, 1991, Matsuzaki, 1999). The next step involves the insertion of these helical peptides vertically into the membrane once a *critical peptide concentration* is reached. The vertical orientation of such peptides is supported by oriented circular dichroism spectroscopy (Huang and Wu, 1991; Ludke *et al.*, 1994) and in-plane neutron scattering studies (Ludke *et al.*, 1996). When the helical peptides are laid in parallel with respect to each other across the membrane, a transmembrane pore is formed with the hydrophobic faces of the peptides facing outwards. These interact with the hydrophobic alkyl chains of the phospholipid bilayer. The polar hydrophilic surface of the peptides are arrayed inwardly allowing the passive flux of ions and small molecules across the membrane, disrupting the osmotic gradient of the cell, ultimately lysing the membrane. A schematic representation of the mechanism is illustrated in Fig. 2.5a and 2.5b.
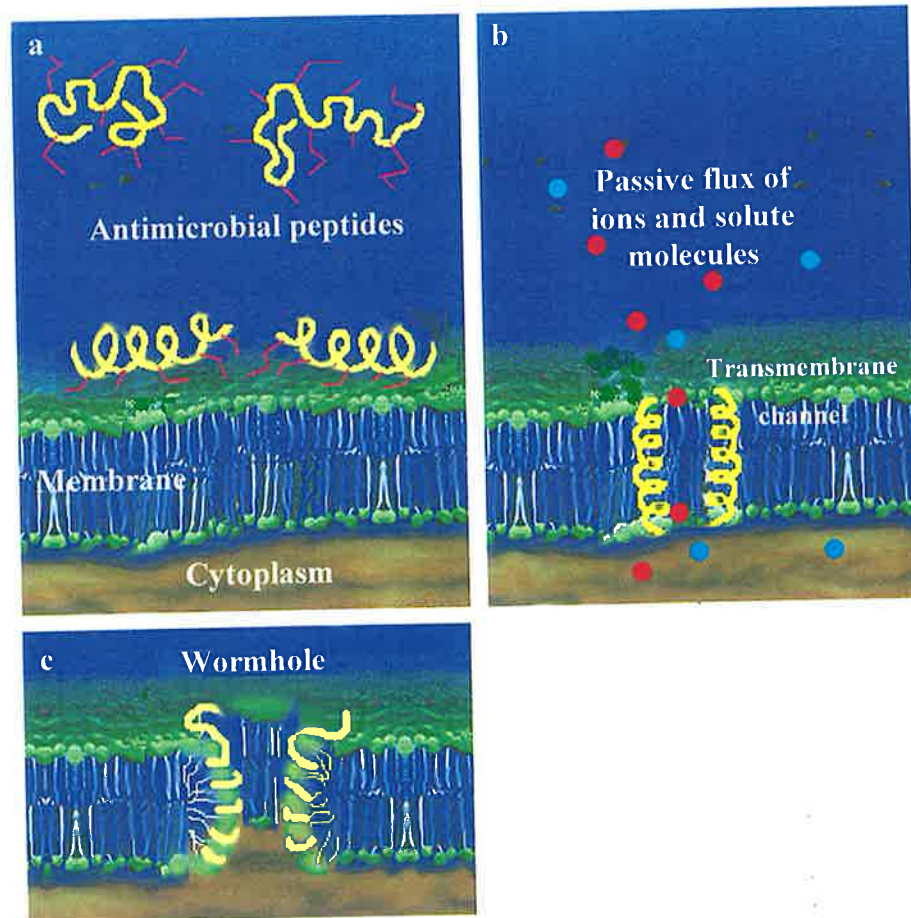
Fig. 2.5 The channel mechanism: (a) Interaction of peptides with membrane followed by (b) transmembrane channel formation resulting in the passive flux of ions and solutes. (c) A wormhole.

Recently, the nature of these channels has come under scrutiny as they involve in a peptide arrangement that result in the accumulation of many cationic residues (e.g. lysine) in a narrow pore (Bechinger, 1997). Such channels would possess a high positive charge-density in the pore region which is energetically unfavourable due to severe electrostatic repulsion. Furthermore, experiments have shown that such pores are selective towards cations, suggesting that the conventional channel model was unacceptable (Cruciani *et al.*, 1992). Recently, the channel model was modified: membrane phospholipids in the vicinity of the peptides are suggested to line the walls along the channel which 'neutralises' the highly positively-charged pore (Ludke *et*

al., 1996; Matsuzaki, 1998). Such channels have been termed *wormholes* (Bechinger, 1999). An example is illustrated in Fig. 2.5c.

The channel mechanism requires channel-forming peptides to be of sufficient length to span the entire phospholipid bilayer. Since each amino acid residue in an α-helix is related to the next by a distance of approximately 1.5 Å (from the N to C terminus), a peptide must have a minimum of 20 residues to be able to span a bacterial membrane typically of about 30 Å in thickness (Kaiser and Kezdy, 1987). Hence, by judging the number of amino acid residues alone, it would appear that most of the peptides listed in Table 1.1 will adopt the barrel-stave mechanism. This, in theory should include: alamethicin, cecropin, defensin, magainin, melittin and pardaxin.

How then, do shorter membrane-lytic peptides exert their biological effects? The next two sections will describe their possible mechanisms of action in detail.

2.6 Dimerisation

Antimicrobial peptides consisting less than twenty residues are too short to penetrate the entire bacterial membrane and thus cannot undergo the barrel-stave mechanism in their monomeric form. However, gramicidin A, a fifteen residue peptide isolated from *Bacillus brevis* was found to possess membrane-lysing properties (Andersen, 1983). In an attempt to explain such a phenomenon, detailed two-dimensional NMR studies were conducted, revealing that gramicidin A formed N-terminal to N-terminal dimers in micelle/water mixtures (Arseniev *et al.*, 1985). In addition, gramicidin A was found to be oriented perpendicular to phospholipid bilayers (Fig. 2.6) (Lazo *et al.*, 1995). End-to-end dimerisation would make them long enough to form transmembrane channels (Urry, 1984; Ketchem *et al.*, 1993; Separovic *et al.*, 1994; Koeppe *et al.*, 1995).
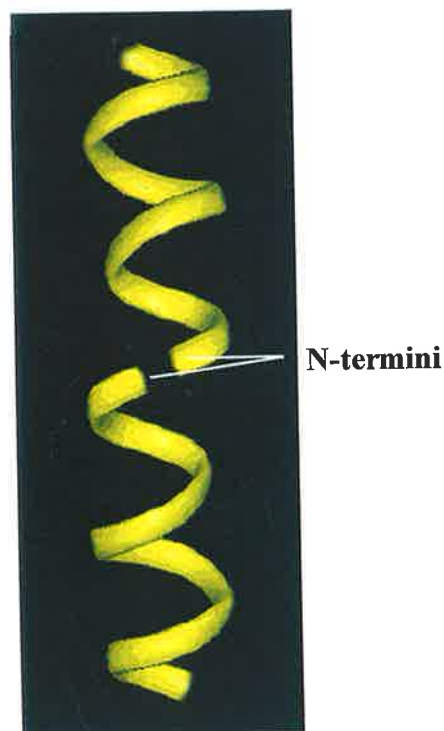
Fig. 2.6   N-terminal to N-terminal dimers of gramicidin A. Monovalent cations are postulated to traverse through the helices.
(Smith *et al.*,1990; Tian and Cross, 1999)

2.7 The Carpet Mechanism

A non-channel forming mechanism known as the *carpet mechanism* has also been suggested which provides another plausible explanation as to why some relatively short peptides possess antimicrobial activities (Epand *et al.*, 1995; Gazit *et al.*, 1995). For example, an eleven residue analogue of sapecin from the flesh fly *Sacrophaga peregrina* (Alvarez-Bravo *et al.*, 1995), a twelve residue defensin analogue from beetle haemolymph (Saido-Sakanaka *et al.*, 1999), thirteen residue peptides from bovine and porcine bone marrow (Selsted *et al.*, 1992; Lawyer *et al.*, 1996), a fifteen residue cecropin hybrid (Andreu *et al.*, 1985; Andreu *et al.*, 1992), a fifteen residue melittin hybrid (Subbalakshmi *et al.*, 1999) and the seventeen residue tachyplesin (Rao, 1999) were found to possess broad-spectrum antibiotic activities.

The initial part of the carpet mechanism is similar to the channel mechanism: electrostatic attraction of cationic residues to the anionic phospholipids on the membrane surface occurs, causing the peptides to adopt an amphipathic α-helical conformation and forming a 'carpet' on the membrane surface. Stoichiometric studies have shown that the threshold concentration of peptide needed to lyse phospholipid vesicles corresponds to the amount of peptide needed to form a 'carpet' monolayer on each vesicle surface (Gazit *et al.*, 1995).

Next, the peptide partially 'immerses' itself into the phospholipid bilayer by rotating and reorienting itself in such a way that only its hydrophobic residues interact with the membrane's hydrophobic core while its hydrophilic face continues to interact

with the polar head groups (and possibly the aqueous solution). Spectrofluorometric studies on N-terminal labelled dermaseptin (Pouny *et al.*, 1992; Strahilevitz *et al.*, 1994) and cecropin (Gazit *et al.*, 1994) showed that N-terminal fluorescent probes relocated to a more hydrophobic region while ^{13}C NMR studies using aqueous shift reagents revealed that such peptides had their hydrophobic residues imbedded in the membrane hydrophobic core while their hydrophilic side chains were immersed in the aqueous phase (Stanislawski and Rüterjans, 1987). In addition, results from attenuated reflection Fourier transform infrared spectroscopy and molecular dynamics simulations have also suggested that cecropins were oriented parallel to the lipid membrane surface and do not insert into the lipid bilayer to form transmembrane channels (Gazit *et al.*, 1996). Finally, solid-state NMR experiments show that the backbone amides of magainin were found near the phospholipid headgroups of artificial lipid bilayers, suggesting that the peptide was near or on the bilayer surface (Hirsch *et al.*, 1996).

This results in the thinning of the phospholipid bilayer to accommodate the peptide 'carpet', as revealed by X-ray diffraction (Ludke *et al.*, 1995), solid-state NMR (Bechiger *et al.*, 1991, 1992, 1993) and stoichiometric studies (Steiner *et al.*, 1988; Oren and Shai, 1997). When a peptide threshold concentration is reached, the membrane disintegrates, resulting in cell death. It has also been suggested that the detergent-like actions of such peptides may lead to the formation of peptide-phospholipid micelles by breaking off portions of the bilayer, destroying the integrity of the membrane (Sanders II and Prestegard, 1990; Bechinger *et al.*, 1999). The mechanisms are shown schematically in Fig. 2.7.
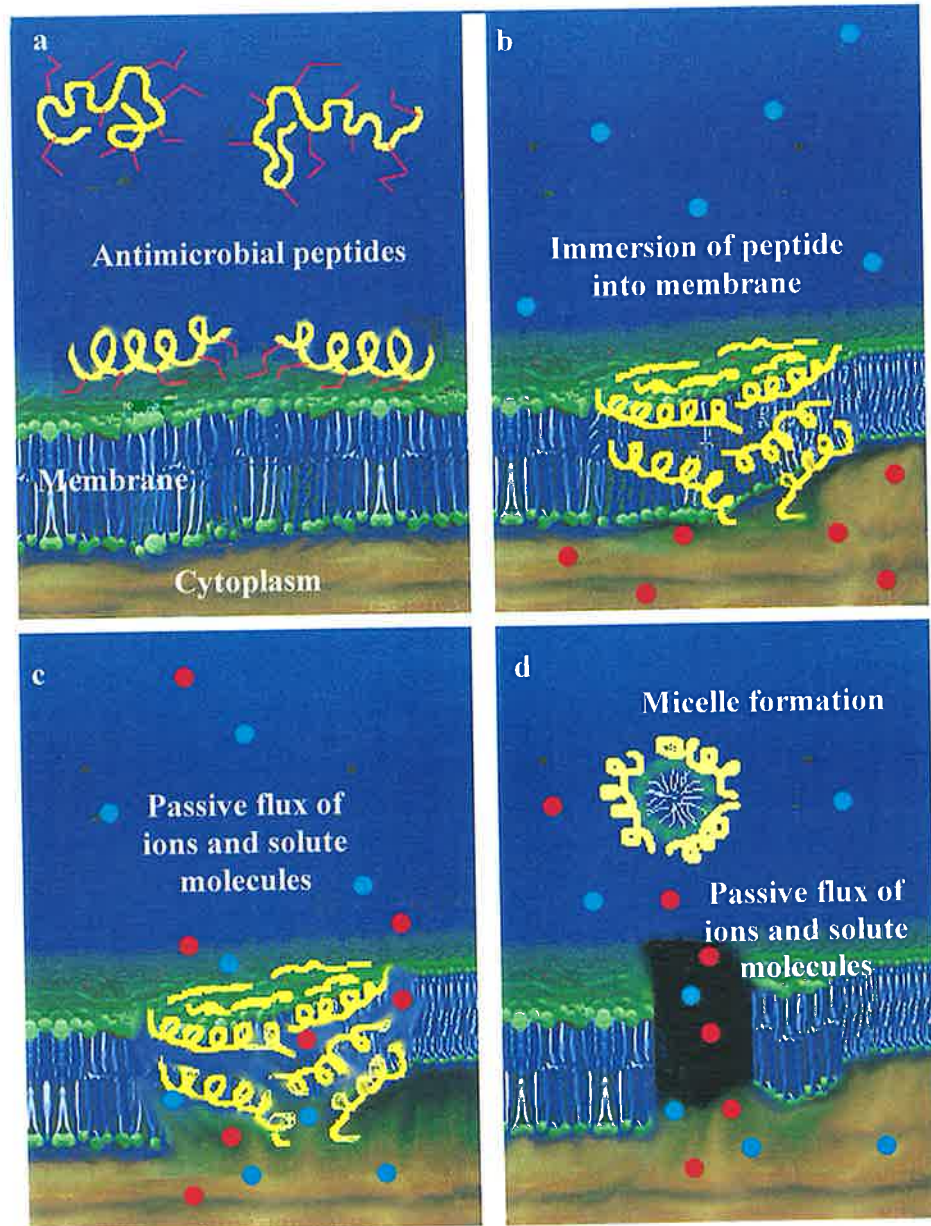
Fig. 2.7 **The carpet mechanism; (a) Peptide-membrane interaction followed by (b) Immersion of peptides into phospholipid bilayer. The final step could either involve: (c) membrane disintegration or (d) peptide-lipid micelle formation. Either pathways will kill the cell.**

Presently, it is not possible to predict which mechanism a membrane-lytic peptide will adopt just by studying its primary structure. However, amphipathic peptides consisting of twenty or more residues were thought to form transmembrane pores *via* the channel mechanism. In the last two decades or so, a variety of experimental techniques have been used to study the orientation and topology of these peptides.

31

Most experiments seem to support the fact that many membrane-lytic peptides (long enough to span a membrane) generally adopt the channel mechanism. Two extensively studied examples are alamethicin and melittin (Table 1.1). However, a number of exceptions were discovered. These include the cecropin, dermaseptin and magainin families of peptides (Epand et al., 1995; Bechinger, 1997). Although they were long enough to span a bilayer, experiments suggest that they adopt the carpet mechanism instead. Table 2.1 summarises some of these peptides and the corresponding techniques used to elucidate their membrane-lytic mechanism.

Table 2.1 **Membrane-disrupting peptides and their mechanisms of action.**

Peptide	Experimental method	Mechanism	References
Alamethicin	molecular modelling	Channel	Tieleman et al., 1999
	neutron-scattering	Channel	He et al., 1996
	Raman spectroscopy	Channel	Vogel, 1987
	solid-state NMR	Channel	North et al., 1995
	X-ray diffraction	Channel	Wu et al., 1995
Cecropin	attenuated reflection IR	Carpet	Gazit et al., 1996
	fluorescence spectroscopy and resonance energy transfer	Carpet	Gazit et al., 1995
	molecular modelling	Channel	Durell et al., 1992

	fluorescence spectroscopy	Carpet	Gazit *et al.*, 1994
	solid-state NMR	Carpet	Marassi *et al.*, 1999
	stoichiometry	Carpet	Gazit *et al.*, 1995
Dermaseptin	fluorescence spectroscopy	Carpet	Pouny *et al.*, 1992 Strahilevitz *et al.*, 1994
Magainin	attenuated reflection IR	Carpet	Bechinger *et al.*, 1999b
	differential scanning calorimetry	Carpet	Matsuzaki *et al.*, 1991
	fluorescence spectroscopy	Carpet	Matsuzaki *et al.*, 1994 Schumann *et al.*, 1997
	nitroxide spin-labelling	Carpet	Ludke *et al.*, 1994
	Raman spectroscopy	Carpet	Williams *et al.*, 1990
	solid-state NMR	Carpet	Bechinger *et al.*, 1991, 1992, 1993, 1998. Hirsch *et al.*, 1996
	X-ray	Carpet	Ludke *et al.*, 1995
Melittin	attenuated reflection IR	Channel	Frey and Tamm, 1991
	fluorescence spectroscopy	Channel	Pramanik *et al.*, 2000
	molecular modelling	Channel	Bachar and Becker, 1999
	neutron-scattering	Channel	Strom *et al.*, 1983 Yang *et al.*, 1999

Raman spectroscopy	Channel	Vogel, 1987
solid-state NMR	Channel	Smith *et al.*, 1994
surface potential measurements	Channel	Maget-Dana, 1999

Which mechanism will the antimicrobial peptides of Australian amphibians adopt? In the next two chapters, experiments that can be used as probes to give a better insight to their mechanism(s) of action will be discussed in greater detail.

Chapter 3

Three-Dimensional Structural Studies
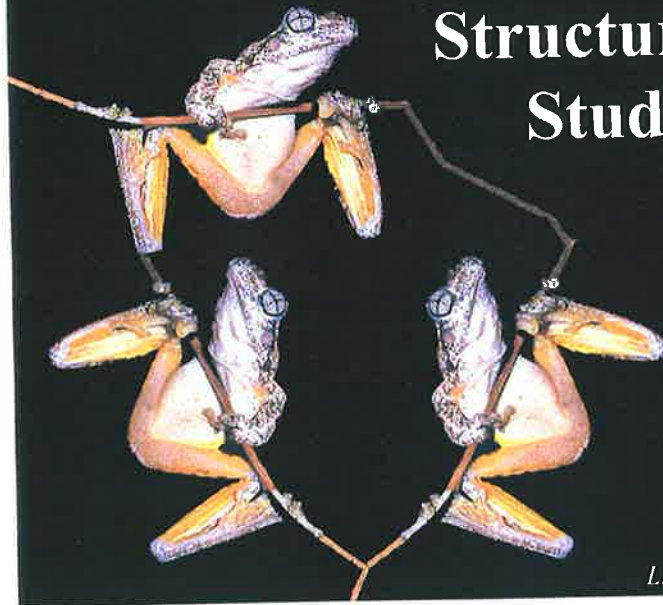
Litoria peroni

3.1 Structural Studies of Bioactive Peptides

Naturally occurring peptides have evolved to perform specific functions such as binding to biological receptors. Their functional properties depend largely on their conformation, i.e., their 3D structures. In order to gain a better understanding of their biological functions and mechanisms of action, their 3D structures must first be determined in appropriate physiological conditions.

A number of techniques have been developed to probe structural elements present in peptides and proteins. Automated Edman sequencing (Hunkapiller *et al.*, 1983) and electrospray mass spectroscopy (Marina *et al.*, 1999) are now routine techniques used for elucidating primary amino acid sequences. The number of new peptide sequences being discovered is increasing exponentially but primary sequences, by themselves, do not provide us with the overall picture of their biological functions. Presently, only a fraction of known bioactive peptides and proteins have had their 3D structures elucidated. Techniques such as circular dichroism (CD) (see Section 3.2), Fourier-transform and Raman IR spectroscopy (Krimm, 1963; Williams 1983; Williams *et al.*, 1990) can reveal the presence of certain structural elements (such as α-helices and β-sheets) while ultraviolet (UV) spectroscopy can provide information on the mobility and orientation of aromatic groups in a peptide (Matsuzaki *et al.*, 1994 and references cited therein). Although such techniques provide general information concerning the structural features of the peptide, they do not provide any quantitative structural data.

Detailed structural information can be obtained from protein crystals using techniques such as X-ray (Glusker *et al.*, 1994) and neutron diffraction (Kossiakoff, 1985; Helliwell, 1997; Niimura *et al*, 1997; Bradshaw *et al.*, 1998). In addition, the accuracy and resolution of peptide and protein structures have been greatly improved using synchrotron radiation as an X-ray source (Helliwell, 1998a, 1998b and 1992). Such techniques have a major disadvantage: the sample has to be crystallised first. If suitable crystals are available, structures with resolution ranging from 1.0-3.5 Å are generally obtainable. However with larger peptides and proteins, it is also necessary to prepare heavy-atom (e.g. cadmium and mercury) derivatives of the crystals to help with phasing of the electron density maps obtained. In addition, crystal packing forces can sometimes distort the overall conformation of a sample, giving different results when compared to solution structures (Blundell and Johnson, 1976; Schulz and Schirmer, 1979). Furthermore, crystallographic techniques only reveal the most stable conformation of the sample in the solid phase, they do not indicate the conformation in aqueous or membrane-mimetic environments. Hence, structural data obtained from crystallographic techniques must be treated with caution in particular instances.

High-resolution electron cryomicroscopy is another diffraction technique employed to determine the 3D structures of large proteins. Presently, it is limited to a resolution of 7 Å (although work is progressing rapidly to bring this down to 3 Å) and it cannot be used to resolve structures of smaller proteins and peptides with molecular masses less than 20 kDa (Chiu and Schmid, 1997; Walz and Grigorieff,

1998). Thus, this technique is unsuitable for use with the small peptides which are the subject of this thesis.

Techniques such as nuclear magnetic resonance spectroscopy (NMR) have emerged as alternative methods for 3D peptide structure determination. These new approaches, with NMR in particular, enables detailed structural studies of peptides in solution. This provides new insights of the molecular mechanisms by which membrane-lytic peptides fulfil their biological functions. The next few sections will decribe these two methods *CD and NMR techniques* in greater detail.

3.2 Circular Dichroism

The majority of naturally occurring peptides are constituted from L amino acids (with the exception of glycine which is not chiral). This stereo-isomeric property results in L and D peptides interacting differently with a beam of left and right-circularly polarised light. Such interactions cause both left and right-circularly polarised light to travel at different speeds as they traverse the peptide, thereby rotating the refracted beam (Brahms and Brahms, 1980; Cantor and Timasheff, 1982). The extent of rotation is measured by its *molecular ellipticity* (θ) and is primarily dependent on the conformational structure of the peptide. If a peptide is unstructured (i.e., random coil), a plot of θ against the wavelength of light (λ) will produce a curve with a broad, low absorbance minimum near 200 nm in the far-UV region. Peptides which adopt an α-helical conformation in solution will display a curve with characteristic minima in the vicinity of 208 nm (π-π^* transition) and 220

nm (n-π* transition) (Crabbe, 1965; Crabbe, 1972; Johnson, 1990). Fig. 3.1

illustrates a schematic CD spectrum of an unstructured and an α-helical peptide.
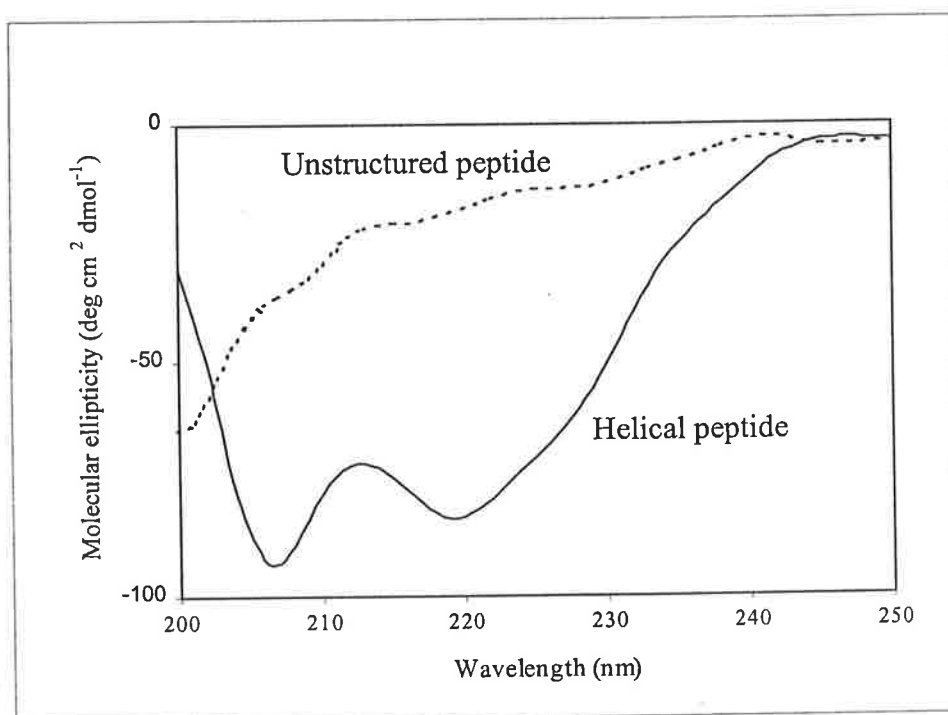
Fig. 3.1   A hypothetical CD spectrum of an unstructured and α-helical peptide.

Small deviations from α-helical geometry yield a CD spectrum with greatly

diminished intensities at 208 and 220 nm. Used qualitatively, CD spectra can

provide valuable information concerning the 3D structure of the peptide (Dyson and

Wright, 1991).

3.3 Nuclear Magnetic Resonance Spectroscopy

In the last two decades, nuclear magnetic resonance (NMR) has emerged as an

indispensable tool for the structural elucidation of biological molecules in solution,

particularly proteins and peptides (Wright, 1989; Wüthrich, 1989a; Clore and

Gronenborn, 1991). This is in part due to the significant developments in NMR

methodologies and hardware; in particular the introduction of multi-dimensional NMR methods, isotopic labelling techniques, superconducting high-field magnets and the use of more powerful computers for data processing. We now have a formidable second approach (alongside X-ray diffraction techniques) for accurate structural determination of peptides with molecular masses up to 40,000 Daltons (Wüthrich, 1989b; Wüthrich, 1998). NMR spectroscopy is an essential technique for structural studies of peptides because it is the only method that can provide us with high-resolution structural information of molecules in solution. In the next section, an introduction to the basic theory underlying NMR spectroscopy will be given followed by an introduction to the more complex two-dimensional (2D) NMR experiments required to obtain inter-nuclei distance restraints required for structural calculations.

3.4 The NMR Phenomenon

When a sample (dissolved in an appropriate solvent) is subjected to an external magnetic field $\mathbf{B_0}$, all its nuclei with a non-zero nuclear spin quantum number (I) will orient themselves in one of the possible ($2I+1$) directions within the field. Thus, biologically important nuclei (e.g. ^{1}H, ^{13}C, ^{15}N) which have $I = \frac{1}{2}$ will therefore be aligned in two possible orientations: parallel or antiparallel to $\mathbf{B_0}$. It is energetically more favourable for spins to align parallel to the magnetic field so the low energy spin state will be slightly more populated (Fig. 3.2). This results in the formation of a *net macroscopic magnetisation* $\mathbf{M}$ - the sum of the magnetisation of all individual spins. It is this net magnetisation which is manipulated to generate NMR spectra .
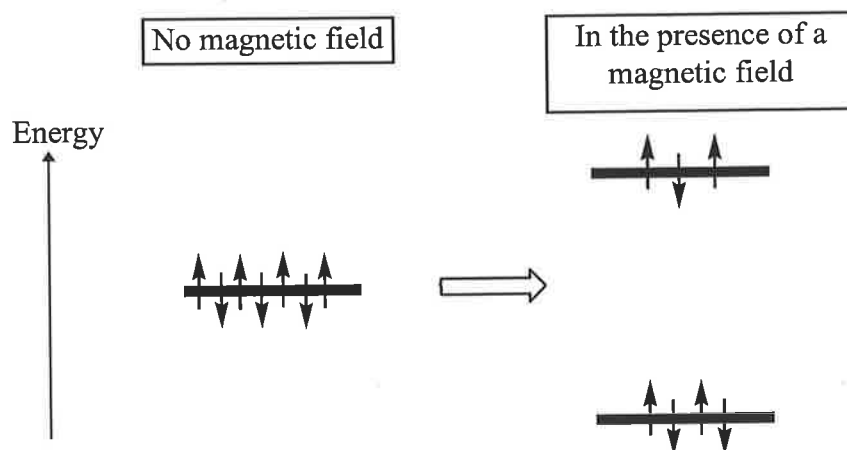
Fig. 3.2 **A schematic representation of the relative population of spins in the two energy states of a magnetised sample.**

3.5 One-Dimensional NMR Spectroscopy

Instead of using the 'energy states' analogy, the behaviour of **M** can be more conveniently described using vector diagrams (Fig. 3.3). When a radio-frequency pulse ($90°_x$) is applied along the X axis, it exerts a torque on **M**, represented by the movement of **M** into the XY plane along the Y axis.

Orientation of **M** *under a magnetic field*   *Application of radio-frequency pulse*   *Precession of magnetisation*
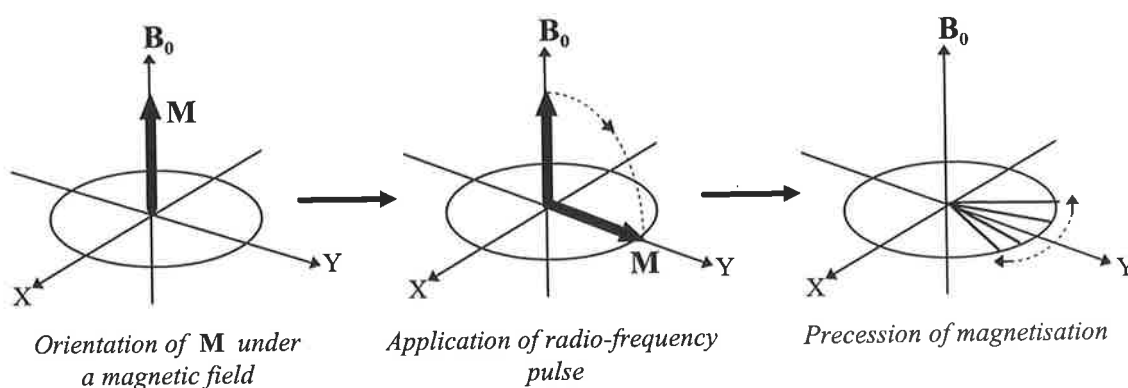
Fig. 3.3 **Vector diagrams showing effects of a radio-frequency pulse on M.**

Once **M** is brought into the XY plane, it precesses under the influence of B_0 at its resonance frequency. This induces an electric current in a detector coil wound

41

around an axis perpendicular to B_0. As the system relaxes back to the initial equilibrium stage, its transverse magnetisation decays with time. This free induction decay (FID) is recorded in the time domain and Fourier transformation (FT) of the transient signals into the frequency domain yields a one-dimensional (1D) NMR spectrum as illustrated in Fig. 3.4.

time domain   *frequency domain*
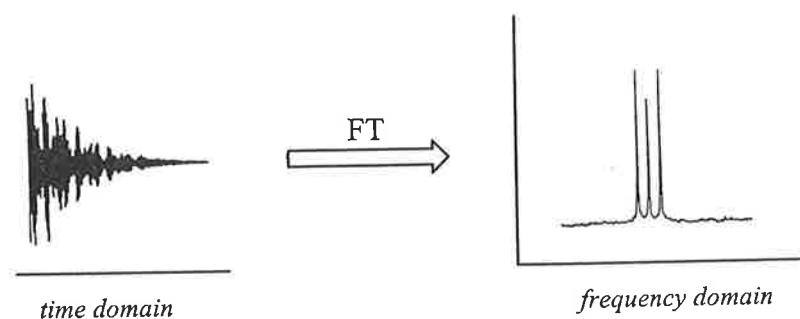
Fig. 3.4 Fourier transformation of a FID.

Since the resonance frequency exhibited by each nucleus depends primarily on its individual magnetic environment, a typical NMR spectrum contains a series of resonances from various nuclei at different frequencies relative to an internal standard expressed in parts per million (ppm) (Duncan, 1990). This makes it possible to compare the relative resonance frequencies of a particular nucleus in different compounds or when using magnets of different field strength. The internal standard of choice for biological samples (in aqueous solvent) is 2,2-dimethyl-2-silapentane-5-sulphonate (DSS) for which the most upfield signal is referenced at 0.015 ppm (Wishart *et al.*, 1995b; Gesell *et al.*, 1997).

3.6 Chemical Shifts and Secondary Structures

It is known that the magnetic environment of a nucleus is sensitive not only to local electronic effects, i.e., electron withdrawing and donating elements, but also to *shielding effects* that result from the formation of secondary structures. For example, the ^{1}H and ^{13}C chemical shifts of amino acid residues in a peptide usually differ from random-coil values, particularly at the α positions. Theoretical calculations (Clayden and Williams, 1982) and statistical analysis (Szilagyi and Jardetzky, 1989) have shown that ^{1}H and ^{13}C α-CH chemical shifts can be used to probe the presence of structural elements in proteins and peptides (Zhou *et al.*, 1992).

The random-coil chemical shifts of the twenty common amino acids have been determined (Wishart *et al.*, 1995b). For example, in a typical α-helical peptide, for a window of n = $\pm$ 2 residues, the smoothed plots of ^{1}H chemical shifts will exhibit a distinct upfield shift and those for the ^{13}C resonances will show a distinct downfield shift along the peptide, relative to the corresponding random-coil amino acids. This suggests that chemical shift deviations can be used to identify the presence of secondary structural elements in a peptide (Pastore and Saudek, 1990; Wishart *et al.*, 1991; Asakura *et al.*, 1995; Wishart *et al.*, 1995a). Fig. 3.5 illustrates a schematic plot representing a hypothetical helical peptide.
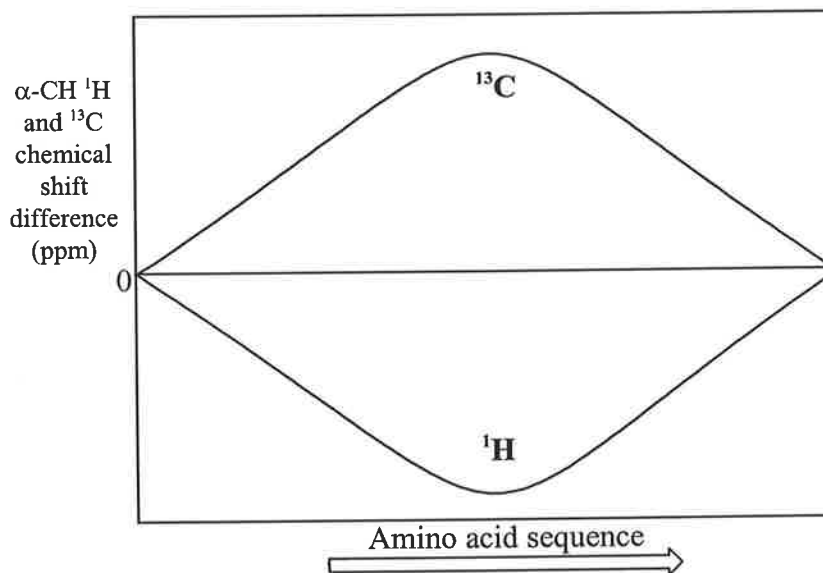
Fig. 3.5 **Deviation from random-coil chemical shifts for the ^{1}H and ^{13}C α-CH resonances of a hypothetical helical peptide.**

3.7 3D Structural Elucidation: The Strategy

So far, the techniques that provide information about the general structural elements present in a peptide have been described. However, these methods do not provide details of a 3D structure at the molecular level. To achieve this, quantitative information from other NMR techniques must be used to provide stringent structural constraints (e.g. inter-nuclei angles and distances). These data can then be used as inputs for calculations to produce realistic 3D models with structural parameters that are in agreement with constraints derived from NMR experiments. The following sections will discuss the appropriate NMR techniques in greater detail.

3.8 Coupling Constants and Dihedral Angles

The conformation of a peptide is influenced by the dihedral angles of the amide bonds (Markley *et al.*, 1998). Fig. 3.6 defines the ϕ dihedral angle ($\phi = 0°$ when the carbonyl C' is in the *trans* position to the amide ^{1}H).

Newman projection   *ϕ angle of a typical α-helix*
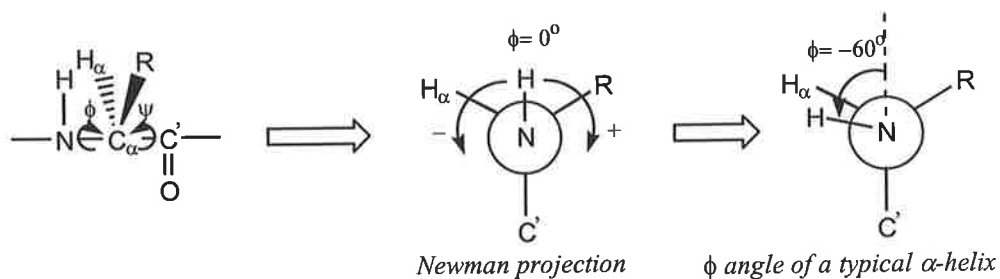
Fig. 3.6 The ϕ dihedral angle. The Newman projection is produced by viewing along the axis of N-C$_\alpha$-C' from the N-terminus.

The dihedral angle ϕ can be obtained from the magnitude of coupling constants between vicinal NH and C$_\alpha$H protons. The three-bond coupling constant (^3J) is related to ϕ by the relationship:

$$^3J_{HNC\alpha H} = 6.4 \cos^2 \left| \phi - 60° \right| + 1.4 \cos \left| \phi - 60° \right| + 1.9$$

A *Karplus plot* can be obtained from the above equation by correlating the ϕ angles of bovine trypsin inhibitor (BPTI) protein and $^3J_{HNC\alpha H}$ values measured in solution is shown in Fig. 3.7 (Karplus, 1959; Pardi *et al.*, 1987; Creighton, 1993).
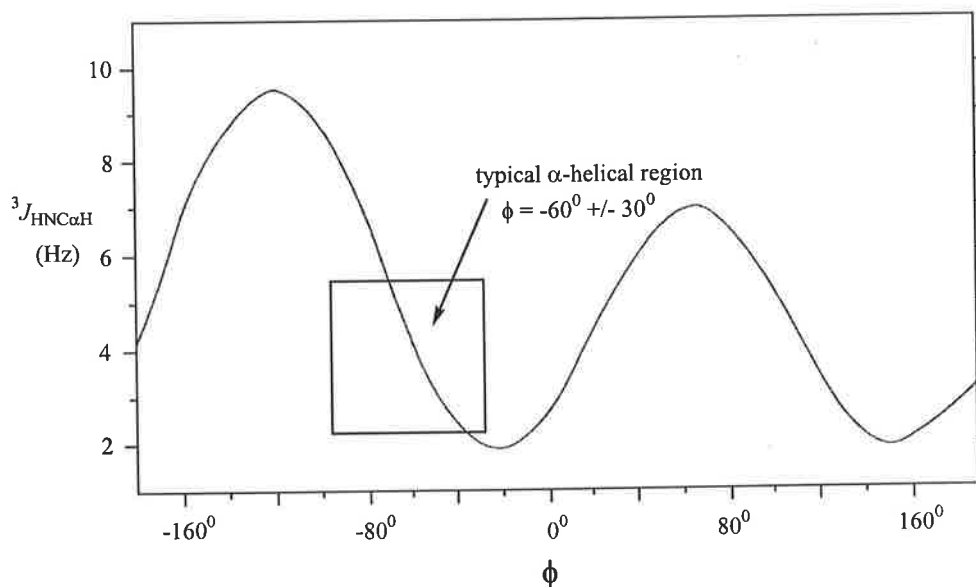
Fig. 3.7 Karplus plot showing relationship between coupling constant (Hz) and the ϕ dihedral angle.

When vicinal coupling constants are correlated with the dihedral angle ϕ, some ambiguities may occur since as many as four different values of ϕ may correlate with a particular coupling constant. This problem can be solved by analysing the range of values allowed for ϕ in known protein structures. For example in α-helices, ϕ values for all residues (with the exception of glycine and proline) are approximately between $-30°$ to $-90°$. As a general rule, four or more consecutive residues exhibiting a coupling constant of less than 5 Hz indicates that a helical region is present. For the purpose of structural calculations, an angular restraint of $-60 \pm 30°$ is typically used in helical regions. Coupling constants between 5 and 6 Hz are used to restrain ϕ to $-60 \pm 40°$ (Richardson, 1981; Wüthrich, 1986).

In summary, $^{3}J_{HNC\alpha H}$ values can provide supporting evidence for α-helical secondary structures. The observation of segments of three or more sequential residues with

small coupling constants (less than or equal to 5 Hz) has been considered a reliable and independent criterion for identification of helical regions in a polypeptide (Wüthrich, 1986).

3.9 Two-dimensional NMR Spectroscopy

Large molecules possess a large number of magnetically non-equivalent spins. In ^{1}H NMR spectra, this results in severe overlapping of NMR resonances in the spectra due to two or more different nuclear spins resonating at similar frequencies. Hence, two-dimensional (2D) NMR techniques are required to further separate these resonances to resolve much of the overlap.

2D experiments involve a basic scheme; *viz* (i) a preparation period (d_1), (ii) an evolution period (t_1) during which spins are labelled according to their resonance frequencies (or chemical shifts), (iii) a mixing period (τ_m) during which the spins are correlated to each other and finally, (iv) a detection period (t_2) where the FID is recorded (Wüthrich, 1986). A number of experiments are recorded with successive incremented values of t_1 to generate a data matrix. Fourier transformation of the data matrix in both dimensions then yields the 2D frequency spectrum. The process is summarised in Fig. 3.8.
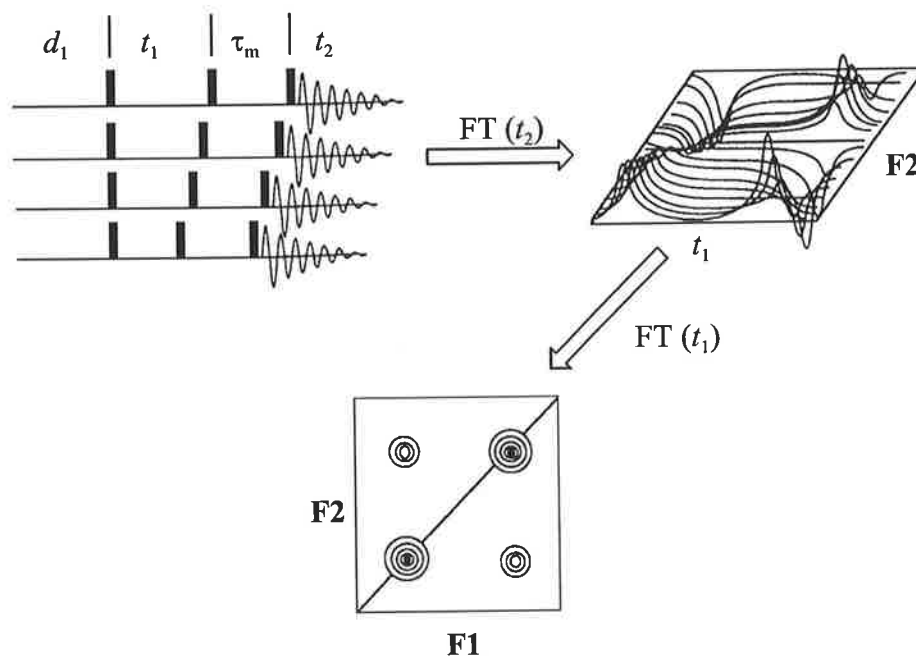
Fig. 3.8 Generating a 2D NMR experiment.

Such spectra have both axes corresponding to the same chemical shift and are symmetrical about the diagonal. The diagonal corresponds to the one-dimensional (1D) spectrum and the off-diagonal, symmetrical *cross-peaks* indicate the existence of interactions between two ^{1}H nuclei, with coordinates corresponding to their respective chemical shifts.

3.10 2D NMR Techniques

Information on through-bond and through-space interactions between specific nuclei can be obtained by manipulating the radio-frequency pulse sequences of 2D NMR experiments. Thus, by conducting a series of 2D experiments, it is possible to obtain the complete ^{1}H and ^{13}C assignments of proteins consisting up to about 100 amino acid residues (Chazin and Wright, 1988). The next four sections describe the essential 2D techniques in detail.

3.11 Correlation Spectroscopy

Correlation Spectroscopy (COSY) enables the analysis of through-bond (scalar) interactions between pairs of ^1H nuclei (Aue *et al.*, 1975). The pulse sequence (Fig. 3.9a) involves the application of an initial 90° pulse which sends the magnetisation from the Z axis to the XY plane. Immediately after, the magnetisation evolves in the XY plane during t_1, leading to the labelling of nuclei that are spin-spin coupled to each other. As a consequence, each COSY cross-peak represents ^1H-^1H couplings *via* three bonds (^3J coupling).

(a)

$$d_1 \quad 90°_x \quad t_1 \quad 90°_x \quad t_2 \text{ (acquire)}$$

(b)

$$d_1 \quad 90°_x \quad t_1 \quad 90° \quad d_2 \quad 90° \quad t_2 \text{ (acquire)}$$
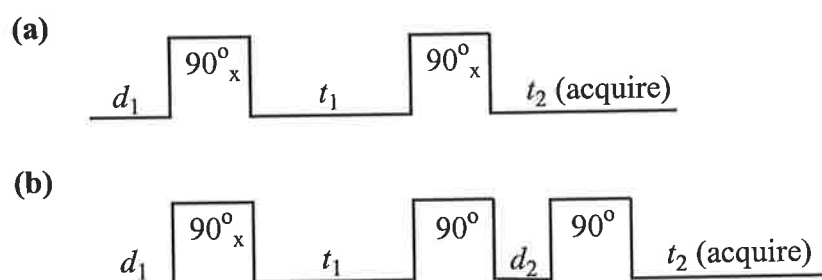
Fig. 3.9 (a) The COSY and (b) double-quantum filtered COSY pulse sequences.

A drawback of the experiment is that the diagonal produced is a dispersion signal. This results in a 'tailing effect' that can obscure cross-peaks near the diagonal. To circumvent this problem, double-quantum filtering (DQF) is incorporated into the pulse sequence (Fig. 3.9b): the first 90° pulse rotates ^1H magnetisation into the XY plane. The incremental delay (t_1) allows evolution of scalar-coupled chemical shifts. The second 90° pulse generates multiple quantum coherence between coupled spins. Scalar-coupled spins are rotated back to observable single-quantum coherence by the third 90° pulse and signals from uncoupled spins are eliminated *via* phase cycling.

DQF-COSY is the method of choice over conventional COSY, not only are the 'tailing' effects of the diagonal minimised, strong singlet peaks (e.g. from water) produced by uncoupled protons are also significantly reduced (Rance *et al.*, 1993b).

3.12 Total Correlation Spectroscopy

COSY-type experiments are used to demonstrate connectivities up to three bonds in length. This is of limited value due to spectral overlap, especially for analysing ^{1}H nuclei in the side chains of amino acids which tend to have chemicals shifts between 1.0 to 3.5 ppm. For this reason, total correlation spectroscopy (TOCSY) is employed to produce *relayed* scalar connectivities (Davies and Bax, 1985). The TOCSY experiment is similar to COSY except that the magnetisation of scalar-coupled protons is extensively transferred across all coupled spins. As a result, distant protons (up to 7 bonds apart) will show up as off-axis cross-peaks in the resultant plots unless they are isolated by a quaternary or carbonyl carbon (Braunschweiler and Ernst, 1983). This feature is essential for the identification of the different spin systems belonging to each specific residue of a peptide i.e., different residues can be identified by their distinct TOCSY pattern. Compared to the COSY pulse sequence, the TOCSY pulse sequence (Fig. 3.10) has an additional *spin-lock* pulse during the mixing time. This induces exchange of magnetisation between the spins of a particular spin system, causing them to temporarily become magnetically equivalent. As a consequence, the 'relayed' through-bond connectivities are observed in a spin system.
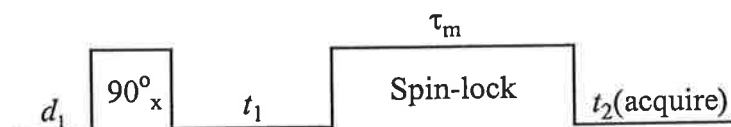
Fig. 3.10 The TOCSY pulse sequence.

3.13 Heteronuclear Single-Quantum Coherence Spectroscopy

The heteronuclear single-quantum coherence (HSQC) experiment provides heteronuclear ^{13}C-^1H correlation information, i.e., the chemical shifts of hydrogen to carbon nuclei. It is basically similar to the COSY experiment but in this case, scalar magnetisation transfer occurs between two types of nuclei. It is an *inverse-detection* technique where the ^1H signal is observed rather than the ^{13}C signal (due to the greatly increased sensitivity of ^1H nucleus). The basic HSQC pulse sequence is illustrated in Fig. 3.11.
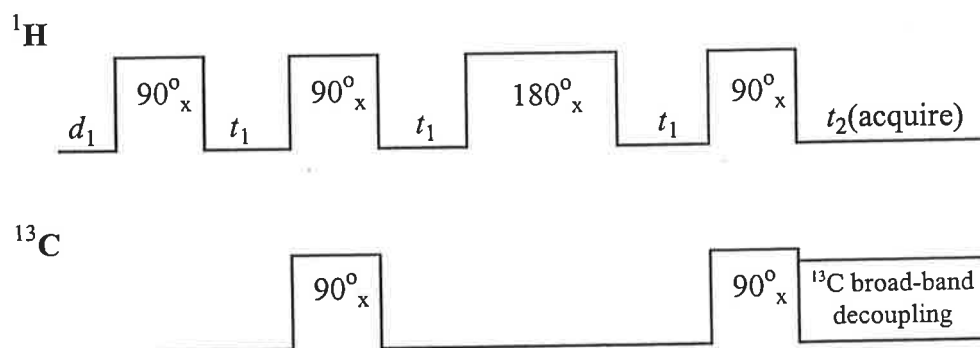
Fig. 3.11 The HSQC pulse sequence. The sequence on the top represents the ^1H transmitter pulse sequence and bottom represents the ^{13}C decoupler pulse sequence.

The experiment involves the use of two separate channels for the ^1H and ^{13}C nuclei. Once the ^1H pulse brings the magnetisation into the XY plane, the first ^{13}C pulse forms double (and zero) quantum coherence between scalar-coupled ^1H and ^{13}C

spins. This coherence undergoes evolution during t_1. Next, a 180° ^{1}H pulse refocuses the ^{1}H chemical shift evolution, leaving the magnetisation labelled only by the ^{13}C chemical shifts. The second ^{13}C pulse converts the double-quantum coherence back to a single-quantum coherence. The ^{1}H (^{13}C decoupled) spectrum detected is modulated by the ^{13}C chemical shift as a function of t_1. Finally, ^{1}H transverse magnetisation is observed after the refocusing period. Following Fourier transformation, cross-peaks are observed between the directly-bonded ^{1}H and ^{13}C nuclei.

3.14 Nuclear Overhauser Effect Spectroscopy

Nuclear Overhauser effect spectroscopy (NOESY) is a crucial technique that determines inter-proton through-space interactions. (Jeener *et al.*, 1979; Wagner and Wüthrich, 1979). In this experiment, each cross-peak represents a nuclear Overhauser effect (NOE) produced by through-space dipolar interactions between ^{1}H nuclei. The pair of nuclei in question need not belong to the same residue; they simply have to be near each other in space. The NOESY pulse sequence is shown in Fig. 3.12. The second 90° pulse is applied after the t_1 period to bring the magnetisation to the –Z axis immediately followed by a mixing period, τ_m. During this period, dipolar coupling occurs between nuclei of close proximity ($\leq$ 5 Å apart).
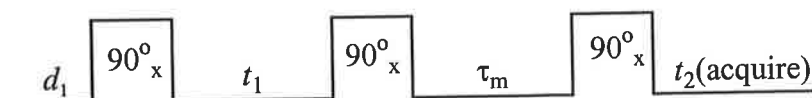
Fig. 3.12 The NOESY pulse sequence.

The relative intensities of cross-peaks reflects the magnitude of spatial separation between two nuclei: the closer apart the two nuclei are, the more intense the cross-peak. As a consequence, NOESY experiments can be utilised to deduce inter-proton distances, imposing stringent constraints on the number of possible conformations a peptide can adopt in solution.

3.15 Cross-peak Intensities and Inter-proton Distances

NOESY cross-peak intensities depend on the inter-proton distance r and is a *are* function of the rotational correlation time (τ_c) of the molecule (Ernst *et al.*, 1987):

$$\text{NOE intensity} \propto r^{-6} \cdot f(\tau_c) \qquad \dots\dots(1)$$

It can be seen that the NOE intensity is inversely proportional to r^6 (i.e., a very short-range effect) but is also dependent on τ_c which gives a measure of the rate of molecular tumbling. Large biomolecules have a long τ_c which can result in the observation of negative NOE intensities. Fig. 3.13 illustrates the relationship between NOE intensity to τ_c.
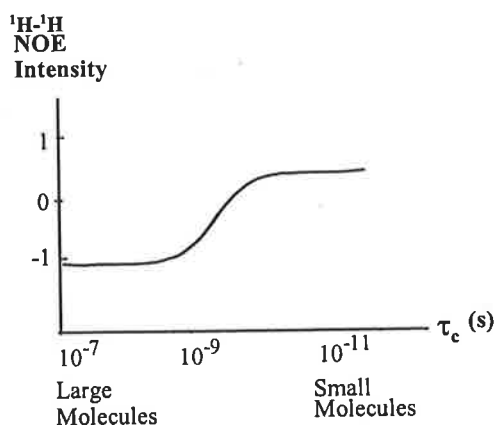
Fig. 3.13 Plot of NOE intensity versus log τ_c (B_0 = 11.7 T, 25°C).
(Diagram modified from Wüthrich, 1986)

Equation (1) assumes that *all* protons in the molecule possess the same τ_c. In reality, however, this is not so. Intra-molecular mobility leads to non-linear averaging of distances for different ^1H nuclei in a molecule. For example, the methyl protons of alanine and valine in a peptide may have different τ_c. For this reason, it is necessary to put upper and lower limits on the distance *r* before they can be used as distance restraints during calculations to avoid over-restraining the molecule. This will be discussed in the next section.

3.16 Measuring NOESY Cross-peak Intensities

In 1D NMR, the intensity of a peak is represented by its integral value and does not depend upon the line-shape or multiplet structure. In the 2D NOESY spectra however, the integral corresponds to the *volume* of the cross-peak. Volume integration is achieved by fitting all rows and columns of the NOESY spectrum to a set of reference line-shapes (Denk *et al.*, 1986; Olejniczak *et al.*, 1989). These line-shapes are defined along the F1 and F2 dimensions for each resonance by using a row (or column) containing a well-resolved crosspeak which has been unambiguously assigned to its resonance. In cases of overlapping cross-peaks, the row and column integral can be evaluated by computerised *curve fitting* methods. This fitting procedure is completely independent of the reference line-shapes as it uses theoretical (Lorentzian) line-shapes produced by NMR resonances (Roberts, 1995).

3.17 Notations for Inter-proton Distances in Peptides

The distance between a pair of ^{1}H nuclei A and B located in two different residues (at positions i and j) of a peptide sequence is denoted by $d_{AB}(i,j)$. Distances are defined from the N to the C terminus of the peptide sequence. Some examples are given below:

$$d_{\alpha N}(i,j) \equiv d(\alpha H_i, NH_j)$$

$$d_{NN}(i,j) \equiv d(NH_i, NH_j) \equiv d_{NN}(j,i)$$

Inter-proton interactions and their corresponding notations between adjacent residues are illustrated in Fig. 3.14. Arrows indicate through-space interactions between the amide proton of residue $i+1$ and the $C_\alpha H$ ($d_{\alpha N}$), NH (d_{NN}) and $C_\beta H$ ($d_{\beta N}$) of residue i. In peptides and proteins, these distances are short enough to give rise to strong NOEs and are used for the identification of adjacent residues during the sequential assignment procedure (see Section 3.19).
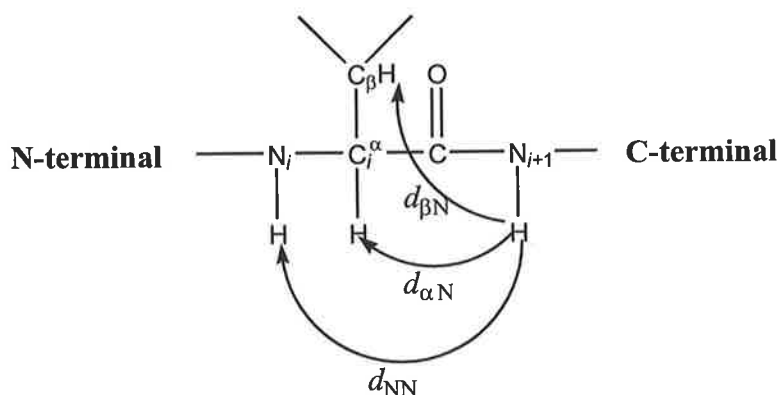
Fig. 3.14 Nomenclature used for defining inter-proton distances in peptides.

3.18 NOESY Patterns in an α-Helical Peptide

NOESY cross-peaks can indicate the presence of secondary structures present in a peptide. For example in amphipathic helical peptides, inter-residue hydrogen bonding takes place between the carbonyl oxygen nuclei and amide protons four residues apart (Fig. 3.15a) resulting in the formation of a α-helix (Jeffrey and Saenger, 1991). Due to this relatively stable conformation, inter-residue NOEs are usually observed between protons belonging to residues that are three to four residues apart in the sequence (Fig. 3.15b).

(a)

(b)
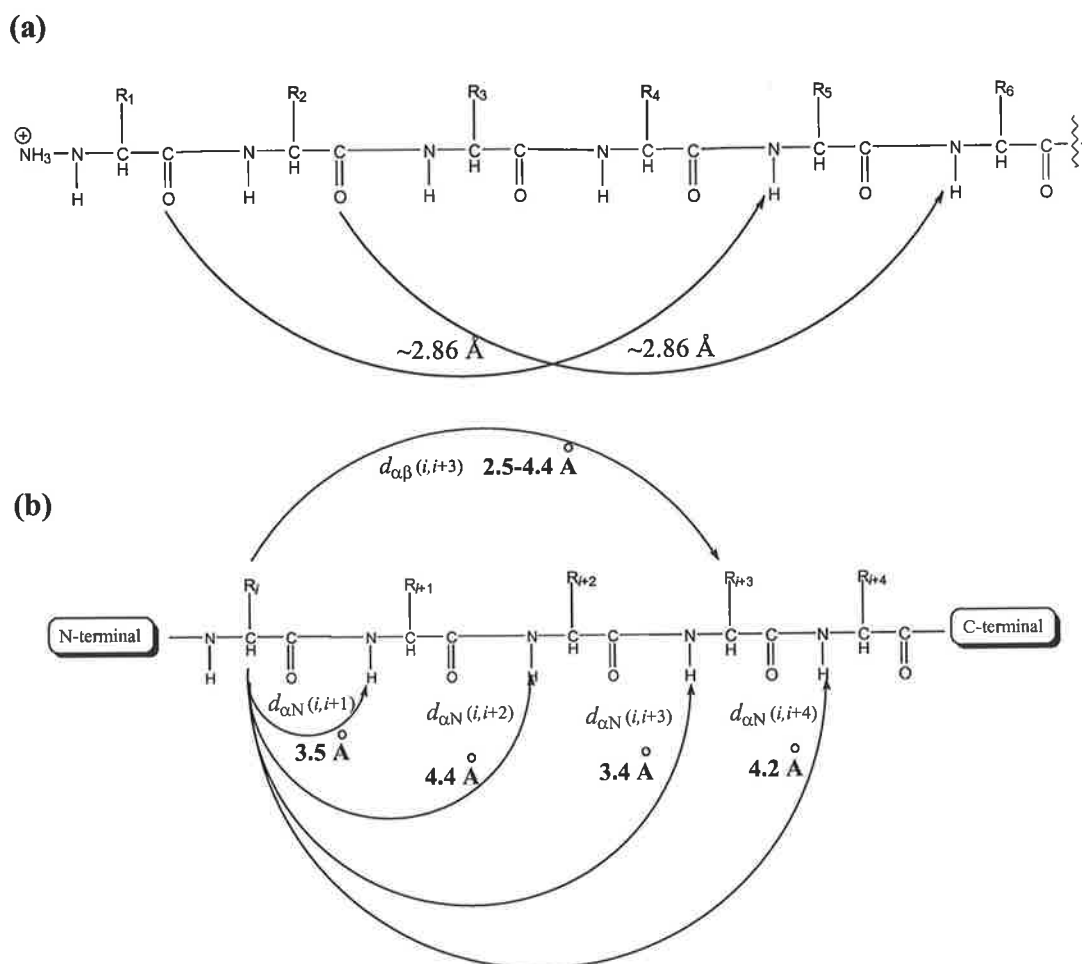
Fig. 3.15 Schematic representations of (a) hydrogen bonding (curved arrows) and (b) typical NOESY inter-residue interactions in an α-helix.

Some of the inter-residue NOESY interactions present in an α-helix are shown in Fig.

3.16 while the corresponding inter-proton distances are listed in Table 3.1.
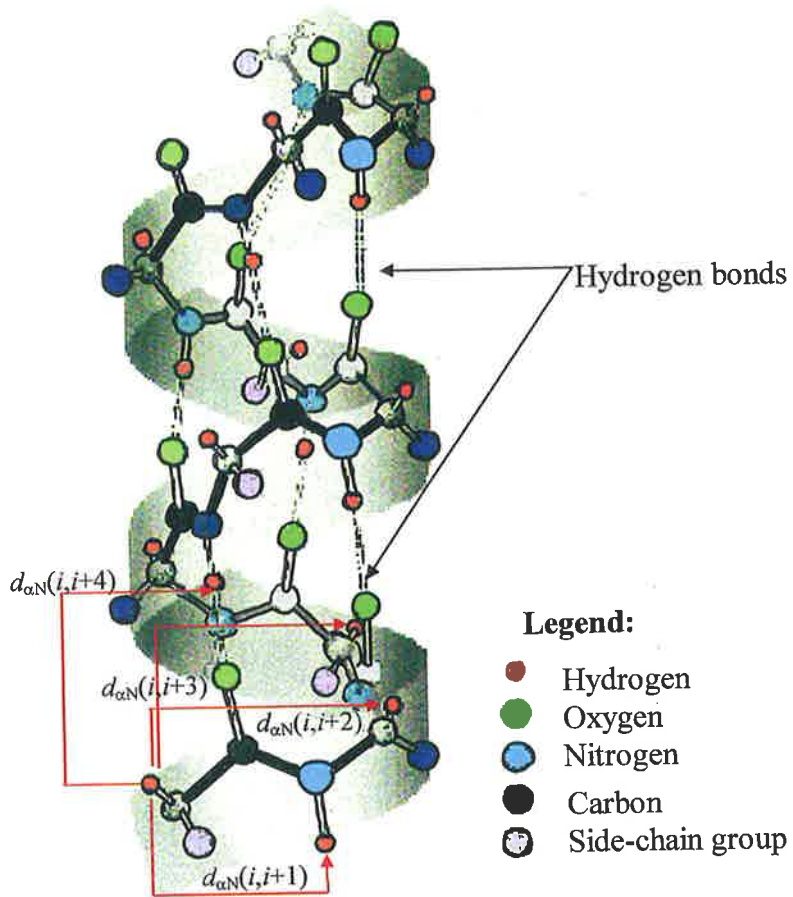
Fig. 3.16 Schematic 3D view of an α-helix showing typical inter-residue NOESY interactions. (Diagram modified from Lewin, 1990).

Table 3.1 Types of inter-proton interactions observed in an α-helix.

Type of Interaction	Approximate distance (Å)
$d_{\alpha N}(i,i+1)$	3.5
$d_{\alpha N}(i,i+2)$	4.4
$d_{\alpha N}(i,i+3)$	3.4
$d_{\alpha N}(i,i+4)$	4.2
$d_{NN}(i,i+1)$	2.8
$d_{NN}(i,i+2)$	4.2
$d_{\beta N}(i,i+1)$	2.5-4.1
$d_{\alpha\beta}(i,i+3)$	2.5-4.4

3.19 The Sequential Assignment of Cross-peaks

Assigning ^{1}H nuclei resonances to specific amino acids of a peptide is a necessary task which must be completed before detailed structural analysis can be undertaken. Central to the sequence-specific assignment of ^{1}H resonances is the use of the *sequential assignment* procedure proposed by Wüthrich and co-workers (Billeter *et al.*, 1982). In essence, it employs the combined analysis of TOCSY and NOESY experiments. Sequence-specific assignments can be achieved using through-space ^{1}H-^{1}H interactions (obtained from the NOESY spectrum) to identify neighbouring amino acid residues. A seventeen residue peptide, uperin 3.6 (GVIDA AKKVV NVLKN LF) is used as an illustrative example.

The first step involves the identification and assignment of proton resonances according to their respective residue type using the TOCSY experiment. For example, the side-chains protons of Gly, Ala, Ile, Leu, Val, Pro, Lys, Arg and Thr residues give unique connectivity patterns which can usually be identified unambiguously. By using the TOCSY spectrum alone, it is possible to assign most of the peptide amide protons couplings to their respective α and side-chain protons (Fig. 3.17).
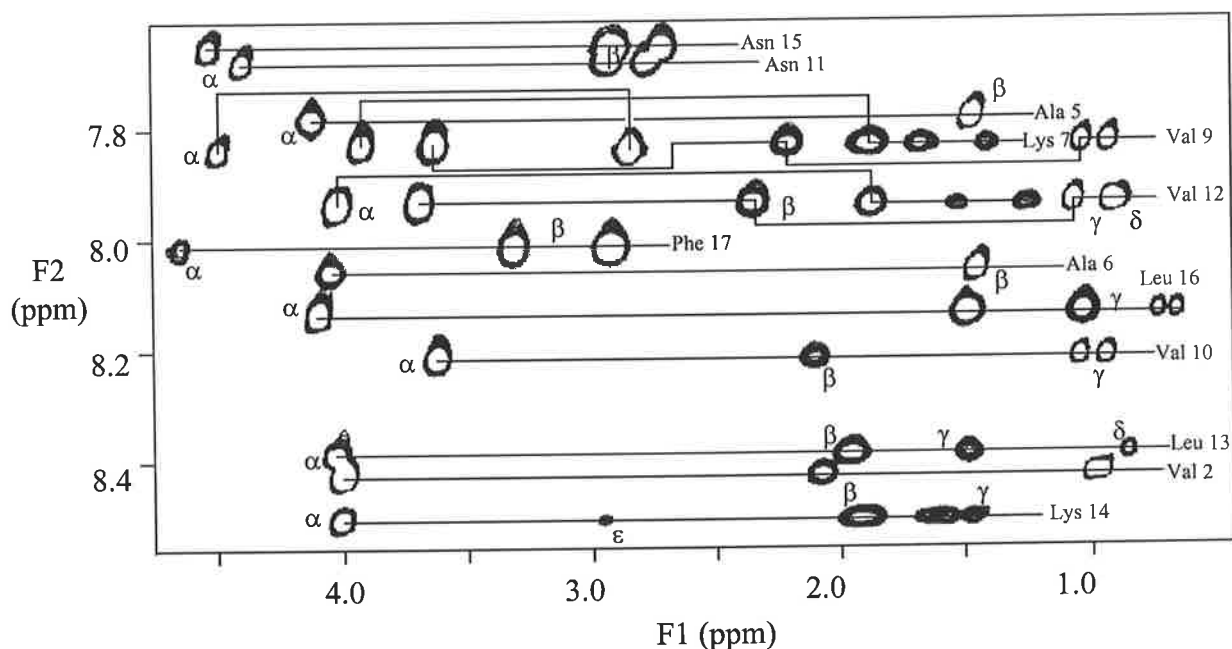
Fig. 3.17 TOCSY showing NH-side chain ¹H region of of uperin 3.6 in TFE/H₂O (1:1 by vol.), pH 2.4, 25°C. (α and side-chain protons are indicated for each residue).

Ambiguity occurs when two or more of the same type of residue is present in the peptide. For example, two asparagine (N) residues are present at positions 11 and 15 in uperin 3.6. To resolve this problem, the NOESY experiment is employed.

The next step involves the sequential assignment of ^{1}H resonances with respect to the peptide sequence by analysing $d_{NN}(i,i+1)$ NOESY cross-peaks (Fig. 3.18). In α-helices, the $d_{NN}(i,i+1)$ distances are typically about 2.8 Å and thus show up as intense NOEs (Table 3.1). This allows the elucidation of the chemical shift of the adjacent amide proton resonance. Using this information, the TOCSY experiment confirms the particular residue type by analysis of the side-chain ^{1}H pattern. This procedure is repeated sequentially along the length of the peptide.
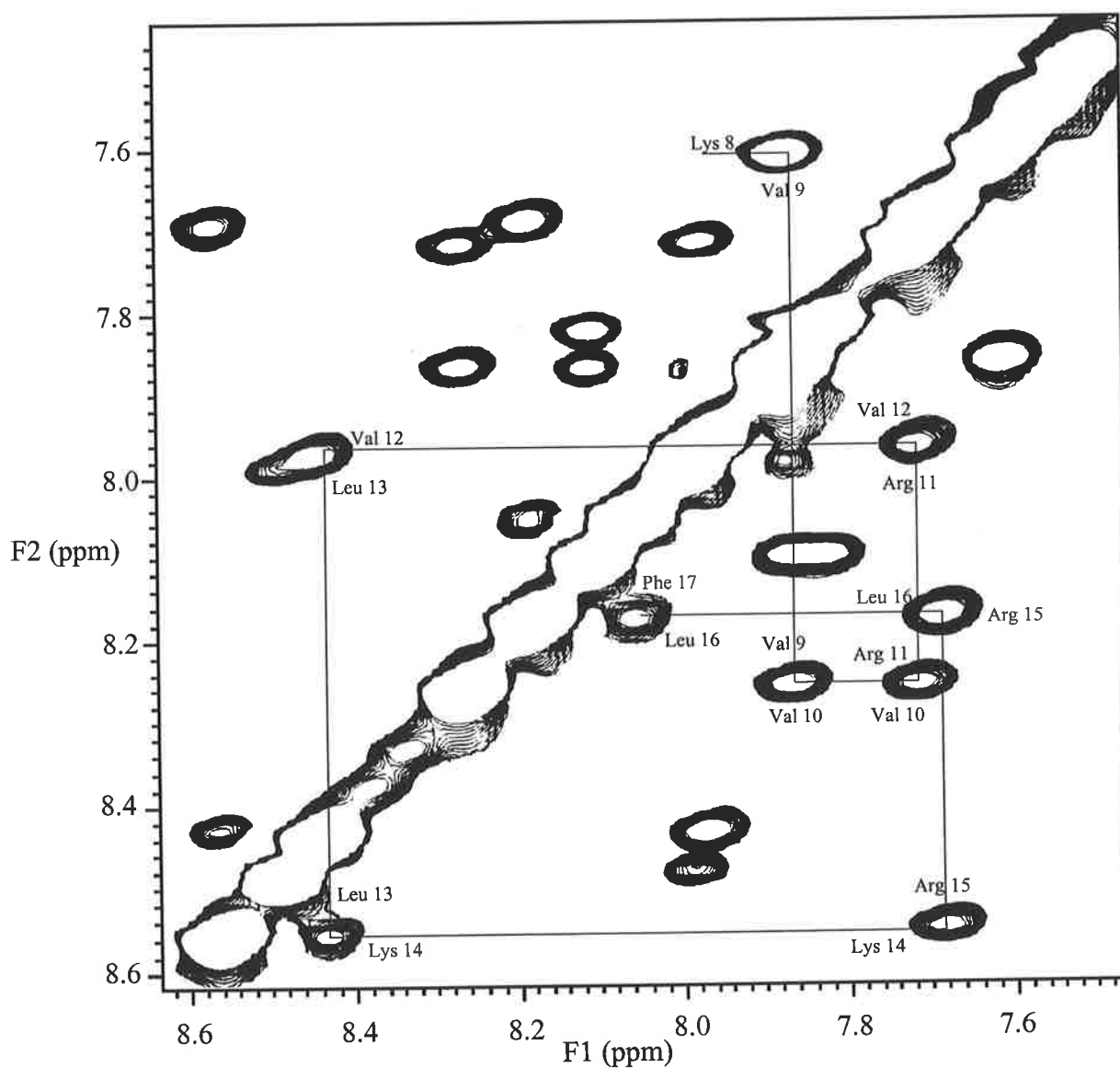
Fig. 3.18 NOESY showing the NH-NH region of uperin 3.6 in TFE/H$_2$O (1:1 by vol.), pH 2.4, 25°C. NOEs between sequential NH protons of residues 8-17 are shown.

Spin systems can thus be sequentially assigned to each individual residue in the primary sequence. When the NH chemical shift of each residue has been determined, the TOCSY spectrum can be employed again to establish the chemical shifts of every proton in the peptide .

When all the ^{1}H nuclei have been assigned, inter-proton distances can be calculated from NOESY cross-peak volumes as discussed in Section 3.16. This, with the angular restraints obtained from 1D NMR (Section 3.8) are used as structural constraints during molecular dynamics calculations as discussed in the following section.

3.20 Restrained Molecular Dynamics

Molecular dynamics (MD) is the science of simulating the motions of a system of particles over a period of time. This technique is now extensively employed for studying structure-energy relationships of large particles, in particular, biological molecules (Sternberg, 1996). In addition, MD can also be used for carrying out energy optimisation procedures in order to minimise the strain energy in calculated structures (McCammon and Harvey, 1987; Moore *et al.*, 1988; Karplus and Petsko, 1990).

Molecular dynamics simulates the motions of a system of atoms with respect to the forces which are present based on classical Newtonian equations of motion solved as a function of time (Brünger *et al.*, 1986; Grant and Richards, 1995):

$$\mathbf{F}_i = m_i \mathbf{a}_i$$

where $\mathbf{F}_i$ is the force, m_i is the mass and $\mathbf{a}_i$ is the acceleration of an atom i. By

expressing acceleration as the second derivative of displacement $\mathbf{r}_i$,

$$\mathbf{F}_i = m_i \, d^2\mathbf{r}_i \, /dt^2$$

Rearranging,

$$\mathbf{F}_i \, /m_i = d^2\mathbf{r}_i \, /dt^2$$

Integrating with respect to time t,

$$(\mathbf{F}_i \, /m_i)t + c_1 = d\mathbf{r}_i \, /dt$$

where c_1 is a constant. Since $\mathbf{a}_i = \mathbf{F}_i \, /m_i$, this equation can be rewritten as:

$$d\mathbf{r}_i \, /dt = \mathbf{a}_i \, t + c_1$$

When $t = 0$, the velocity $d\mathbf{r}_i \, /dt$ is given by c_1. Further integration with respect to

time gives:

$$\mathbf{r}_i = \tfrac{1}{2} \, \mathbf{a}_i \, t^2 + c_1 \, t + c_2 \qquad \text{....................} \; ①$$

where c_2 is the current position of the atom.

So far no account has been taken of the thermal motion of the atoms. The

temperature T of the system can be calculated from the mean kinetic energies of all

the atoms in the system:

$$(3N/2) \, k_B T = \sum_{i=1}^{N} \tfrac{1}{2} \, m_i v_i^2$$

where k_B is the Boltzmann's constant, m_i and v_i are the mass and velocity of atom i respectively. N is the total number of atoms ($3N$ being the number of degrees of freedom of the system). The system is heated by randomly assigning initial velocities (c_1) to all atoms according to a Maxwellian distribution for the given temperature (Berendsen, 1984). Once the initial velocities have been assigned, the molecular dynamics simulation is self-perpetuating; acceleration of an atom i can be calculated from the forces according to the potential used:

$$a_i = F_i / m_i = (dE_i / dr_i)/m_i$$

Therefore, equation ① allows calculation of the future position or displacement r_i of an atom at time t from its initial velocity c_1.

3.21 Potential Energy Terms

To perform calculations on every single atom in a large molecule will require extremely long computing times, even using modern-day supercomputers. A set of *potential energy functions* have been developed to simplify the calculations. Briefly, these functions consist of potential energy terms describing bonding and non-bonding interactions between nuclei (Flores and Moss, 1991). From this, the potential energy E of a molecule can be described as a complex function of Cartesian coordinates of all its atoms being studied, i.e., $E = E(r_1, r_2, r_3 \ldots\ldots r_N)$ from which the potential energy function, E_{total} is derived. E_{total} consists of a number of terms:

$$E_{total} = E_{bonds} + E_{angles} + E_{improper} + E_{repel} + E_{NOE} + E_{cdih}$$

The first four empirical energy terms describe physical interactions between atoms.

Bonded interactions are defined by the E_{bonds}, E_{angles} and $E_{improper}$ terms which keep

bond lengths (b), bond angles (θ) and dihedral angles (ϕ) at their equilibrium values

respectively. In addition, $E_{improper}$ serves to maintain planarity and chirality, i.e.,

peptide bonds are considered *trans* planar while aromatic rings are considered

planar. These terms are either harmonic or sinusoidal and are summarised as

follows:

$$E_{bonds} = \sum_{bonds} \tfrac{1}{2} K_b (b-b_0)^2$$

$$E_{angles} = \sum_{angles} \tfrac{1}{2} K_\theta (\theta-\theta_0)^2$$

$$E_{improper} = \sum_{improper} K_\phi [1+ \cos n\phi]$$

K_b, K_θ and K_ϕ are force constants which are employed as weighting factors that can

be varied during the course of the experiment. b_0 and θ_0 are the equilibrum bond

lengths and angles respectively and n is the periodicity of the rotation.

Non-bonded interactions are represented by the van der Waals repulsion term E_{repel}:

$$E_{repel} = \begin{cases} 0 & \text{if } r \geq r_{min} \\ K_{repel} (r^2_{min} - r^2)^2 & \text{if } r < r_{min} \end{cases}$$

where K_{repel} is the van der Waals repulsion force constant and r_{min} is the sum of the

van der Waals radii between a pair of nuclei.

The last two terms, E_{NOE} and E_{cdih} do not correspond to any real physical force but

are a means of including NMR information. Both terms allow for the introduction

of additional inter-proton distance and angular restraints during computation. E_{NOE} contains NOESY restraints and has the effect of restraining proton pairs that exhibit NOE interactions to their respective coordinates r_i and r_j. As a consequence, their measured inter-proton distance r_{ij} would be restrained to a specific distance during computation. These potentials are pseudo-square-well potentials and are defined as follows:

$$
\mathbf{E}_{NOE} = \begin{cases} K_{NOE}(r_{ij} - r^u{}_{ij})^2 & \text{if } r_{ij} > r^u{}_{ij} \\ 0 & \text{if } r^l{}_{ij} \leq r_{ij} \leq r^u{}_{ij} \\ K_{NOE}(r_{ij} - r^l{}_{ij})^2 & \text{if } r_{ij} < r^l{}_{ij} \end{cases}
$$

where $r^u{}_{ij}$ and $r^l{}_{ij}$ are the upper and lower limits of the target distances respectively and K_{NOE} is the NOE force constant. $r^l{}_{ij}$ is typically set to 1.79Å, the sum of the van der Waals radii of two protons.

E_{cdih} contains ^3J coupling information restraints based on, for example, high-resolution 1D ^1H spectra and has the effect of restraining ϕ dihedral angles, e.g., -60 $\pm$ 30° for ^3J < 5 Hz. Similarly, dihedral angle restraints can be incorporated into pseudo-square-well potentials of the form:

$$
\mathbf{E}_{cdih} = \begin{cases} K_{cdih}(\phi_i - \phi^u{}_i)^2 & \text{if } \phi_i > \phi^u{}_i \\ 0 & \text{if } \phi^l{}_i \leq \phi_i \leq \phi^u{}_i \\ K_{cdih}(\phi_i - \phi^l{}_i)^2 & \text{if } \phi_i < \phi^l{}_i \end{cases}
$$

where $\phi^u{}_i$ and $\phi^l{}_i$ are the upper and lower limits/bounds of the dihedral angle restraints, ϕ_i is its calculated value and K_{cdih} is the torsion force constant.

The essence of *restrained molecular dynamics* (RMD) has been described in reasonable detail. The term 'restrained' is used because NMR angular and distance

constraints are incorporated during MD calculations. An energy minimisation procedure that produces more 'realistic' 3D structures after MD calculations is described in the next section.

3.22 Simulated Annealing

The way the energy of a molecule varies with small changes in its structure is specified by its *potential energy surface* (PES). A PES is basically a mathematical relationship that links molecular structure to the corresponding potential energy. The PES can be used to illustrate the relative stabilities of different, but possible structures a molecule can adopt (Foresman and Frisch, 1993). The PES of any system consists of many dimensions but can be schematically represented in three dimensions as shown in Fig. 3.19. A typical PES contains several *local* potential minima but only one true *global* minimum.
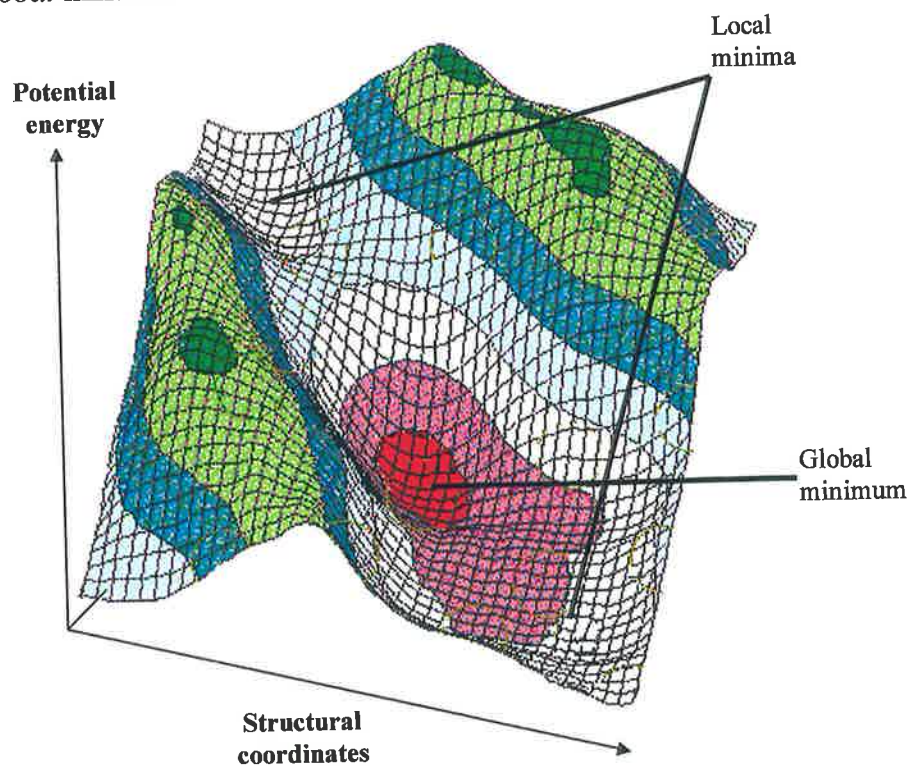
Fig. 3.19 Schematic representation of a hypothetical PES showing local minima and the global minimum.

Calculated structures based entirely on RMD may not be entirely accurate as their potential energies may represent those existing as local minima rather than the global minimum. As a consequence, these calculated structures may not correspond to the most stable conformation and may be quite different to that of the global minimum.

To circumvent this problem, simulated annealing (SA) is introduced after RMD calculations in order to locate the global minimum (Nilges *et al.*, 1988a, 1988b and 1991) This involves simulating the introduction of kinetic energy to the molecule by raising the temperature of the system (typically to 2000 K) followed by slow cooling (to 100 K). This enables any molecule that is initially 'trapped' in a local minima to 'jump out' and reach the global minimum (shown schematically in Fig. 3.20).
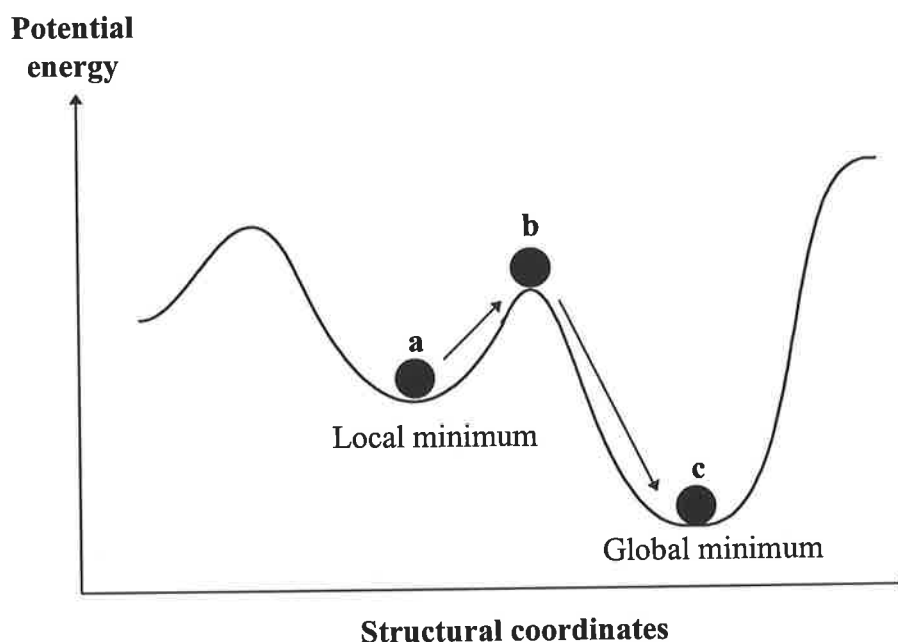
Fig. 3.20 **Schematic diagram showing a molecule [represented by the black circle (a)] trapped in a local minimum. Introduction of kinetic energy enables the molecule to 'jump' out of the local minimum (b) into the global minimum (c).**

3.23 Calculation Protocol

The typical procedure of obtaining structures consistent with the NMR data constraints involves generating an ensemble of structures with random conformations using known experimental geometries (e.g. bond lengths and angles) but with random dihedral angles (Nilges *et al.*, 1988a). Such structures are usually incompatible with most of the NMR data. The next step involves introducing inter-proton distance and ϕ dihedral angle restraints based on NOE intensities and coupling constants respectively before subjecting them to RMD and SA calculations. A flow chart showing the computational strategy is shown in Fig. 3.21.

```
              Random structures

              NOESY and φ
              angle restraints

              Restrained Molecular Dynamics

              Simulated Annealing

    No        Convergence ?

                        Yes

              Final Structures
```
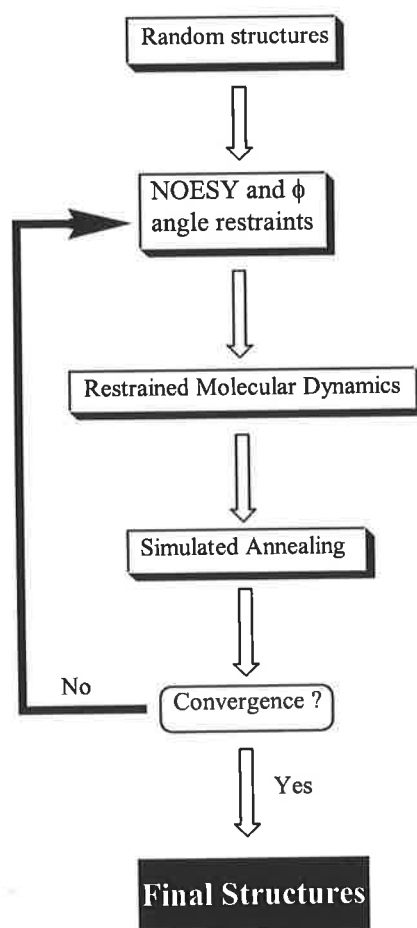
Fig. 3.21 Calculation strategy used to solve 3D structures.

3.24 Floating Stereospecific Assignments

In the past where cases of distinguishable but unassignable resonances of methylene ($-CH_2-$) and isopropyl groups [$-CH(CH_3)_2$] were observed, distance constraints were measured relative to a *pseudoatom*, located centrally with respect to these protons (Wüthrich, 1983). An appropriate *correction term* was added to allow for the maximum possible error since experimental NOEs involve protons rather than the pseudoatom. This results in the loss of valuable NOE information. The *floating stereospecific assignment* method was developed to circumvent such problems (Folmer *et al.*, 1997). Instead of using pseudoatoms, NOEs are measured for both individual resonances of a methylene or isopropyl group which are arbitrarily assigned (i.e., simply denoted $H_{\beta 2}$ and $H_{\beta 3}$ in the case of a β-methylene group). Force constants (e.g. K_θ and K_ϕ) used to enforce a defined chirality at the prochiral centre are initially reduced to allow stereo-related nuclei or methyl groups to 'float' between the *pro*-R and *pro*-S configurations to find the energetically most favourable conformation. These are slowly increased during the course of RMD/SA calculations. The final positions of the respective protons will denote the correct stereospecific assignment. The advantage of such an approach is that no correction factors have to be introduced and therefore no NOE information is lost (Weber *et al.*, 1988; Holak *et al.*, 1989).

3.25 Quality of Generated Structures

How is it determined whether a particular generated structure is 'realistic' and comparable to the final ensemble of generated structures? The conventional way to

gauge this is by calculating the root-mean-square deviation (RMSD) of a selection of structures (typically twenty of the lowest energy structures are chosen). This value is generated by superimposing the centroids of the chosen structures and then calculating an 'average structure' that represents the overall ensemble:

$$\text{RMSD} = [(1/N) \sum_{i=1}^{N} (r_i - r'_i)^2]^{\frac{1}{2}}$$

where N is the number of atoms being compared, r_i and r'_i are the atomic co-ordinates for the respective calculated and average structures respectively. Generally, a RMSD of less than 2.0 Å indicates that the calculated structures are structurally similar and close to the calculated 'average structure'. If the RMSD is too large, then it is necessary to re-analyse the NMR spectra. Large proteins typically show RMSD of the order of 1.5 Å for all atoms in the molecule (Evans, 1995).

3.26 Angular Order Parameters

The angular order parameter (S) is a statistical parameter used to describe how well-defined dihedral angles (ϕ and ψ) of a peptide are over a family of structures. For example, the value of S for the dihedral angles, α_I, of residue number i (where $\alpha = \phi$ or ψ) is defined as:

$$S = 1/N \left| \sum_{j=1}^{N} \alpha_i{}^j \right|$$

where N is the total number of structures, j represents the number of the calculated structures ($j = 1, 2, ... N$) and $\alpha_i{}^j$ is a 2D unit vector with phase equal to the dihedral angle α_i. The relation of S to the standard deviation of the dihedral angles (σ) is given by:

$$1 + 0.5 \log S = \cos (\sigma/2)$$

and is graphically represented in Fig. 3.22 (Hyberts et $al.$, 1992). If the dihedral angles are the same for all the structures, then S will have a value of 1.00. A value of $S = 0.9$ corresponds to a σ of $\pm 24°$ while a value of $S = 0.99$ corresponds to a σ of $\pm 8°$. A value of 0.01 indicates a totally disordered structure.
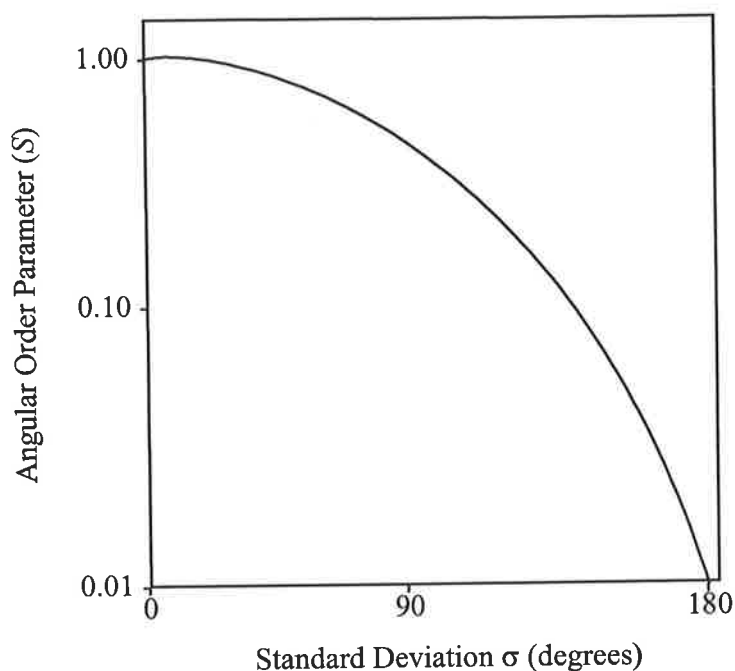
Fig. 3.22 Plot of angular order parameter (S) vs. standard deviation (σ).

Why is the use of S favoured over the more conventional standard deviation? The reason is because S is easier to calculate and it gives a better 'mental picture' when

describing the precision of dihedral angles of a particular structure. It clearly defines the two limits: a totally well-defined dihedral angle ($S=1$) and a completely random distribution ($S=0$). In contrast, the standard deviation is undefined for a completely random distribution (Pallagy *et al.*, 1993).

3.27 Ramachandran Plots

Most combinations of ϕ and ψ angles do not occur as they lead to unfavourable steric interactions between atoms of adjacent residues. This reduces the number of possible conformations a peptide can adopt. Possible combinations of ϕ and ψ angles that do not lead to clashes can be plotted on a conformation map known as a *Ramachandran plot* (Fig. 3.23) (Ramachandran *et al.*, 1963; Ramachandran and Sassiekharan, 1968; Zubay, 1986). The plot is divided into shaded regions which indicate if a particular (non-proline) residue adopts a particular secondary structure. These regions are basically population density plots produced from known experimental ϕ and ψ angles as determined from the analysis of 121,870 non-glycine residues obtained from 463 protein structures available from the Brookhaven databank (Morris *et al.*, 1992). Shaded regions labelled A, B and L represent *'favoured'* combinations of ϕ and ψ angles corresponding to dihedral angles found in α-helices, β-sheets and left-handed α-helices respectively. Shaded regions labelled a, b and l represent *'allowed'* ϕ and ψ combinations while regions labelled ~a, ~b and ~l represent *'generous'* ϕ and ψ combinations. Unshaded regions represent disallowed combinations. Proline and glycine residues were omitted from the study because of their atypical dihedral angle distribution. Glycine residues are roughly

symmetrical around the centre of the Ramachandran plot due to the ability of glycine

to adopt both right-handed and left-handed versions of any allowed conformation.

Values of ϕ and ψ angles for each residue (with the exception of glycine and proline)

can be obtained from an ensemble of calculated structures and plotted to check for

dihedral angle abnormalities. This method provides another way to assess the degree

of 'correctness' of calculated structures.

Legend:		
α-helix	β-sheet	
■	■	favoured
■	■	allowed
▓	▓	generous
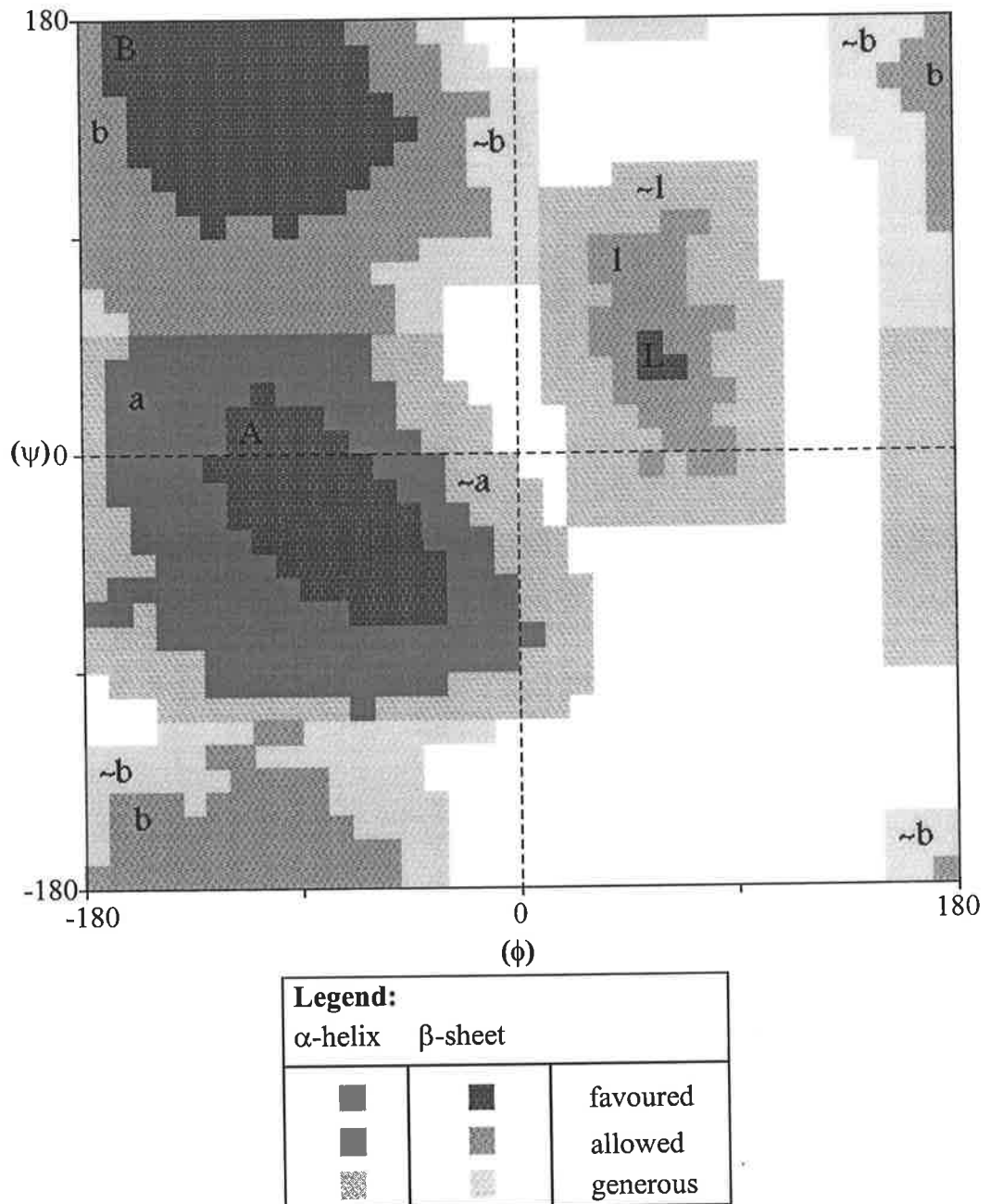
Fig. 3.23 A Ramachandran plot. (Diagram modified from Richardson, 1981).

3.28 Membrane-Mimetic Media

To determine 3D conformations of membrane-disrupting peptides, it is necessary to conduct structural studies using suitable membrane-mimicking solvents or phospholipids. Studies have shown that 2,2,2-trifluoroethanol (TFE, Fig 3.24) is a good candidate because it promotes intra-molecular hydrogen bonding in regions of a peptide with α-helical propensity but does not induce structures in regions lacking structural tendency (Goodman *et al.*, 1971; Marion *et al.*, 1988; Bruch and Gierasch, 1990; Blanco *et al*, 1994; Gesell *et al*, 1997). Thus, TFE is not a helix-inducing solvent, i.e., it will not induce helix formation independently of the sequence. It is rather a *helix enhancing solvent* which stabilises helices in peptides with helical propensity (Dyson *et al.*, 1992; Sönnichsen *et al.*, 1992). Previously, it has been shown that glucagon analogs adopt similar conformations in TFE/water mixtures and in phospholipid micelles, suggesting that TFE/water mixtures are suitable membrane mimicking solvents (Braun *et al.*, 1983; Clore *et al.*, 1986).

TFE possesses several properties responsible for its unique helix stabilising capabilities. Firstly, its dielectric constant is only about a third of that of water, enhancing electrostatic interactions between charged groups of the peptide (Llinas and Klein, 1975; Rajan and Balaram, 1996). Secondly, TFE strengthens intra-molecular hydrogen bonding in a peptide as it is a significantly weaker base (poorer proton acceptor) than water (TFE pKa $\approx$ 12.4 vs. $\approx$ 15.7 for water) (Nelson and Kallenbach, 1986). This reduces the amount of water molecules around the peptide. As a consequence, intra-molecular hydrogen bonds between

amide protons and carbonyl oxygen atoms in the peptide remain unperturbed, stabilising the overall secondary structure (Berliner and Reuben, 1980; Storrs *et al.*, 1992; Brooks and Nilsson, 1993; Cammers-Goodwin *et al.*, 1996). Based on these factors, peptides with significant helical propensity (amphipathic peptides in particular) often adopt helical structures in 30-50% (by vol.) TFE/water mixtures (Lehrman *et al.*, 1990; Zhou *et al.*, 1990). However, the use of TFE as a membrane-mimetic is still a subject of contention

Detergent micelles such as sodium dodecyl sulphate (SDS), dodecylphosphocholine (DPC), 1,2-dihexanoyl-sn-glycero-3-phosphocholine (DHPC) and 1,2-dimyristoyl-sn-glycero-3-phosphocholine (DMPC) (Fig. 3.24) are now commonly utilised as membrane-mimetics to study peptide-membrane interactions (Brown and Wüthrich, 1977; Lauterwein *et al.*, 1979; Brown and Wüthrich, 1981; Brown *et al.*, 1982; Kaiser and Kezdy, 1983; Kaiser and Kezdy, 1984; Deber and Li, 1995; Blondelle *et al.*, 1997).
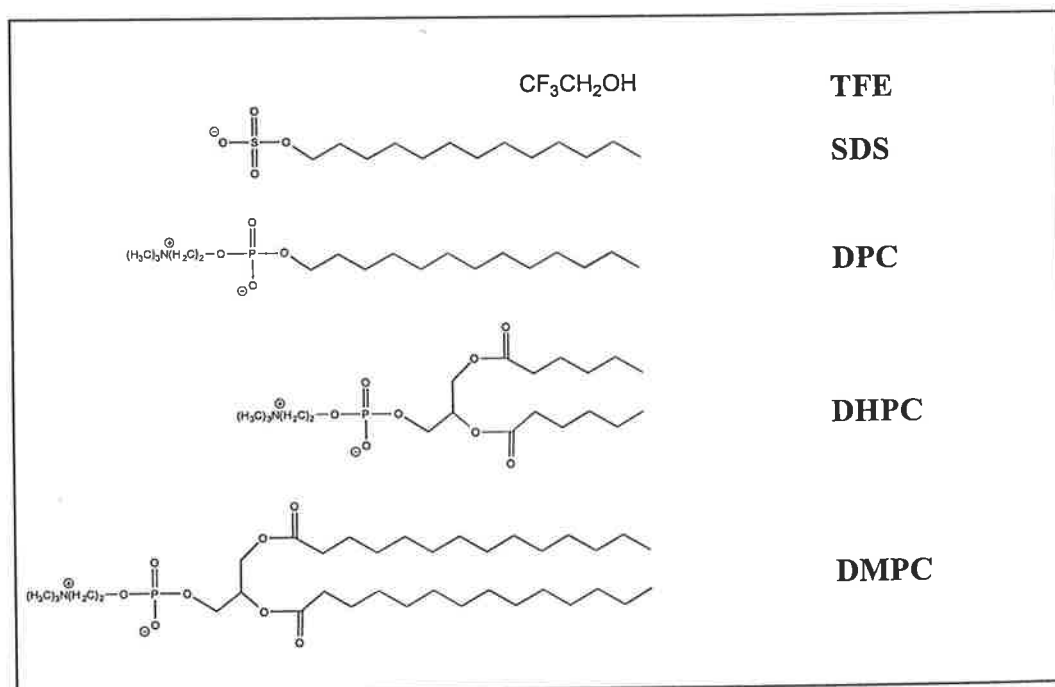
Fig. 3.24 Structures of TFE, SDS, DPC, DHPC and DMPC.

Detergent micelles are generally considered to provide a more 'realistic' membrane-mimetic environment for structural studies compared to TFE. The structure-inducing driving forces in isotropic solvents such as TFE and the natural, non-isotropic membrane-peptide interface are generally different. For example, TFE can weaken non-local hydrophobic interactions and favour local polar interactions such as the intra-molecular hydrogen bonding in peptides (Shiraki *et al.*, 1995). In artificial lipid membranes, the hydrophobic interactions between amino acid sidechains and lipid alkyl chains have been suggested to be the primary forces driving secondary structure formation. (Blondelle *et al.*, 1997). As a result of different driving forces, the solution structure of membrane-lytic peptides may be quite different. In the following chapters, TFE and the above mentioned phospholipids will be used as membrane mimetics. In particular, Chapter 5 will compare how TFE and DPC micelles influence the solution structure of the membrane-disrupting peptide maculatin 1.1.

Chapter 4
Orientation
Studies
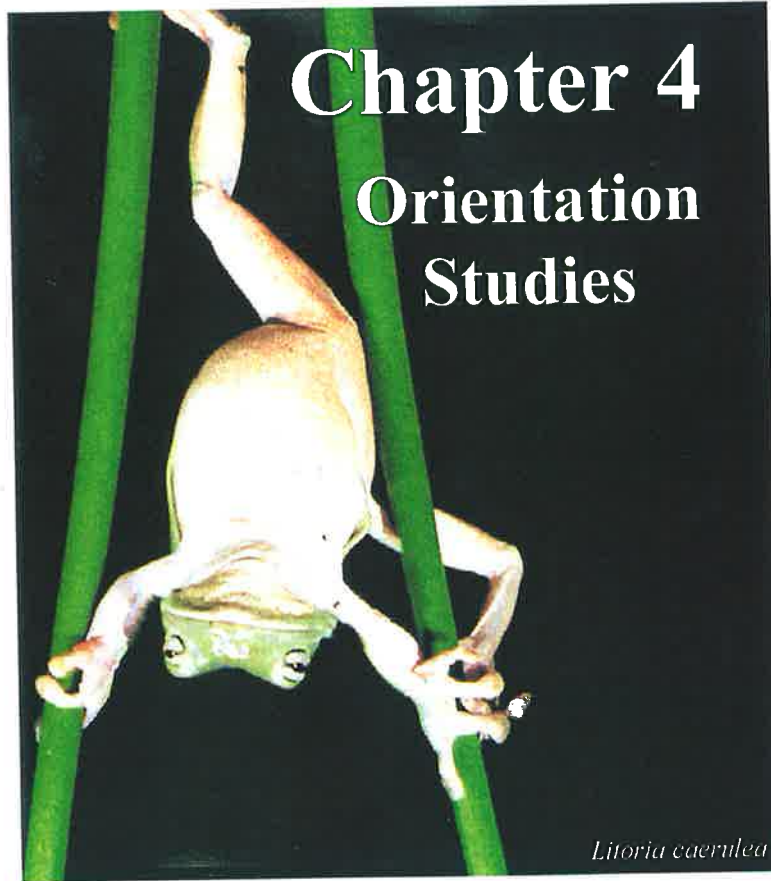
Litoria caerulea

4.1 Solid-State NMR Spectroscopy

Solid-state NMR spectroscopy is fast becoming one of the methods for examining the structure and function of biological systems. In particular, it is extremely useful in studies involving membrane-associated peptides and proteins (Opella, 1997; Marassi and Opella, 1998). Both solid-state and solution NMR spectroscopy provide complementary windows on molecular information because the effects of rapid molecular reorientation present in solution are absent in the relatively immobile samples accessible to solid-state NMR methods (Opella *et al.*, 1997). This chapter describes how solid-state NMR spectroscopy is employed to study the orientation and topology of antibiotic peptides when associated with lipid bilayers in an effort to shed light into their membrane-lytic mechanisms.

4.2 The Origin of Chemical Shifts and Powder Patterns

When a nucleus ($I \neq 0$) is introduced to an external magnetic field $\mathbf{B_0}$, the moving electric charges of the surrounding electron cloud induce a local magnetic field which opposes $\mathbf{B_0}$. The effective field experienced by the nucleus will become:

$$\mathbf{B_{effective}} = \mathbf{B_0} - (\sigma)\mathbf{B_0}$$

The nucleus is said to be 'shielded' and the extent of shielding is given by the *shielding constant*, also known as the *chemical shift tensor* (σ). σ consists of three principal components: σ_{11}, σ_{22} and σ_{33}. These *principal elements* are basically vectors used to characterise the 3D nature of shielding experienced by the nucleus

and are prerequisites for the interpretation of spectral features. The chemical shift tensor of the ^{15}N nucleus of a peptide bond has been determined (Mehring, 1983; Wu et al., 1995). Fig. 4.1 illustrates the principal elements relative to the orientation of the N-H peptide bond and $\mathbf{B_0}$.
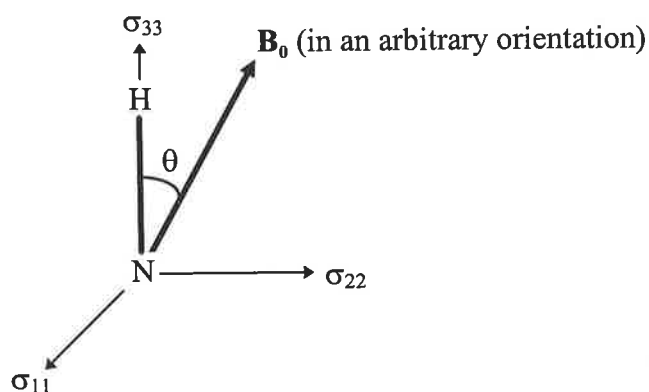
Fig. 4.1 The principal elements used to relate the orientation of the N-H peptide bond relative to $\mathbf{B_0}$ (not drawn to scale).
Diagram modified from Evans (1995).

In the solution-state, the principal elements are averaged out due to rapid molecular tumbling and only the isotropic shift tensor (σ_{iso}) is observed:

$$\sigma_{iso} = 1/3 \ (\sigma_{11} + \sigma_{22} + \sigma_{33})$$

Hence, only a single, averaged peak is observed for each respective nucleus in the molecule. In solids or immobile systems, however, molecular motion is severely restricted so little averaging occurs. Therefore, the observed chemical shift ($\sigma_{observed}$) for a nucleus is described as the sum of its isotropic and anisotropic parts:

$$\sigma_{observed} = \sigma_{iso} + \sigma_{aniso}$$

where σ_{aniso}, the chemical shift anisotropy, is an orientation-dependent parameter.

Thus, each nucleus with a unique orientation with respect to B_0 will give rise to a particular resonance frequency. In immobile powders, the nucleus of interest (e.g., ^{15}N) will have totally random orientations with respect to B_0. This results in the formation of a broad, continuum of peaks known as a *powder pattern*. The shape of a powder pattern depends on the magnitude of the principal elements involved. When two of the principal shielding elements are identical, we obtain an axially symmetric powder pattern like that shown in Fig. 4.2.
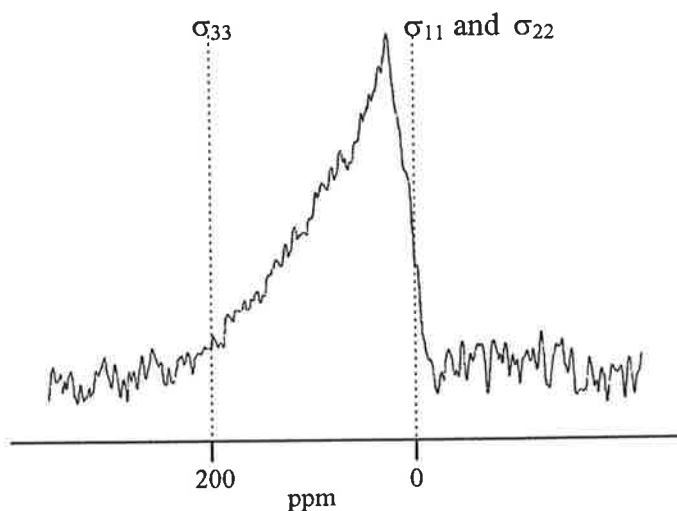
Fig. 4.2 ^{15}N (**^{1}H decoupled) NMR powder pattern of randomly oriented ^{15}N-Ala15 labelled magainin 2.** (Diagram modified from Bechinger *et al.*, 1992).

When the N-H bond axis is parallel to B_0, the ^{15}N resonance appears downfield near the principal element σ_{33}. If the N-H bonds are perpendicular to B_0, this results in upfield resonances close to that of the principal elements σ_{11} and σ_{22}. It is the observation of resonance frequencies near either extremes of the powder pattern which allows for the qualitative determination of peptide orientations in uniaxially aligned phospholipid bilayers with respect to B_0 (Teng and Cross, 1989; Bechinger *et al.*, 1991).

4.3 Mechanical Orientation of Phospholipid Bilayers

Phospholipid bilayers can be oriented by shear mechanical forces when multi-lamellar vesicles are sandwiched between two plates. Geometric considerations suggest that the use of large glass microscope coverslips results in optimal bilayer alignment since edge effects are minimised (de Vries and Berendsen, 1969; Moll and Cross, 1990; Ketchum *et al.*, 1993; Grobner *et al.*, 1997; Marassi *et al.*, 1997). Experiments have shown that the bilayers are large 'onion-shaped' structures separated by 10-30 Å thickness of water (Fig. 4.3a) (Rand and Parsegian, 1989; Cevc, 1990; Sanders *et al.*, 1994). When a phospholipid bilayer is oriented with its axes of symmetry parallel (or perpendicular) to B_0, a single resonance peak will be observed as shown in Fig. 4.3b.
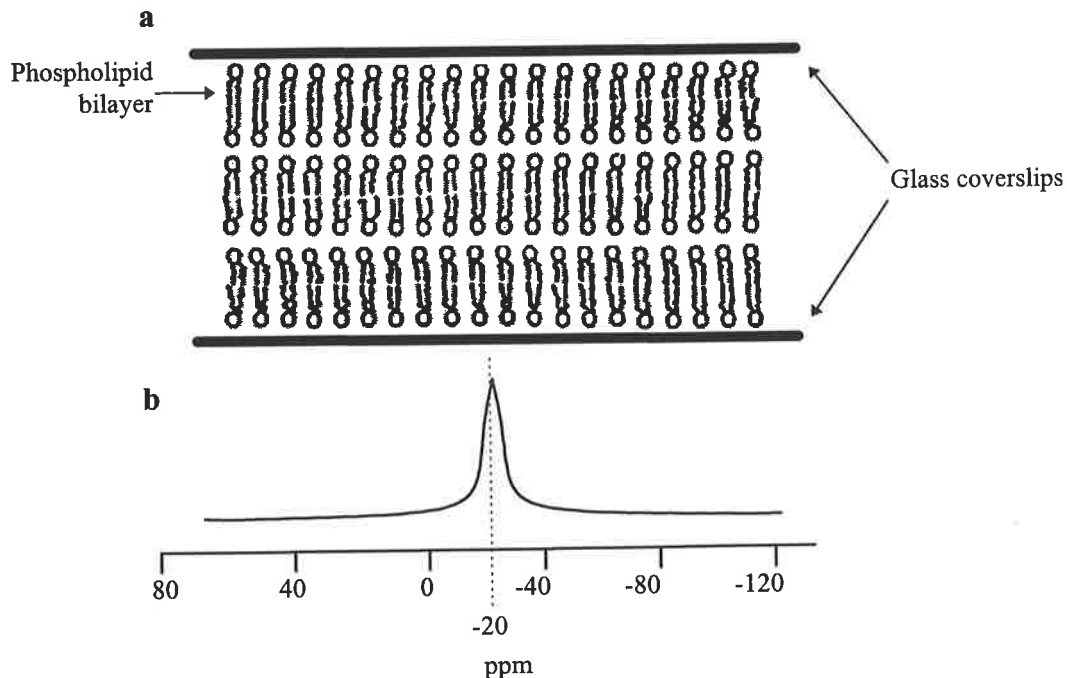
Fig. 4.3 Schematic representations of (a) oriented bilayers formed by mechanical alignment of lipids between glass plates, (b) ^{31}P NMR spectrum of uniaxially oriented phospholipid bilayers between glass plates oriented with bilayer normal perpendicular to B_0.

4.4 Peptide Orientation in Phospholipid Bilayers

The orientation of a peptide incorporated into a lipid bilayer can be deduced from solid-state NMR using ^{15}N-labelled peptides. In these experiments, the chemical shift of the ^{15}N peptide amide resonance reflects the orientation of the labelled ^{15}N-H peptide bond relative to the bilayer normal and $\mathbf{B_0}$. Since the amide N-H bond of an α-helix is aligned approximately along its length (Fig. 3.16), it is possible to deduce the general orientation of the helical peptide with respect to the lipid bilayer surface. For example, if the N-H bond is found to be oriented parallel to $\mathbf{B_0}$, it would indicate that the peptide is oriented with the α-helical axis parallel to $\mathbf{B_0}$. Fig. 4.4a shows a simulation of the ^{15}N powder pattern of ^{15}N-Ala15 labelled magainin 2 while Fig. 4.4b shows the spectrum of an aligned sample oriented with the bilayer normal parallel to $\mathbf{B_0}$. The former gives a single resonance near the σ_{11} and σ_{22} edge, indicating that the N-H amide bond of Ala15 (and those of other residues in the peptide) are oriented approximately perpendicular to the bilayer normal. This suggests that magainin 2 adopts the carpet mechanism (shown schematically in Fig. 4.4c). In contrast, the resonance of ^{15}N-Ala15 labelled melittin (aligned in a phospholipid bilayer) appears near σ_{33}, therefore, the N-H bond of Ala15 is oriented approximately parallel to the bilayer normal (Fig. 4.4d and 4.4e). This suggests that melittin forms transmembrane pores *via* the channel mechanism (Fig. 4.4f) as discussed in Chapter 2. Note that for simplicity, Fig. 4.4c and 4.4f illustrate only one peptide to represent the relative orientation. In reality, the peptides are most likely to be associated as oligomers, with each peptide having a similar orientation.

a

σ_{33} σ_{11} and σ_{22}

b

200   0

ppm

d

σ_{33} σ_{11} and σ_{22}

e

200   0

ppm

B_0

c

f

B_0
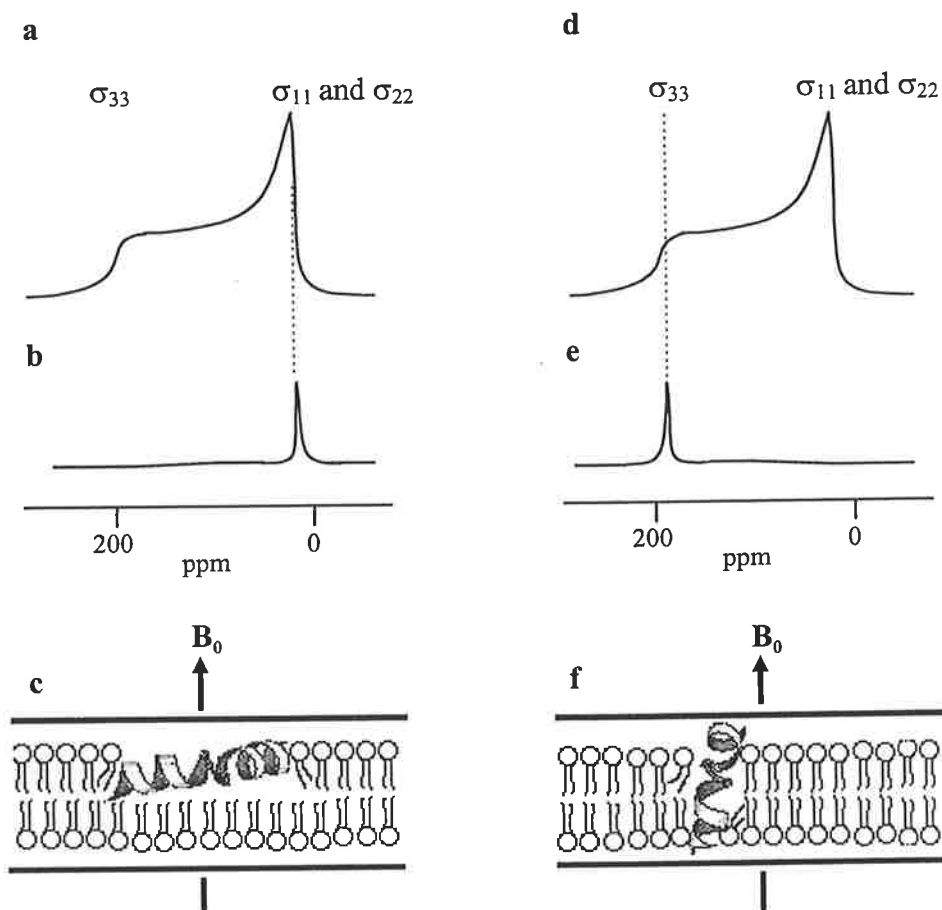
Fig. 4.4 Schematic ^{15}N solid-state NMR spectra of ^{15}N-Ala15 labelled peptides: (a) powder pattern of magainin (b) magainin in oriented phospholipid bilayers (c) orientation of magainin in a phospholipid bilayer (d) powder pattern of melittin (e) melittin in oriented phospholipid bilayers (f) orientation of melittin in a phospholipid bilayer. (Diagrams not drawn to scale).

Hence, by using ^{15}N labels, the orientation of membrane-interacting peptides relative to the bilayer can be determined using solid-state NMR. Peptide-lipid interactions can further be investigated using deuterium NMR and this will be discussed in the next section.

4.5 Deuterium Quadrupolar Splittings

Deuterium (^{2}H) quadrupolar splittings reflect the dynamic and orientational order of deuterated molecules including membrane phospholipids. Since ^{2}H has $I = 1$, a doublet is observed for each ^{2}H resonance in the sample. For deuterated phospholipids, the magnitude of the splitting ($\Delta\nu_Q$) is dependent on the average orientation of the C-^{2}H vector with respect to $\mathbf{B_0}$ and can be defined by the equation:

$$<\Delta\nu_Q> = Q <\mathbf{S}_{CD}(n)>$$

where $< >$ represent the time average of molecular conformations and orientations on the NMR timescale, Q is the quadrupolar coupling constant (typically 170 kHz for C-^{2}H bonds) and $\mathbf{S}_{CD}$ is the orientational order parameter and is defined as:

$$\mathbf{S}_{CD}(n) = \tfrac{1}{2} <3\cos^2\theta_n - 1>$$

where θ_n is the angle between the for C-^{2}H bond for the (n)th carbon position and the axis of symmetry of the lipid acyl chain (Seelig and Niederberger, 1973; Davies, 1983).

When a peptide penetrates a phospholipid bilayer, the lipid chains become more disordered and mobile, causing a decrease in $<\mathbf{S}_{CD}(n)>$. This decreases the magnitude of deuterium splitting and results in the narrowing of the ^{2}H powder pattern. Fig. 4.5 illustrates the decrease in ^{2}H order parameter of DMPC-^{2}H$_{54}$ bilayers after the addition of magainin. The broad wings with the largest splitting arise from the relatively immobile methylene doublets near the hydrocarbon-water interface.

The less intense doublets with smaller splittings result from the stepwise decrease in order parameter occurring near the terminal portion of the lipid chain. The relatively mobile terminal methyl groups give rise to an intense doublet with the smallest splitting (Seelig and Niederberger, 1973; Howard and Opella, 1996).
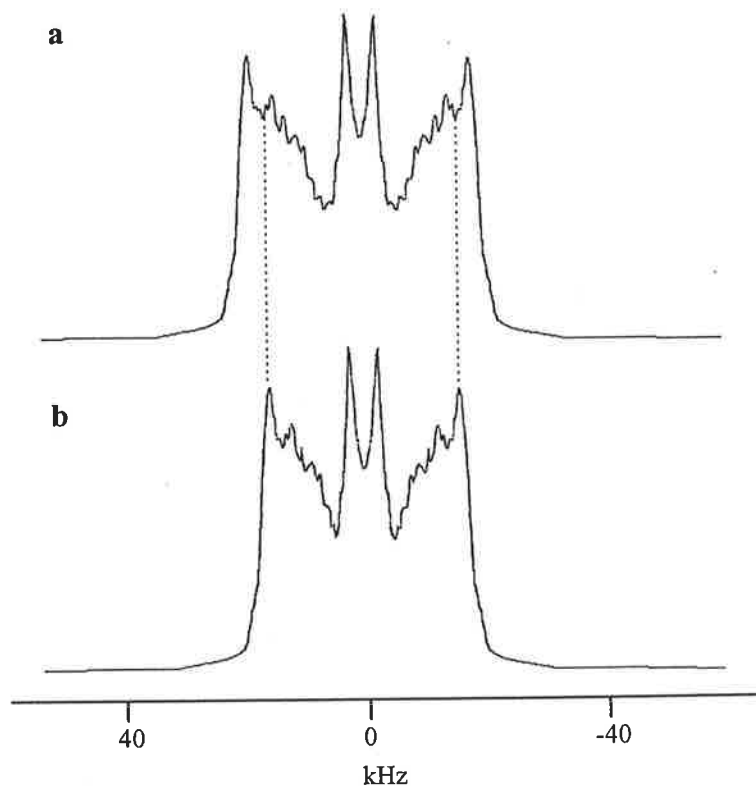
Fig. 4.5 ^{2}H NMR spectra of DMPC bilayer (a) without magainin (b) after adding magainin. (Diagram modified from Bechinger *et al.*, 1992).

4.6 Chapter Summary

This chapter describes how solid-state NMR spectroscopy can be employed to determine the orientation of membrane-disrupting peptides when associated with lipid bilayers, providing valuable insights into their mechanism of action. The next chapter will deal with one such peptide, maculatin 1.1, in greater detail.

Chapter 5

Maculatin 1.1
and
Analogues
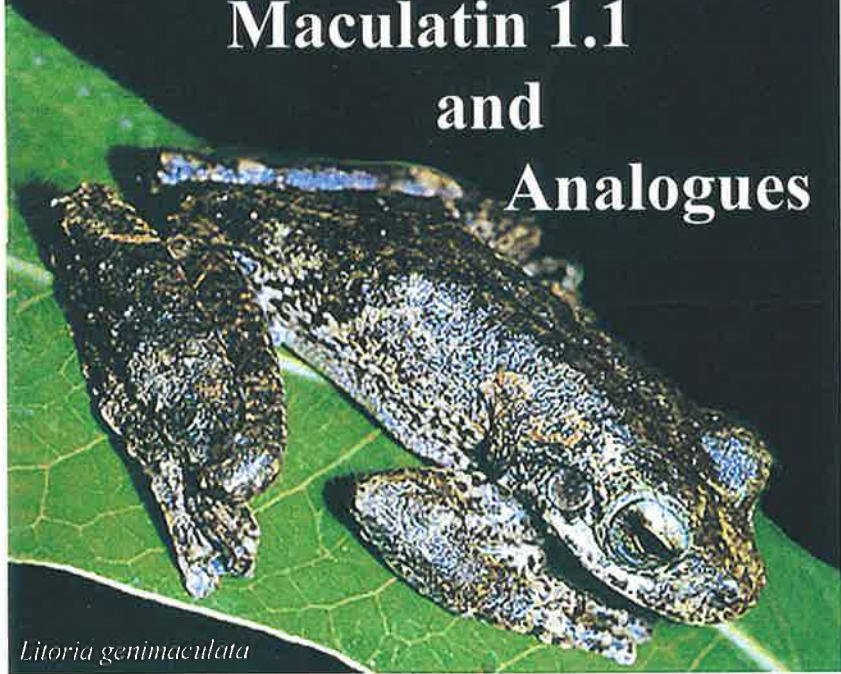
Litoria genimaculata

5.1 Maculatin 1.1 and Analogues

The dermal secretions of Australian tree frogs (*Litoria caerulea, L. chloris, L. ewingi, L. gilleni, L. splendida* and *L. xanthomera*) (see Fig. 1.8) all contain wide-spectrum antimicrobial peptides of the caerin 1 family as discussed in the first chapter. Nine members of the caerin 1 family have been identified to date; the most widespread of these peptides is caerin 1.1 which has the sequence:

GLLSV LGSVA KHVLP HVVPV IAEHL-NH$_2$

2D NMR spectroscopic studies in TFE/water (1:1 vol.:vol.) together with molecular dynamics calculations indicate that caerin 1.1 adopts two well-defined α-helices (Leu2 to Lys11 and Val17 to His23) separated by a hinge region of greater flexibility. Pro15 is an integral part of this region due to the flexibility that this residue imparts because of the absence of a hydrogen bonding NH group (Wong *et al.*, 1997). A computed low-energy conformation of caerin 1.1 is shown in Figure 5.1; this representation shows hydrophilic and hydrophobic zones on opposite sides of the peptide backbone. The amphipathic nature of caerin 1.1 together with the flexibility imparted by the central hinge region allows the basic peptide to interact with a variety of membrane surfaces, resulting in its wide-spectrum antibiotic activity.
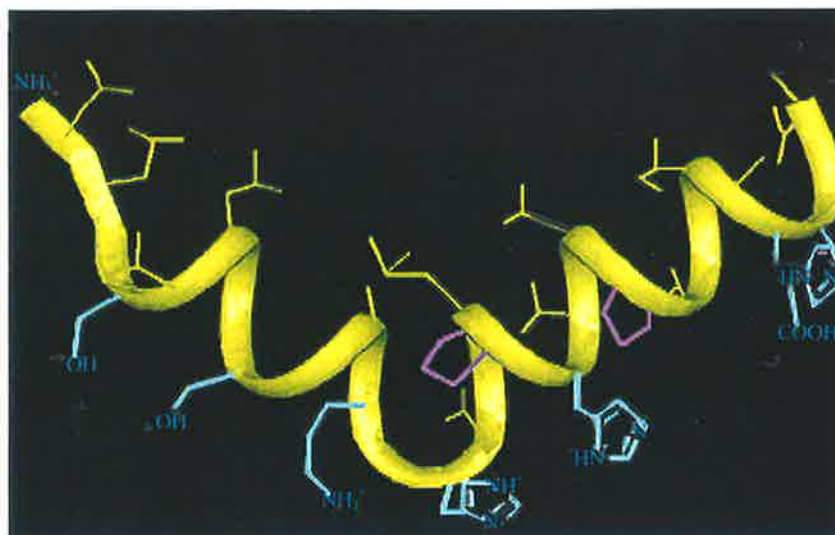
Fig. 5.1 A low-energy structure of caerin 1.1. The marked amphipathic nature of the helical peptide is apparent from this representation with the hydrophobic side above and hydrophilic side below the polypeptide backbone, which is represented by the ribbon. Hydrophilic groups are shown in blue. The proline pyrrolidine ring is coloured purple.

Recently, another antimicrobial peptide, maculatin 1.1, was isolated from the Australian tree frog *Litoria genimaculata* (Rozek *et al.*, 1998). These frogs are found in the coastal rainforests of northern Queensland and New Guinea and typically grow up to 5cm in length (Barker *et al.*, 1995) (Fig. 5.2). Maculatin 1.1 has the primary structure:

GLFGV LAKVA AHVVP AIAEH F-NH$_2$

It is apparent from this sequence that maculatin 1.1 shares significant sequence similarity to caerin 1.1 except that in the former, four of the central residues (His12 to Pro15 of caerin 1.1) are missing, including the central proline residue within the hinge region in caerin 1.1. It is therefore conceivable that the solution structure of maculatin 1.1 is different from that of caerin 1.1, possibly *via* adoption of a more

rigid helix along its entire length. Interestingly, both caerin 1.1 and maculatin 1.1 are subjected to proteolytic cleavage which removes the first two residues of each peptide after it has been on the skin for about five to ten minutes. As a result, the bioactivity of the peptide is destroyed (Steinborner *et al.*, 1997a; Steinborner *et al.*, 1997b).
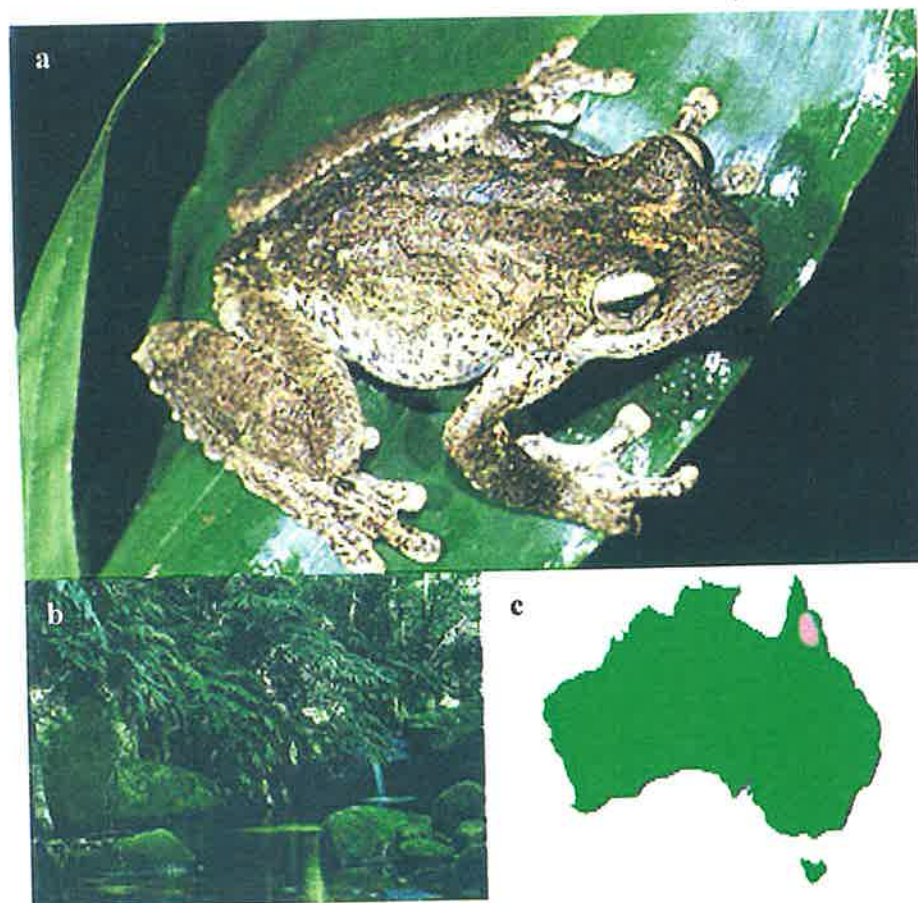
Fig. 5.2 (a) *Litoria genimaculata* **(b) a rainforest in northern Queensland (c) geographical distribution of the frog (coloured pink).**

Although shorter in length than caerin 1.1 and lacking a Pro15 of caerin 1.1, maculatin 1.1 has been shown to possess similar broad-spectrum antibiotic activities against a range of pathogens (Table 5.1). The primary goal of the work presented in this chapter is to obtain insights into the mechanism of action of maculatin 1.1 and

its structure-activity relationship (SAR) when interacting with biological membranes. Towards this goal, a number of synthetically modified analogues have been synthesised in order to evaluate their ability to inhibit the growth of various pathogens:

First, the all *D*-amino acid form of maculatin 1.1 [(*D*) M1.1] was synthesised. All '*D*' amino acids are known to form left handed α-helices as opposed to the right hand α-helices formed by naturally-occurring '*L*' amino acids. Thus, in terms of chiral recognition, an enzyme's active site which has evolved to recognise a right-handed helix will not recognise the same peptide consisting of '*D*' amino acids. If both '*D*' and '*L*' forms are shown to possess identical biological activities, it would indicate that the peptides interact *via* a gross conformational feature (e.g. an amphipathic helix) and not due to some specific feature of the peptide.

Second, many bacteria have negatively charged phospholipid head groups on their membrane surface making them specific to cationic cytolytic peptides as mentioned in chapter 2. If this is true, then increasing the number of negative charges on the peptide will reduce its bioactivity because of a reduction of electrostatic attraction between the peptide and the membrane. This is investigated by synthesising the C-terminal carboxyl (-COOH) form of maculatin 1.1, i.e. without an amidated group (M1.1 acid).

Third, we would like to ascertain the effects of replacing proline with the helix forming residue, alanine, in order to determine if proline is crucial for the

antimicrobial activity of maculatin 1.1. This was investigated by synthesising maculatin 1.1 with Pro15 substituted with an alanine (A15 M1.1). The reason why proline was chosen for replacement is due to its unique properties: proline is an imino acid and thus lacks an amide proton for hydrogen bonding (see Table 3.1). As a consequence, proline cannot participate in hydrogen bonding to proton acceptors such as backbone carbonyl oxygen atoms in the peptide chain. In an α-helix, amide protons of the $i+4$ residue will hydrogen-bond to the carbonyl oxygen of the i residue. Proline will therefore disrupt the hydrogen-bonding pattern of a peptide chain. Also, due to the highly rigid nature of the pyrrolidine ring, proline sterically prevents hydrogen bonding between the amide proton of its $i+1$ neighbour to the carbonyl oxygen in the preceding turn of the helix (Vanhoof *et al.*, 1995). Both consequences allow proline to act as a 'helix breaker': as a result, a flexible hinge or 'kink' will be created in the α-helix (Kuchel and Ralston, 1988).

Lastly, we will investigate how a peptide's helical dipole moment affects the mechanism of bactericidal action. This is done with a synthetic retro maculatin 1.1 [(R) M1.1] where the *L*-amino acid peptide has its primary sequence reversed (i.e., the peptide bond directions are reversed). This has the effect of inducing an equal but opposite helical dipole moment as compared to the natural isomer. If such a dipole moment makes a critical contribution to its bioactivity, then the retro isomer will be expected to lose its activity.

These synthetic analogues and the primary sequences of other natural maculatins (1.1, 1.1.1 and 1.2) (Steinborner *et al.*, 1998) are shown on the next page.

Caerin 1.1	GLLSV LGSVA KHVLP HVVPV IAEHL-NH$_2$
Maculatin 1.1	GLFVG LAKVA AHVVP AIAEH F-NH$_2$
D-Maculatin 1.1	GlfvG lakva ahvvp aiaeh f-NH$_2$
Maculatin 1.1 acid	GLFVG LAKVA AHVVP AIAEH F-OH
Maculatin 1.1.1	FVG LAKVA AHVVP AIAEH F-NH$_2$
Ala15 maculatin 1.1	GLFVG LAKVA AHVVA AIAEH F-NH$_2$
Retro maculatin 1.1	FHEAI APVVH AAVKA LGVFL G-NH$_2$
Maculatin 1.2	GLFVG LAKVA AHNNP AIAEH FQA-NH$_2$

The bioactivities of the above mentioned peptides are listed in Table 5.1.

Table 5.1 **Antimicrobial activities of caerin 1.1, maculatin 1.1 and some synthetic modifications of maculatin 1.1.**

Organism	MIC (µg/mL)							
	C1.1[a]	M1.1[b]	(D) M1.1	M1.1 acid	M1.1.1[b]	A15 M1.1	(R) M1.1	M1.2[b]
Bacillus cereus	50	50	25	>100	>100	>100	>100	>100
Escherichia coli	>100	>100	>100	>100	>100	>100	>100	>100
Leuconostoc lactis	1.5	3	3	50	>100	12	50	>100
Listeria innocua	25	100	100	>100	>100	100	>100	>100
Micrococcus luteus	12	12	12	>100	>100	50	>100	>100
Pasteurella multocida	25	50	25	>100	>100	>100	>100	>100
Staphylococcus aureus [c]	3-12	6-12	12	>100	>100	50-100	>100	50
Staphylococcus epidermidis	12	12	25	>100	>100	100	>100	>100
Streptococcus faecalis	25	25	25	>100	>100	>100	>100	>100
Streptococcus uberis	12	3	6	>100	>100	50	>100	6

[a]The data for caerin 1.1 were taken from Wong et al. (1997).

[b]The data for maculatin 1.1, 1.1.1 and 1.2 were taken from Steinborner et al. (1998).

[c]Tested against two strains (ATCC type strains 25923 and 29213).

Chapter 5

Specific observations which arise from these data are:

(i) the spectrum of activities of caerin 1.1 and maculatin 1.1 is very similar, suggesting that the four central amino acids in caerin 1.1 are not essential for complete activity.

(ii) the antibiotic activities of natural (*L*) maculatin 1.1 and synthetic (*D*) maculatin 1.1 are the same within experimental error (to within one dilution factor), indicating that maculatin 1.1, like caerin 1.1, is a membrane-active antimicrobial peptide, i.e., activity is not dependent on interaction with chiral receptor sites or enzymes (Wong *et al.*, 1997).

(iii) the C-terminal carboxyl analogue of maculatin 1.1 is significantly diminished in activity, suggesting that the mechanism of bactericidal action involves electrostatic peptide-membrane interactions. These data support similar SAR studies of other analogues of natural antimicrobial peptides with their amide groups substituted for carboxyl groups at their C-terminus (Li *et al.*, 1988; Callaway *et al.*, 1993; Mor *et al.*, 1994).

(iv) Substituting the Pro15 residue of maculatin 1.1 with an alanine results in a peptide with greatly reduced bioactivity. This suggests that the central 'kink' in the helix is necessary for antimicrobial activity.

(v) the retro form of maculatin 1.1 is essentially inactive, suggesting that both H_2N-Gly1 and Phe21-$CONH_2$ are necessary for the activity of maculatin 1.1, i.e., the helical dipole moment is involved in the bactericidal mechanism. In contrast, similar studies on retro melittin have shown that it retains its antimicrobial properties (Juvvadi *et al.* 1995). This suggests that the mechanism of bactericidal action of maculatin and melittin could be different.

(vi) maculatin 1.1.1 (which arises from the action of an endogenous endoprotease to remove the first two residues of maculatin 1.1) is essentially inactive (Steinborner *et al.*, 1998) while maculatin 1.2, which has two more residues at its C-terminus than maculatin 1.1, has markedly reduced activity compared to that of maculatin 1.1.

5.2 Structural Studies

Maculatin 1.1 and caerin 1.1 do not display any amphipathic character when presented on a Edmundson helical wheel (Fig 5.3). As a consequence, neither exhibit well-defined hydrophobic and hydrophilic faces. However, the proline residue(s) in the central region of these peptides may orient the C-terminal part of the helix into an appropriate conformation to allow the formation of an amphipathic α-helix. A rotation of approximately $60°$ and $140°$ of the polypeptide chain after Pro15 is required to give such a distribution for maculatin 1.1 and caerin 1.1 respectively (Wong *et al.*, 1997; Chia *et al.*, 2000). Since caerin 1.1 needs to rotate at a greater angle than maculatin 1.1, it may need four additional central residues to enhance its flexibility. This may explain the extra central residues in caerin 1.1.
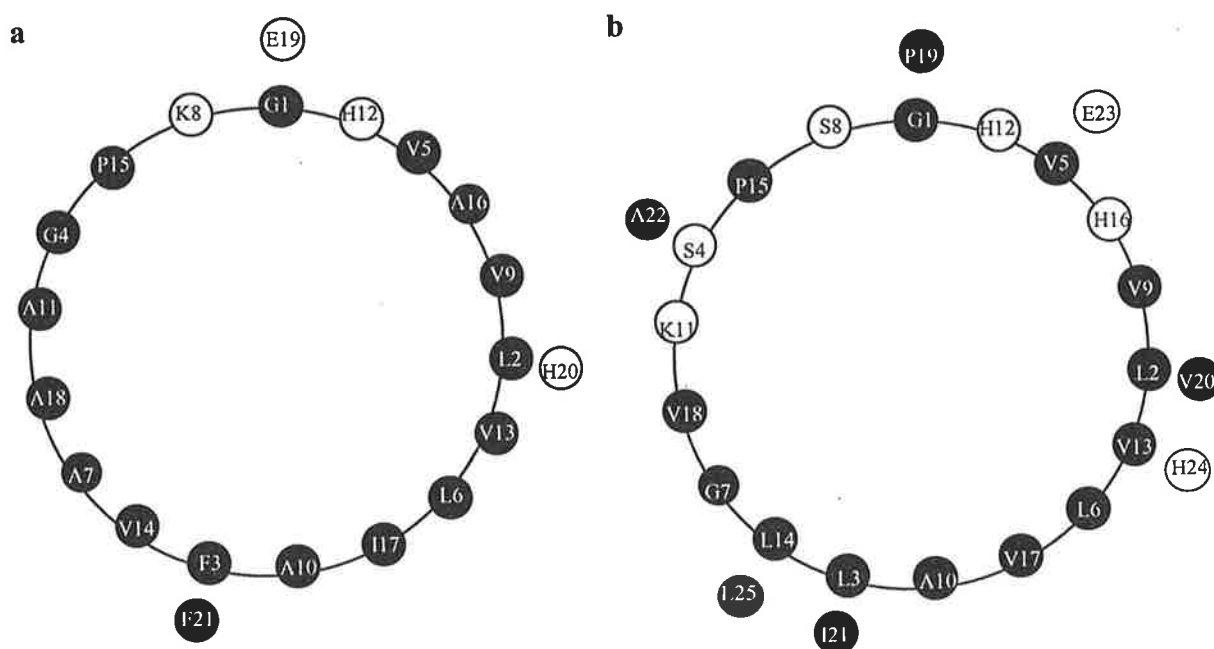
Fig. 5.3   Edmundson helical wheel representation of (a) maculatin 1.1 and (b) caerin 1.1. Hydrophobic and hydrophilic residues are represented by black and white circles respectively.

5.3   Circular Dichroism Studies

CD spectra were acquired on maculatin 1.1 in increasing concentrations from 0 to 50% (by vol.) of TFE in water (see Fig. 5.4). In low amounts of TFE (0-10%), maculatin 1.1 exhibits a far UV CD spectrum characteristic of an unstructured peptide, i.e., a broad minimum at 200 nm was observed. With increasing TFE, the CD spectrum underwent a marked change to one indicative of a predominantly α-helical structure, i.e. two minima in the vicinity of 208 nm (π-π* transition) and 220 nm (n-π* transition) were observed. The spectra at 40% and 50% TFE showed greatest ellipticity at these minima, indicative of maximum helical conformation.
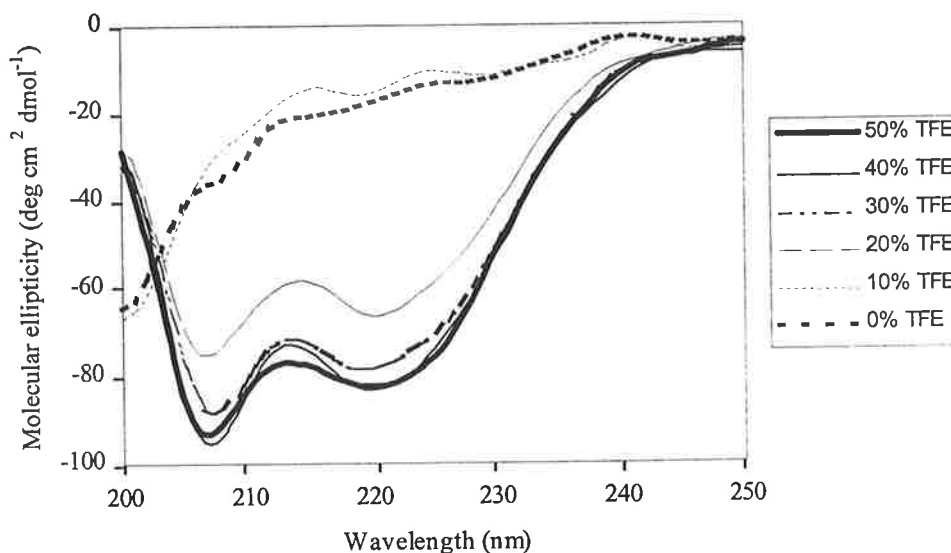
Fig. 5.4 CD spectra of maculatin 1.1 at varying concentrations (by vol.) of TFE.

5.4 Nuclear Magnetic Resonance Studies

On the basis of the CD results, NMR spectra of maculatin 1.1 were acquired under conditions which exhibited maximal helical structure, i.e., 50% (by vol.) TFE. Spectra of Ala15 maculatin 1.1 were also acquired under the same conditions whilst a third set of spectra were acquired on maculatin 1.1 dissolved in DPC micelles. In all cases, the ^{1}H-NMR spectrum was assigned *via* the standard methods discussed in chapter 3. Figs. 5.5a and 5.5b show a region of the TOCSY spectrum and the NH region of the NOESY spectrum of maculatin 1.1 in DPC/water respectively. Lines are drawn between spectra to correlate the series of side-chain proton resonance to sequential $d_{NN}(i,i+1)$ NOEs observed along the length of the peptide. Weaker $d_{NN}(i,i+2)$ NOEs were also present in this region. Similar spectra are also illustrated for maculatin 1.1 in TFE/water (Fig. 5.5c and 5.5d) and Ala15 maculatin 1.1 in TFE/water (Fig. 5.5e and 5.5f).
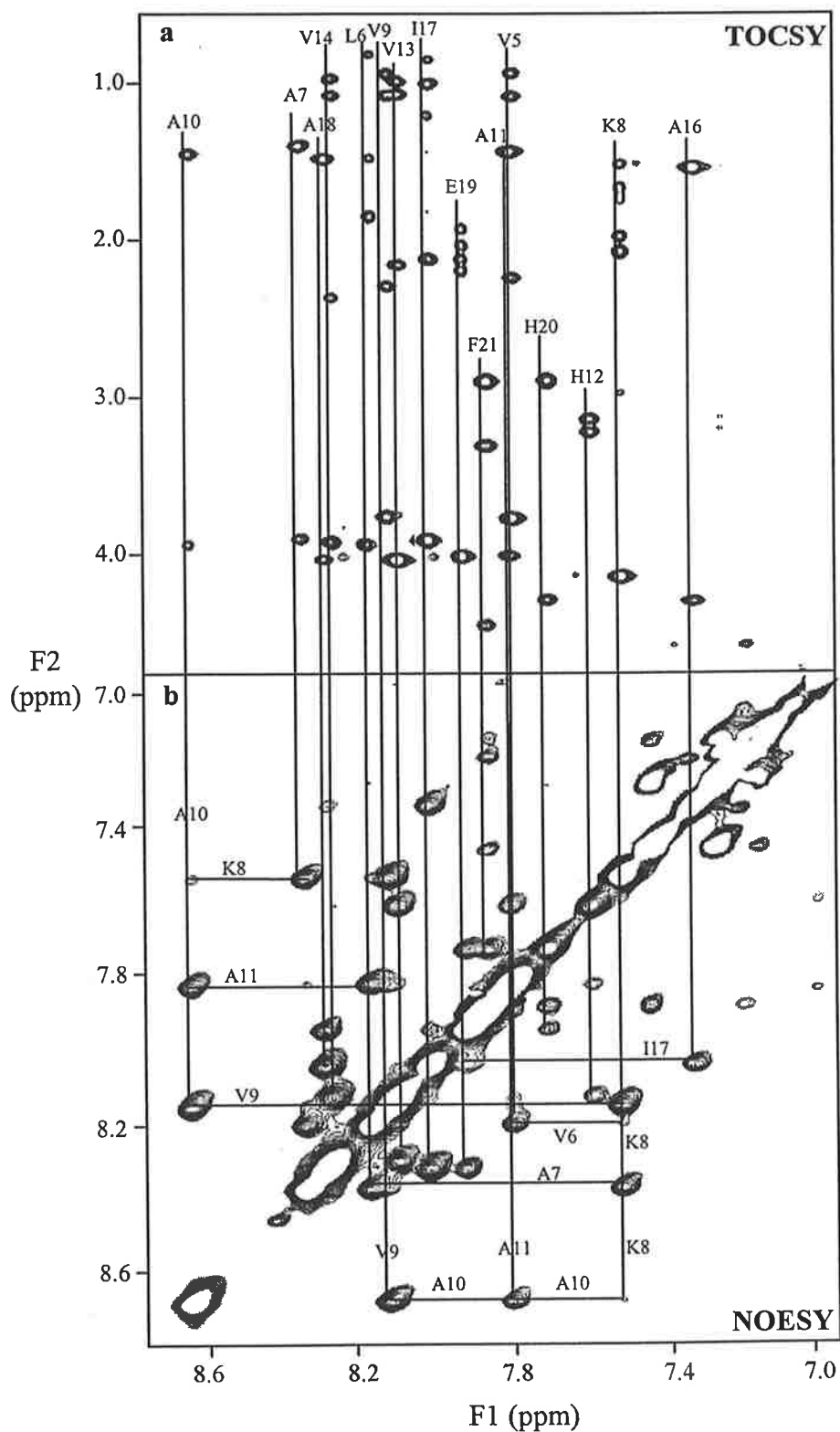
Fig 5.5 **(a) A region of the TOCSY spectrum showing NH to sidechain proton couplings, (b) NH region of the NOESY spectrum of maculatin 1.1 in DPC/water.** Connectivities between side-chain and backbone amide protons are indicated.
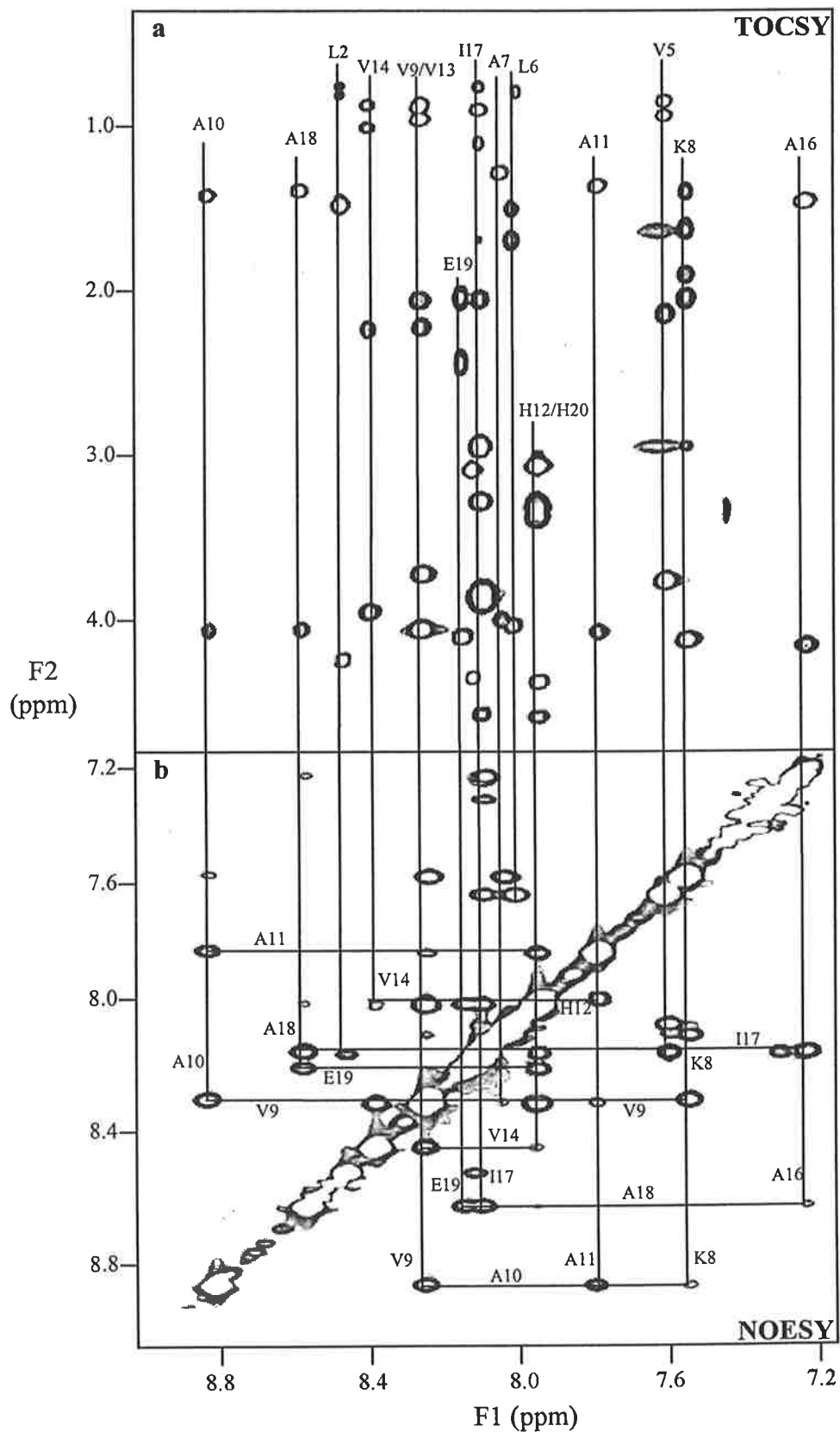
Fig 5.5 (c) A region of the TOCSY spectrum showing NH to sidechain proton couplings, (d) NH region of the NOESY spectrum of maculatin 1.1 in TFE/water. Connectivities between side-chain and backbone amide protons are indicated.
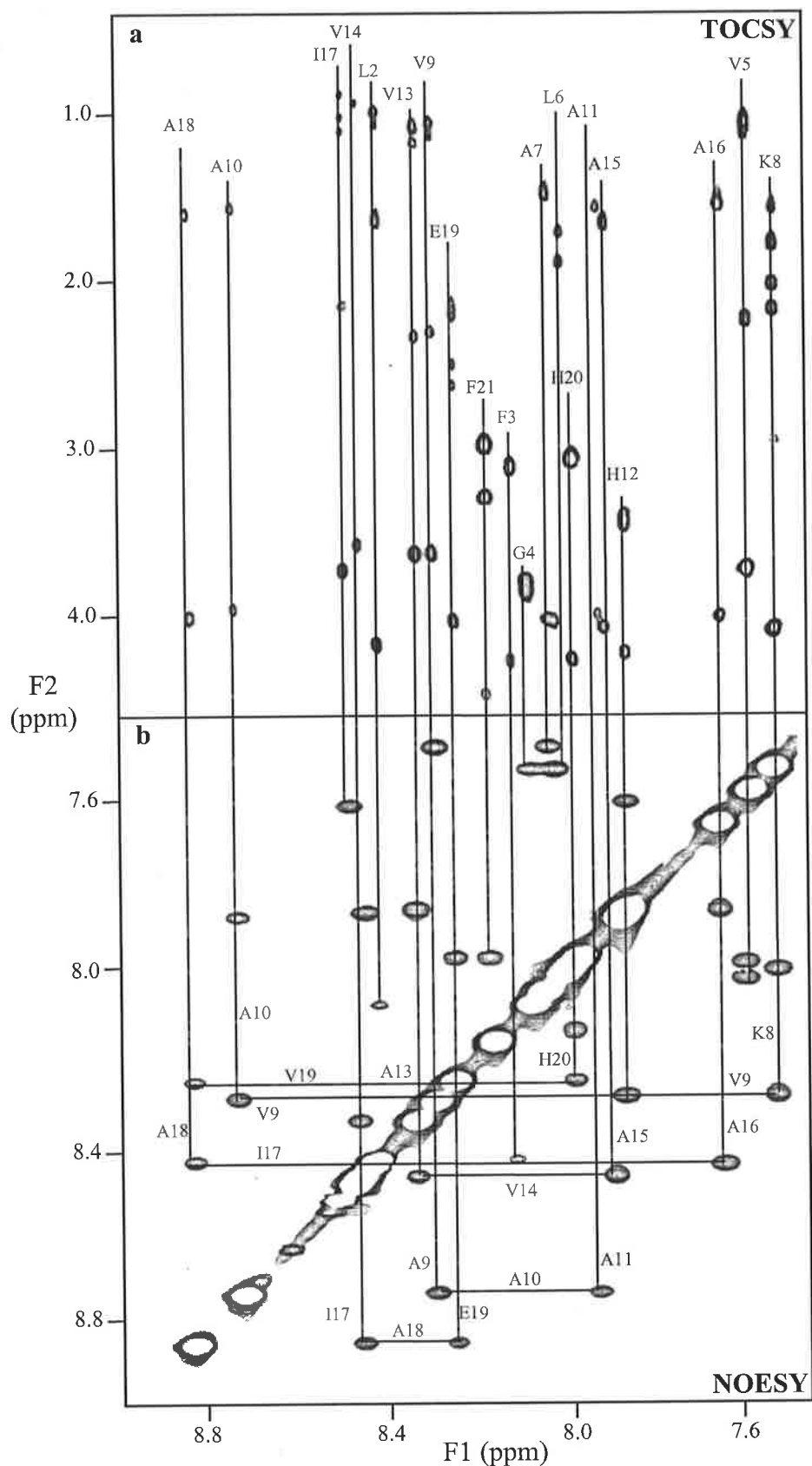
Fig 5.5 **(e) A region of the TOCSY spectrum showing NH to sidechain proton coupling, (f) NH region of the NOESY spectrum of Ala15 maculatin 1.1 in TFE/water.** Connectivities between side-chain and backbone amide protons are indicated.

Cross-peaks in the presence of DPC were observed to be broader than those in TFE/water mixtures, consistent with the incorporation of maculatin 1.1 into the large DPC micelle. The higher pH value of the DPC solution could also contribute to the broader NH resonances due to increased rate of exchange of NH protons with water. Using the $d_{\alpha N}(i,i+1)$ and $d_{NN}(i,i+1)$ sequential connectivities, the vast majority of ^{1}H resonances of maculatin 1.1 and its Ala15 analogue were assigned under the three solvent conditions. Assignments of these resonances and the ^{13}C α-CH resonances are tabulated in Table 5.2.

Table 5.2a ^{1}**H and** ^{13}**C NMR chemical shifts for maculatin 1.1 in DPC/water, pH 7.0, 37°C.**

Residue	Chemical Shifts (ppm)				
	NH	C$^{\alpha}$H	C$^{\beta}$H	others	C$^{\alpha}$
Gly 1	not observed	not observed	-	-	not observed
Leu 2	8.03	4.04	1.82	γ-CH=1.45 δ-CH$_3$=0.90, 1.01	54.00
Phe 3	not observed	4.20	3.14, 3.21	Aromatic H=7.27, 7.45	61.02
Gly 4	8.25	3.85, 3.99	-		42.99
Val 5	7.81	4.05	2.25	γ-CH$_3$=0.94, 1.09	57.80
Leu 6	8.19	3.94	1.85	γ-CH=1.49 δ-CH$_3$=0.83	57.51
Ala 7	8.36	3.92	1.42	-	54.91
Lys 8	7.53	4.14	1.98, 2.08	γ-CH$_2$=1.42, 1.52 δ-CH$_2$=1.67, 1.74 ε-CH$_2$=2.98	58.59
Val 9	8.13	3.77	2.30	γ-CH$_3$=0.95, 1.08	65.09
Ala 10	8.65	3.95	1.47	-	54.99
Ala 11	7.81	3.78	1.45	-	56.12
His 12	7.60	4.12	3.14, 3.22	δ-H=7.27, ε-H=7.01	58.59

Val 13	8.11	4.05	2.17	γ-CH$_3$=0.99, 1.08	64.10
Val 14	8.29	3.93	2.37	γ-CH$_3$=0.98, 1.09	66.45
Pro 15	-	4.34	1.90, 2.37	γ-CH$_2$=1.93, 2.16 δ-CH$_2$=3.51, 3.59	65.24
Ala 16	7.33	4.31	1.54	-	54.09
Ile 17	8.03	3.92	2.13	γ-CH$_2$=1.21, 1.83 γ-CH$_3$=1.01 δ-CH$_3$=0.85	63.81
Ala 18	8.31	4.04	1.49	-	54.88
Glu 19	7.94	4.02	1.94, 2.04	γ-CH$_2$=2.13, 2.20	57.30
His 20	7.72	4.30	2.90	δ-H=6.31, ε-H=7.93	58.09
Phe 21	7.87	4.44	2.91, 3.31	Aromatic H=7.16, 7.21, 7.35 CONH$_2$=7.28 , 7.45	58.24

Table 5.2b ^{1}H and ^{13}C NMR chemical shifts for maculatin 1.1 in d_3-TFE/water (1:1 by vol.) pH 2.5, 25°C.

	Chemical Shifts (ppm)				
Residue	NH	C$^\alpha$H	C$^\beta$H	others	C$^\alpha$
Gly 1	not observed	3.87, 3.95	-	-	42.26
Leu 2	8.45	4.27	1.58	γ-CH=1.57 δ-CH$_3$=0.86, 0.93	56.01
Phe 3	8.11	4.37	3.15	Aromatic H=7.25	59.52
Gly 4	8.08	3.86, 3.93	-	-	45.57
Val 5	7.60	3.81	2.23	γ-CH$_3$=0.98, 1.05	64.91
Leu 6	8.00	4.06	1.78	γ-CH=1.61 δ-CH$_3$=0.91	56.81
Ala 7	8.03	4.04	1.38	-	54.18
Lys 8	7.53	4.16	2.00, 2.14	γ-CH$_2$=1.38, 1.51 δ-CH$_2$=1.73 ε-CH$_2$=3.02	58.13
Val 9	8.23	3.76	2.30	γ-CH$_3$=0.98, 1.07	65.70
Ala 10	8.80	4.08	1.51	-	54.50
Ala 11	7.78	4.10	1.47	-	53.10

His 12	7.94	4.62	3.35, 3.43	δ-H=7.44, ε-H=8.53	56.59
Val 13	8.23	4.09	2.14	γ-CH$_3$=0.98, 1.07	63.93
Val 14	8.37	3.98	2.31	γ-CH$_3$=1.00, 1.12	66.21
Pro 15	-	4.29	1.84, 2.32	γ-CH$_2$=1.92, 2.18 δ-CH$_2$=3.50, 3.74	64.83
Ala 16	7.23	4.20	1.58	-	53.94
Ile 17	8.08	3.88	2.14	γ-CH$_2$=1.21, 1.77 γ-CH$_3$=1.01 δ-CH$_3$=0.88	63.68
Ala 18	8.56	4.08	1.49	-	54.10
Glu 19	8.13	4.13	2.14	γ-CH$_2$=2.48, 2.53	56.50
His 20	7.94	4.40	3.12	δ-H=6.86, ε-H=8.49	56.69
Phe 21	8.09	4.60	3.01, 3.33	Aromatic H=7.41 CONH$_2$=6.94 , 7.31	57.23

Table 5.2c ^{1}H and ^{13}C NMR chemical shifts for Ala15 maculatin 1.1 in d_3-TFE/water (1:1 by vol.) pH 2.5, 25°C.

	Chemical Shifts (ppm)				
Residue	NH	CαH	CβH	others	Cα
Gly 1	not observed	3.83, 3.94	-	-	42.18
Leu 2	8.43	4.24	1.55	γ-CH$_3$=1.55 δ-CH$_3$=0.85, 0.90	56.00
Phe 3	8.09	4.35	3.13	Aromatic H=7.23, 7.31	59.43
Gly 4	8.06	3.82, 3.92	-	-	45.39
Val 5	7.60	3.79	2.22	γ-CH$_3$=0.95, 1.04	64.50
Leu 6	8.01	4.37	1.78	γ-CH$_3$=1.58 δ-CH$_3$=0.88	57.05
Ala 7	8.03	4.04	1.39	-	56.83
Lys 8	7.53	4.17	1.98, 2.15	γ-CH$_2$=1.50, 1.74 δ-CH$_2$=1.73 ε-CH$_2$=3.00	58.18
Val 9	8.30	3.67	2.28	γ-CH$_3$=0.95, 1.04	66.20
Ala 10	8.71	4.02	1.49	-	54.22
Ala 11	7.91	4.05	1.52	-	53.10

His 12	7.89	4.31	3.45, 3.49	δ-H=7.35, ε-H=8.35	58.44
Val 13	8.34	3.67	2.31	γ-CH$_3$=0.97, 1.07	65.90
Val 14	8.46	3.61	2.10	γ-CH$_3$=0.85, 0.96	65.90
Ala 15	7.89	4.15	1.59	-	58.12
Ala 16	7.65	4.08	1.48	-	56.64
Ile 17	8.48	3.77	2.10	γ-CH$_2$=1.13, 1.91 γ-CH$_3$=1.00 δ-CH$_3$=0.85	64.71
Ala 18	8.82	4.09	1.53	-	54.26
Glu 19	8.26	4.10	2.10, 2.18	γ-CH$_2$=2.49, 2.63	56.67
His 20	7.99	4.35	3.10	δ-H=6.77, ε-H=8.49	56.89
Phe 21	8.17	4.57	2,99, 3.31	Aromatic H=7.32, 7.41 CONH$_2$=6.90, 7.32	57.47

NOEs connecting the NH, C$^\alpha$H and C$^\beta$H protons can be summarised in a bar chart (Fig. 5.6) which provides a basis for a qualitative interpretation of the secondary structure of the peptides under these solvation conditions (Wüthrich *et al.*, 1984).

a
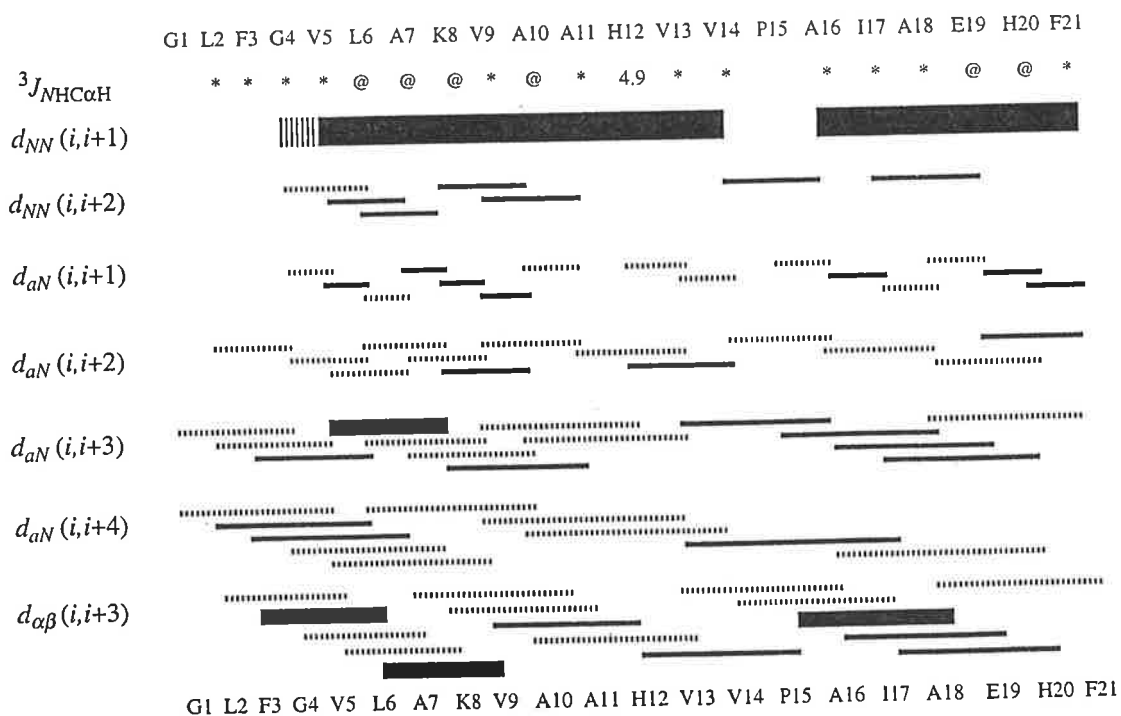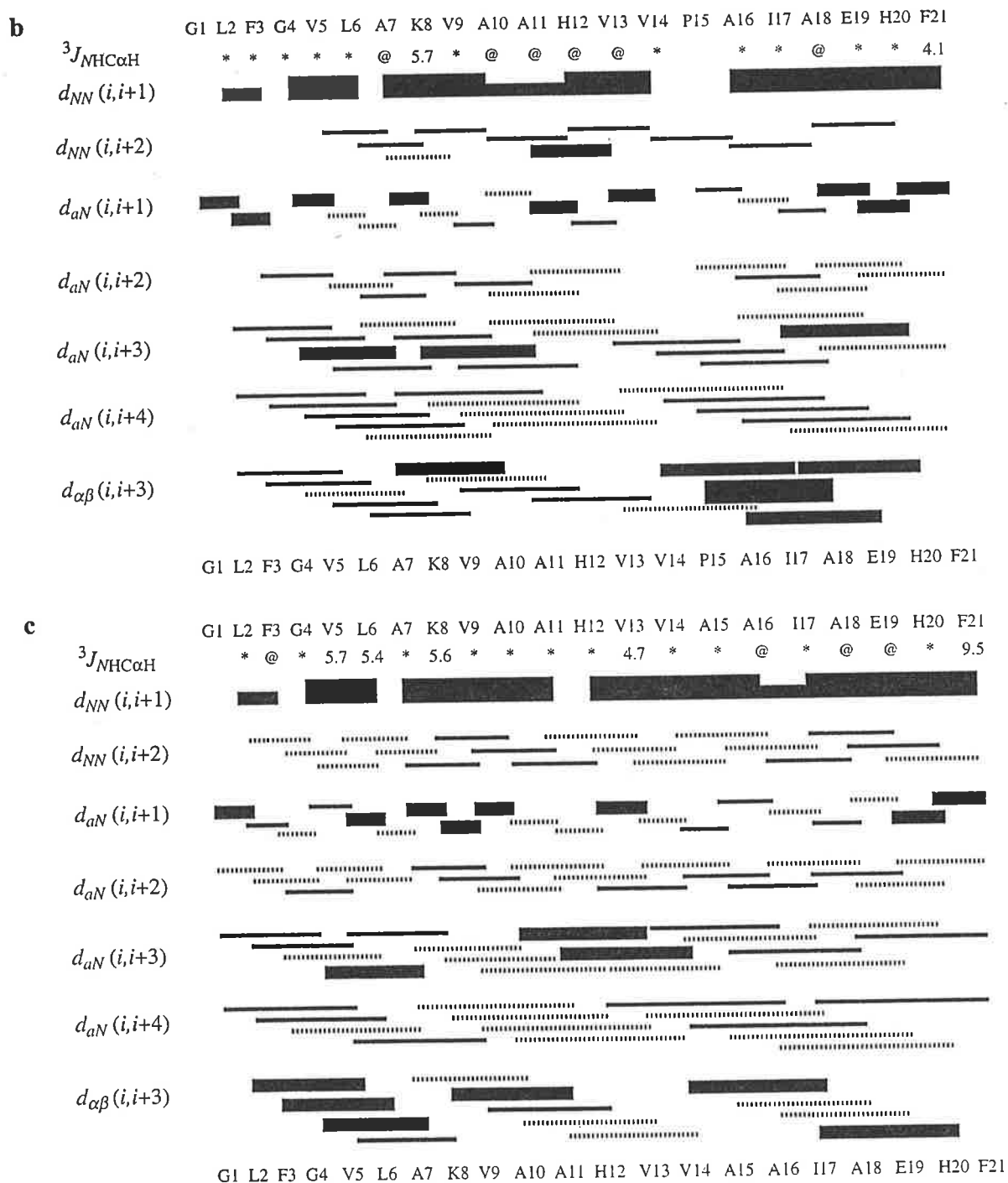
Fig. 5.6 Summary of NOEs used for structure calculation of maculatin 1.1 in (a) DPC/water pH 7.0, 37°C (b) TFE/water (1:1 by vol.) pH 2.5, 25°C and (c) Ala15 maculatin 1.1 in TFE/water (1:1 by vol.) pH 2.5, 25°C respectively. The amino acid sequence of the peptide is given at the top of the diagram and the values of $^3J_{NHC\alpha H}$ were obtained from high-resolution 1D ^{1}H spectra. Asterisks (*) indicate coupling constants could not be unambiguously assigned due to overlap. @ indicates no coupling constant was detected for the particular residue. The various types of NOEs and their relative strengths are indicated by the thickness of the bars (strong, medium and weak). For this diagram, NOEs are classified on the basis of strong (< 2.7 Å), medium (between 2.7 to 3.5 Å) and weak (> 3.5 Å). Dashed lines represent connectivities that could not be unambiguously assigned due to overlap, e.g. with an intraresidue NOE.

From inspection of Fig. 5.6, it is apparent that a large number of connectivities indicative of α-helical structure are present for all three systems (Wüthrich, 1986). For example, the presence of strong $d_{NN}(i,i+1)$ NOEs complemented by weaker $d_{\alpha N}(i,i+1)$ NOEs, a series of NOEs from residues three and four amino acids apart in the peptide, i.e., $d_{\alpha N}(i,i+3)$, $d_{\alpha\beta}(i,i+3)$, $d_{\alpha N}(i,i+4)$ and some weak $d_{NN}(i,i+2)$ NOEs were observed. Finally, $^3J_{HNC\alpha H}$ values that could be measured mostly had values less than 5 Hz, consistent with a helical structure. The NOE data and their relative intensities suggest that maculatin 1.1 adopts a helical secondary structure along the majority of its polypeptide chain in both TFE/water and DPC/water mixtures. In examining and comparing these figures for maculatin 1.1, the NOE pattern suggests that in both cases the helix commences at Leu2 and continues to His12, is partially interrupted in the vicinity of Pro15 before regaining its helical structure between Ala16 to Phe21. By contrast, the NOE pattern shown in Fig. 5.5f suggests that the Ala15 analogue of maculatin 1.1 (which does not contain the proline residue) adopts an uninterrupted α-helix along its entire length.

The presence of a helical structure is also indicated from an examination of the deviation from random coil chemical shift values of the ^1H and ^{13}C α-CH resonances (Wishart et al., 1995a). Using a window of n = ±2 residues was used (Pastore and Saudek, 1990). In all three cases, the ^1H resonances showed a distinct upfield shift and the ^{13}C resonances and a distinct downfield shift along the peptide (see Fig. 5.7). Statistical analysis of the ^1H and ^{13}C α-CH chemical shifts in structured regions of proteins has shown that α-helical regions have a marked upfield ^1H and downfield

^{13}C chemical shift respectively compared to random-coil values (Wishart *et al.*, 1991, Wishart *et al.*, 1992). The pattern for the ^{1}H and ^{13}C chemical shifts of maculatin 1.1 in TFE/water and DPC are similar, implying that the peptide adopts similar structures in both solvent systems. In particular, the ^{1}H chemical shift data indicate a greater helical nature in the N- and C-terminal regions. The more random-coil nature of the chemical shifts in between these regions (i.e., near Pro15) suggests that the middle portion of the molecule does not have as a strong helical preference and is thus more flexible. By contrast, the same plots for Ala15 maculatin 1.1 in TFE/water show a bell-shaped trend along the peptide sequence implying that this analogue is helical along its entire length with maximal helicity in the central region. Furthermore, the ^{1}H and ^{13}C chemical shift deviations in the centre of Ala15 maculatin 1.1 are greater than those of maculatin 1.1 in TFE and DPC implying that a tighter helix is present in this region of the Ala15 variant.
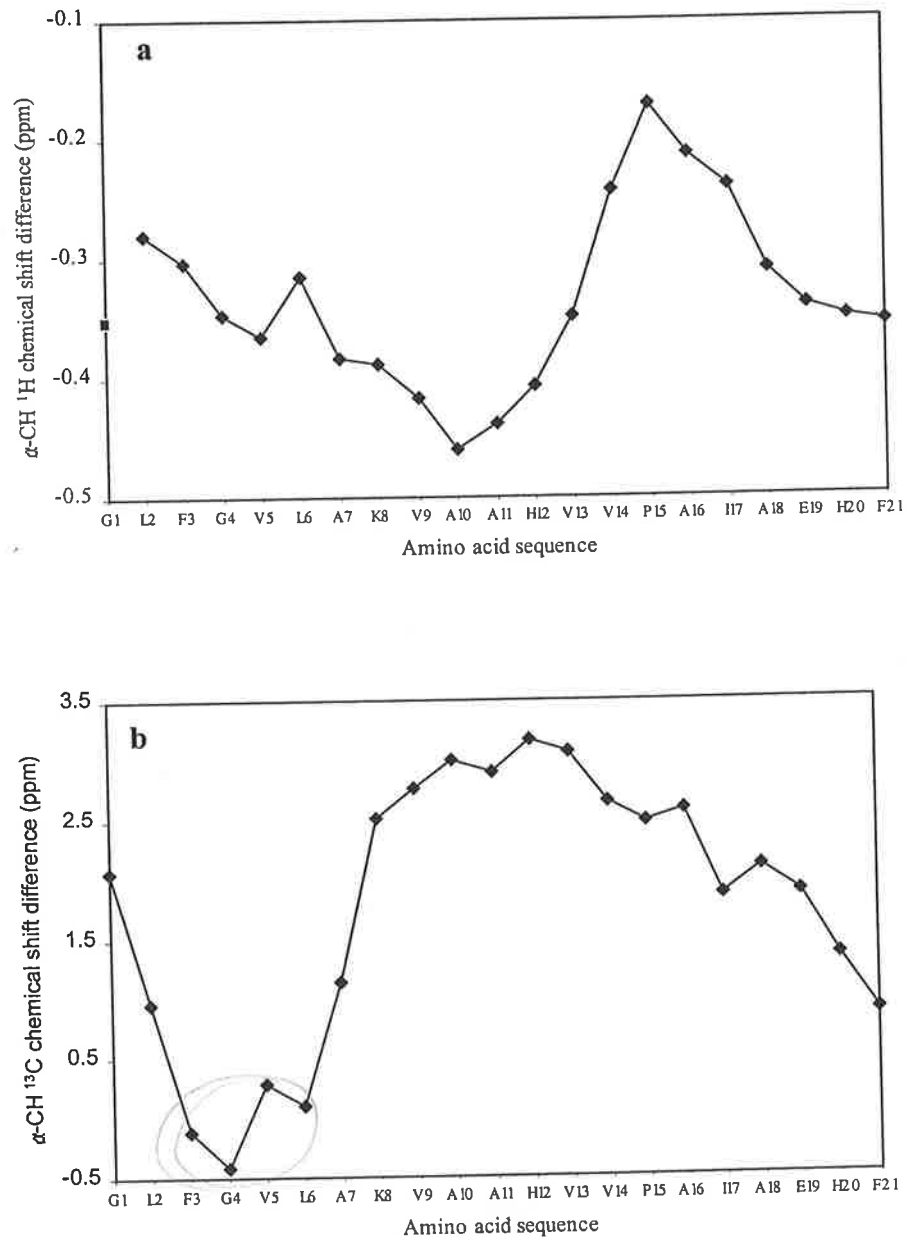
Fig. 5.7 Deviation from random coil chemical shifts of (a) ^{1}H α-CH resonances of maculatin 1.1 in DPC/water mixture, (b) ^{13}C α-CH resonances of maculatin 1.1 in DPC/water mixture. A window of ± 2 residues was used. Upfield and downfield chemical shifts are indicated by negative and positive values respectively.

✱ Nobody has given a good reason for this behaviour. It maybe that when an α-helix is formed, the α-carbons are more shielded due to the proximity of the C=O group. Thus the ^{13}C plot shows a distinctive downfield shift.
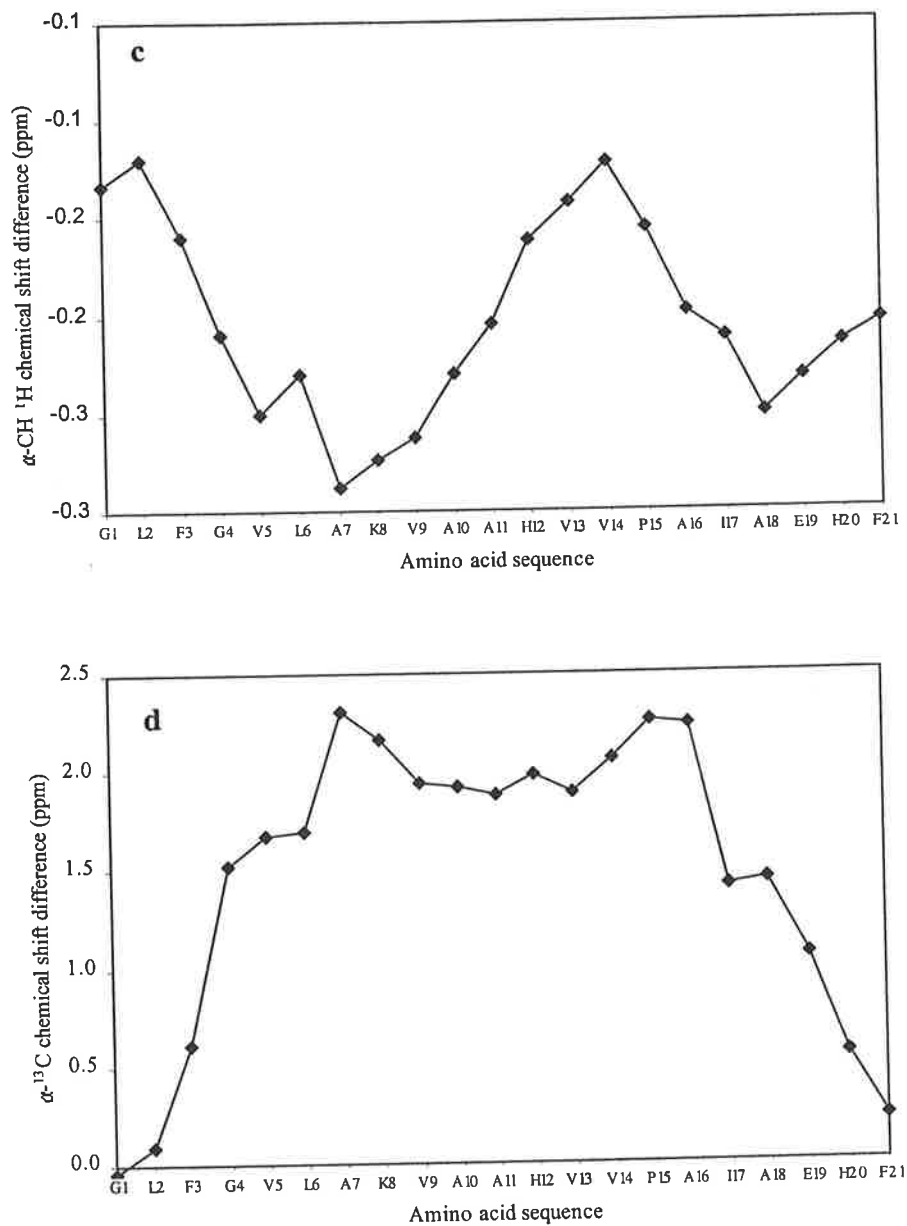
Fig. 5.7 **Deviation from random coil chemical shifts of (c) ^{1}H α-CH resonances of maculatin 1.1 in 50% (by vol.) TFE, (d) ^{13}C α-CH resonances of maculatin 1.1 in 50% (by vol.) TFE.** A window of ± 2 residues was used. Upfield and downfield chemical shifts are indicated by negative and positive values respectively.
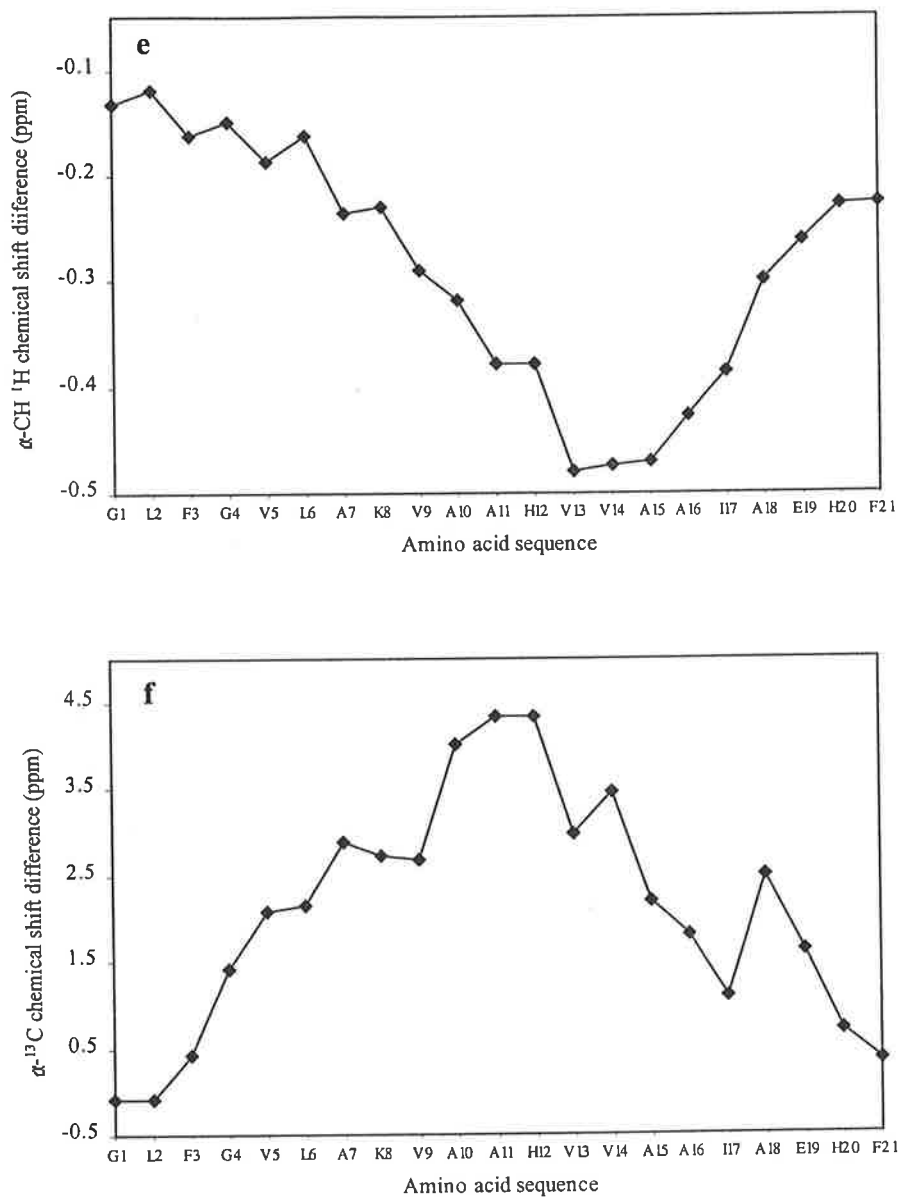
Fig. 5.7 **Deviation from random coil chemical shifts of (e) ^{1}H α-CH resonances of Ala15 maculatin 1.1 in 50% (by vol.) TFE, (f) ^{13}C α-CH resonances of Ala15 maculatin 1.1 in 50% (by vol.) TFE.** A window of ± 2 residues was used. Upfield and downfield chemical shifts are indicated by negative and positive values respectively.

5.5 Structural analysis

The 1D coupling constants and 2D NOESY data were used as input for calculation of the solution structures of maculatin 1.1 and Ala15 maculatin 1.1. Structural calculations for maculatin 1.1 in DPC/water were based on a total of 414 NOE distance restraints comprising of 164 intra-residue restraints, 116 sequential restraints, 132 medium and 2 long-range restraints. In the TFE/water mixture, a total of 437 NOE distance restraints comprising of 167 intra-residue restraints, 121 sequential restraints, 146 medium and 3 long-range restraints were used. For the Ala15 analogue of maculatin 1.1, a total of 366 NOE distance restraints comprising of 137 intra-residue restraints, 86 sequential restraints, 139 medium and 4 long-range restraints were employed. Following RMD, structures were minimised with respect to potential energy *via* conjugate-gradient methods (Sutcliffe and Dobson, 1991). The final run produced 60 conformers from which the most stable (lowest potential energy) 20 conformers were chosen for examination (Table 5.3). It is apparent from the data presented in Table 5.3 that all three structures are well ordered with very similar low RMSD values for the backbone N, C^α and C' atoms along the amino acid sequence. Fig. 5.8 shows the superimposition of the 20 structures over the backbone atoms of maculatin 1.1 and its Ala15 analogue.

Table 5.3a Structural statistics of maculatin 1.1 in DPC/water pH 7.0, 37°C following RMD/SA calculations.[*]

RMSD from mean geometry (Å)	$<SA>$	$(SA)_r$
All heavy atoms	0.80 ± 0.021	
All heavy backbone atoms (N, C^α and C')	0.38 ± 0.016	
X-PLOR energies (kcalmol^{-1})		
E_{tot}	235.43 ± 3.39	225.93
E_{bond}	17.61 ± 0.74	16.83
E_{angle}	84.63 ± 2.07	81.84
E_{impr}	12.96 ± 0.85	11.37
E_{repel}	32.81 ± 1.71	32.17
E_{NOE}	86.33 ± 2.53	82.21
E_{cdih}	1.09 ± 0.14	0.933

* $<SA>$ is the ensemble of the 20 final structures, (SA) is the mean structure obtained by best-fitting and averaging the coordinates of the backbone N, C^α and C' atoms of the 20 final structures. (SA)r is the representative structure obtained after restrained energy minimization of the mean structure. Number of NOEs violate > 0.2 Å $= 29$. Maximum violation is 2.90 Å.

Table 5.3b **Structural statistics of maculatin 1.1 in d_3-TFE/water (1:1 by vol.) pH 2.5, 25°C.**

RMSD from mean geometry (Å)	<SA>	(SA)$_r$
All heavy atoms	0.79 ± 0.011	
All heavy backbone atoms (N, C$^\alpha$ and C')	0.37 ± 0.012	
X-PLOR energies (kcalmol^{-1})		
E_{tot}	200.84 ± 6.06	194.23
E_{bond}	19.15 ± 0.75	14.39
E_{angle}	66.16 ± 2.10	54.91
E_{impr}	11.56 ± 0.73	8.76
E_{repel}	16.10 ± 1.21	19.98
E_{NOE}	83.35 ± 4.31	89.39
E_{cdih}	4.55 ± 1.14	6.80

Number of NOEs violate > 0.2 Å = 26. Maximum violation is 2.90 Å.

Table 5.3c **Structural statistics of Ala15 maculatin 1.1 in d_3-TFE/ H_2O (1:1 by vol.) pH 2.5, 25°C.**

RMSD from mean geometry (Å)	<SA> *	(SA)$_r$
All heavy atoms	0.80 ± 0.017	
All heavy backbone atoms (N, C$^\alpha$ and C')	0.38 ± 0.020	
X-PLOR energies (kcalmol^{-1})		
E_{tot}	196.16 ± 4.83	175.10
E_{bond}	15.02 ± 0.77	13.47
E_{angle}	58.72 ± 2.08	52.27
E_{impr}	20.91 ± 0.73	18.78
E_{repel}	12.24 ± 1.09	12.13
E_{NOE}	88.37 ± 4.21	78.21
E_{cdih}	0.91 ± 0.32	0.22

Number of NOEs violate > 0.2 Å = 24. Maximum violation is 2.80 Å.
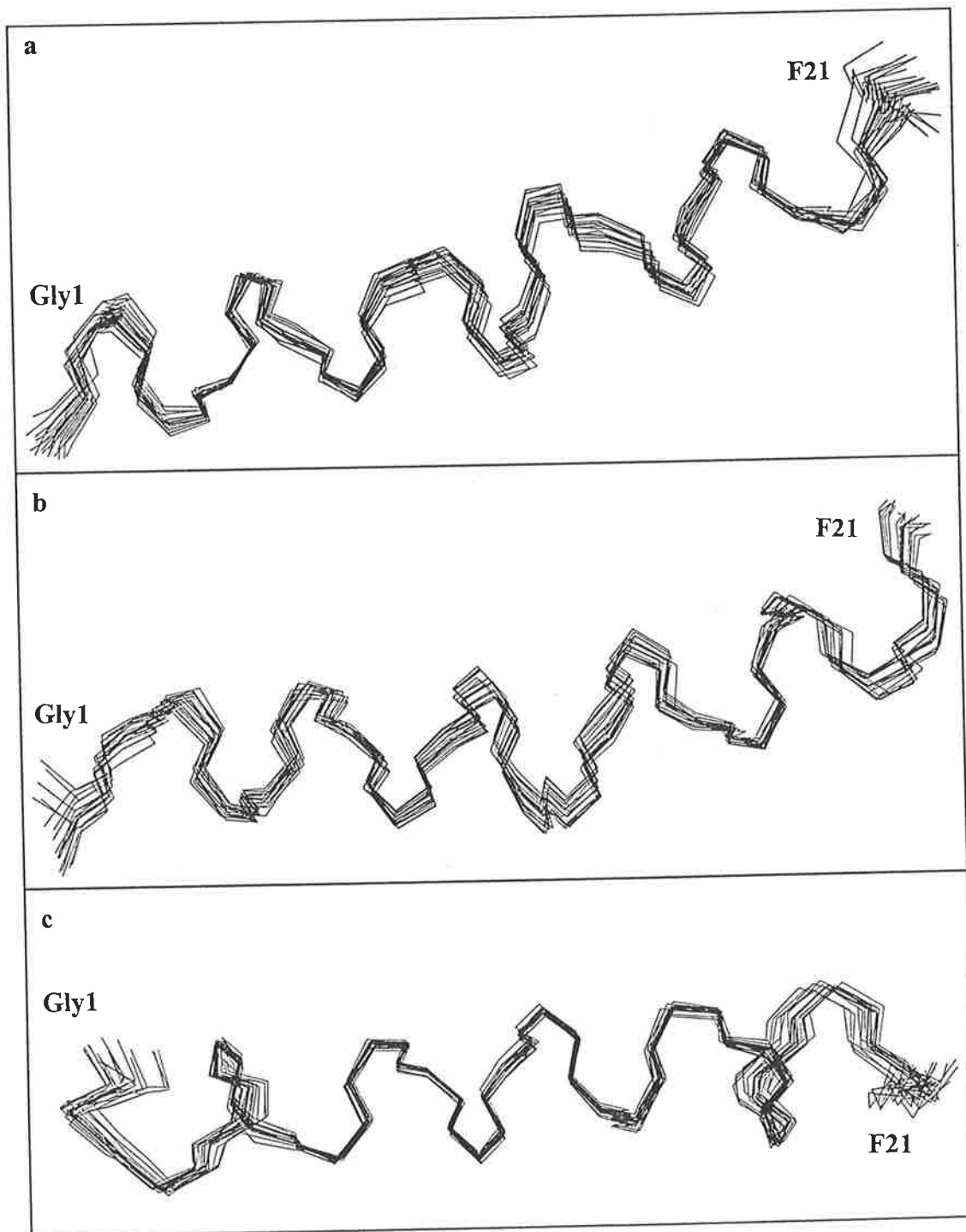
Fig. 5.8 Superposition of backbone atoms of the 20 most stable structures of (a) maculatin 1.1 in DPC/water (b) TFE/water and (c) Ala15 maculatin 1.1 in TFE/water.

Analysis of the angular order parameters (S, ϕ and ψ) of all three groups of the twenty structures indicates that all non-terminal residues are well defined (Leu2 to His20) with $S > 0.9$ for both their ϕ and ψ angles (Fig. 5.9).
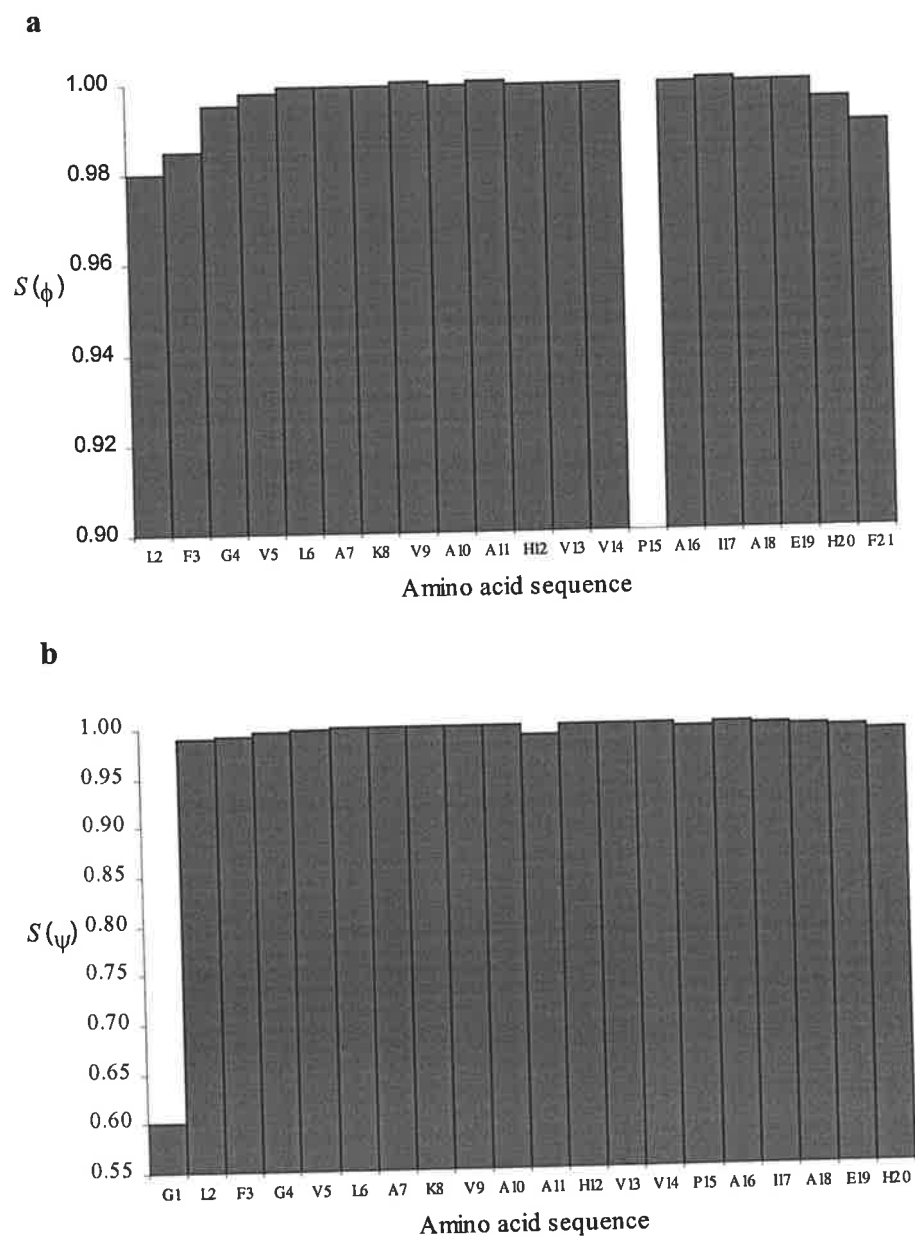
Fig. 5.9   Plots of Angular order parameters (a) $S(\phi)$ and (b) $S(\psi)$ against amino acid sequence for maculatin 1.1 in DPC/water.

c

d
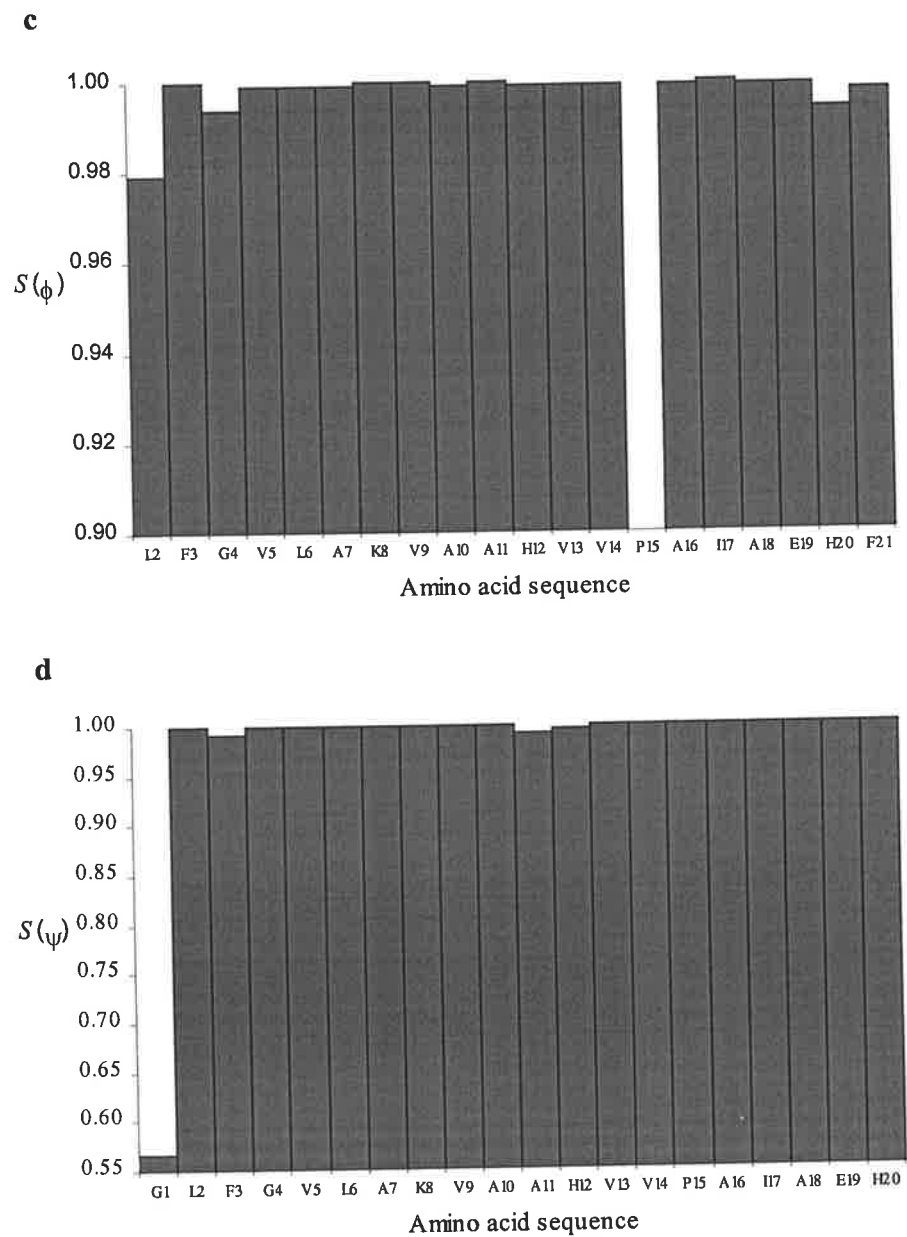
Fig. 5.9 **Plots of Angular order parameters (c) $S(\phi)$ and (d) $S(\psi)$ against amino acid sequence for maculatin 1.1 in TFE/water.**

e

f
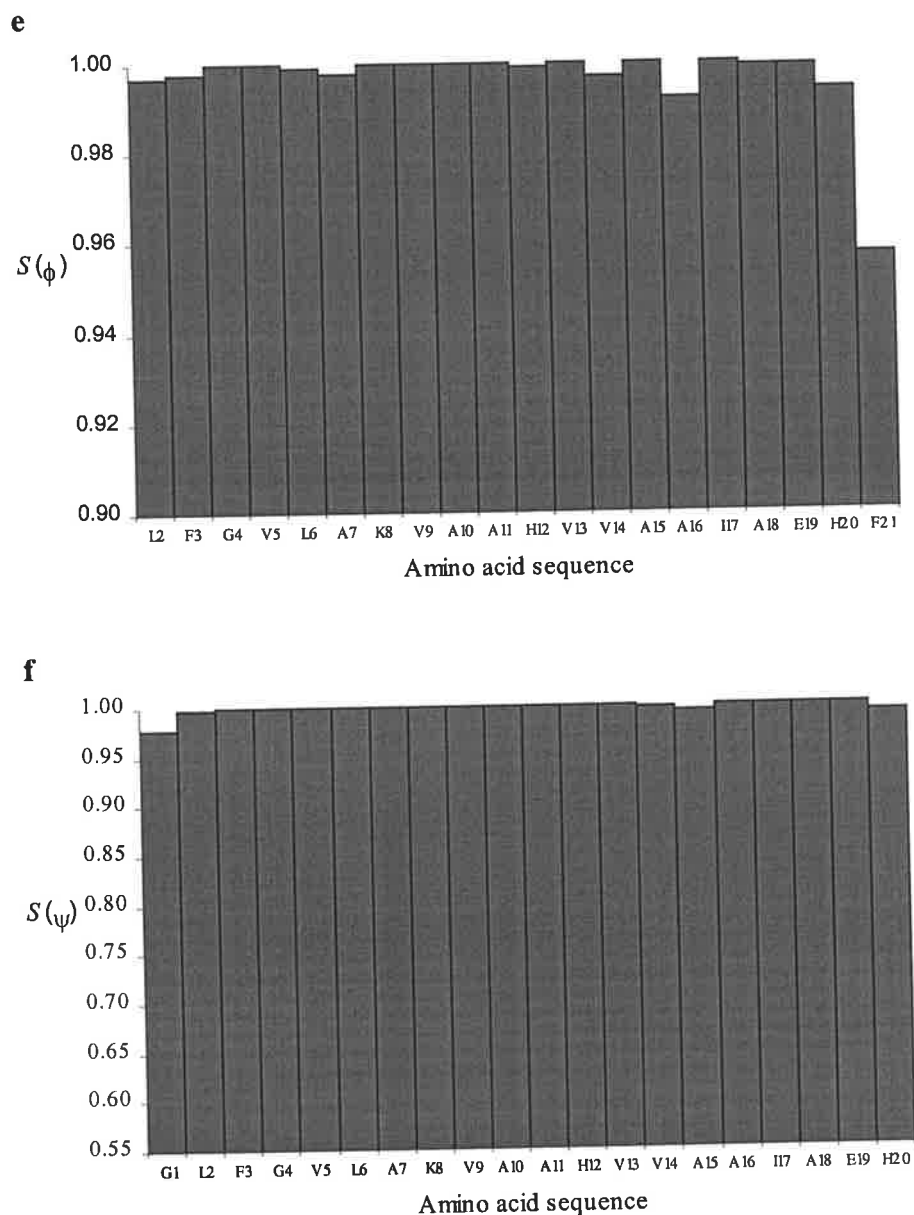
Fig. 5.9 **Plots of Angular order parameters (e) $S(\phi)$ and (f) $S(\psi)$ against amino acid sequence for Ala15 maculatin 1.1 in TFE/water.**

Ramachandran plots averaged over these twenty structures indicated that in all three cases, the dihedral angles of all the 18 non-glycine and non-proline amino acids were in the sterically favoured or allowed regions for α-helical conformation (Fig. 5.10).
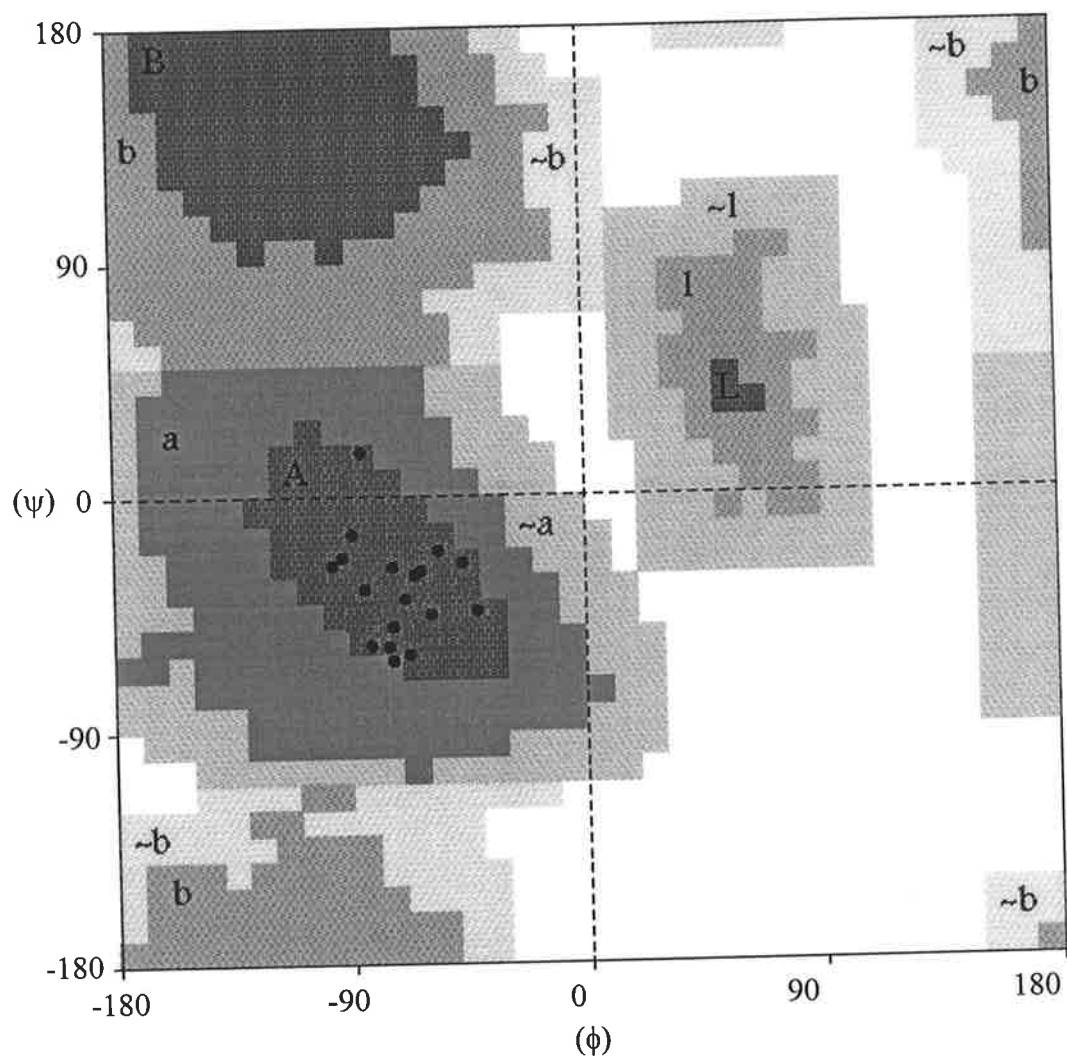
Fig. 5.10a Ramachandran plot of maculatin 1.1 in DPC/water.
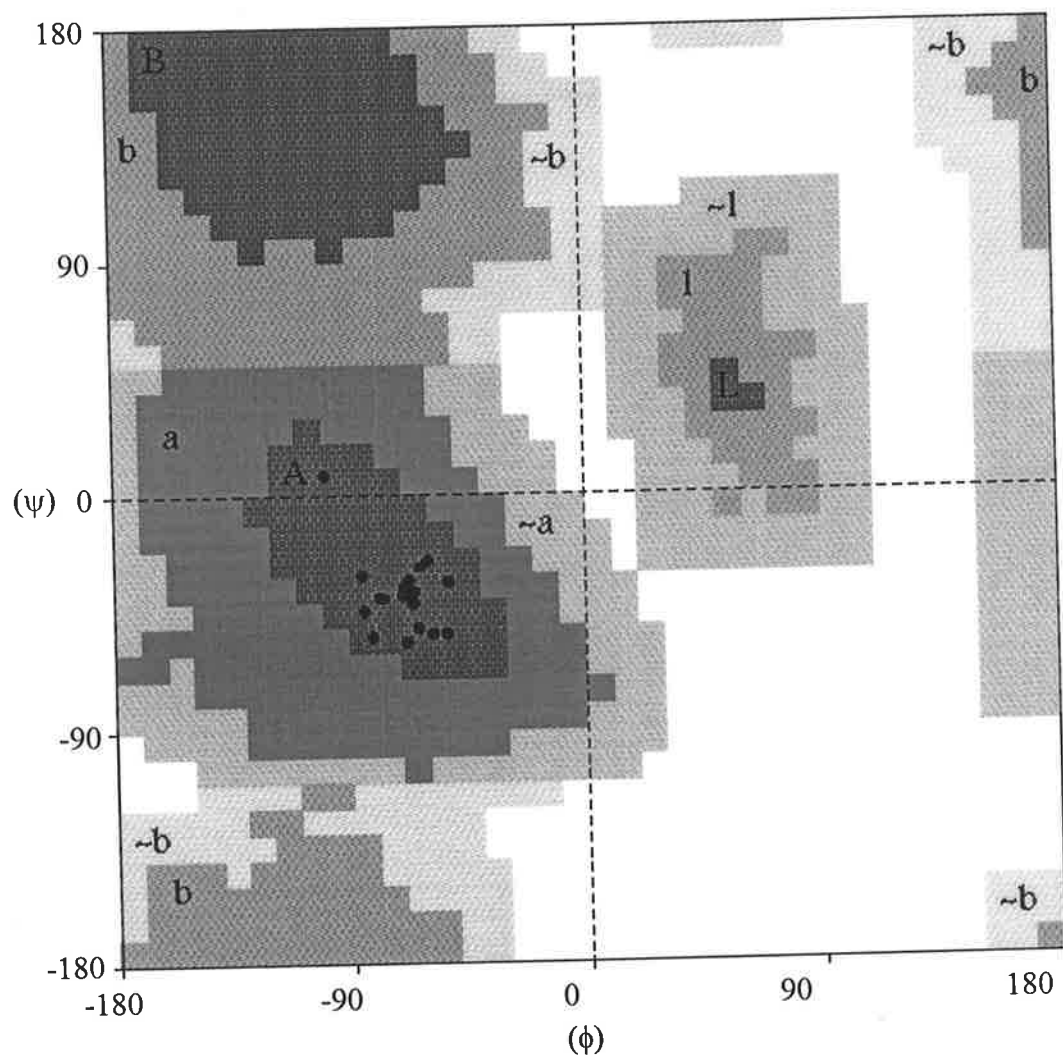
Fig. 5.10b Ramachandran plot of maculatin 1.1 in TFE/water.
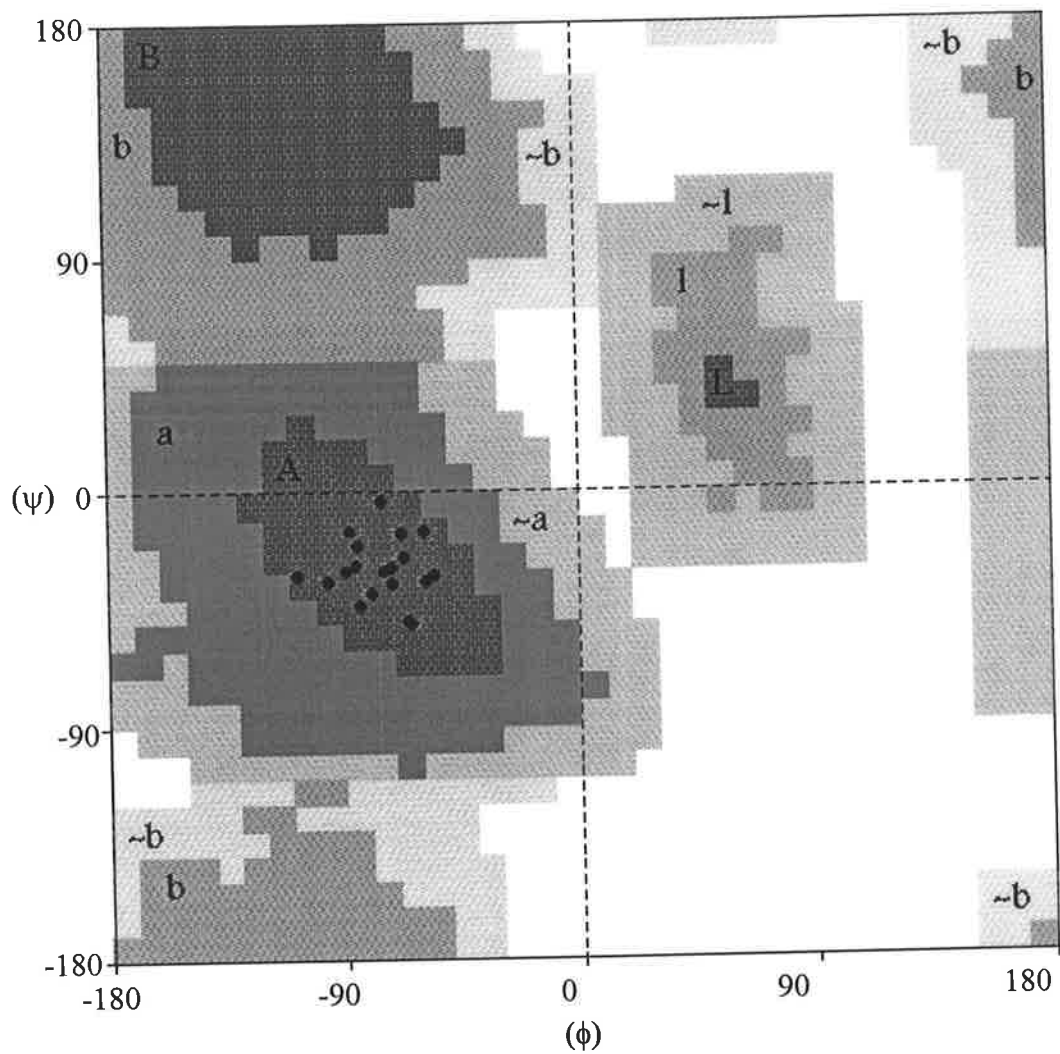
Fig. 5.10c   Ramachandran plot of Ala15 maculatin 1.1 in TFE/water.

The structure calculations confirmed the conclusions derived from analysis of the NOE and α-CH chemical shift data (Figs. 5.6 and 5.7). Fig. 5.11 shows the lowest energy structures of maculatin 1.1 in TFE/water and DPC and its Ala15 analogue in TFE/water. In the first two cases, maculatin 1.1 adopts an overall amphipathic helical conformation with well-defined hydrophobic and hydrophilic zones. The Ala15 analogue is predominantly amphipathic apart from the sidechain of His20 occurring on the hydrophobic side of the peptide (Fig. 5.11). For maculatin 1.1, a kink exists in the peptide in both solvent systems. The angle between the two helical regions in TFE/water and DPC is $20.7 \pm 6.0^{\circ}$ and $9.6 \pm 5.4^{\circ}$ respectively (from Leu2 to Ala10 and Val13 to His20 in the TFE/water structures and Leu2 to His12 and Pro15 to Glu19 in the DPC structures). The kink in maculatin 1.1 imparts some additional flexibility in the central region as is apparent in the greater variability in this region in the calculated structures of maculatin 1.1 in TFE/water and DPC compared to Ala15 maculatin 1.1 (Fig. 5.8). The Ala15 analogue adopts a much more linear helix. However, it does exhibit slight curvature along its length with a radius of curvature of 25 Å in the lowest energy structure of Fig. 5.11.
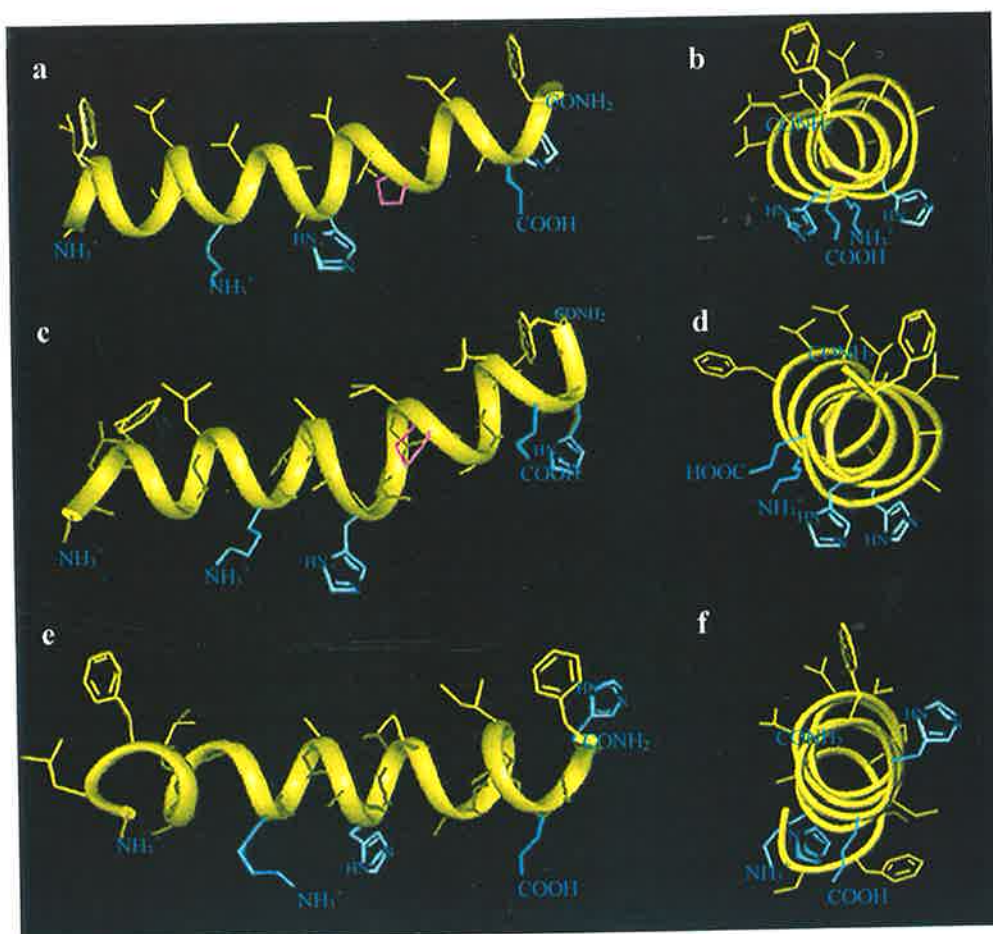
Fig. 5.11 **Lowest energy structures illustrating (a) the side-view of maculatin 1.1 in DPC/water (b) showing axial view, (c) maculatin 1.1 in TFE/water showing side view, (d) showing axial view and (e) Ala15 maculatin 1.1 in TFE/water showing side view, (f) showing axial view.** Hydrophilic groups are shown in blue. The proline pyrrolidine ring is coloured pink.

5.6 Orientation Studies using Solid-State NMR

As discussed in Chapter 4, DMPC phospholipid multilayers were prepared on glass coverslips. Solid-state ^{31}P NMR spectra of the sample showed a single peak at –16 ppm, indicating that the phospholipids were uniaxially oriented (Fig. 5.12) (Seelig, 1984; Crowell and McDonald, 1999).

121
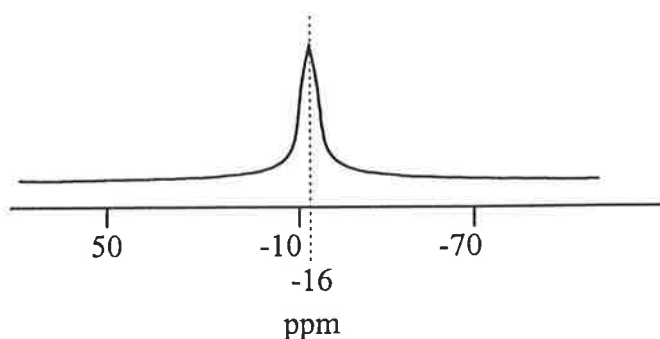
Fig. 5.12 ^{31}P NMR spectrum of DMPC multilayers on glass coverslips (35°C).

Addition of maculatin 1.1 to the sample caused the spectral width of the ^{2}H NMR spectrum to decrease by approximately 4000 Hz. This decrease in order parameter of the lipid alkyl chains suggests that maculatin 1.1 has been incorporated into the lipid bilayer (see Fig. 5.13 and Section 4.5). Similar behaviour has also been observed for magainin interacting with DMPC model membranes (Bechinger *et al.*, 1991 and 1992).
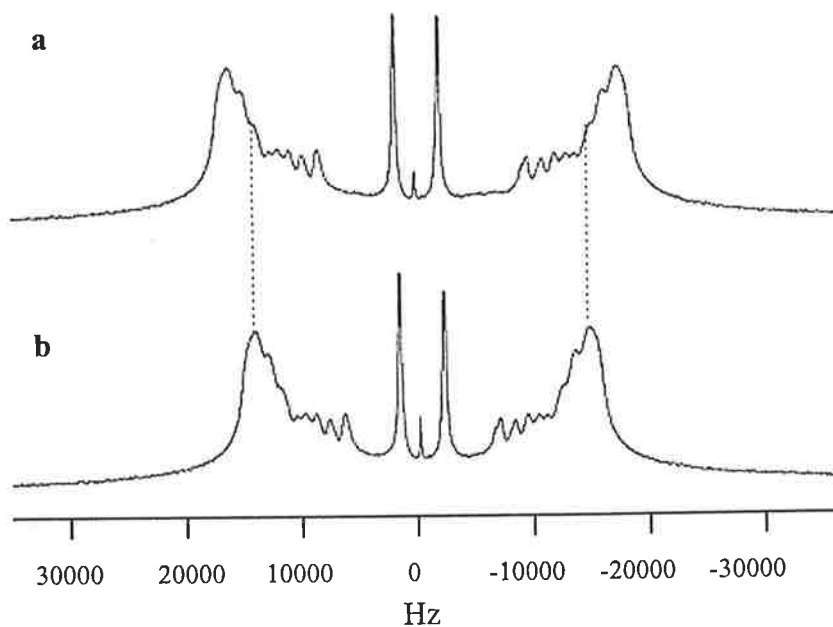
Fig. 5.13 ^{2}H-NMR spectra of aligned multilayers (DMPC-^{2}H$_{54}$, 35°C) before (a) and after (b) adding maculatin 1.1 (lipid/peptide ratio 15:1, 35°C).

Fig. 5.14 compares the ^{15}N-NMR spectra of ^{15}N-Ala7 labelled maculatin 1.1: (a) in its pure form revealing a powder pattern and (b) when incorporated into multilayers. [(Note that the glass coverslips in this experiment were oriented such that the bilayer normal was perpendicular to $\mathbf{B_0}$. This is unlike the experiments conducted by Bechinger and co-workers (1991, 1992) who orient their glass slides with the bilayer normal parallel to $\mathbf{B_0}$ (Fig. 4.4)].
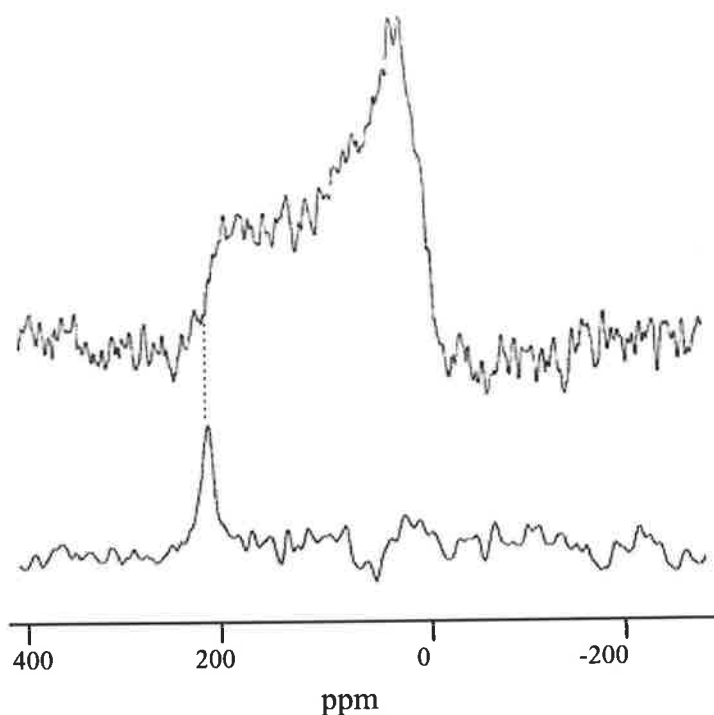
Fig. 5.14 ^{15}**N NMR spectra of** ^{15}**N-Ala7 maculatin 1.1 (a) showing powder pattern, (b) when incorporated into DMPC multilayers (lipid/peptide ratio 15:1, 35°C).**

Fig. 5.15a and 5.15b show the schematic representation of the ^{15}N solid-state NMR spectra of ^{15}N-Ala7 labelled maculatin 1.1 while 5.15c depicts the parallel orientation of maculatin 1.1 with respect to the lipid bilayer surface. Whereas only one monomer of the peptide is shown, the NMR data are consistent with a

mechanism of membrane interaction which involves maculatin 1.1 aggregating as oligomers, forming a 'carpet' layer on the membrane surface.
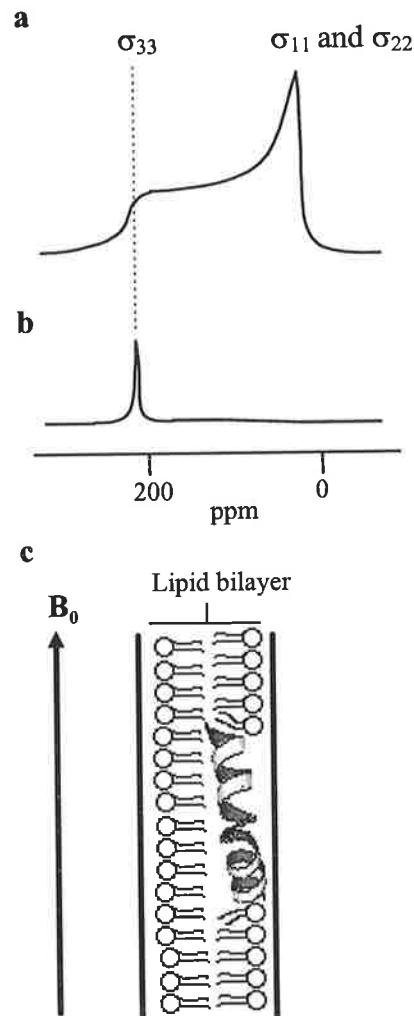
Fig. 5.15 Schematic ^{15}N solid-state NMR spectra of ^{15}N-Ala7 labelled maculatin 1.1: (a) powder pattern of maculatin 1.1 (b) maculatin 1.1 in oriented phospholipid multilayers. (c) Schematic representation of the 'carpet' conformation of maculatin 1.1 in a lipid bilayer. (Diagrams not drawn to scale).

The ^{15}N spectrum in Fig. 5.15b exhibits amide resonances at the downfield end of the chemical shift range, suggesting that maculatin 1.1 orients with its helical axis parallel to the bilayer surface i.e., it adopts the carpet mechanism. This behaviour has also been observed by solid-state NMR of magainin in lipid bilayers (Bechinger et al., 1991 and 1992).

5.7 Discussion

The structures of maculatin 1.1 dissolved in TFE co-solvent and DPC micelles are very similar with a definite kink in the middle of both helices [although the angle between the two helical regions is greater in the former (Figs. 5.8 and 5.11)]. The angle of this kink in both solvent systems is less than the average value for kinked helices in proteins as determined in a recent statistical survey (Kumar and Bansal, 1998) and earlier work (Barlow and Thornton, 1988). The twenty-three amino acid antimicrobial peptide, magainin 2 also adopts very similar helical structures in TFE/water and DPC micelles (Gesell *et al.*, 1997). Likewise, the structures of the helical peptide, δ-hemolysin, are similar in DPC micelles (Lee *et al.*, 1987) and in methanol (Tappin *et al.*, 1988). These studies suggest that organic solvents (e.g. TFE/water mixtures or methanol solutions) give rise to representative structures for amphipathic helices in a lipid environment.

Other NMR studies have shown that other amphipathic helices containing a central proline residue have a similar central bend, e.g. melittin in methanol has a kink of 20° between the two helical portions (Bazzo *et al.*, 1988; Dempsey *et al.*, 1991), alamethicin in methanol has a central bend (Esposito *et al.*, 1987), cecropin A in hexafluoroisopropylalcohol/water has a large degree of flexibility in its middle (Holak *et al.*, 1988), buforin II in TFE/water is similar (Yi *et al.*, 1996) and caerin 1.1 in TFE/water has a large kink and flexibility in its middle (Wong *et al.*, 1997). Barlow and Thornton (1988) observed similar behaviour for these types of helices in X-ray crystal structures of proteins. In proline-containing peptides, the enhanced

flexibility in the vicinity of the proline arises from the extra freedom available to the peptide in this region due to the backbone hydrogen bonding pattern being disrupted by the absence of an NH group on the proline (Bazzo *et al.*, 1988). Using X-ray crystallographic data, Woolfson and Williams (1990) examined the structural features of proline-containing helices within proteins. They found that in all these bent helices, the relatively hydrophobic proline residue is found on the hydrophilic side of the helix. In maculatin 1.1, Pro15 is similarly placed on the hydrophilic side of the peptide (Fig. 5.11). Likewise, in caerin 1.1, Pro15 and Pro19 are found on this side of the peptide (Fig. 5.1). From the crystal structures, the kink in these types of helices enables water or hydrogen bonding acceptor amino acid sidechains to perform the hydrogen bonding role that is lost due to the presence of the proline, i.e., to the carbonyl of the amino acid four residues earlier in the amino acid sequence (Woolfson and Williams, 1990).

Magainin 2 does not have a central proline residue but adopts an α-helical structure in DPC with a bend in the middle of its sequence centred about a phenylalanine-glycine moiety such that the angle between the two helical segments is 16° (Gesell *et al.*, 1997). Other non-proline-containing amphipathic helices are often curved (Barlow and Thornton, 1988; Zhou *et al.*, 1992; ; McLeish *et al.*, 1994; Kumar and Bansal, 1998; Wegener *et al.*, 1999). Zhou *et al.* (1992) discovered that there is a periodic distribution of NH chemical shifts in amphipathic helices which is due to the curvature of the peptide leading to shorter hydrogen bonds on the hydrophobic face of the peptide. For maculatin 1.1 in TFE/water and DPC, this is consistent with the kink in the peptide which leads to hydrophobic amino acid side-chains being

localised on the concave side of the peptide (Fig. 5.11). The majority of helices in proteins are curved with a mean radius of curvature of 65 ± 30 Å (Barlow and Thornton, 1988; Blundell *et al.*, 1983; Kumar and Bansal, 1998) which is approximately 2.5 times greater than that observed for Ala15 maculatin 1.1. Thus, Ala15 maculatin 1.1 has only a small amount of curvature and there is reduced flexibility in the central portion compared to maculatin 1.1 (Figs 5.8 and 5.11). The greater kink and flexibility imparted by the central proline residue in maculatin 1.1 (and other proline-containing amphipathic peptides) would enable optimal amphipathic distribution of its amino acids and thereby precise interaction of the peptide with the membrane surface, e.g. the positively charged amino acids with the anionic phospholipids as discussed in Section 2.4.

In agreement with the above discussion, the structure/bioactivity data on maculatin 1.1 indicate that changing Pro15 to an alanine reduces the bioactivity of the peptide by a factor of 5-10 fold (Table 5.1). Thus, Pro15 is a necessary prerequisite for the full activity of maculatin 1.1 possibly due to its ability to rotate the C-terminal helical segment to form an amphipathic helix (Fig. 5.11). In the Ala15 analogue, however, the relative rigidity of the helix causes hydrophilic His20 to be positioned on the hydrophobic side of the peptide (Fig. 5.11). As a consequence, the amphipathic nature of the helix is lost, causing a significant decrease in bactericidal activity.

The mechanism of membrane lysis by antimicrobials is still a matter of some debate (Shai, 1995; Bechinger, 1997). Solid state NMR studies of magainin and cecropin

incorporated into lipid bilayers have shown that these peptides lie parallel to the surface of synthetic model membranes, suggesting that they both adopt the carpet mechanism when permeabilising membranes (Bechinger *et al.*, 1992 and 1993; Marassi *et al.*, 1999). In contrast, experimental evidence has shown that cytolytic peptides such as alamethicin and melittin adopt the channel mechanism to form transmembrane pores (see table 2.1). Both maculatin 1.1 and caerin 1.1 have central proline residues and are long enough (> 20 amino acids) to span a membrane when in a helical conformation. It is conceivable, therefore, that both peptides could utilise the channel mechanism. However, solid-state NMR studies have revealed that antimicrobial amphibian peptides magainin and its analogue, PGLa adopt the carpet mechanism (Bechinger *et al.*, 1991, 1992, 1993, 1996 and 1998). Similar conclusions have been obtained for maculatin 1.1 using the same technique (Section 5.6). These peptides are found with their helical axis oriented parallel to the plane of the bilayer, suggesting that they exert their bactericidal action *via* the carpet mechanism. In this model, the peptide is most likely to be arranged so that its hydrophobic side is within the hydrocarbon chains of the lipids and its hydrophilic side interacts with the lipid polar headgroups and aqueous solution. This results in membrane thinning and destabilisation to accommodate the peptide, ultimately lysing the cell (Durell *et al.*, 1992, Bechinger, 1999).

Presently, it is unknown why both maculatin 1.1 and caerin 1.1 are not active against Gram-negative bacteria. Although these bacteria have outer membranes which act as effective barriers against various antibiotics (Hancock, 1984), they should still be susceptible to membrane-disrupting peptides. One reason could be due to the

presence of lipopolysaccharide (LPS) on the outer membrane surface. Being anionic in nature, they may bind irreversibly to cationic bactericidal peptides, preventing the latter from reaching and disrupting the bacterial membrane. Orientation studies (using solid-state NMR techniques in particular) and molecular dynamics simulations involving maculatin 1.1 and phospholipids/LPS bilayers may resolve this issue.

Chapter 6
Uperin 3.6 and Analogues

Uperoleia mjobergii

6.1 Uperin 3.6 and Analogues

Toadlets of the genus *Uperoleia* have host defence peptides which fulfil similar roles to those from tree frogs of the genus *Litoria*. However, the sequences of the peptides from the two genera are quite different. These include the two related wide-spectrum antibiotic peptides named uperin 3.5 and uperin 3.6 isolated from the toadlet *Uperoleia mjobergii* (Bradford *et al.*, 1996). These amphibians are found in the flood plains of the Kimberley region of Western Australia (Fig 6.1) and adult specimens typically grow up to an average of 2 cm in length.
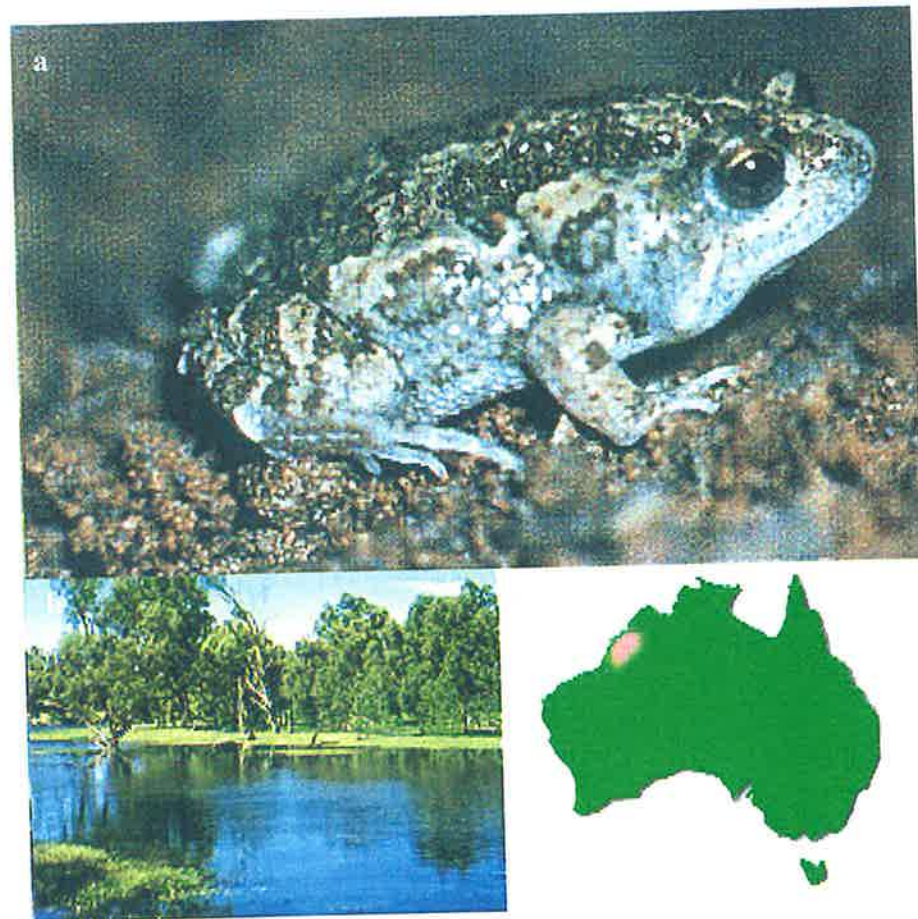
Fig. 6.1 **(a)** *Uperoleia mjobergii* (note warty protuberances on the dorsal surface of the skin), **(b) a flood plain in the Kimberly region of western Australia (c) geographical distribution on the toadlet (shaded pink).**

The skin secretions of these toadlets are stored in granular glands which can be seen as warty protuberances on the dorsal surface of the animal (Fig 6.1). They deliver a number of peptides onto the skin surface when the animal is stressed or attacked, in particular, the antimicrobial peptides uperin 3.5 and 3.6. Both have similar bioactivities to those of caerin 1.1 and maculatin 1.1 (see Table 6.1). Both peptides contain 17 amino acids and are therefore significantly shorter in length than the twenty-five residue caerin 1.1 and twenty-one residue maculatin 1.1 (see Section 5.1). This raises the question as to why such dissimilar structures should have similar spectra of antibiotic activities. Another interesting question is whether the positively charged residues in the uperin peptides are essential for its bactericidal properties. Most natural antibacterial and haemolytic peptides are positively charged [see Dathe and Wieprecht (1999) and Sitaram and Nagaraj (1999) for reviews]. The role of positive charges is essential for the electrostatic interaction with the anionic cytoplasmic membranes of bacteria. For example, the electrically neutral twenty-seven residue δ-haemolysin is highly haemolytic but devoid of antimicrobial activity. Substituting certain residues with lysines induced potent antibacterial activities in the peptide (Dhople and Nagaraj, 1995). Increasing the number of positive charges of magainin 2 also enhanced its bactericidal potency (Bessale *et al.*, 1992) while a reduction of the number of positive charges resulted in the loss of antimicrobial activity (Matsuzaki *et al.*, 1997b).

In an effort to gain a deeper insight on their mechanisms of bactericidal action, a number of synthetically modified analogues were synthesised. The primary sequences of the natural uperin peptides and their analogues are shown overleaf:

Uperin 3.5   GVGDL IRKAV SVIKN IV-NH$_2$

Uperin 3.6   GVIDA AKKVV NVLKN LF-NH$_2$

Ala4 uperin 3.6   GVIAA AKKVV NVLKN LF-NH$_2$

Ala7 uperin 3.6   GVIDA AAKVV NVLKN LF-NH$_2$

Ala14 uperin 3.6   GVIDA AKKVV NVLAN LF-NH$_2$

The antibiotic activities of the uperin peptides and their synthetic analogues are summarised in Table 6.1.

Table 6.1   Antimicrobial activities of the uperin 3.5, 3.6 and three synthetic analogues.

Organism	MIC (µg/mL)						
	Caerin 1.1[a]	Maculatin 1.1[b]	Uperin 3.5	Uperin 3.6	Ala4 uperin 3.6	Ala7 uperin 3.6	Ala14 uperin 3.6
Bacillus cereus	50	50	25	25	25	100	100
Escherichia coli	>100	>100	>100	>100	>100	>100	>100
Leuconostoc lactis	1.5	3	3	3	3	12	12
Listeria innocua	25	100	50	50	25	>100	>100
Micrococcus luteus	12	12	25	50	12	>100	100
Pasteurella multocida	25	50	100	>100	>100	>100	>100
Staphylococcus aureus[c]	3-12	6-12	50	25	25-50	>100	>100
Staphylococcus epidermidis	12	12	12	12	12	>100	100
Streptococcus faecalis	25	25	12	12	>100	>100	>100
Streptococcus uberis	12	3	12	12	25	50	100

[a]The data for caerin 1.1 were taken from Wong *et al.* (1997).
[b]The data for maculatin 1.1 were taken from Chia *et al.* (2000).
[c]Two strains were tested (ATCC type strains 25923 and 29213).

It can be clearly seen that substituting positively charged lysines with neutral alanine results in a significant reduction of antimicrobial activity. This suggests that positive electric charges are important for the antimicrobial activity of uperin 3.6. In the subsequent sections, detailed studies will be conducted on uperin 3.6 in order to gain a better understanding to its mechanism of action.

6.2 Structural Studies

Uperin 3.6 displays a distinct amphipathic α-helical distribution of amino acids when represented on an Edmundson helical wheel (Fig 6.2).
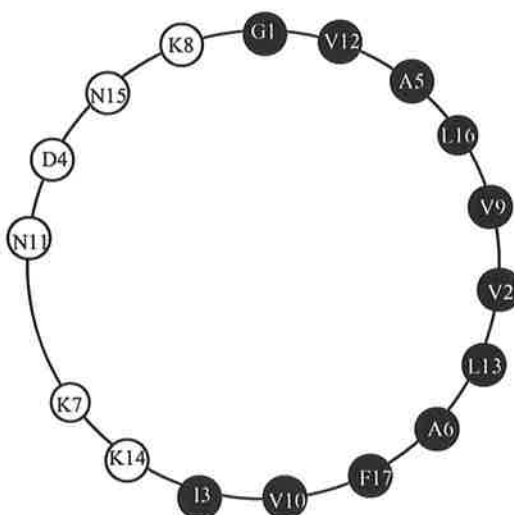
Fig. 6.2 Edmundson helical wheel representation of uperin 3.6. Hydrophobic and hydrophilic residues are represented by black and white circles respectively.

In this chapter, CD, NMR spectroscopy and computer based modelling techniques were used to determine the 3D structure of uperin 3.6 in TFE/water mixtures.

6.3 Circular Dichroism Studies

CD spectra of uperin 3.6 were measured under increasing concentrations from 0-50% (by vol.) of TFE in water (see Fig. 6.3). At low concentrations of TFE (0-10%), uperin 3.6 exhibits a spectrum characteristic of an unstructured peptide, i.e. a broad minimum at 200 nm was observed. On increasing the TFE concentration, the spectra underwent a marked change to one indicative of a predominantly α-helical structure, i.e. two minima in the vicinity of 208 nm (π-π* transition) and 220 nm (n-π* transition) were observed. Spectra at intermediate concentration (20-30% TFE) showed reduced helical content as evidenced by both a lower ellipticity and a shift of the minima around 208 nm to lower wavelengths. The spectra at 40% and 50% TFE showed greatest ellipticity at these minima, indicative of maximum helical conformation. Based on this evidence, NMR studies were undertaken in a 50% TFE/water mixture. (It should be noted that a 50% (by vol.) TFE/water mixture corresponds to a mole fraction of 20:80 respectively, i.e. to relatively small amounts of TFE on a molar basis).
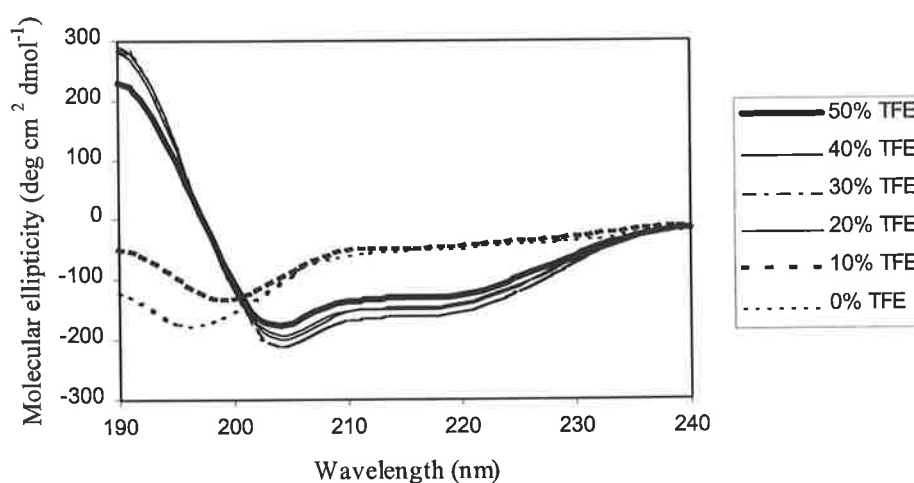
Fig 6.3 CD spectra of uperin 3.6 at varying amounts (by vol.) of TFE.

6.4 NMR Studies

On the basis of the CD results, NMR spectra of uperin 3.6 were acquired under conditions which exhibited maximal helical structure, i.e. 50% (by vol.) TFE. Fig. 6.4 shows a region of the TOCSY spectrum and the NH region of the NOESY spectrum of uperin 3.6 in which a series of strong sequential NH to NH NOEs $[d_{NN}(i,i+1)]$ were observed along the length of the peptide. Weaker $d_{NN}(i,i+2)$ NOEs can also be observed in this region. Using $d_{NN}(i,i+1)$ and $d_{\alpha N}(i,i+1)$ sequential connectivities, all proton resonances of uperin 3.6 were assigned. Assignments for all ^{1}H and ^{13}C$^\alpha$ resonances are tabulated in Table 6.2.

A summary of NOEs involving the NH, C$^\alpha$H and C$^\beta$H protons obtained from the NOESY spectra are presented in a connectivity diagram (Fig. 6.5). This figure shows a large number of connectivities indicative of an α-helix. For example, the presence of strong $d_{NN}(i,i+1)$ NOEs complemented by weaker $d_{\alpha N}(i,i+1)$ NOEs, a series of NOEs from residues three and four amino acids apart in the peptide, i.e., $d_{\alpha N}(i,i+3)$, $d_{\alpha\beta}(i,i+3)$, $d_{\alpha N}(i,i+4)$ and eight $d_{NN}(i,i+2)$ NOEs were observed. Finally, $^3J_{HNC\alpha H}$ values that could be measured mostly had values less than 5 Hz, consistent with a helical structure. In summary, the NOE data and intensities suggest that a helical secondary structure for uperin 3.6 commences at Val2 and continues to Phe17.
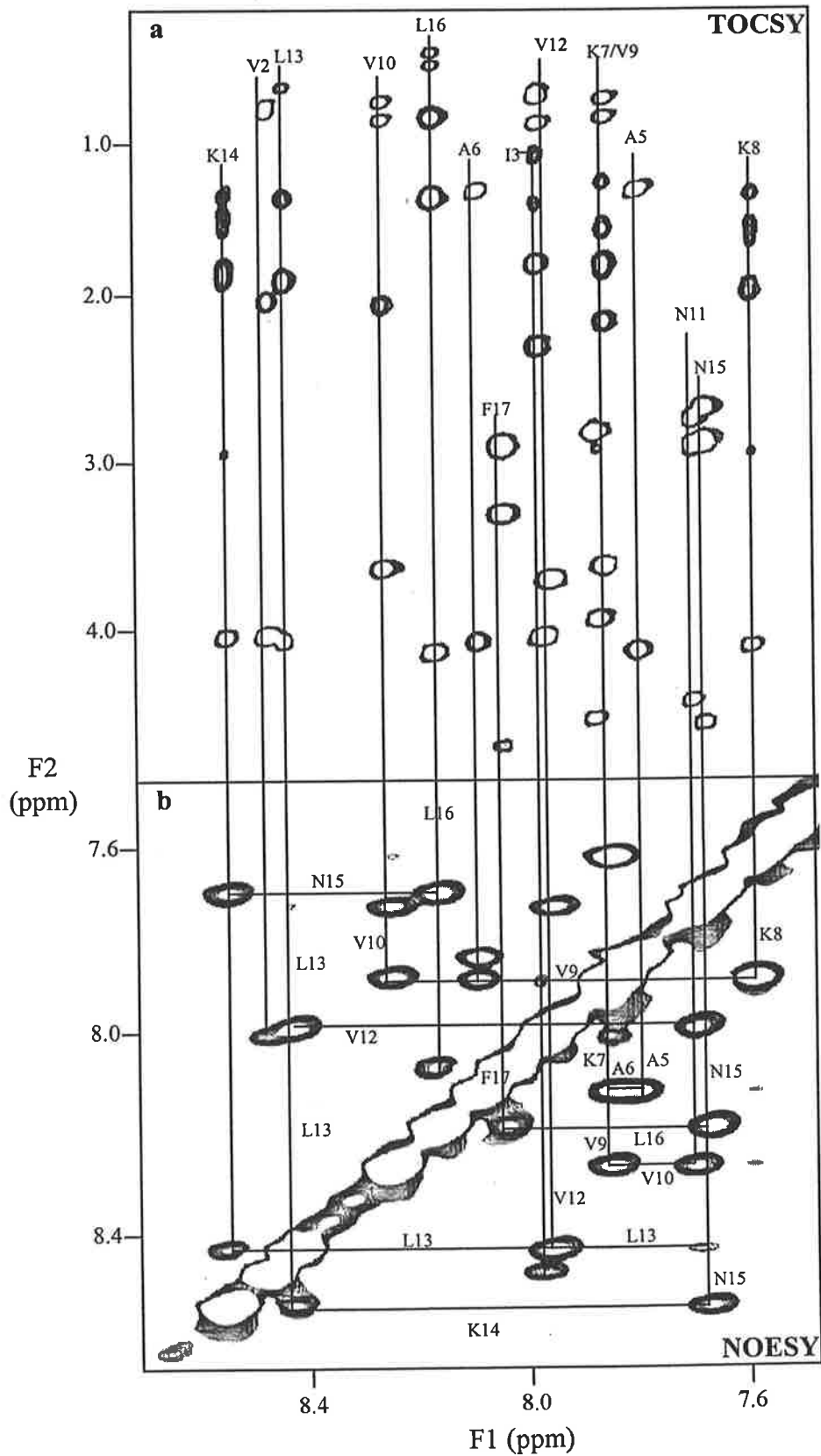
Fig 6.4 (a) A region of the TOCSY spectrum showing NH to sidechain proton couplings, (b) NH region of the NOESY spectrum of uperin 3.6 in TFE/water. Connectivities between sidechain and backbone amide protons are indicated.

137

Table 6.2 ^{1}H and ^{13}C NMR chemical shifts for uperin 3.6 in d_3-TFE/water (1:1 by vol.) pH 2.4, 25°C.

Residue	Chemical Shifts (ppm)				
	NH	C$^\alpha$H	C$^\beta$H	others	C$^\alpha$
Gly 1	not observed	3.93, 3.99	-	-	42.3
Val 2	8.46	4.04	2.11	γ-CH$_3$=1.03, 1.03	63.5
Ile 3	7.98	4.04	1.90	γ-CH$_2$=1.28, 1.56 γ-CH$_3$=0.94 δ-CH$_3$=1.00	61.6
Asp 4	7.88	4.52	2.87	-	54.2
Ala 5	7.82	4.14	1.49	-	54.2
Ala 6	8.10	4.08	1.49	-	54.1
Lys 7	7.87	3.94	1.91	γ-CH$_3$=1.44, 1.49 δ-CH$_2$=1.70 ε-CH$_2$=2.97	58.5
Lys 8	7.62	4.12	1.90, 2.01	γ-CH$_2$=1.47 δ-CH$_2$=1.61, 1.71 ε-CH$_2$=2.95	58.4
Val 9	7.87	3.66	2.24	γ-CH$_3$=0.96, 1.07	65.8
Val 10	8.25	3.65	2.14	γ-CH$_3$=0.97, 1.09	65.8
Asn 11	7.72	4.42	2.81, 2.95	δ-CONH$_2$=6.77, 7.51	55.9
Val 12	7.96	3.72	2.38	γ-CH$_3$=0.96, 1.10	65.8
Leu 13	8.42	4.06	1.97	γ-CH$_3$=1.52 δ-CH$_2$=1.61, 1.71	57.4
Lys 14	8.54	4.04	1.92, 1.98	γ-CH$_3$=1.52 δ-CH$_2$=1.62 ε-CH$_2$=2.95	58.3
Asn 15	7.69	4.55	2.74, 2.93	δ-CONH$_2$=6.77, 7.42	54.7

Leu 16	8.17	4.12	1.52	γ-CH$_3$=1.07 δ-CH$_2$=0.69, 0.77	56.2
Phe 17	8.05	4.63	2.96, 3.34	Aromatic H=7.27, 7.31, 7.32 CONH$_2$=6.94 , 7.17	56.8

G1 V2 I3 D4 A5 A6 K7 K8 V9 V10 N11 V12 L13 K14 N15 L16 F17

$^3J_{\text{NHC}\alpha\text{H}}$ 4.3 3.0 * 3.6 @ * @ * @ @ @ @ @ 6.7 5.3 8.0

G1 V2 I3 D4 A5 A6 K7 K8 V9 V10 N11 V12 L13 K14 N15 L16 F17
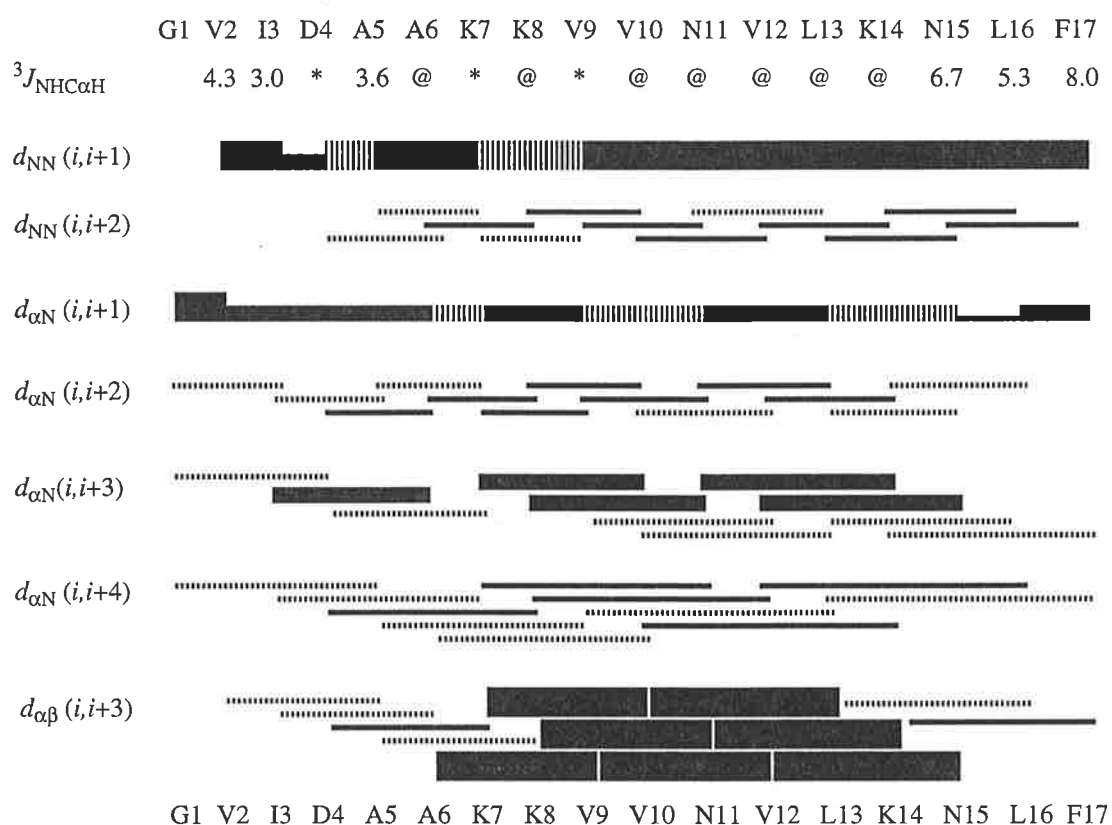
Fig. 6.5 **A summary of NOEs used for structure calculation of uperin 3.6 in 50% (by vol.) d_3-TFE, pH 2. 4, 25°C.** The amino acid sequence of the peptide is given at the top of the diagram and the values of $^3J_{\text{NHC}\alpha\text{H}}$ were obtained from high-resolution 1D ^{1}H spectra. @ indicates no coupling constants were detected for the corresponding residue. Asterisks (*) indicate that coupling constants could not be unambiguously assigned due to overlap. The various types of NOEs and their relative strengths are indicated by the thickness of the bars (strong, medium and weak). For the basis of this diagram, NOEs are classified on the basis of strong (< 2.7 Å), medium (between 2.7 to 3.5 Å) and weak (> 3.5 Å). Dashed lines represent connectivities that could not be unambiguously assign due to overlap, e.g. with an intraresidue NOE.

The presence of a helical structure is also indicated from an examination of the deviation from random coil chemical shift values of the α–CH ^{1}H and ^{13}C resonances. Although a complete set of random coil chemical shifts are not available for amino acids in TFE, those which have been tabulated indicate that there is little difference between random coil chemical shifts in TFE and water (Merutka *et al.*, 1995). A comparison was made with random coil chemical shifts determined in water. For a window of n = ±2 residues, smoothed plots for the ^{1}H resonances showed a distinct upfield shift (see Fig. 6.5a) and those for the ^{13}C resonances exhibited a distinct downfield shift along the peptide (see Fig. 6.5b). A negative chemical shift difference indicates an upfield chemical shift compared to the random coil value. Statistical analysis of the α–CH ^{1}H and ^{13}C chemical shifts in structural regions of proteins has shown that α-helical regions give more to a marked upfield ^{1}H and downfield ^{13}C chemical shift compared to random-coil values. The directions of the deviations from random coil chemical shifts in uperin 3.6 are thus consistent with helical structure for the peptide with maximum helicity being present in the central region of the peptide.
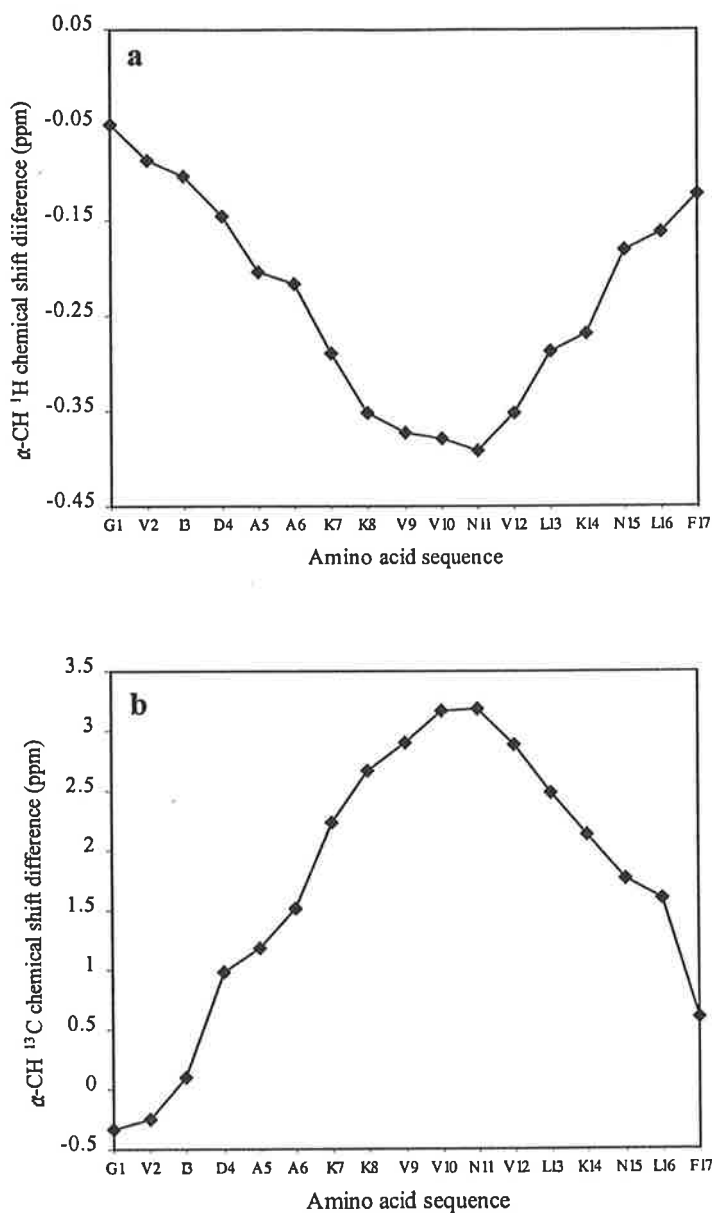
Fig. 6.6 **Deviation from random coil chemical shifts of (a) ^{1}H α-CH resonances and (b) ^{13}C α-CH resonances of uperin 3.6 in 50% (by vol.) d_3-TFE, pH 2. 4, 25°C. A window of ±2 residues was used. Upfield and downfield chemical shifts are indicated by negative and positive values respectively.**

6.5 Structural Analysis

The conclusions derived from the examination of the NMR data presented above are confirmed when the NOESY data were used as input for calculations. Structural

calculations were based on a total of 319 NOE distance restraints comprising of 132 intra-residue restraints, 77 (i, i+1) sequential restraints, 110 medium-range restraints and 13 ϕ angle restraints. Following calculations, structures were minimised with respect to potential energy *via* conjugate-gradient methods. The final run produced 60 conformers from which the 20 of the most stable (lowest potential energy) conformers were chosen for detailed examination. The statistics for these structures are presented in Table 6.3.

Table 6.3 Structural statistics of uperin 3.6 in 50% (by vol.) d_3-TFE, pH 2. 40, 25°C following RMD/SA calculations*.

RMSD from mean geometry (Å)	<SA> *	(SA)$_r$
All heavy atoms	0.42 ± 0.10	
All heavy backbone atoms (N, C$^\alpha$ and C')	0.10 ± 0.04	
X-PLOR energies (kcalmol^{-1})		
E_{tot}	129.16 ± 12.30	127.70
E_{bond}	10.12 ± 1.46	10.76
E_{angle}	40.49 ± 2.81	40.89
E_{impr}	7.51 ± 1.14	6.63
E_{repel}	16.72 ± 2.97	16.73
E_{NOE}	53.64 ± 7.28	52.67
E_{cdih}	0.66 ± 0.64	0.12

* <SA> is the ensemble of the 20 final structures, (SA) is the mean structure obtained by best-fitting and averaging the coordinates of the well-defined heavy backbone N, C$^\alpha$ and C' atoms of the 20 final structures. (SA)$_r$ is the representative structure obtained after restrained energy minimisation of the mean structure.

Number of NOEs violate > 0 2Å = 18. Maximum violation is 2.80 Å.

Chapter 6

The superimposition of the twenty most stable structures over the entire backbone N,

C^α and C' atoms is shown in Fig. 6.7.

Gly 1

Phe 17
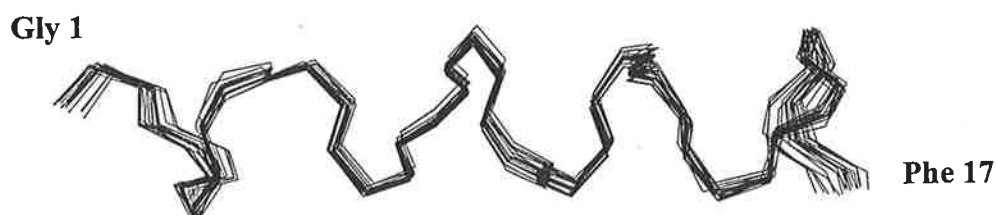
Fig. 6.7   Superposition of backbone atoms of the 20 most stable structures of uperin 3.6 in 50% (by vol.) d_3-TFE, pH 2. 4, 25°C

Analysis of the angular order parameters (S, ϕ and ψ) of all three groups of the

twenty structures indicates that all non-terminal residues are well defined (Val2 to

Phe17) with $S > 0.9$ for both their ϕ and ψ angles (Fig. 6.8).
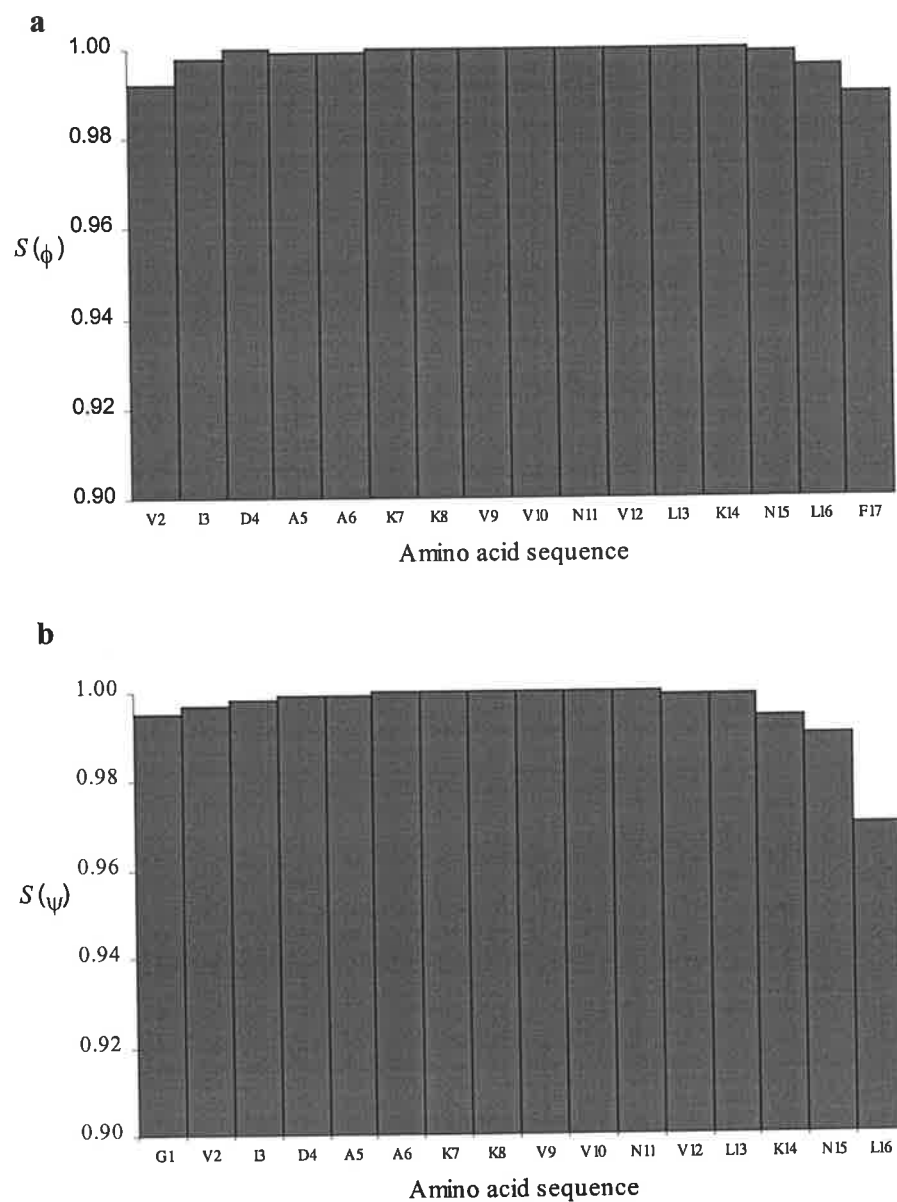
Fig. 6.8 **Plots of Angular Order Parameters (a) $S(\phi)$ and (b) $S(\psi)$ against amino acid sequence for uperin 3.6 in 50% (by vol.) d_3-TFE, pH 2. 4, 25°C.**

The Ramachandran plot of uperin 3.6 (Fig 6.9) showed all non-glycine residues had their averaged backbone dihedral angles (ϕ and ψ) within the 'favoured' (A) α-helical region, the only exception being Leu16 which is in the 'allowed' (a) region, possibly indicating a region of flexibility near the C-terminal.
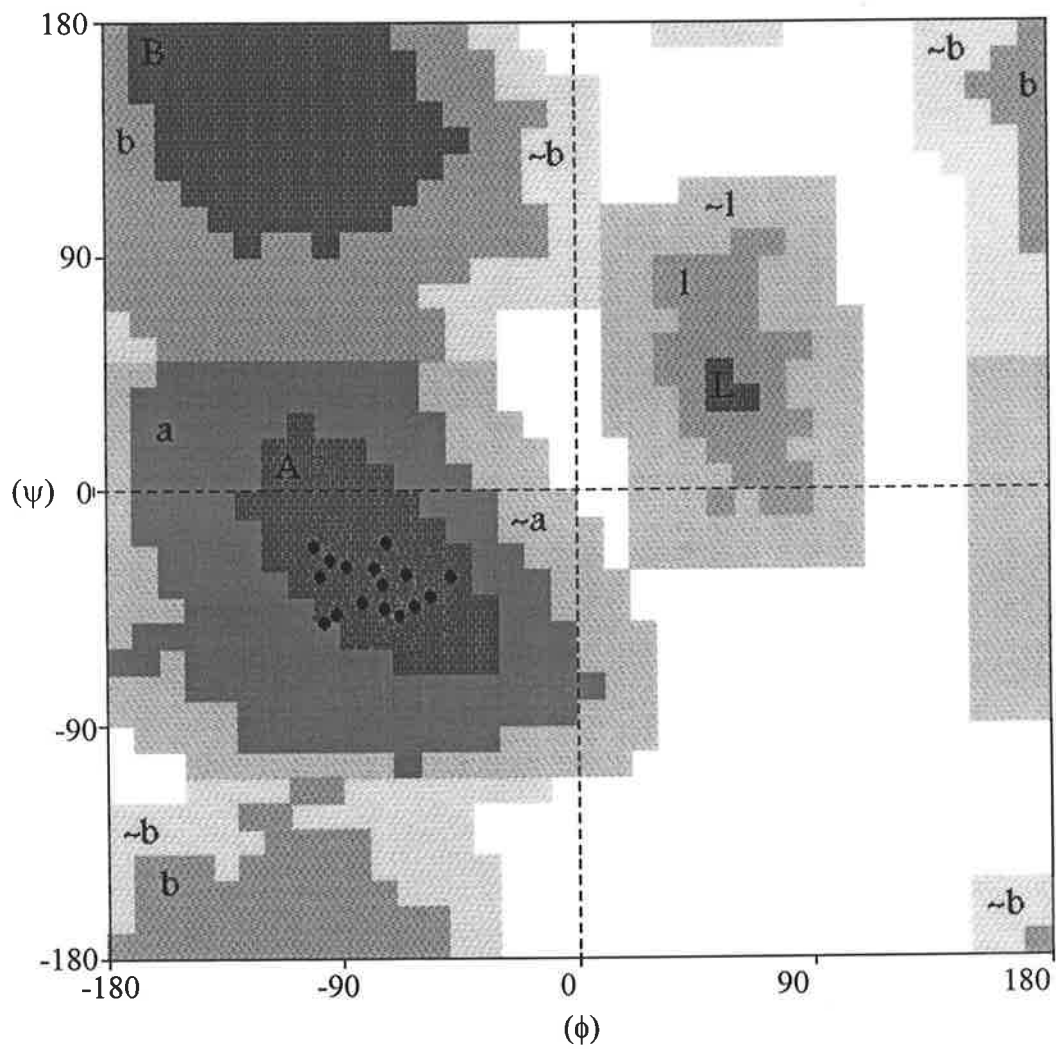
Fig 6.9   Ramachandran plot of the average backbone ϕ and ψ angles of uperin 3.6.

The most stable structure (lowest potential energy) of uperin 3.6 is shown in Fig. 6.10. It is apparent from this representation that uperin 3.6 has an amphipathic helical structure with distinct hydrophobic and hydrophilic faces.
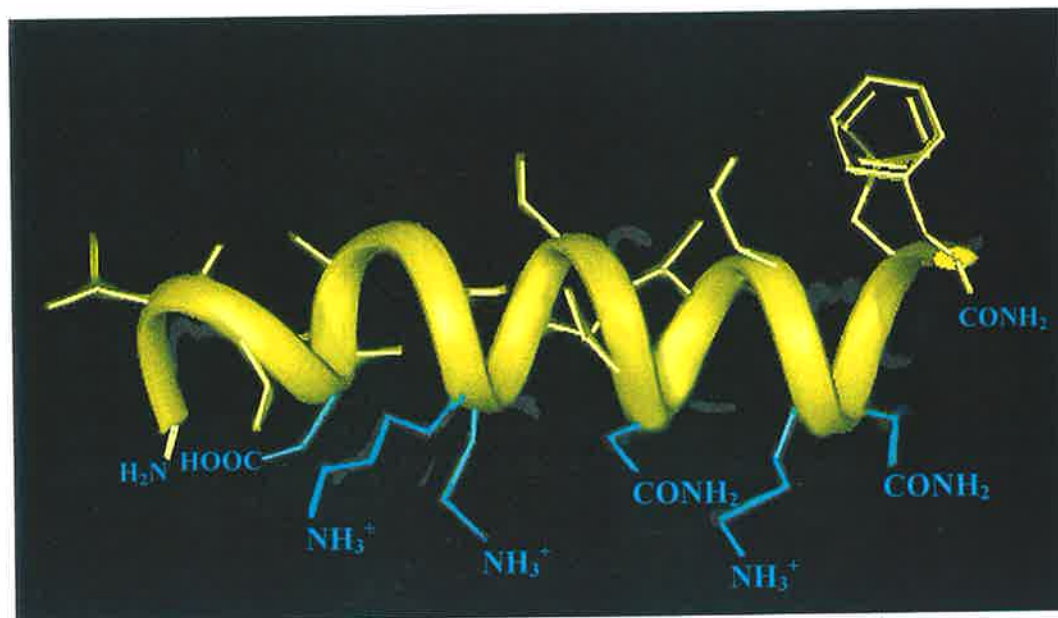
Fig 6.10 The most stable structure (lowest potential energy) of uperin 3.6.
The projection demonstrates the well-defined hydrophobic and hydrophilic zones (blue). The polypeptide backbone is represented by the ribbon.

6.6 Discussion

The antibiotic activities of the membrane-active amphipathic uperin peptides are listed in Table 6.1. With the exception of the activity against *Staphylococcus aureus*, the spectra of activities of uperin 3.5 and uperin 3.6 are quite similar to that of caerin 1.1 and maculatin 1.1. Both caerin 1.1 and maculatin 1.1 are helical with a region of flexibility about Pro15 (see Chapter 5). This flexibility enables both peptides to interact with a variety of membrane surfaces by rearranging their backbone conformations to optimise their interactions with the bacterial membrane surface.

Such an ability would account, at least in part, for both their broad-spectrum antibiotic activities. In contrast, neither uperin 3.5 and 3.6 have proline residues and the three-dimensional solution structure of uperin 3.6 shows that it adopts a well-defined amphipathic helix along its entire length with no central region of flexibility (Fig 6.7 and 6.10). Despite these differences, uperin 3.5 and 3.6 exhibit similar broad-spectrum antibiotic activities to caerin 1.1 and maculatin 1.1 (see Table 6.1). One reason for their similar activity profile may be that the two peptides have different overall charges. Caerin 1.1 has three histidine residues and assuming that these have similar pK_a values for an isolated histidine, they will be uncharged at neutral pH. Thus at pH 7, caerin 1.1 will have an overall charge of +1, whereas uperin 3.5 and 3.6 (which have no histidine residues) will possess an overall charge of +3. This suggests that the significantly higher overall charge of uperin 3.5 and 3.6 compared to caerin 1.1 would enable the former to interact electrostatically more strongly with the anionic phospholipids on a typical bacterial membrane. For this reason, uperin 3.6 may be able to compensate for the lack of flexibility in its central region that caerin 1.1 possess. This proposal is supported by the bioactivity data for alanine-substituted uperin 3.6 peptides listed in Table 6.1. Substitution of the negatively charged Asp4 by an uncharged alanine residue induces only minor changes in the activity data, while replacement of either Lys7 or Lys15 with alanine reduces the activity significantly.

The studies above emphasise the importance of the overall cationic peptide charge for the interaction with bacterial membranes. However, a simple correlation between

the number and position of cationic residues on the one hand and antimicrobial specificity on the other hand does not seem to exist.

In Chapter 5, solid-state NMR studies suggest that maculatin 1.1 adopts the carpet mechanism in favour of the transmembrane channel-forming mechanism. Which mechanism will uperin 3.6 adopt? As mentioned in Chapter 2, a typical bacterial cytoplasmic membrane is about 30 Å in thickness. Since the distance between successive amino acids in an α-helix is 1.5 Å, a minimum of 20 amino acids is required for an α-helical peptide to span a membrane. Uperin 3.6, with only 17 amino acids, is not long enough to traverse a bacterial membrane. Therefore, it is unlikely that it would follow the channel mechanism, unless the peptide forms head-to-head or head-to-tail dimers in a similar manner to gramicidin A (see Section 2.6). 2D NMR results in TFE/water do not indicate uperin 3.6 undergoing dimerisation. NMR studies of the peptide incorporated into phospholipid micelles may shed light into this.

The NMR and activity data presented herein for uperin 3.6 are consistent with the initial phase of the carpet and channel mechanism, i.e., the formation of an amphipathic helix followed by electrostatic interaction to the bacterial membrane. However, the next step involving the way the peptide penetrates a phospholipid membrane is yet to be determined. Solid-state NMR studies involving the peptide interacting with phospholipid bilayers may resolve this issue.

Chapter 7
The Caerin 4 Peptides
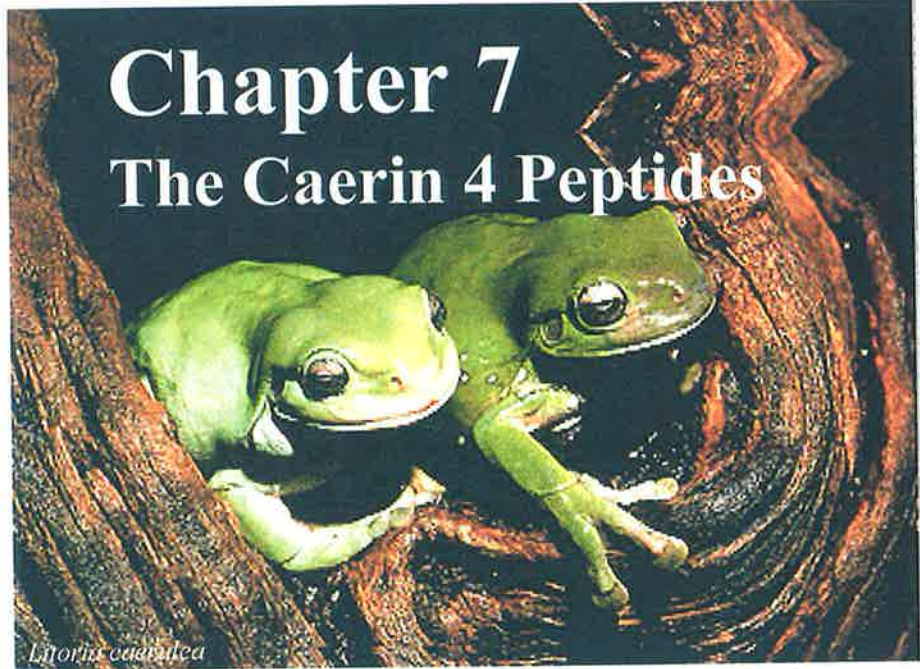
Litoria caerulea

7.1 The Caerin 4 Antimicrobial Peptides

The caerin 4 family of antimicrobial peptides (shown below) are isolated from the Australian green tree frog *Litoria caerulea* (Stone *et al*., 1993). It is a medium sized tree frog measuring from 6 to 11 cm in length and is found in tropical rainforests of Australia (Barker *et al*., 1995) (Fig 7.1).

Caerin 4.1   GLWQK IKSAA GDLAS GIVEG IKS-NH$_2$

Caerin 4.1   GLWQK IKSAA GDLAS GIVEG IKS-NH$_2$

Caerin 4.3   GLWQK IKNAA GDLAS GIVEG IKS-NH$_2$
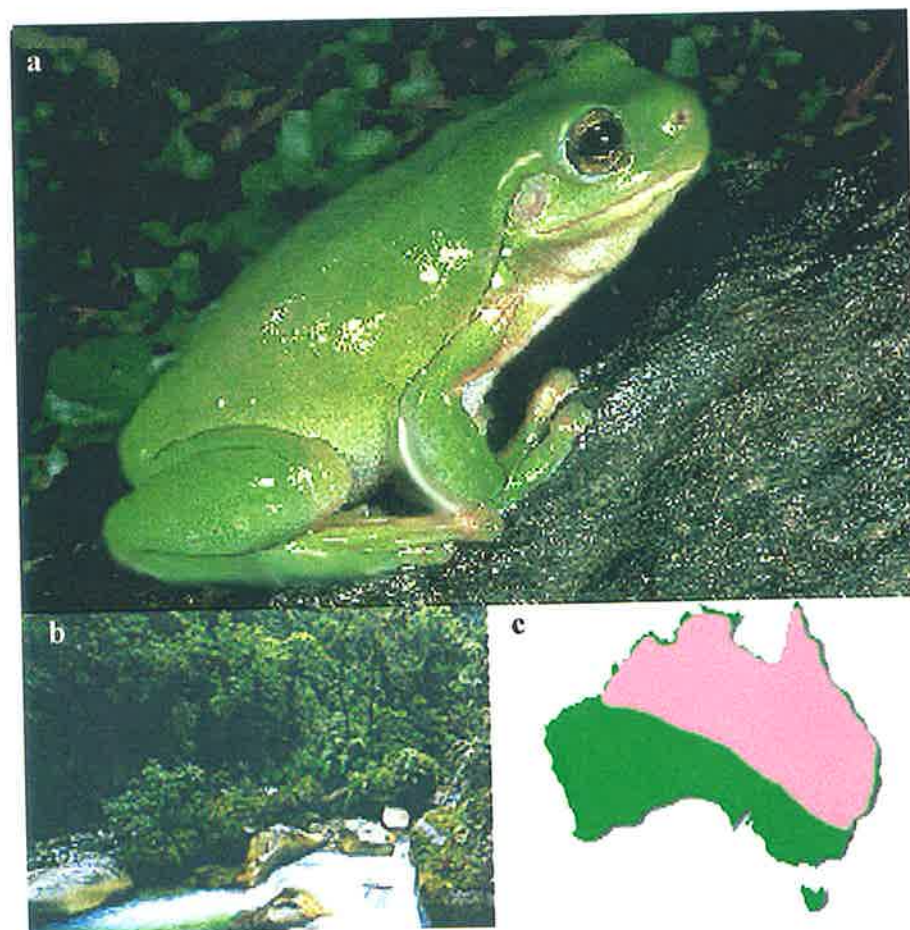
Fig. 7.1   (a) *Litoria caerulea* (b) a tropical rainforest in Australia (c) geographical distribution of the frog (shaded pink).

Chapter 7

The antibiotic activities of the caerin 4 family of peptides are summarised in Table 7.1.

Table 7.1   Antibiotic activities of the caerin 4 family of peptides as shown by MIC* tests (values given in µg/ml).

| Organism | MIC (µg/mL) | | |
	Caerin 4.1[a]	Caerin 4.2	Caerin 4.3
Bacillus cereus			
Escherichia coli	25	50	50
Leuconostoc lactis			
Listeria innocua			
Micrococcus luteus	12.5	6	25
Pasteurella multocida	< 0.4	< 0.4	< 0.4
Staphylococcus aureus			
Streptococcus faecalis			
Streptococcus uberis			

If there is no figure indicated, the MIC value is > 100 µg/ml.
All data are taken from Bradford *et al.* (1996)
[a] Caerin 4.1 has also been tested against several viruses (HIV 1, *Herpes simplex* 1 and 2) and cancers (L1210 mouse leukaemia and SKOV ovarian cancer). Unlike caerin 1.1 (see Chapter 5), caerin 4.1 showed no significant activity against these pathogens.

Caerin 4.1 is a narrow spectrum antibiotic which shows potent activity against *Pasteurella multocida* (swine fever); this activity is high enough to suggest that the

peptide should be investigated as a veterinary product. It is also interesting to note that caerin 4.1 is active against Gram-negative *Escherichia coli*, which is not a general feature of amphibian peptides studied. Indeed, the bioactivity of caerin 4.1 against *Escherichia coli* is the best yet recorded for a peptide from an Australian amphibian (MIC = 25μg/mL). The 3D structure of caerin 4.1 was investigated using NMR spectroscopy and computer based modelling techniques in order to provide an insight into the mechanism of bactericidal action. This chapter reports the results of an NMR spectroscopic determination of the solution structure of caerin 4.1.

7.2 Structural Studies

Caerin 4.1 does not display a well-defined amphipathic α-helical distribution of amino acids when represented on an Edmundson helical wheel (Fig 7.2).
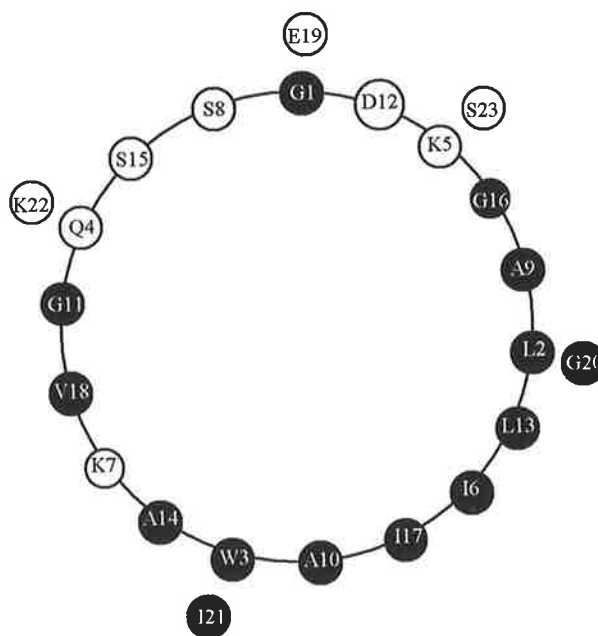
Fig 7.2 Edmundson helical wheel representation showing the non-amphipathic nature of caerin 4.1. Hydrophobic and hydrophilic residues are represented by black and white circles respectively.

From Fig. 7.2, it is apparent that caerin 4.1 is not amphipathic based on the helical wheel representation. More detailed structural studies on the peptide were conducted using CD, NMR spectroscopy and computer based modelling techniques.

7.3 Circular Dichroism Studies

The CD spectra were acquired on caerin 4.1 in the presence of an increasing proportion [from 0 to 50% (by vol.)] of TFE in water (see Fig 7.3). At low amounts of TFE (0-10%), caerin 4.1 exhibits a CD spectrum characteristic of an unstructured peptide, i.e., a broad minimum at 200 nm was observed. On increasing the amount of TFE, the CD spectra indicated the presence of a predominantly α-helical structure, i.e. two minima in the vicinity of 208 nm (π-π^* transition) and 220 nm (n-π^* transition) were observed. The spectra at 40% and 50% TFE showed greatest ellipticity at these minima, indicative of maximum helical conformation. Based on this evidence, NMR studies were undertaken in a 50% (by vol.) TFE/water mixture.
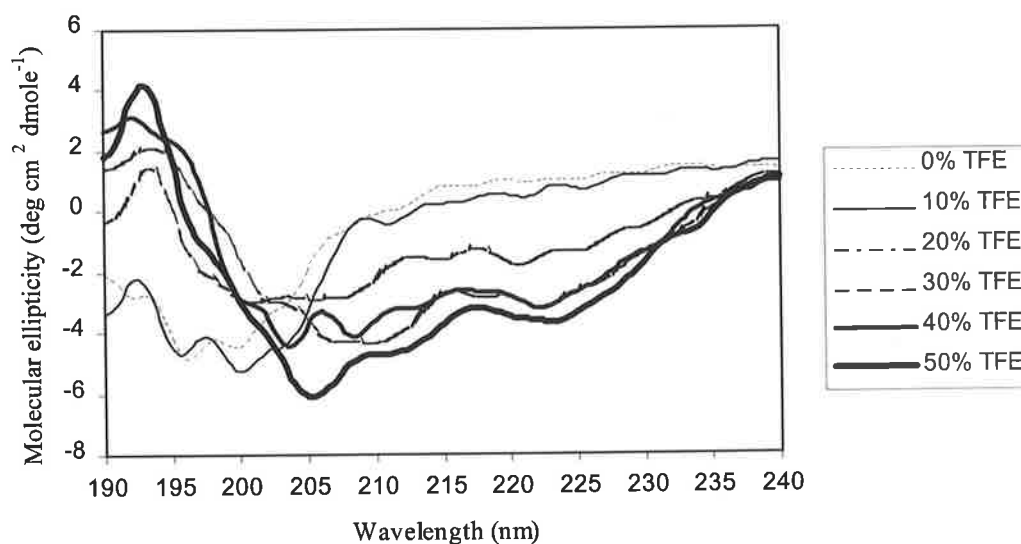
Fig 7.3 CD spectra of caerin 4.1 at varying concentrations (by vol.) of TFE.

7.4 NMR Spectroscopy

The ^{1}H NMR spectrum of caerin 4.1 in 50% (by vol.) TFE was assigned *via* standard methods as discussed in Chapter 3. ^{13}C NMR resonances were assigned from the HSQC spectrum from correlations of the ^{13}C resonances to the assigned ^{1}H resonances. Fig. 7.4 shows a region of the TOCSY spectrum and the NH region of the NOESY spectrum of caerin 4.1 in which a series of strong sequential NH to NH NOEs [$d_{NN}(i,i+1)$] were observed along the length of the peptide. Weaker $d_{NN}(i,i+2)$ NOEs can also be observed in this region. Using $d_{NN}(i,i+1)$ and $d_{\alpha N}(i,i+1)$ sequential connectivities, all proton resonances of caerin 4.1 were assigned. Assignments for all ^{1}H and ^{13}C$^\alpha$ resonances are tabulated in Table 7.2.

A summary of NOEs involving the NH, C$^\alpha$H and C$^\beta$H protons obtained from the NOESY spectra are presented in a connectivity diagram (Fig. 7.5). This figure shows a large number of connectivities indicative of an α-helix. For example, the presence of strong $d_{NN}(i,i+1)$ NOEs complemented by weaker $d_{\alpha N}(i,i+1)$ NOEs, a series of NOEs from residues three and four amino acids apart in the peptide, i.e., $d_{\alpha N}(i,i+3)$, $d_{\alpha\beta}(i,i+3)$, $d_{\alpha N}(i,i+4)$ and three $d_{NN}(i,i+2)$ NOEs were observed. Finally, $^3J_{HNC\alpha H}$ values that could be measured mostly had values less than 5 Hz, consistent with a helical structure. In summary, the NOE data and intensities suggest that a helical secondary structure for caerin 4.1.
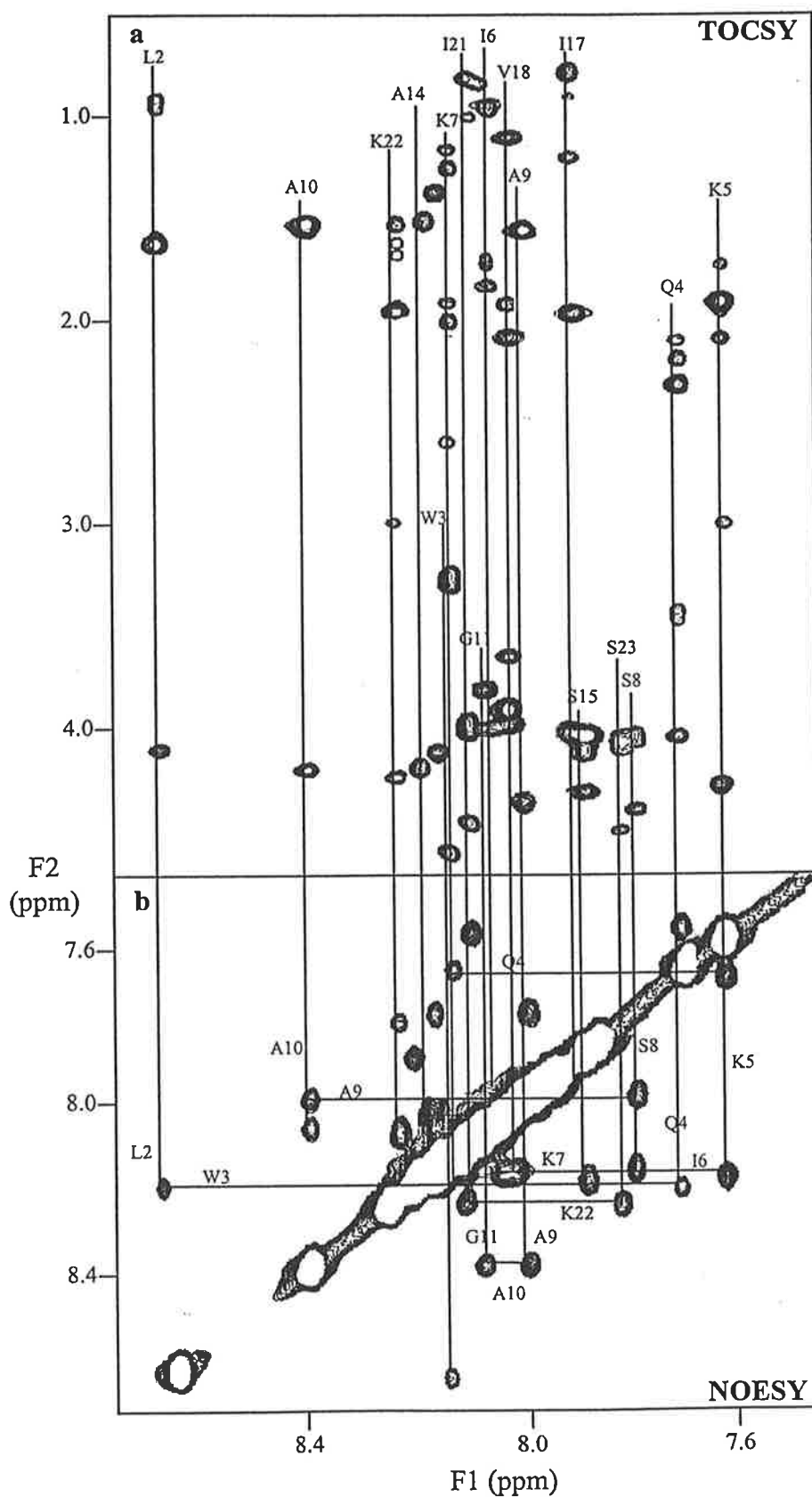
Fig 7.4 (a) A region of the TOCSY spectrum showing NH to sidechain
proton couplings, (b) NH region of the NOESY spectrum of caerin
4.1 in TFE/ water. Connectivities between sidechain and backbone
amide protons are indicated.

Table 7.2 ^{1}H and ^{13}C NMR chemical shifts for caerin 4.1 in d_3-TFE/water (1:1 by vol.) pH 2.8, 25°C.

Residue	Chemical Shifts (ppm)				
	NH	C$^\alpha$H	C$^\beta$H	others	C$^\alpha$
Gly 1	not observed	3.86, 3.93	-	-	42.37
Leu 2	8.64	4.10	1.55, 1.55	γ-CH=1.51 δ-CH$_3$=0.79, 0.88	57.26
Trp 3	8.18	4.45	3.24, 3.29	C$^\delta$H=7.20 C$^\varepsilon$H=7.51 C$^{\eta2}$H=7.18 C$^{\zeta2}$H=7.44 C$^{\zeta3}$H=7.08 N$^\varepsilon$H=9.87	58.87
Gln 4	7.77	3.75	2.14, 2.46	γ-CH$_2$=2.15, 2.46	63.58
Lys 5	7.68	4.07	1.97, 1.97	γ-CH$_3$=1.42, 1.65 δ-CH$_2$=1.54 ε-CH$_2$=2.84	57.97
Ile 6	8.11	3.73	1.87	γ-CH$_2$=1.12, 1.64 γ-CH$_3$=0.88 δ-CH$_3$=0.77	65.06
Lys 7	8.17	3.84	2.15, 2.15	γ-CH$_2$=1.28, 1.32 δ-CH$_2$=1.64 ε-CH$_2$=2.91	58.61
Ser 8	7.87	4.27	3.90, 3.95	-	59.84
Ala 9	8.00	4.23	1.50	-	53.50
Ala 10	8.39	4.12	1.45	-	53.80
Gly 11	8.08	3.91, 3.91	-	-	45.53
Asp 12	8.12	4.59	2.90, 3.05	-	54.16
Leu 13	8.15	4.19	1.78, 1.78	γ-CH=1.70 δ-CH$_3$=0.89, 0.91	56.68
Ala 14	8.20	4.11	1.49	-	53.90

Ser 15	7.96	4.18	3.97, 4.00	-	60.16
Gly 16	8.05	3.88, 3.90	-	-	45.53
Ile 17	7.98	3.87	2.00	γ-CH$_2$=1.14, 1.50 γ-CH$_3$=0.91 δ-CH$_3$=0.85	61.10
Val 18	8.02	3.65	2.14	γ-CH$_3$=0.95, 1.05	59.20
Glu 19	8.17	4.11	2.16	γ-CH$_2$=2.51, 2.55	57.26
Gly 20	8.05	3.92, 3.92	-	-	45.53
Ile 21	8.09	3.91	1.96	γ-CH$_2$=1.16, 1.71 γ-CH$_3$=0.91 δ-CH$_3$=0.84	58.10
Lys 22	8.25	4.19	1.87, 1.87	γ-CH$_2$=1.48, 1.58 δ-CH$_2$=1.64 ε-CH$_2$=2.95	56.61
Ser 23	7.89	4.36	3.96, 3.96	- CONH$_2$=7.04, 7.21	57.97
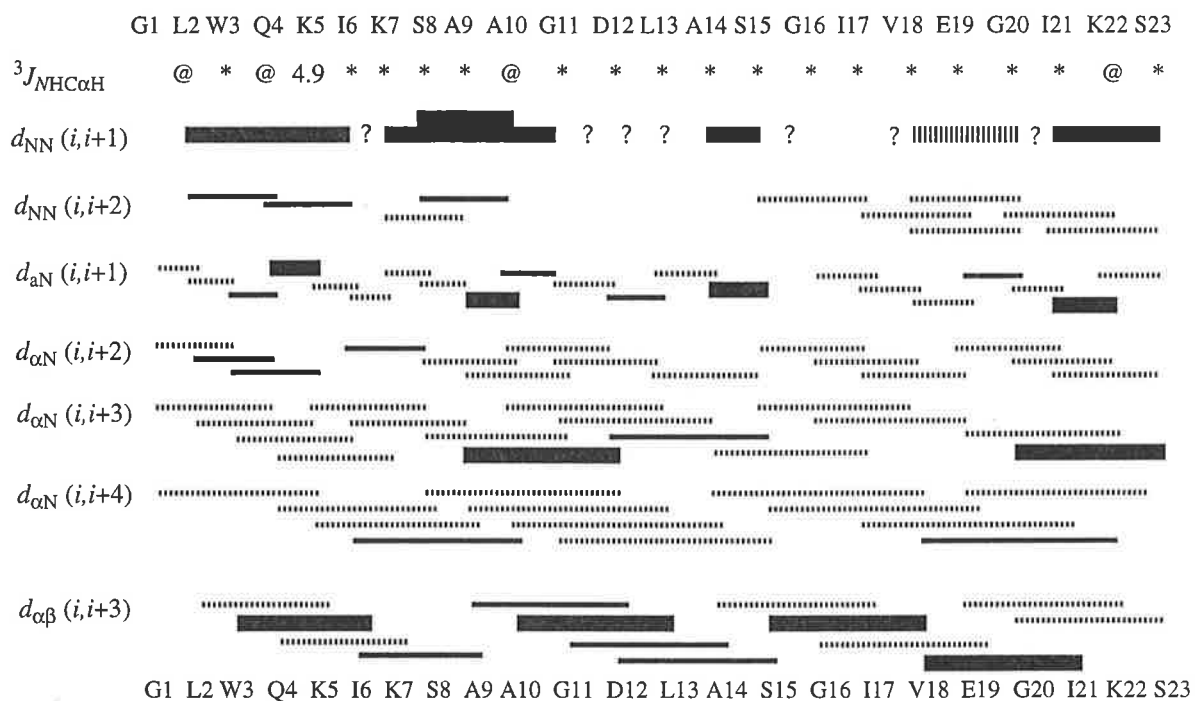
Fig. 7.5 **A summary of NOEs used for structure calculation of caerin 4.1 in 50% (by vol.) d_3-TFE, pH 2.8, 25°C.** The amino acid sequence of the peptide is given at the top of the diagram and the values of $^3J_{NHC\alpha H}$ were obtained from high-resolution 1D ^{1}H spectra. @ indicates no coupling constants were detected for the corresponding residue. Asterisks (*) indicate that coupling constants could not be unambiguously assigned due to overlap. The various types of NOEs and their relative strengths are indicated by the thickness of the bars (strong, medium and weak). For the basis of this diagram, NOEs are classified on the basis of strong (< 2.7 Å), medium (between 2.7 to 3.5 Å) and weak (> 3.5 Å). Dashed lines represent connectivities that could not be unambiguously assigned due to overlap, e.g. with an intraresidue NOE.

The presence of a helical structure is also indicated from an examination of the deviation from random coil chemical shift values of ^1H and ^{13}C α-CH resonances determined in water. For a window of n = ± 2 residues, smooth plots for the ^1H resonances showed a distinct upfield shift and those for the ^{13}C resonances showed a distinct downfield shift along the peptide (Fig 7.6a & b). The directions of the deviations from random coil chemical shifts are consistent with helical structure for the peptide with maximum helicity being present in its central region. However, it is apparent that these deviations do not exhibit a smooth distribution along the entire amino acid sequence. For example, the ^1H α-CH chemical shifts show a marked upfield shift in the region from Lys5 to Ser8 and Gly16 to Gly20 with an intervening region of α-CH chemical shifts which approach random coil values. The implications from these data are that these two aforementioned regions are strongly helical and are separated by a region where the helicity is reduced. In the main, the ^{13}C α-CH chemical shift deviations were opposite in direction to the ^1H deviations, with a significant downfield shift from Gln4 to Ser8 and shifts near random coil values from Gly1 to Trp3 and Ala9 to Gly16. However, a downfield shift was not observed for the α-CH resonances of Ile17 to Gly20 which would have been expected on the basis of the ^1H α-CH shift data. In fact, these residues were shifted upfield. This suggests a degree of flexibility in the C-terminal region.
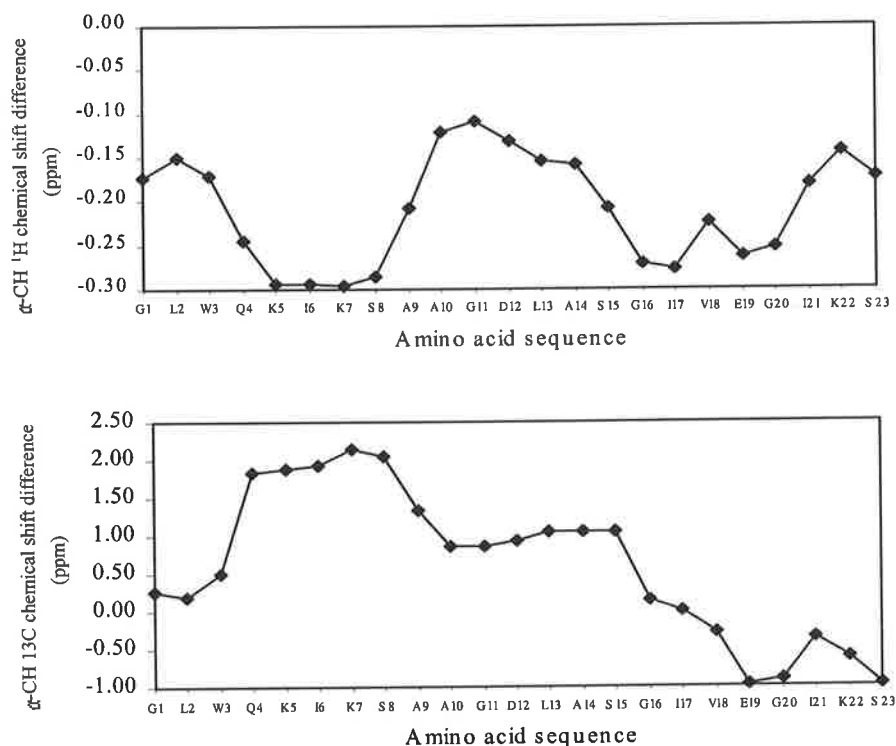
Fig 7.6 Deviation from random coil chemical shifts of (a) ^{1}H α-CH resonances and (b) ^{13}C α-CH resonances of caerin 4.1 in 50% (by vol.) TFE. A window of $\pm$ 2 residues was used. Upfield and downfield chemical shifts are indicated by negative and positive values respectively.

7.5 Structural Analysis

The conclusions derived from the examination of the NMR data presented above were confirmed when the NOESY data were used as input for determination of the solution structure of caerin 4.1. Structural calculations were based on a total of 415 NOE distance restraints comprising of 188 intra-residue restraints, 104 (i, i+1) sequential restraints, 123 medium-range restraints and 5 ϕ torsion angle restraints. Following RMD/SA calculations, structures were energy minimised with respect to potential energy *via* conjugate-gradient methods. The final run produced 60 conformers from which the 20 most stable (lowest potential energy) conformers

were selected for detailed examination. The structural statistics are presented in Table 7.4.

Table 7.4   Structural statistics of caerin 4.1 following RMD/SA calculations *.

RMSD from mean geometry (Å)	<SA> *	(SA)$_r$
All heavy atoms	0.74 ± 0.26	
All heavy backbone atoms (N, C$^\alpha$ and C')	0.50 ± 0.29	
X-PLOR energies (kcalmol^{-1})		
E$_{tot}$	260.39 ± 3.39	241.85
E$_{bond}$	28.12 ± 0.70	26.48
E$_{angle}$	74.82 ± 2.79	67.23
E$_{impr}$	17.56 ± 1.12	14.75
E$_{repel}$	23.14 ± 1.53	19.25
E$_{NOE}$	116.73 ± 3.55	114.12
E$_{cdih}$	0.07 ± 0.02	0.02

* <SA> is the ensemble of the 20 final structures, (SA) is the mean structure obtained by best-fitting and averaging the coordinates of the well-defined heavy backbone N, C$^\alpha$ and C' atoms of the 20 final structures. (SA)$_r$ is the representative structure obtained after restrained energy minimization of the mean structure.

Number of NOEs violate >0.2 Å = 35   Maximum violation is 2.90 Å

The superimposition of the twenty most stable structures over the entire backbone N, C$^\alpha$ and C' atoms show that caerin 4.1 forms a slightly curved helix along its entire length (Fig 7.7). The peptide is well-defined over its entire length with a RMSD of 0.50 ± 0.29 Å for the backbone atoms (Table 7.4).
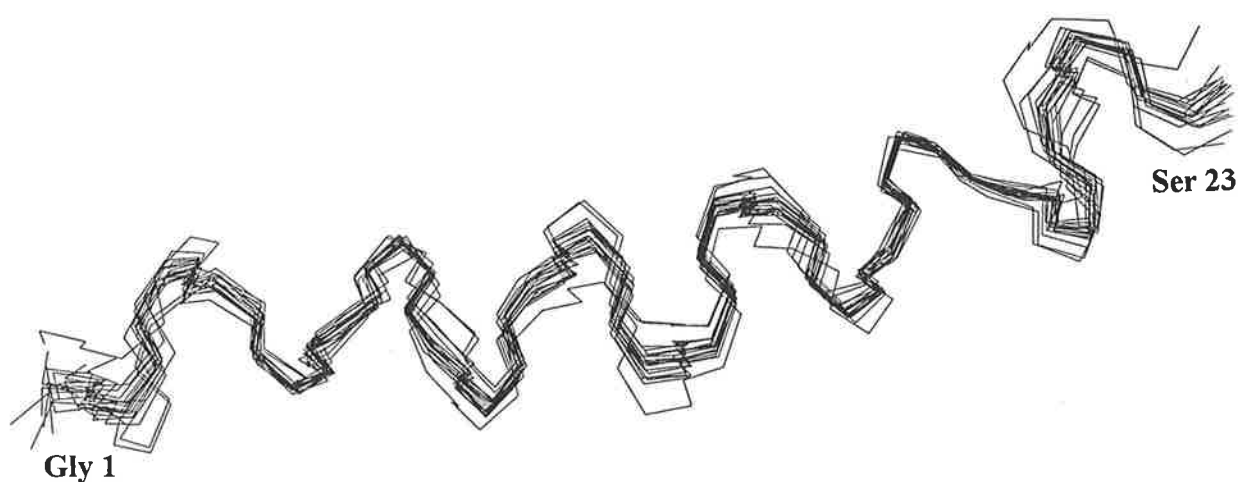
Fig 7.7 Superimposition of backbone atoms (N, C^α and C') of the 20 most
stable structures of caerin 4.1 in 50% (by vol.) d_3-TFE, pH 2. 8, 25°C.

Analysis of the angular order parameters (S , ϕ and ψ) of these twenty structures indicate that eighteen of the nineteen non-glycine residues are well defined with $S >$ 0.9 for both their ϕ and ψ angles. Ser23 at the C-terminus is the exception with (S , ϕ and ψ) values of 0.98 and 0.80 respectively (Fig. 7.8). The N- and C- terminal residues exhibited greater conformational variability.

a

b
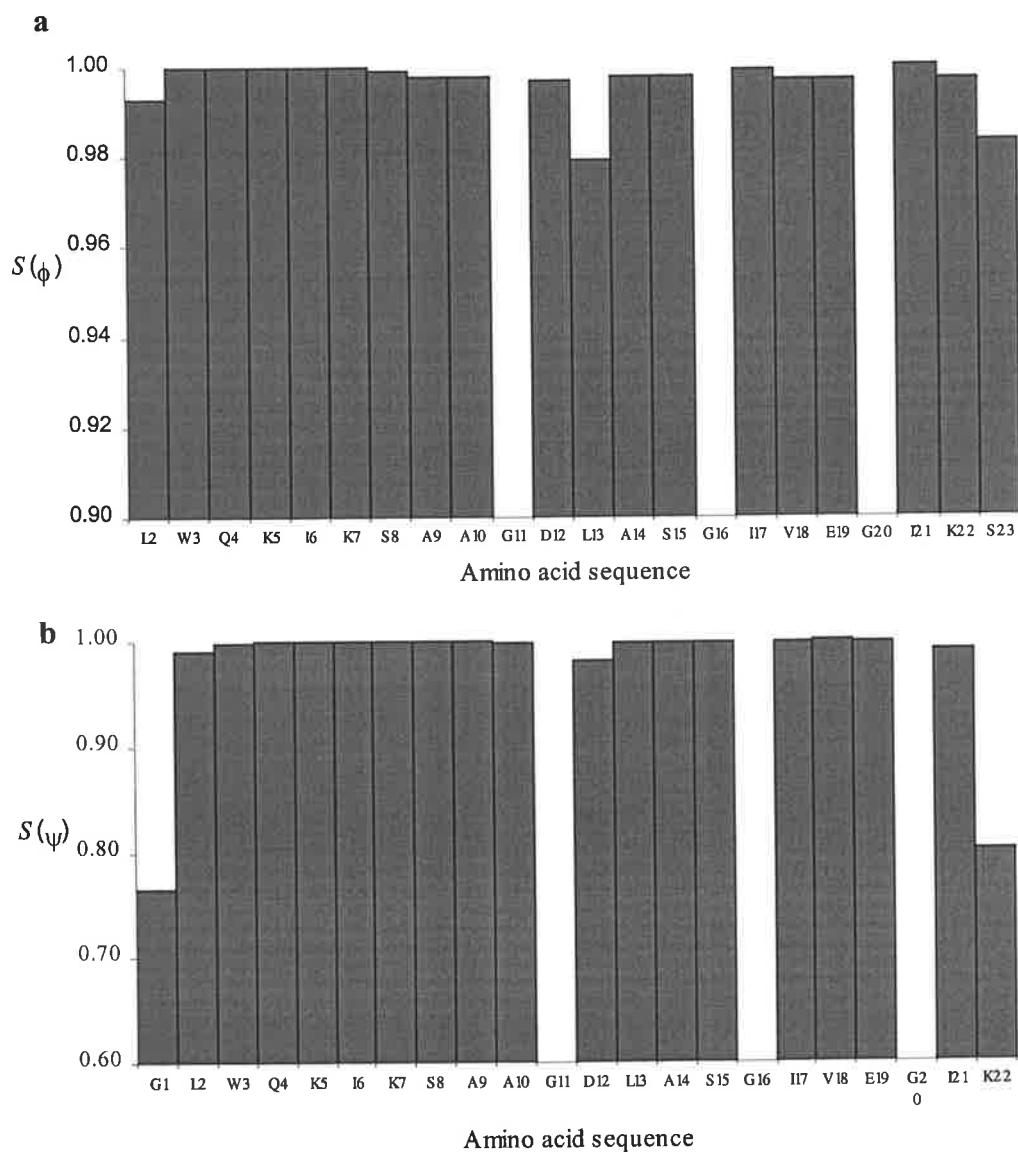
Fig 7.8 **Plots of angular order parameters $S(\phi)$ and $S(\psi)$ against amino acid sequence for caerin 4.1 in 50% (by vol.) d_3-TFE, pH 2. 8, 25°C**

The Ramachandran plot of caerin 4.1 (Fig 7.9) showed seventeen of the nineteen non-glycine residues had their averaged backbone dihedral angles (ϕ and ψ) within the 'favoured' (A) α-helical region, the only exception being Val18 and Glu19 which are in the 'allowed' (a) region, possibly indicating a region of flexibility near the C-terminus.
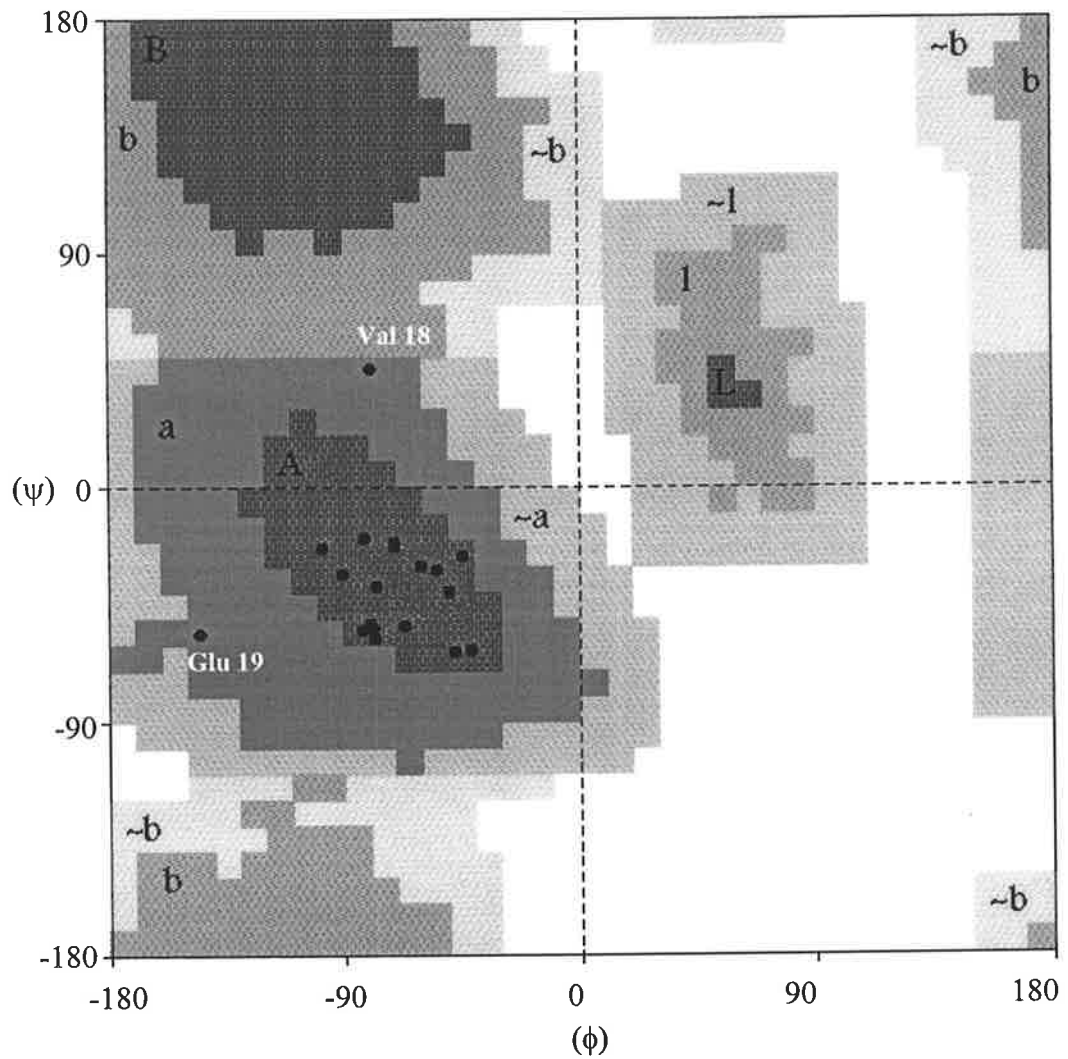
Fig 7.9 **Ramachandran plot of the average backbone φ and ψ angles of caerin 4.1.** The dots represented by Val 18 and Glu 19 are indicated.

The most stable structure of caerin 4.1 (i.e. with the lowest potential energy) is shown in Figure 7.10. Caerin 4.1 adopts a slightly curved helix along its entire length with well-defined hydrophobic and hydrophilic zones. The variation in the

middle of the peptide is due to flexibility associated with two glycine residues at positions 11 and 16, amino acids that are well known as "helix breakers" (Richardson and Richardson, 1988). Likewise, the helicity is disrupted after Gly20 which causes greater variation at the C-terminus than at the N-terminus of the molecule.
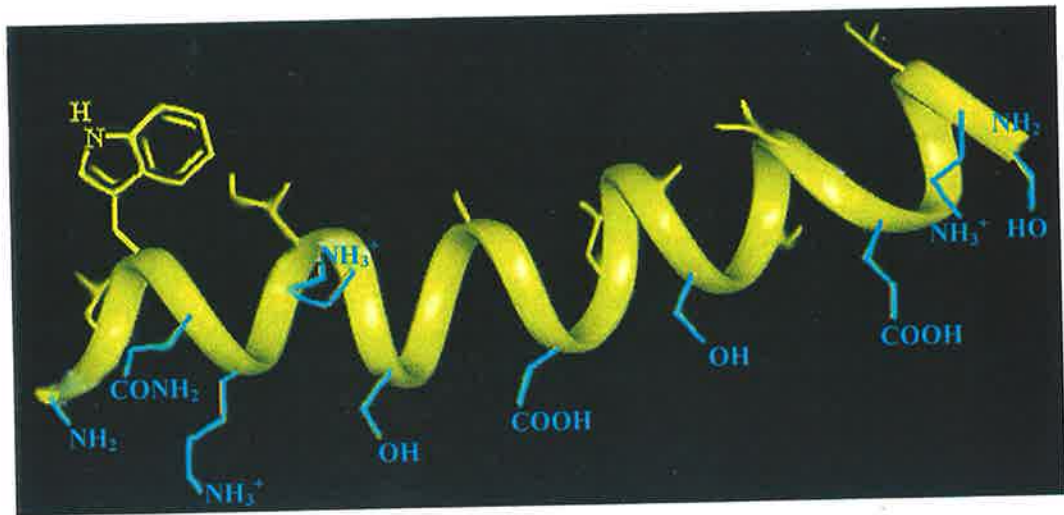
Fig 7.10   The most stable structure (lowest potential energy) of caerin 4.1.
The projection demonstrates the well defined hydrophobic and hydrophilic zones (shown in blue).

7.6 Discussion

There are three members of the caerin 4 family. To date, these have only been found in the skin secretion of the granular glands of the Australian green tree frog *Litoria caerulea* (Chia *et al.*, 2000b). The structure of caerin 4.1 in TFE co-solvent is that of a helical peptide along its entire length (Fig. 7.7 and 7.10). The first part of the peptide (from Gln4 to Ala10) is highly helical. However, the structures shown in Fig. 7.7 exhibit some conformational variation in the middle of the peptide (from

Gly11 to Gly16) which leads to greater flexibility in this portion of the molecule. The region of flexibility from Gly11 to Gly16 is followed by approximately one turn of well-structured helix from Ile17 to Ile21 which leads into a flexible portion at the C-terminus. The structure-disrupting ability of glycine amino acids is apparent from the structures in Fig. 7.7 where the ends of the two highly helical regions in caerin 4.1 correspond to the presence of glycine amino acids at positions 11 and 20.

Central flexibility is common in many unrelated antibiotic amphipathic helical peptides. For example, caerin 1.1 has a central region of greater flexibility than caerin 4.1 which occurs in the vicinity of Pro15 (see Chapter 5). The equivalent residue in caerin 4.1 is a serine. The larger degree of central flexibility in caerin 1.1 may explain its much broader spectrum of antibiotic activity (Table 7.1), i.e., by arranging its amino acid side chains accordingly it can interact more efficiently with membranes from a diversity of bacteria which have different membrane composition and topology. In caerin 4.1, however, its relatively rigid helical backbone conformation cannot undergo a similar conformational change which causes a loss in its wide-spectrum antibiotic capability.

Presently, it is unknown why caerin 4.1 is active only against Gram-negative bacteria and not Gram-positive ones. It has been suggested that since all Gram-negative bacteria have lipopolysaccharide (LPS) in their outer membranes (Brock *et al.*, 1984), it could play a role in bacterial selectivity for certain antimicrobial peptides (Epand and Vogel, 1999). Indeed, cecropin was found to bind to the phosphoryl moiety of LPS (De Lucca *et al.*, 1995) while spectroscopic studies

showed that magainin binds to and disrupt vesicles containing LPS (Rana *et al.*, 1990, 1991a and 1991b; Matsuzaki *et al.*, 1999b) as well as natural Gram-negative bacterial membranes (Skurmik *et al.*, 1999). Hence, it has been suggested that cationic bactericidal peptides initially binds to LPS and disrupt the outer membrane before penetrating the second, inner membrane (Guo *et* al., 1998). These studies, however, do not explain why certain antimicrobial peptides are active against Gram-negative bacteria while others are not. Recently, a novel model membrane system made up of LPS and phospholipids was developed which can be employed as a membrane mimetic for Gram-negative bacteria (Matsuzaki *et al.*, 1999b). Hence, future experiments that can be performed using caerin 4.1 include: (i) NMR structural analysis of the peptide dissolved in a solution of phospholipid bicelles containing LPS, (ii) orientation studies of the peptide when incorporated in LPS multilayers using solid-state NMR techniques and (iii) molecular dynamics simulations involving caerin 4.1 with phospholipid/LPS bilayers. Such studies can be used to probe the 3D structure, topology and dynamics of peptide-membrane systems which may shed some light as to why caerin 4.1 is selective only towards Gram-negative bacteria.

Chapter 8
Future Directions
and Conclusions
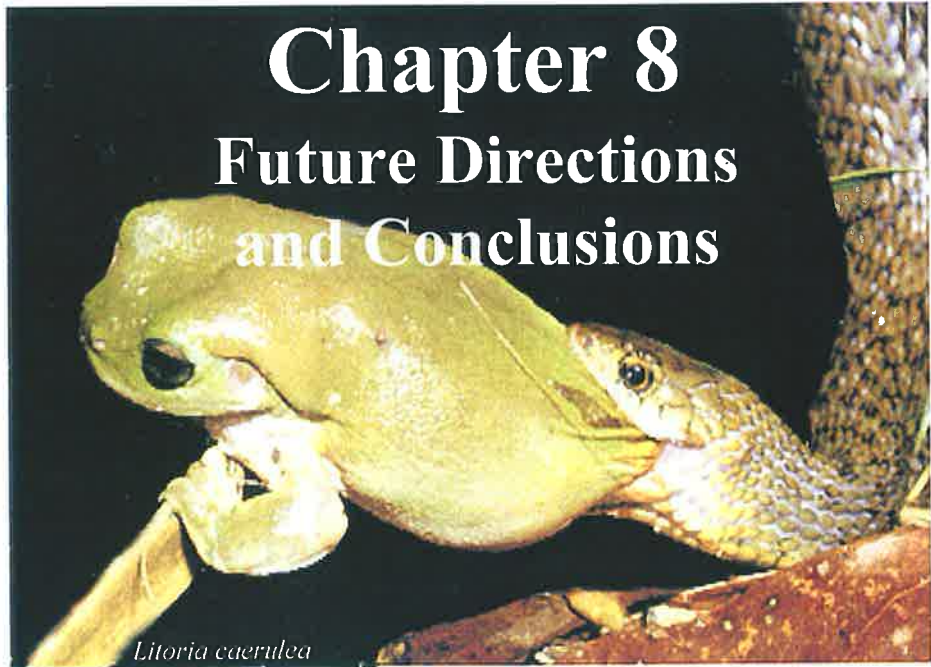
Litoria caerulea

8.1 Antimicrobial Peptides: Antibiotics of the Future?

No new classes of antibiotics have been developed in the past 26 years since the introduction of quinolones in the 1970s (Hancock *et al.*, 1996). Already, a plethora of drug-resistant pathogens are on the rise world-wide and thus there is an urgent need for the introduction of new antibiotics (Davies, 1996; Ewald and Cochran, 1999). Naturally-occurring bactericidal peptides from amphibian skin and other organisms are a potential source of such antibiotics as they possess several features that confer some advantages over existing antibiotics (Hancock, 1997; Hancock and Lehrer, 1998; Boman *et al.*, 1999; Hancock and Chapple, 1999). For example, they are mostly broad-spectrum, highly potent and are known to kill drug-resistant pathogens such as *Staphylococcus aureus* and fungi (de Lucca and Walsh, 1995; Hancock *et al.*, 1995). In addition, some of these peptides have shown remarkable selectivity against bacteria and are not known to induce drug-resistant mutants. These desirable properties make them promising candidates for the development of a new antibiotic class (Hancock and Lehrer, 1998; Hancock, 1999). Furthermore, these peptides are relatively small and hence, are relatively easy to produce in a large scale using solid-phase techniques (Wade *et al.*, 1990; Maloy and Kari, 1995) and recombinant DNA procedures (Simmaco *et al.*, 1998). One such example is an analogue of magainin (MSI-78) which is now commercially available as a topical antibiotic cream (see Fig. 1.4b) (Lipsky *et al.*, 1997).

However, a major problem exists: these peptides are likely to be vulnerable to proteases found in humans (or any host organism in particular). Shemyakin *et al.*

(1969) suggested that this can be circumvented by synthesising and using the all-*D* analogues which would not be targeted by host proteolytic enzymes.

8.2 Peptides and Drug Design

Antimicrobial peptides have been subjected to numerous structure-activity relationship studies which have greatly enhanced our knowledge of their mechanisms of bactericidal action (Bessalle *et al.*, 1993; Tossi *et al.*, 1997). Understanding the structure-function relationships of these peptides has facilitated the design of more potent and/or cell-specific analogues (Bechinger *et al.*, 1997; Hwang and Vogel, 1998). Examples include analogues that: (i) differ at one or more sequence positions, (ii) are shortened or contain deletions or (iii) are hybrids of two different peptides (Boman *et al.*, 1989; Fink *et al.*, 1989; Rivett *et al.*, 1996). Of particular interest are analogues that exhibit tumouricidal activities (see Section 8.3). These studies enable the determination of important residues that modulate biological activities, resulting in the discovery of novel analogues that are more potent than the natural peptides. For example, analogues of cecropin and magainin have been synthesised in the search for potential therapeutic agents (Saberwal and Nagaraj, 1994; Maloy and Kari, 1995) while cecropin-melittin and cecropin-magainin hybrids have been synthesised which possess enhanced activities against a wide range of pathogens without the cytotoxic effects of the natural peptides (Boman *et al.*, 1989; Andreu *et al.*, 1992; Wade *et al.*, 1992; Piers and Hancock, 1994; Fernandez *et al.*, 1996; Shin *et al.*, 1997; Shin *et al.*, 1999; Hedberg *et al.*, 2000). Another approach in the design of novel peptides for use as therapeutic agents is to create peptides with maximum amphipathicity. Towards this end, two

approaches have been utilised. The first involves synthesising peptides with repeating sequences of alternating hydrophilic and hydrophobic residues (Tossi *et al.*, 1997) while the second method involves the use of combinatorial libraries (Blondelle and Houghton, 1996; Blondelle *et al.*, 1996; Dorner *et al.*, 1997). These methods have not only created highly potent membrane-lytic agents, but have also provided a deeper insight to their mechanism(s) of action.

8.3 Development of Anti-Cancer Agents

The conventional treatment for cancer involves chemotherapy. Unfortunately, chemotherapeutic drugs are highly toxic because they are indiscriminate in their killing of cells, including healthy cells. These drugs work by attacking all rapidly proliferating cells, such as those of the gastrointestinal tract. Such serious side-effects restrict the dosage level of drug which can be administered. Thus, new drugs are currently being developed that will selectively target cancerous cells with minimum effect on other healthy cells in the patient. In Section 1.3, it was mentioned that caerin 1.1 is active against many types of cancer cells (see also Section 2.4 on cancer cell membranes). Its mechanism of action is suspected to be similar to the way it, and maculatin 1.1, lyse bacteria membranes (i.e., *via* the carpet mechanism). This makes caerin 1.1 (and possibly most membrane-lytic peptides) potential anti-cancer agents. Cell-specific targeting can be achieved by attaching appropriate immunoglobulins (antibodies) to the peptide which will then be able to seek out specific cancer cells before disrupting their membranes (Fig 8.1). Such a concept is not new, various cytolytic agents have already been chemically linked to

immunoglobulins, including radionuclides, cytolytic drugs, ribonuclease, plant and animal toxins [see Colowick and Kaplan (1985), Neville (1986), McGuire (1988), Pai and Pastan (1994) and Compans *et al.* (1998) for reviews]. For example, the plant toxin ricin and cobra venom have been tested as therapeutic agents for the treatment of cancer (Vallera *et al.*, 1983; Vogel *et al.*, 1985; Bjorn and Villemez, 1988). These studies suggest that it could be feasible to use membrane-lytic peptides as a new class of immunotoxins, thereby offering new opportunities in cancer therapy. For example, a melittin-antibody conjugate is currently under investigation (Dunn *et. al.*, 1996).
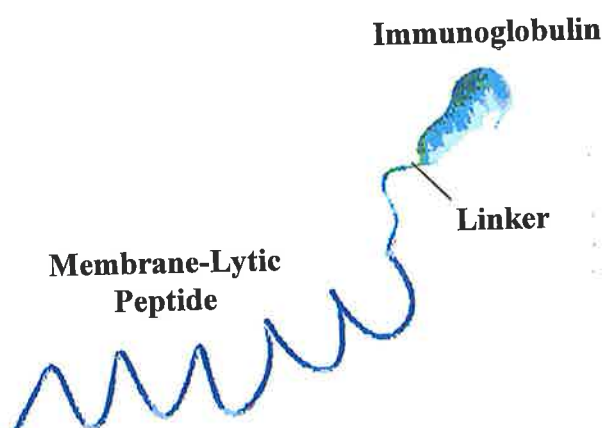
Fig. 8.1 A schematic representation of an immunotoxin, consisting of an immunoglobulin, a linker and the membrane-lytic peptide.
(Figure not drawn to scale).

8.4 Conclusions

In this thesis, a combination of structure-activity studies, CD, NMR and computer modelling techniques were employed to give a deeper insight into the mechanisms of bactericidal action of amphibian antimicrobial peptides. These studies have also enhanced our understanding of the molecular basis of peptide specificity and potency against bacteria. This serves to facilitate the design of more potent and cell-specific antibiotics as well as anti-cancer agents.

The main reason for the difficulties in establishing a correlation between peptide conformation in membrane-mimetic media and their specificity against Gram-positive and Gram-negative bacteria is the lack of experimental model systems that can accurately mimic the highly complex natural cell membranes (Blondelle *et al.*, 1999; Dathe and Wieprecht, 1999). Future studies in this area can be undertaken using more realistic membrane-mimicking solvent systems, including phospholipid bicelles (Vold *et al.*, 1997; Prestegard, 1998) or liposomes containing LPS to mimic Gram-negative bacterial membranes (Matsuzaki, 1999b).

The Toad, Ugly and Venomous,
Wears yet a Precious Jewel in his Skin
-adapted from
William Shakespeare's
"As You Like It".
Act II, Scene I

Chapter 9
Experimental
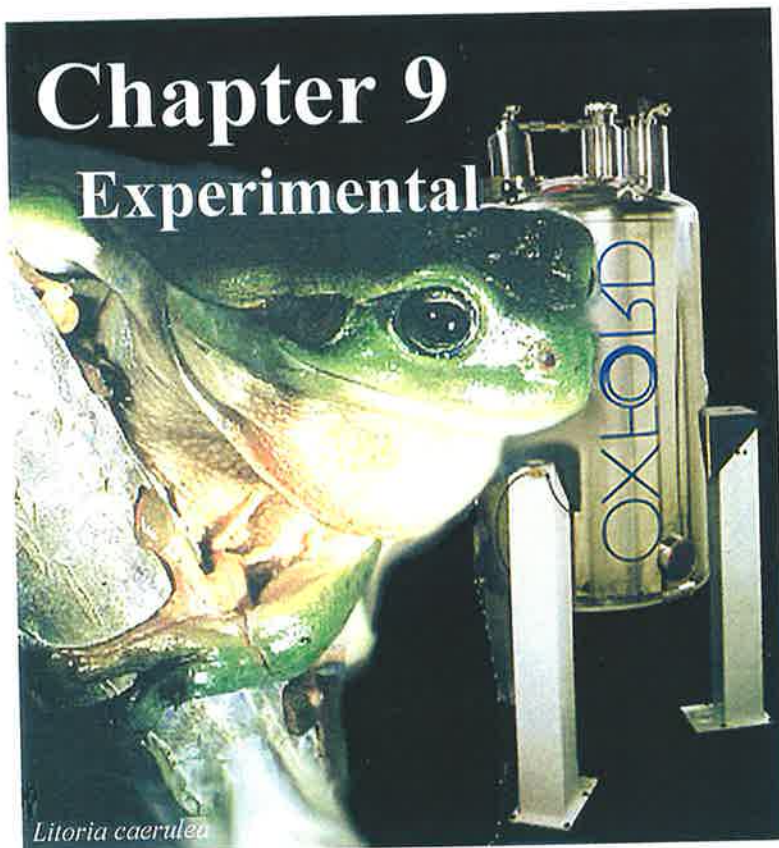
Litoria caerulea

9.1 Preparation of Synthetic Peptides

All peptides and their synthetic analogues were synthesised commercially by Chiron Mimotopes (Clayton, Victoria) using L-amino acids *via* the standard N-α-Fmoc method (Maeji *et al.*, 1995).

9.2 Antimicrobial Testing

Synthetic peptides were tested by the microbiology section of the Institute of Medical and Veterinary Science (Adelaide, South Australia). The method involved the measurement of inhibition zones produced by the applied peptide on a thin agarose plate containing the micro-organisms under study. The procedures are standard and have been fully documented (Jorgensen *et al.*, 1993). Activities were recorded as minimum inhibitory concentration (MIC) values, i.e. the mass of peptide per millilitre of water required to kill or totally inhibit the growth of the test microorganism.

9.3 CD Spectroscopy

All CD spectra were acquired on a Jobin-Yvon CD-6 spectrophotometer (located at the Department of Chemistry, University of Wollongong) at 20°C at varying concentrations of TFE in water (from 0 to 50% by volume) at peptide concentrations listed in table 10.1. Each spectrum represented an average of five scans. The instrument was routinely calibrated with an aqueous solution of recrystallised d_{10}-camphorsulphonic acid (1.0 g/L in a cell of pathlength 1mm). Ellipticity was

calibrated using values of 33.5 mdeg. at λ=290.5 nm and -69.5 mdeg. at λ=192.5 nm.

Table 9.1   Sample details for CD spectroscopy.

Peptide	Concentration (μM)	pH
caerin 4.1	22.9	4.8
maculatin 1.1	23.3	4.8
uperin 3.6	27.3	4.2

9.4 NMR Spectroscopy

The general procedure for the preparation of NMR samples is described below. Details can be found in Table 9.2. The appropriate peptide (**A** mg) was dissolved in 0.7 ml of d_3-TFE/water (1:1 by volume) to give a concentration of **B** mM. For the experiment involving dodecylphosphocholine, 9.6 mg of maculatin 1.1 and 69.8 mg of dodecylphosphocholine-d_{38} (DPC) (Cambridge Isotope Laboratories) was dissolved in 0.63 ml water / D_2O (9:1 by volume) containing 50 mM of NaH_2PO_4 buffer giving a concentration of 6.39 mM of maculatin and 0.70 M of DPC. pH was adjusted to 7.00 by adding appropriate amounts of HCl and NaOH. All pH measurements were made using a Activon Model 210 pH meter and Activon BJ 432 Platinum Electrode (183×6 mm epoxy thin stem, Ag/AgCl reference). Model 535 NMR tubes were used for all NMR experiments.

Table 9.2   Sample details for NMR spectroscopy.

Peptide	Mass of Peptide (A mg)	Concentration (B mM)	pH
Caerin 4.1	10.2	6.30	2.8
Maculatin 1.1	9.6	6.39	2.5
Ala15 maculatin 1.1	10.6	7.21	2.5
Uperin 3.6	10.7	8.36	2.4

All NMR spectra were acquired on a 600 MHz Varian Unity Inova spectrometer at a ^{1}H frequency of 599.12 MHz and ^{13}C frequency of 150.00 MHz. Experiments involving water / d_3-TFE were conducted at 25°C while that involving DPC was conducted at 37°C. Probe temperature was calibrated using ethylene glycol. The methylene resonances of residual TFE were used as ^{1}H and ^{13}C chemical shift references (at 3.918 and 60.975 ppm, respectively) for experiments acquired in TFE/water. Sodium 2,2-dimethyl-2-silapentane-5-sulphonate (DSS) was used as ^{1}H and ^{13}C chemical shift references (at 0.015 and 0.000 ppm, respectively) for experiments involving DPC micelles (Gesell *et al.*, 1997).

^{1}H 2D NMR DQF-COSY (Rance *et al.*, 1983b), TOCSY (Davies and Bax, 1985), NOESY (Jeneer *et al.*, 1979) experiments were conducted in the phase sensitive mode using Time Proportional Phase Incrementation (TPPI) (Marion and Wüthrich, 1983) in the t_1 dimension. Each experiment consisted of 512 t_1 increments with 32 scans recorded per increment. The FID in t_2 consisted of 2048 data points over a spectral width of 5112.5 Hz.

Water suppression was conducted using the presaturation method (Gueron *et al.*, 1991). The transmitter frequency was centered on the water resonance and conventional low power presaturation from the same frequency synthesizer (proton transmitter) was applied during the delay between scans. A 1.5 s presaturation pulse was used to suppress the large water signal in the TOCSY, NOESY and DQF-COSY spectra.

The TOCSY experiments used a 75 ms MLEV-17 spin-lock and employed a modified pulse sequence to minimise cross relaxation effects (i.e. "Clean-TOCSY") (Griesinger *et al.*, 1988). All NOESY spectra were acquired with a mixing time of 200 ms.

HSQC (Kay *et al.*, 1992) experiments using linear prediction (Gmeiner and Babcook, 1997) were acquired to assign the protonated ^{13}C resonances *via* correlations to their attached protons. For this experiment, 512 t_1 increments were acquired over 4096 data points with a spectral width of 5521.8 Hz in the directly detected (^1H, F_2) dimension and a spectral width in the ^{13}C (F_1) dimension of 24146.5 Hz.

9.5 NMR Data Processing

All 2D NMR spectra were processed on a Sun Microsystems Ultra Sparc 1 workstation using VNMR (version 5.3) software. All 2D NMR spectra were multiplied by a gaussian function in both dimensions before zero-filling to 2048 data

points in both dimensions prior to Fourier transformation. The resulting 2D matrices consisted of 2048 × 2048 real data points.

9.6 Cross-peak Assignments and Structural Calculations

Cross-peak assignments were performed using XEASY (version 1.3.13) software (Bartels *et al.*, 1995). Structures were generated on a Sun Microsystems Sparc 4 workstation using X-PLOR (version 3.851) software (Brünger, 1992; Brünger and Nilges, 1993). All restraints were set to a lower limit of 1.80 Å based on the sum of the van der Waals radii of two nuclei. The upper boundary limit was set to the calculated distance plus 20% to avoid excessively restraining the molecule.

NOESY cross-peak volumes was calculated by the approach proposed by Xu *et al.* (1995). It involves converting the cross-peak volumes into a continuum of distance restraints with values determined from the equation:

$$\text{Calculated Distance} = [A(I)/I]^{1/6}$$

where $A(I)$ is an intensity-dependent proportionality factor and I is the observed crosspeak intensity. $A(I)$ can be obtained from equation:

$$A(I) = [(I - I_s)/(I_w - I_s)] [A(I_w) - A(I_s)] + A(I_s)$$

with $A(I_w)$ and $A(I_s)$ representing the average of the 10 weakest and 10 strongest NOE intensities respectively. Both can be calculated as follows:

$$A(I_w) = (5.0 \text{ Å})^6 \, I_w$$

$$A(I_s) = (1.8 \text{ Å})^6 \, I_s$$

The RMD/SA protocol was based on that of Nilges *et al.* (1988b) which included the use of floating stereospecific assignments (Holak *et al.*, 1989). The All Hydrogen Distance Geometry (ALLHDG) force field (version 4.03) was employed for all calculations (Engh and Huber, 1991). The protocol started with a family of 60 initial structures generated from templates with random backbone ϕ and ψ angles. They were next subjected to 6500 steps (19.5 ps) of high temperature dynamics at 2000 K. K_{NOE} and K_{repel} force constants were increased from 10 to 50 kcalmol^{-1}Å^{-2}, from 5 to 200 kcalmol^{-1}rad^{-2} and from 0.02 to 0.1 kcalmol^{-1}Å^{-4}, respectively. (Force constants for all terms were initially set to very low values to ensure that atoms can 'pass through' each other to satisfy experimental restraints if experimental constraints so dictate). This was followed by 2500 steps (7.5 ps) of cooling from 2000 K to 1000 K with K_{repel} is increasing from 0.1 to 4.0 kcalmol^{-1}Å^{-4} while the atomic radii was decreased from 0.9 to 0.75 times those in the ALLHDG parameter set in order to ensure that no close non-bonded contacts existed. The last step involved 1000 steps (3 ps) of cooling from 1000 K to 100 K. Final structures were subjected to 200 cycles of conjugate gradient Powell minimisation (Sutcliffe and Dobson, 1991). Of these, the twenty structures with the lowest potential energy were selected for analysis. INSIGHT II (version 95.0, MSI) was used to display and manipulate the structures. PROCHECK (version 3.0) was used to produce the Ramachandran plots (Laskowski *et al.*, 1994).

9.7 Coupling Constants

$^3J_{NHC\alpha H}$ coupling constants were measured from high-resolution 1D ^1H spectra acquired at 25^0C with 0.0105 Hz/point digital resolution (128,000 data points). Dihedral angles were restrained as follows: $^3J_{NHC\alpha H}$ <5 Hz, $\phi = -60^\circ \pm 30^\circ$, $^3J_{NHC\alpha H}$ between 5 to 6 Hz, $\phi = -60^\circ \pm 40^\circ$, $^3J_{NHC\alpha H} > 8$ Hz, $\phi = -120^\circ \pm 40^\circ$. Where 6 Hz < $^3J_{NHC\alpha H} < 8$ Hz, ϕ angles were not constrained. Similarly, for residues where no coupling constant could be measured, no dihedral constraints were used.

9.8 Solid-State NMR Spectroscopy

DHPC and DMPC were purchased from Avanti Polar Lipids (Alabaster, AL). DMPC-$^2H_{54}$ was purchased from Serdary Research Laboratories (Ontario, Canada).

The bilayer-peptide sample was prepared using ^{15}N-Ala7 labelled maculatin 1.1 (6.0 mg) and DMPC-d_{54} (30.7 mg) to give a 15:1 phospholipid/peptide ratio. The powder was dissolved in chloroform/methanol (4 ml, 3:1 by vol.) and applied evenly to 30 strips of glass coverslips. The solvent was allowed to dry, then evaporated *in vacuo* (4 hours) and hydrated with 50 μl of H_2O. Finally, the plates were stacked, inserted into a 7 mm diameter NMR tube, left to equilibrate with excess water overnight and then sealed.

^{31}P and ^2H experiments were performed on a Varian Unity Plus 400 NMR spectrometer. Spectra were proton-decoupled and acquired using a 10mm broad-band probe. ^{31}P spectra were acquired between 30°-50° C at 161.8 MHz with a

spectral width of 32 kHz and relaxation delay of 2s. Data were acquired for 512 scans with 8192 data points. H_3PO_4 was used as an external reference (0 ppm).

50 Hz line-broadening was applied to the spectra. ^2H NMR spectra were acquired at 61.4 MHz with a spectral width of 100 kHz. The quadrupole echo pulse sequence: $90°-t_1-90°-t_2$-acquire was employed with phase cycling and quadrature detection (Davis *et al.*, 1976). t_1 and t_2 were set to 40 µs and 30 µs respectively. A relaxation delay of 0.30 s was used. Data were acquired over 36,000 scans and 16,384 data points. D_2O was used as reference (0 ppm). Proton-decoupled ^{15}N NMR spectra were acquired on a Bruker AMX-500 spectrometer operating at 50 MHz and using saturated *NH_4NO_3 solution as reference (0 ppm) (Levy and Lichter, 1979). 42 000 scans were used and the FID consisted of 32 000 data points over a spectral width of 21 000 Hz.

References

Litoria chloris

References

Alvarez-Bravo, J., Kurata, S. and Natori, S. *J. Biochem.* 1995, **117**, 6, 1312-6.

Amiche, M., Seon, A.A., Pierre, T.N. and Nicolas, P. *FEBS. Lett.* 1999, **456**, 352-6.

Anastasi, A., Erspamer, V. and Bertaccini, G. *Comp. Biochem. Physiol.* 1965, **14**, 43-9.

Anastasi, A., Erspamer, V. and Endean, R. *Arch. Biochem. Biophys.* 1968, **125**, 57-63.

Andersen, O.S. *Biophys. J.* 1983, **41**, 119-65.

Andersen, O.S. *Annu. Rev. Physiol.* 1984, **46**, 531-48.

Andreu, D., Merrifield, R.B., Steiner, H. and Boman, H.G. *Biochemistry.* 1985, **24**, 7, 1683-8.

Andreu, D., Bach, J., Boman, A., Wahlin, B., Wade, D., Merrifield, R.B. and Boman, H.G. *FEBS. Lett.* 1992, **296**, 190-4.

Arseniev, A.S., Barsulov, I.L., Bystrov, V.F., Lomize, A.L. and Ovchinnikov, Y.A. *FEBS. Lett.* 1985, **186**, 2, 168-74.

Asakura, T., Taoka, K., Demura, M., Williamson, MP. *J. Biomol NMR.* 1995, **6**, 227-36.

Aue, W.P., Bartholdi, E. and Ernst, R.R. *J. Chem. Phys.* 1975, **64**, 2229-46.

Bachar, M. and Becker, O.M. *J. Chem. Phys.* 1999, **111**, 18, 1872-85.

References

Baker, M.A., Maloy, W.L., Zasloff, M. and Jacob, L.S. *Cancer Res.* 1993, **53**, 3052-7.

Barra, D. and Maurizio, S. *Trends Biotech.* 1995, **13**, 205-9.

Barker, J., Grigg, G.C. and Tyler, M.J. in *A Field Guide to Australian Frogs.* Surrey Beatty and Sons, Australia. 1995. p.49-53.

Barlow, D.J. and Thornton, J.M. *J. Mol. Biol.* 1998, **201**, 601-619.

Bartels, C., Xia, T.H., Billeter, M., Güntert, P. and Wüthrich, K. *J. Biomol. NMR.* 1995, **6**, 1-10.

Barthalmus, G.T. and Zielinski, W.J. *Pharmacol. Biochem. Behav.* 1988, **30**, 4, 957-9.

Bazzo, R., Tappin, M.J., Pastore, A., Harvey, T.S., Carver, J.A. and Campbell, I.D. *Eur. J. Biochem.* 1988, **173**, 139-146.

Bechinger, B., Kim, Y., Chirlian, L.E., Gesell, J., Neumann, J.M., Montal, M., Tomich, J., Zasloff, M. and Opella, S.J. *J. Biomol. NMR.* 1991, **1**, 167-73.

Bechinger, B., Zasloff, M. and Opella, S.J. *Biophys. J.* 1992, **62**, 12-4.

Bechinger, B., Zasloff, M. and Opella, S.J. *Protein. Sci.* 1993, **2**, 2077-84.

Bechinger, B., Gierasch, L.M., Montal, M., Zasloff, M. and Opella, S.J. *Solid State NMR.* 1996, **7**, 185-92.

Bechinger, B. *J. Membr. Biol.* 1997, **156**, 197-211.

185

References

Bechinger, B., Zasloff, M. and Opella, S.J. *Biophys. J.* 1998, **74**, 981-7.

Bechinger, B. *Biochim. Biophys. Acta.* 1999, **1462**, 157-83.

Bechinger, B., Kinder, R., Helmle, M., Vogt, T.B., Harzer, U. and Schinzel, S. *Biopolymers.* 1999a, **51**, 174-90.

Bechinger, B., Ruysschaert, J.M., and Goormaghtigh, F. *Biophys. J.* 1999b, **76**, 552-63.

Bertaccini, G., Cei, J.M. and Erspamer, V. *Br. J. Pharmac.* 1963, **25**, 380-9.

Berendsen, J. *J. Chem. Phys.* 1984, **81**, 3684-91.

Berkowitz, B.A., Bevins, C.L. and Zasloff, M. *Biochem. Pharmacol.*, 1990, **39**, 625-629

Berliner, L. J. and Reuben, J. in *Biological Magnetic Resonance.* Vol. 2. Plenum Press, New York. 1980. p.282.

Bessalle, R., Kaptkovsky, A., Gorea, A., Shalit, I. and Fridkin, M. *FEBS. Lett.* 1990, **274**, 151-5.

Bessalle, R., Haas, H., Goria, A., Shalit, I. and Fridkin, M. *Antimicrob. Agents Chemother.* 1992, **36**, 313-7.

Bessalle, R., Gorea, A., Shalit, I., Metzger, J.W., Dass, C., Desiderio, D.M. and Fridkin, M. *J. Med. Chem.* 1993, **36**, 1203-9.

Beven, L., Helluin, O., Molle, G., Ducloheir, H. and Wroblewski, H. *Biochem. Biohys. Acta.* 1999, **1421**, 53-63.

References

Bevins, C.L. and Zasloff, M. *Annu. Rev. Biochem.* 1990, **59**, 395-414.

Bhakdi, S., Fussle, R. and Tranum-Jensen, J. *Proc. Natl. Acad. Sci. USA.* 1981, **78**, 5475-9.

Billeter, M., Braun, W. and Wüthrich, K. *J. Mol. Biol.* 1982, **155**, 321-46.

Bjorn, M.J. and Villemez, C.L. in *Immunotoxins.* (Frankel, A.E. Ed.) Kluwer Academic Publishers, Boston. 1988.

Blanco, F., Rivas, G. and Servano, L. *Nature Struct. Biol.* 1994, **1**, 584-90.

Bloch, K. in *Biochemistry of lipids, lipoproteins and membranes.* (Vance, D.E. and Vance, J.E. Eds.) Elseiver, Amsterdam. 1991. p.363-81.

Blondelle, S.E. and Houghton, R.A. *Biochemistry.* 1992, **31**, 12688-84.

Blondelle, S.E. and Houghton, R.A. *Trends Biotech.* 1996, **14**, 60-5.

Blondelle, S.E., Takahashi, E., Houghton, R.A. and Perez-Paya, E. *Biochem. J.* 1996, **313**, 141-7.

Blondelle, S.E., Forood, B., Houghten, R.A. and Perez-Paya, E. *Biopolmers.* 1997, **42**, 489-98.

Blondelle, S.E., Lohner, K. and Aguilar. M.I. *Biochim. Biophys. Acta.* 1999, **1462**, 89-108.

Blundell, T.L. and Johnson, L.N. in *Protein Crystallography.* Academic Press, New York. 1976.

References

Blundell, T.L., Barlow, D., Borkakoti, N. and Thornton, J. *Nature.*1983, **306**, 281-3.

Bohlmann, H. *Crit. Rev. Plant Sci.*. 1994, **13**, 1-16.

Boman, H.G. and Hultmark, D. *TIBS.* 1981, 306-9.

Boman, H.G., Wade, D., Boman, I.A., Wahlin, B. and Merrifield, R.B. *FEBS Lett.* 1989, **259**, 103-6.

Boman, H.G. *Cell.* 1991, **65**, 205-7.

Boman, H.G. *Annu. Rev. Immun.* 1995, **13**, 61-92.

Boman, H.G., Broekaert, W.F. and Willem, F. *Immunologist.* 1999, **6**, 234-8.

Bösch, C., Brown, L.R. and Wüthrich, K. *Biochim. Biophys. Acta.* 1980, **603**, 298-312.

Bowie, J.H., Chia, B.C.S. and Tyler, M.J. *Pharm. News.* 1998, **5**, 6, 16-21.

Bowie, J.H., Wegener, K.L., Chia, B.C.S., Wabnitz, P.A., Carver, J.A., Tyler, M.J. and Wallace, J.C. *Prot. Pept. Lett.* 1999, **6**, 259-69.

Bradford, A.M., Bowie, J.H., Tyler. M.J. and Wallace, J.C. *Aust. J. Chem.* 1996, **49**, 1325-31.

Bradshaw, J.P., Davies, J.M. and Hauss, T. *Biophys. J.* 1998, **75**, 889-95.

Brahms, S. and Brahms, J. *J. Mol. Biol.* 1980, **138**, 149-78.

Braun, W., Wider, G., Lee, K.H. and Wüthrich, K. *J. Mol. Biol.* 1983, **169**, 921-48.,

References

Braunschweiler, L. and Ernst, R.R. *J. Mag. Reson.* 1983, **53**, 521-8.

Brown, L.R. *Biochim. Biophys. Acta.* 1979, **557**, 135-48.

Brown, L.R. and Wüthrich, K. *Biochim. Biophys. Acta.* 1977, **468**, 389-410.

Brown, L.R. and Wüthrich, K. *Biochim. Biophys. Acta.* 1981, **647**, 95-111.

Brown, L.R., Braun, W., Kumar, A. and Wüthrich, K. *Biophys. J.* 1982, 37, 319-28.

Brock. T.D. in *Biology of Microorganisms*. 4th Ed. Prentice Hall Inc., New Jersey. 1984.

Brooks III C.L. and Nilsson, L. *J. Am. Chem. Soc.* 1993, **115**, 11034-5.

Bruch, M.D. and Gierasch, L.M. *J. Mol. Biol.* 1990, **265**, 351-8.

Brünger, A.T., Clore, G.M., Gronenborn, A.M amd Karplus, M. *Proc. Natl. Acad Sci. USA.* 1986, **83**, 3801-9.

Brünger, A.T. in *X-PLOR: A system for X-ray Crystallography and NMR*. Yale University, New Haven, Connecticut. 1992.

Brünger, A.T. and Nilges, M. *Q. Rev. Biophys.* 1993, **26**, 49-125.

Büssing, A., Stein, G.M., Wagner, M., Wagner, B., Schaller, G., Pfüller, U and Schietzel, M. *Eur. J. Biochem.* 1999, **262**, 79-87.

Callaway, J.E., Lai, J., Haselbeck, B., Baltaian, M., Bonnesen, S.P., Weickmann, J., Wilcox, G. and Lei, S.P. *Antimicrob. Agents. Chemother.* 1993, 37, 1614 -9.

References

Cammers-Goodwin, A., Allen, T.J., Oslick, S.L., McClure, K.F., Lee, J.H. and Kemp, D.S. *J. Am. Chem. Soc.* 1996, **118**, 3082-90.

Cantor, C.R. and Timasheff, S.N. in *Optical Spectroscopy of Proteins*. 3rd Ed. Vol. 5. (Neurath, H. and Hill, R.L. Eds.) Academic Press, New York. 1982. p.145-306.

Carraway, R.E. and Cochrane, D.E. *J. Biol. Chem.* 1987, **261**, 15886-9.

Castano, S., Cornut, I, Büttner, K., Dasseux, J.L. and Dufourcq, J. *Biochim. Biophys. Acta.* 1999, **1416**, 161-75.

Cevc, G. *Biochim. Biophys. Acta.* 1990, **1031**, 311-5.

Chazin, W.J. and Wright, P.E. *J. Mol. Biol.* 1988, **202**, 623-36.

Chia, B.C.S., Carver, J.A., Mulhern, T.D. and Bowie, J.H. *Eur. J. Biochem*, 2000a. In press.

Chia, B.C.S., Carver, J.A., Bowie, J.H., Wong, H. and Lie, W. *Aust. J. Chem.* 2000b. In press.

Chen, H.C., Brown, J.H., Morell, J.L. and Huang, C.M. *FEBS. Lett.* 1988, **36**, 462-6.

Chiu, W. and Schmid, M.F. *Nature Struct. Biol.* 1996, **4**, 5, 331-3.

Christensen, B., Fink, J., Merrifield, R.B. and Mauzerall, D. *Proc. Natl. Acad. Sci. USA.* 1988, **85**, 5072-6.

References

Clark, D.P., Durell, S., Maloy, W.L. and Zasloff, M. *J. Biol. Chem.* 1994, **269**, 14, 10849-55.

Clayden, N.J. and Williams, R.J.P. *J. Mag. Reson.* 1982, **49**, 383.

Clore, G.M., Martin, S.R. and Gronenborn, A.M. *J. Mol. Biol.* 1986, **191**, 553-61.

Clore, G.M. and Gronenborn, A.M. *Annu. Rev. Biophys. Biophys. Chem.* 1991, **20**, 29-63.

Clore, G.M., Robien, M.A. and Gronenborn, A.M. *J. Mol. Biol.* 1993, **231**, 82-102.

Cociancich, S., Ghazi, A., Hetru, C., Hoffman, J.A. and Letellier, L. *J. Biol. Chem.* 1993, **268**, 19239-48.

Coghlan, A. *Nature.* 1997, **387**, 861-9

Colowick, S.P. and Kaplan, N.O. in "Drug and Enzyme Targeting. Part A". *Methods in Enzymology.* Vol. 112. Academic Press Inc., Orlando. 1985.

Compans, R.W., Cooper, M., Hogle, J.H., Ito, Koprowski, Y.H., Melchers, F., Oldstone, M., Olsnes, M. S., Potter, M., Saedler, H., Vogt, P.K. and Wagner, H. in *Current Topics in Microbiology and Immunology.* Vol. 234. Springer-Verlag, New York. 1998.

Conner, J., Bucana, C., Fidler, I.J. and Schroit, A.J. *Proc. Natl. Acad. Sci .USA.* 1989, **86**, 3184-8.

Crabbe, P. in *Optical Rotatory Dispersion and Circular Dichroism in Organic Chemistry.* Holden Day Pub., San Francisco. 1965. p.7-26 and 325-35.

References

Crabbe, P. in *Optical Rotatory Dispersion and Circular Dichroism in Chemistry and Biochemistry*. Academic Press, New York. 1972. p.7-10.

Crease, R. *Science*. 1989, **246**, 883-4.

Creighton, T.E. in *Proteins: Structures and Molecular Properties*. 2nd Ed. W.H. Freeman, New York. 1993. p.238-45.

Crook, G.A. and Tyler, M.J. *Trans. R. Soc. S. Aust*. 1981, **105**, 2, 49-52.

Cruciani, R.A., Barker, J.L., Durell, S.R., Zasloff, M., Chen, H.-C. and Colamonic, O. *Proc. Natl. Acad. Sci*. 1991, **88**, 3792-6.

Cruciani, R.A., Barker, J.L., Durell, S.R., Raghunathan, G., Guy, H.R., Zasloff, M. and Stanley, E. *Eur. J. Pharm*. 1992, **226**, 287-96.

Dathe, M. and Wieprecht, T. *Biochim. Biophys. Acta*. 1999, **1462**, 71-87.

Davies, G.D. and Bax, A. *J. Am. Chem. Soc*. 1985, **107**, 2820-1.

Davis, J. *Biochim. Biophys. Acta*. 1983, **737**, 117-71.

Davies, J. *Nature*. 1996, **383**, 219-220.

Davis, J., Jeffrey, K., Bloom, M., Valic, M. and Higgs, T. *Chem Phys. Lett*. 1976, **42**, 390-4.

Deber, C.M. and Li, S.C. *Biopolymers*. 1995, **37**, 295-318.

de Lucca, A.J. and Walsh T.J. *Antimicrob. Agents Chemother*. 1995, **43**, 1-11

References

de Lucca, A.J., Jacks, T.J. and Borgden, K.A. *Mol. Cell Biochem.* 1995, **151**, 141-8.

Dempsey, C.E. *Biochim. Biophys. Acta.* 1990, **1031**, 143-61.

Dempsey, C.E., Bazzo, R., Harvey, T.S., Syperek, I., Boheim, G. and Campbell, I.D. *FEBS. Lett.* 1991, **281**, 12, 240-4.

Denk, W., Bauman, R. and Wagner, G. *J. Mag. Reson.* 1986, 67, 386-9.

de Vries, J.J. and Berendsen, H.J.C. *Nature.* 1969, **221**, 1139-40.

de Waal, A., Gomes, A.V., Mensink, A. and Grootegoed, J. A. *FEBS. Lett.* 1991, **293**, 219-23.

Dhople, V.M. and Nagaraj, R. *Protein Eng.* 1995, **8**, 315-8.

Dorner, B., Ostresh, J.M., Blondelle, S.E., Dooley, C.T. and Houghten, R.A. *Adv. Amino Acid Mimetics Peptidomimetics.* 1997, **1**, 109-125

Duckworth, D.H., Becers, E.M., Verkleij, A.J., Kamp, J.A.F. and Deenen, L.L.M. Arch. Biochem. Biophys. 1974, **165**, 379-87.

Ducloheir, H., Molle, G. and Spach, G. *Biophys. J.* 1989, **56**, 1017-21.

Ducloheir, H., Snook, C.F. and Wallace, B.A.. *Biochim. Biophys. Acta.* 1998, **1415**, 255-60.

Duncan, T.M. in *A Compilation of Chemical Shifts Anisotropies.* Farragu Press, Chicago. 1990.

References

Dunn, R.D., Weston, K.M., Longhurst, T.J., Lilley, G.G., Rivett, D.E., Hudson, P.J. and Rasion, R.L. *Immunotech*. 1996, **2**, 229-240.

Durell, S.R., Raghunathan, G. and Guy, H.R. *Biophys. J.* 1992, **63**, 1623-70.

Dyson. H.J. and Wright, P.E. *Ann. Rev. Biophys. Chem.* 1991, **20**, 519-38.

Dyson, H.J., Merutka, G., Waltho, J.P., Lerner, R.A. and Wright, P.E. *J. Mol. Biol.* 1992, **226**, 795-817.

Ehret-Sabatier, L., Loew, M., Goyffon, M., Fehlbaum, P., Hoffman, J.A. and Bulet, P.H. *J. Biol. Chem.* 1996, **271**, 29537-44.

Eisenberg, D. *Annu. Rev. Biochem.* 1984, **53**, 595-623.,

Engh, R.A. and Huber, R. *Acta Crystallog. sect. A*. 1991, **47**, 392-400.

Epand, R.M., Shai, Y., Segrest, J.P. and Anantharamaiah, G.M. *Biopolymers*.1995, **37**, 319-38.

Epand, R.M. and Vogel, H.J. *Biochim. Biophys. Acta*. 1999, **1422**, 11-28.

Ernst, R.R., Bodenhausen, G. and Wokaun, A. in *Principles of Nuclear Magnetic Resonance in One and Two Dimensions*. Clarendon Press, Oxford. 1987.

Erspamer, V. in *Amphibian Biology: The Integument*. Vol.1. Surrey Beatty and Sons, Australia. 1994. p.178-350.

Erspamer, V. and Melchiorri, P. *Pure. Appl. Chem.* 1973, **35**, 463-94.

Erspamer, V. and Melchiorri, P. *Trends Pharmacol. Sci.* 1980, **1**, 391-5.

References

Erspamer, V. and Melchiorri, P. in *Growth Hormone and Other Biologically Active Peptides*. (Pecile, A. and Muller, E. Eds.) Excerpta Medica, Amsterdam. 1980b. p.185-94.

Erspamer, V., Roseghini, M., Endean, R. and Anastasi, A. *Nature (London)*. 1966a, **212**, 204-9.

Erspamer, V., de Caro, G. and Endean, R. *Experientia.* 1966b, **22**, 738-45.

Erspamer, V., Erspamer, G.F., Inselvini, M. and Negri, L. *Brit. J. Pharmacol.* 1972, **45**, 333-9.

Erspamer,V., Melchiorri, P., Nakajima, T., Yasyuhara, T. and Endean, R. *Experimentia.* 1979, **35**, 1132-9.

Erspamer, V., Erspamer, G.F., Mazzanti, G. and Endean, R. *Comp. Biochem. Physiol.* 1984, **77C**, 1, 99-108.

Erspamer, W. Erspamer, G.F. and Cei, J.M. *Comp. Biochem. Physiol.* 1986, **85**, 1, 125-37.

Erspamer, V., Erspamer, G.F., Severini, C., Potenza, R.L., Barra, D., Mignogna, G. and Bianchi, A. *Toxicon.* 1993, **31**, 9, 1099-111.

Esposito, G., S. Carver, J.A., Boyd, J. and Campbell, I.D. *Biochemistry.* 1987, **26**, 4, 1043-50.

Evans, J.S. in *Biomolecular NMR Spectroscopy*. Oxford University Press, Oxford. 1995.

Ewald, P.W. and Cochran, G. *Nat. Hist.* 1999, **2**, 34-47.

References

Fernandez, I., Ubach, J., Fuxreiter, M., Andreu, J.M., Andreu, D. and Pos, M. *Chem. Eur. J.* 1996, **2**, 7, 838-46.

Fink, J., Boman, A., Boman, H.G. and Merrifield, R.B. *Int. J. Pept. Prot. Res.* 1989, **33**, 412-21.

Fitton, J., Dell, A., Shaw, W. *FEBS. Lett.* 1980, **115**, 209-12.

Flores, T.P. and Moss, D.S. in *Molecular Dynamics: Application in Molecular Biology*. (Goodfellow, J.M. Ed.) Macmillian Press Inc., London. 1991. p.1-26.

Folmer, R.H.A., Hilbers, C.W., Konings, R.N.H. and Nilges, M. *J. Biomol. NMR.* 1997, **9**, 245-58.

Foresman, JB. and Frisch, A. in *Exploring Chemistry with Electronic Structure Methods*. Gaussian Inc., Pittsburg. 1993. p.57-8.

Frey, S. and Tamm, L.K. Biophys. J. 1991, 60, 922-30.

Frieden T.R., Munsiff S.S. and Low D.E. *Lancet.* 1993, **342**, 76-9.

Fuchs, P.C., Barry, A.L. and Brown, S.D. *Antimicrob. Agents Chemother.* 1998, **42**, 1213-6.

Garcia-Olmedo, F., Molina, A., Alamillo, J.M. and Rodriguez-Palanzuèla, P. *Biopolymers.* 1998, **47**, 479-494.

Ganz, T. in *Antimicrobial Peptides: Ciba Symposium 186*. Wiley and Sons, New York. 1994. 62-76.

Ganz, T. and Lehrer, R. *Curr. Opin. Hematol.* 1997, **4**, 53-8.

References

Gazit, E., Lee, W.J., Brey, P.T. and Shai, Y. *Biochemistry.* 1994, **33**, 10681-92.

Gazit, E., Boman, A., Boman, H.G. and Shai, Y. *Biochemistry*, 1995, **34**, 11479-88.

Gazit, E., Miller, I.R., Biggin, P.C., Sansom, M.S.P. and Shai, Y. *J. Mol. Biol.* 1996, **258**, 860-70.

Gennaro, R., Skerlavaj, B. and Romeo, D. *Infect. Immun.* 1989, **57**, 3142-6.

Gesell, J., Zasloff, M. and Opella. S.J. *J. Biomol. NMR.* 1997, **9**, 127-35.

Gibson, B.W., Poulter, L., Williams, D.H. and Maggio, J.E. *J. Biol. Chem.* 1986, **261**, 5341-9.

Giovannini, M.G., Poulter, L., Gibson, B.W. and Williams, D.H. *Biochem. J.* 1987, **243**, 113-9.

Glusker, J.P., Lewis, M.G. and Rossi, M. in *Crystal Structure Analysis for Chemists and Biologists.* VCH Publishers, New York. 1994. p.643-5.

Gmeiner, W.H. and Babcook, D.M. *Magnetic Moments.* 1997, **8**, 4, 3-4.

Goodman, M., Naider, F. and Toniolo, C. *Biopolymers.* 1971, **10**, 1719-30.

Goormaghtigh, E., Raussens, V. and Ruysschaert, J.M. *Biochim. Biophys. Acta.* 1999, **1422**, 105-85.

Grant, G.H. and Richards, W.G. in *Computational Chemistry.* Oxford University Press, Oxford. 1995. p.52-4.

Green, D.M. *Canadian. J. Zoology.* 1970, **57**, 2033-46.

References

Griesinger, C., Otting, G., Wüthrich, K. and Ernst, R.R. *J. Am. Chem. Soc.* 1988, **110**, 7870-2.

Grobner, G., Taylor, A., Williamson, P.T.F., Choi, G., Glaubitz, C., Watts, J.A. de Grip, W.J. and Watts, A. *Anal. Biochem.* 1997, **254**, 132-8.

Gudmundsson, G.H., Lidholm, D.A., Asling, B., Gan, R. and Boman, H.G. *J. Biol. Chem.* 1991, **266**, 11510-9.

Guéron, M., Plateu, P. and Decorps, M. *Prog. NMR Spectrosc.* 1991, **23**, 135-209.

Guo, L., Lim, B.K., Podiye, C.M., Danial, M., Gunn, J.S., Hackett, M. and Miller, S.I. *Cell.* 1998, **95**, 189-98.

Hancock, R.E.W. *Annu. Rev. Microbiol.* 1984, **38**, 237-64.

Hancock, R.E.W., Falla, T. and Brown, M.H. *Adv. Microb. Physiol.* 1995, **37**, 135-75.

Hancock, R.E.W., Piers, K., Brown, M., Falla, T., Gough, M., Wu. M. and Fidai, S. in *Molecular Biology of Pseudomonads.* (Nakazawa, T. Ed.) ASM Press, Washington. 1996. p.441-50.

Hancock, R.E.W. *Lancet.* 1997, **349**, 418-22.

Hancock, R.E.W. and Lehrer, R. *Trends in Biotech.* 1998, **16**, 82-8.

Hancock, R.E.W. *Drugs.* 1999, **57**, 469-73.

Hancock, R.E.W. and Chapple, D.D. *Antimicrob. Agents Chemother.* 1999, **43**, 1435-40.

References

Hanzawa, H., Shimada, I., Kuzuhara, T., Komano, H., Kohda, D., Inagaki, F., Natori, S. and Arata, Y. *FEBS. Lett.* 1990, **269**, 413-9.

Hara, S. and Yamakawa, M. *J. Biol. Chem.* 1995, **270**, 50, 29923-7.

He, K., Ludtke, S.J., Worcester, D.L. and Huang, H.W. *Biophys. J.* 1996, **70**, 2659-66.

Hedberg, O.H., Wade, D. and Edlund, C. *Antimicrob. Agents Chemother*. 2000, **441**, 1, 68-72.

Helliwell, J.R. in *Macromolecular Crystallography with Synchrotron Radiation.* Cambridge University Press, Cambridge. 1992.

Helliwell, J.R. *Nature Struct. Biol.* 1997, **4**, 11, 874-6.

Helliwell, J.R. *Nature Struct. Biol.* 1998a, **5**, Synchrotron Special Issue, 615-7.

Helliwell, J.R. *Acta Cryst. A* 1998b, **A54**, 738-749.

Hirsch, D.J., Hammer, W.L., Maloy, W.L. , Blazyk, J. and Schaefer, J. *Biochemistry*. 1996, **35**, 12733-41.

Holak, T.A., Engström, Å, Kraulis, P.J., Lindeberg, G., Bennich, H., Jones, T.A., Gronenborn, A.M. and Clore, G.M. *Biochemistry* 1988, **27**, 7620-7629.

Holak, T.A., Nilges, M. and Oschkinat, H. *FEBS. Lett.* 1989, **242**, 649-54.

Hiramatsu, K., Aritaka, N., Hanaki, H., Kawasaki, S., Hosoda, Y., Hori, S., Fukuchi, Y. and Kobayashi, I. *Lancet.* 1997, **350**, 1670-3.

References

Howard, K.P. and Opella, S.J. *J. Mag. Reson. Ser. B.* 1996, **112**, 91-4.

Huang, H.W. and Wu,Y. *Biophys. J.* 1991, **60**, 1079-87.

Hunkapiller, M.W., Hewick, R.M., Drewer, W.J. and Hood, L.E. *Methods Enzymol.* 1983, **91**, 399-406.

Hwang, P.M. and Vogel, H.J. *Biochem. Cell. Biol.* 1998, **76**, 235-46.

Hyberts, S.G., Goldberg, M.S., Havel, T.F. and Wagner, G. *Protein. Sci.* 1992, **1**, 736-51.

Ikura, T., Go, N. and Inagaki, F. *Proteins: Struct, Function and Gen.* 1991, **9**, 81-9.

Inagaki, F., Shimada, I., Kawaguchi, K., Hirano, M, Terasawa, I., Ikura, T. and Go, N. *Biochemistry.* 1989, **28**, 14, 5985-91.

Jack, R., Tagg, J. and Ray, B. *Microbiol. Rev.* 1995, **59**, 171-200.

Jacob, L. and Zasloff, M. *Ciba Found. Symp.* 1994, **186**, 197-223

Jeffrey, G.A. and Saenger, W. in *Hydrogen Bonding in Biological Structures.* Springer-Verlag, New York. 1991.

Jeneer, J., Meier, B.H., Bachmann, P. and Ernst, R.R. *J. Chem. Phys.* 1979, **71**, 11, 4546-53.

Jorgensen, J.H., Cleeland, R., Craig, W.A., Doern, G., Ferraro, M.J., Fingold, D.A., Hansen, S.L., Jenkins, S.G., Novick, W.J., Pfaller, M.A., Preston, D.A., Reller, L.B. and Swenson, J.M. in *Methods for Dilution - Antimicrobial Susceptibility Tests for*

References

Bacteria that Grow Aerobically. 3rd Ed. *National Committee for clinical Laboratory Standards*. 1993, **13**, 1-12.

Juvvadi, P., Vunnam, S. and Merrifield, R.B. *J. Am. Chem. Soc.* 1996, **118**, 38, 8989-97.

Jeneer, J., Meier, B.H., Bachmann, P. and Ernst, R.R. *J. Chem. Phys.* 1979, **71**, 11, 4546-53.

Johnson., W.C. *Proteins*. 1990, **7**, 205-14.

Kagan, B.L., Selsted, M.E., Ganz, T. and Lehrer, R.I. *Proc. Natl. Acad. Sci. USA.* 1990, **87**, 210-4.

Kaiser, E.T. and Kezdy, F.J. *Proc. Natl. Acad. Sci. USA*. 1983, **80**, 1137-43.

Kaiser, E.T. and Kezdy, F.J. *Science.* 1984, **223**, 249-55.

Kaiser, E.T. and Kezdy, F.J. *Annu. Rev. Biophys.Chem.* 1987, **16**, 562-9.

Karle, I.L., Flippen-Anderson, J.L., Agarwalla, S. and Balaram, P. *Biopolymers* 1994, **34**, 721-735.

Karplus, M. *J. Phys.Chem.* 1959, **30**, 11-5.

Karplus, M. and Petsko, G. A. *Nature.* 1990, **347**, 631-9.

Katz, E. and Demain, A.L. *Bacteriol. Rev.* 1977, **41**, 449-74.

Kay, L.E., Keifer, P. and Saarinen, T. *J. Am. Chem. Soc.* 1992, **114**, 10663-5.

References

Ketchem, R.R., Hu, W. and Cross, T.A. *Science.* 1993, **261**, 1457-60.

Koeppe, R.E., Killian, J.A., Vogt, T.C., de Kruijff, B., Taylor, M.J., Mattice, G.L. and Greathouse, D.V. *Biochemistry.* 1995, **34**, 29, 9299-306.

Kokryakov, V.N., Harwig, S.L., Panyutich, E.A., Shevchenko. A.A., Aleshina, G.M., Shamova, O.V., Korneva, H.A. and Lehrer, R.I. *FEBS. Lett.* 1993, **327**, 231-9.

Kossiakoff, A.A. *Annu. Rev. Biochem.* 1985, **54**, 1195-204.

Krimm, S. in *Infra-red Spectroscopy and Molecular Structure.* (Davies, M. Ed.) Elsevier Co., Amsterdam. 1963. p.307-9.

Kuchel, P.W. and Ralston, G.B. in *Theory and Problems in Biochemistry.* Magraw Hill Book Co., New York. 1988. p.84-5

Kumar, S. and Bansal, M. *Biophys. J.* 1998, **75**, 1935-1944.

Labler, L., Keilova, H., Sorm, F. and Styblova, S. *Toxicon.* 1968, **5**, 247-51.

Lange, Y. and Ramos, B.V. *J. Biol. Chem.* 1983, **258**, 15130-4.

Laskowski, R.A., MacArthur, M.W., Smith, D.K., Jones, D.T., Hutchinson, E.G., Morris, A.L., Naylor, D., Moss, D.S. and Thornton, J..M. in *PROCHECK v.3.0.: Programs to check the Stereochemical Quality of Protein Structures.* 1994.

Lauterwein, J., Bösch, C., Brown, L.R. and Wüthrich, K. *Biochim. Biophys. Acta.* 1979, **556**, 244-64.

Lawyer, C., Pai, S., Watabe, M., Borgia, P., Eagleton, L. and Watabe, K. *FEBS. Lett.* 1996, **390**, 95-8.

References

Lazarovic, P., Primor, N. and Loew, L.M. *J. Biol. Chem.* 1986, **261**, 16704-13.

Lazarus, L.H. and Attila, M. *Prog. in Neurobiology.* 1993, **41**, 473-507.

Lazo, N.D., Hu, T.A. and Cross, T.A. *J. Magn. Res.* 1995, **107**, 43-50.

Lee, K.H., Fitton, J.E. and Wüthrich, K. *Biochim. Biophys. Acta.* 1987, **911**, 144-153.

Lehrer, R.I., Ganz, T. and Selsted, M.E.. *Cell.* 1991, **64**, 229-32.

Lehrer, R.I., Lichtenstein, A.K. and Ganz, T. *Ann. Rev. Immunol.* 1993, **11**, 105-9.

Lehrman, S.R., Tuls, J.L. and Lund, M. *Biochemistry.* 1990, **29**, 5590-6.

Levy, G.C. and Lichter, R.L. in *Nitrogen-15 Nuclear Magnetic Resonance Spectroscopy.* John Wiley and Sons, New York. 1979.

Lewin, B. in *Genes.* 4th Ed. Oxford University Press, Oxford. 1990.

Li, Z.Q., Merrifield, R.B., Boman, A. and Boman, H.G. *FEBS. Lett.* 1988, **231**, 2, 299-302.

Lipsky, B.A., MacDonald, D. and Litka, P.A. *Diabetologia.* 1997, **40**, 482-7.

Llinas, M. and Klein, M.P. *J. Am Chem. Soc.* 1975, **97**, 4731-7.

Lohner, K. and Prenner, E.J. *Biochim. Biophys. Acta.* 1999, 1462, 141-56.

Ludke, S.J., He, K., Wu.,Y. and Huang, H.W. *Biochim. Biophys. Acta.* 1994, **1190**, 181-84.

References

Ludke, S.J., He, K. and Huang, H.W. *Biochemistry*. 1995, **34**, 16764-9.

Ludke, S.J., He, K., Heller, W.T., Harroun, T.A., Yang, L. and Huang, H.W. *Biochemistry*. 1996, **35**, 13723-8.

Lugtenberg, B. and van Alpen, L. *Biochim. Biophys. Acta*. 1983, **737**, 51-115.

Maeji, N.J., Bray, A., Valerio, R. and Wang, W. *Peptide Res*. 1995, **8**, 33-8.

Maget-Dana, R. *Biochim. Biophys. Acta*. 1999, **1462**, 109-40.

Maloy, W.L. and Kari, U.P. *Biopolymers*. 1995, **37**, 105-22.

Marassi, F.M., Ramamoorthy, A. and Opella, S.J. *Proc. Natl. Acad. Sci. USA*. 1997, **94**, 8551-56.

Marassi, F.M. and Opella, S.J. *Curr. Opin. Struct. Biol*. 1998, **8**, 640-8.

Marassi, F.M., Opella, S.J., Juuvadi, P. and Merrifield, R.B. *Biphys. J*. 1999, **77**, 6, 3152-55.

Marina, A., Carcia, M.A., Albar, J.P., Yague, J., Lopez de Castro, J.A. and Vazquez, J. *J. Mass Spectrom*. 1999, **34**, 17-27.

Marion, D. and Wüthrich, K. *Biochem. Biophys. Res. Comm*. 1983, **113**, 3, 967-74.

Marion, D., Zasloff, M. and Bax, A. *FEBS Lett*. 1988, **227**, 1, 21-5.

Markley, J.L., Bax, A., Arata, Y., Hilbers. C.W., Kaptein, R., Sykes, B.D., Wright, P.E. and Wüthrich, K. *J. Mol. Biol*. 1998, **280**, 933-52.

References

Marshall, D.A., Mertz, P.M., Cazzaniga, A.L., Eaglstein, W.H., Weber, A., Berkowitz, B. and Jacob, L.S. *Clin. Res.* 1991, **39**, 566-72.

Matsuzaki, K., Harada, M. and Funakoshi, S. *Biochem. Biophys. Acta.* 1989a, **981**, 130-4.

Matsuzaki, K., Harada, M., Handa, T., Funakoshi, S., Fujii, N., Yajima,H and Miyajima, K. *Biochim. Biophys. Acta.* 1989b, **981**, 130-4.

Matsuzaki, K., Harada, M., Funakoshi, S., Fujii, N and Miyajima, K. *Biochim. Biophys. Acta.* 1991, **1063**, 162-70.

Matsuzaki, K., Murase, O., Tokuda, H., Funakoshi, S, Fujii, N. and Miyajima, K. *Biochemistry.* 1994, **33**, 3342-9.

Matsuzaki, K., Sugishita, K., Fujii, N. and Miyajima, K. *Biochemistry.* 1995, **34**, 3423-9.

Matsuzaki, K., Murase, O., Fujii, N. and Miyajima, K. *Biochemistry.* 1996, **35**, 11361-8.

Matsuzaki, K., Nakamura, A., Murase, K., Sugishita, N., Fujii, N. and Miyajima, K. *Biochemistry.* 1997, **36**, 2104-11.

Matsuzaki, K., Sugishita, K., Harada, M., Fujii, N. and Miyajima, K. *Biochim. Biophys. Acta.* 1997b, **1327**, 119-30.

Matsuzaki, K. *Biochim. Biophys. Acta.* 1998, **1376**, 391-400.

Matsuzaki, K., Nakamura, A., Ishibe, N., Nakata, S. and Miyajima, K. *Biochemistry.* 1998, **37**, 11856-63.

References

Matsuzaki, K. *Biochim. Biophys. Acta.* 1999, **1462**, 1-10.

Matsuzaki, K., Sugishita, K. and Miyajima, K. *FEBS. Lett.* 1999, **449**, 221-4.

McCammon, J.A. and Harvey, S.C. in *Dynamics of Proteins and Nucleic Acids.* Cambridge University Press, Cambridge. 1987.

McDonnell, P.A. and Opella, S.J. *J. Magn. Reson., Series B.* 1993, **102**, 120-5.

McGuire, W.L. in *Immunotoxins.* Kluwer Academic Publishers, Boston. 1988.

McLeish, M., Nielsen, K.J., Najbar, L.V., Wade, J.D., Lin, F., Doughty, M.B. and Craik, D.J. *Biochemistry* 1994, **33**, 11174-11183.

Mehring, M. in *Principles of High Resolution NMR in Solids.* 2nd Ed. Springer-Verlag, Berlin. 1983. p.233-258.

Merutka, G., Dyson, H.J. and Wright, P.E. *J. Biomol. NMR.* 1995, **5**, 14-24.

Miteva, M., Anderson, M., Karshikoff, A. and Otting, G. *FEBS. Lett.* 1999, **462**, 155-8.

Moll, F. and Cross, T.A. *Biophys. J.* 1990, **57**, 351-9.

Moore, J.M., Case, D.A., Chazin, W.J., Gippert, G.P., Havel, T.F., Powls, R. and Wright, P.E. *Science.* 1988, **140**, 314-31.

Moore, K.S., Bevins, C.L., Brasseur, M.M., Tomassini, N., Turner, K., Eck, H. and Zasloff, M. *J. Biol. Chem.* 1991, **266**, 29, 19851-7.

References

Mor, A and Nicolas, P. *J. Biol. Chem.* 1994, **269**, 1934-9.

Mor, A., Nguyen, V.H., Delfour, A., Miglior-Samour, D., and Nicolas, P. *Biochemistry.* 1991, **30**, 8824-30.

Mor, A., Hani, K. And Nicolas, P. *J. Biol. Chem.* 1994, **269**, 50, 31635-41.

Morris, A.L., MacArthur, M.W., Hutchinson, E.G. and Thornton, J.M. *Proteins.* 1992, **12**, 345-64.

Nakajima, T. *Trends Pharmacol. Sci.* 1981, **2**, 202-5.

Nakajima, Y., Qu, X.M. and Natori, S. *J. Biol. Chem.* 1987, **262**, 1665-9.

Nakamura, T., Furunaka, H., Miyata, T., Tokunaga, F., Muta, T., Iwanaga, S., Niwa, M., Takao, T. and Shimonishi, Y. *J. Biol. Chem.* 1988, **263**, 16709-13.

Negri, L., Lattanzi, R. and Melchiorri, P. *Brit. J. Pharm.* 1995, **114**, 57-66.

Nelson, J.W. and Kallenbach, N.R. *Proteins.* 1986, **1**, 211-7.

Neu, H.C. *Science.* 1992, **257**, 1064-73.

Neville, D.M. in *CRC Critical Review in Therapeutic Drug Carrier Systems.* Vol. 2. CRC Press Inc., London. 1986. p.329-52.

Nicolas, P. and Mor, A. *Annu. Rev. Microbiol.* 1995, **49**, 277-304.

Niimura, N., Minezaki, Y., Nonaka, T., Castagna, J.C., Cipriani, F., Høghøj, P., Lehmann, M.S. and Wilkinson, C. *Nature Struct. Biol.* 1997, **4**, 11, 909-14.

References

Nikaido, H. and Vaard, M. *Microbiol. Rev.* 1985, **49**, 1-32.

Nilges, M., Clore, G.M. and Gronenborn, A.M. *FEBS. Lett.* 1988a, **239**, 129-36.

Nilges, M., Gronenborn, A.M., Brünger, A.T. and Clore, G.M. *Prot. Eng.* 1988b, **2**, 27-38.

Nilges, M., Kuszewski, J. and Brünger, A.T. in *Computational Aspects of the Study of Biological Macromolecules by NMR.* (Hoch, J.C. Ed.) Plenum Press, New York. 1991.

North, C.L., Barranger-Mathys, M., Cafiso, D.S. *Biophys. J.* 1995, **69**, 2392-7.

Ojcius, D.M. and Young, J.D.E. *Trends. Biochem. Sci.* 1991, **16**, 225-9.

Olejniczak, E.T., Gampe, R.T. and Fesik, S.W. *J. Mag. Reson.* 1989, **81**, 178-84.

Opella, S.J. *Nature. Struct. Biol.* 1997, **4**, 845-8.

Opella, S.J., Chirlian, L.E. and Bechinger, B. in *Biological NMR Spectroscopy.* (Markley, J.L. and Opella, S.J. Eds.) Oxford University Press, Oxford. 1997. p.161-79.

Oren, Z. and Shai, Y. *Eur. J. Biochem.* 1996, **237**, 303-10.

Oren, Z. and Shai, Y. *Biochemistry.* 1997, **36**, 1826-35.

Oren, Z., Hong, J. and Shai, Y. *Biochemistry.* 1997, **272**, 14643-9.

Ovchinnikov, Y.A. and Ivanov, V.T. in *The Proteins.* (Neurath, H. and Hill, R.L. Eds.) Academic Press, New York. 1982. p. 391-8.

References

Pai, L.H. and Pastan, I. in *Biologic Therapy of Cancer*. (DeVita, V.T., Hellman, S. and Rosenberg, S.A. Eds.) Lippincott Publishers, Philadelphia. 1994. p. 521-533.

Pallagy, P.K., Duggan, B.M., Pennington, M.W. and Norton, R.S. *J. Mol. Biol.* 1993, **234**, 405-20.

Pardi, A., Billeter, M. and Wüthrich, K. *J. Mol. Biol.* 1984, **180**, 741-51.

Park, C.B., Kim, M.S. and Kim, S.C. *Biochem. Biophys. Res. Commun.* 1996, **218**, 408-13.

Pastore, A. and Saudek, V. *J. Magn.Reson.* 1990, **90**, 165-76.

Pescher, A., Otto, M., Jack, R.W., Halbacher, H., Jung, C. and Gotz, F. *J. Biol. Chem.* 1999, **274**, 8405-10.

Piers, K.L. and Hancock, R.E.W. *Mol. Microbiol.* 1994, **12**, 6, 951-8.

Polozov, I.V., Polozova, A.I., Molotkovsky, J.J. and Epand, R.M. *Biochim. Biophys. Acta.* 1997, **1328**, 125-39.

Pouny, Y., Rapaport, D., Mor, A., Nicolas, P. and Shai, Y. *Biochemistry.* 1992, **31**, 12416-23.

Pramanik, A., Thyberg, P. and Rigler, R. *Chem. Phys. Lipids.* 2000, **104**, 1, 35-47.

Prenner, E.J., Lewis, N.A.H., Kondejewski, L.H., Hodges, R.S. and McElhaney, R.N. *Biochim. Biophys. Acta.* 1999, **1417**, 211-23.

References

Prenner, E.J., Lewis, N.A.H. and McElhaney, R.N. *Biochim. Biophys. Acta.* 1999, **1462**, 201-21.

Prestegard, J.H. *Nature. Struct. Biol.* 1998, **5**, 517-22.

Rajan, R. and Balaram, P. *Int. J. Peptide. Protein. Res.* 1996, **48**, 328-36.

Ramachandran, G.N., Ramakrishnan, C. and Sassiekharan, V. *J. Mol. Biol.* 1963, **7**, 95-9.

Ramachandran, G.N. and Sassiekharan, V. *Adv. Prot. Chem.* 1968, **28**, 283-437

Rana, F.R., Sultany, C.M. and Blazyk, J. *FEBS. Lett.* 1990, **261**, 2, 464-7.

Rana, F.R. and Blazyk, J. *FEBS. Lett.* 1991a, **293**, 1, 2, 11-5

Rana, F.R., Marcias, E.A., Sultany, C.M., Modrzakowski, M.C. and Blazyk, J. *Biochemistry.* 1991b, **30**, 5858-67

Rance, M., Sørensen, O.W., Bodenhausen, G., Wagner, R., Ernst, RR and Wüthrich, K. *Biochim. Biophys. Res. Comm.* 1983a, **27**, 157-62.

Rance, M., Sørensen, O.W., Bodenhausen, G., Wagner, G., Ernst, R.R. and Wüthrich, K. *Biochem. Biophys. Res. Comm.* 1983b, **117**, 479-85.

Rand, R.P. and Parsegian, V.A. *Biochem. Biophys. Acta.* 1989, **988**, 351-7.

Rao, A.G. *Arch. Biochem. Biophys.* 1999, **361**, 1, 127-34.

Ratledge, C. and Wilkinson, S.G. in *Microbial Lipids.* Vol 1. Academic Press, London. 1988.

References

Richardson, J.S. *Adv. Protein Chem.* 1981, **34**, 167-339.

Richardson, J.S. and Richardson, D.C. *Science.* 1988, **240**, 1648-54.

Rivett, D.E., Kirkpatrick, A., Hewish, D.R., Reilly, W. and Werkmeister, J. A. *Biochem. J.* 1996, **316**, 525-529.

Roberts, G.C.K. *NMR of Macromolecules.* IRL Press, Oxford. 1995. p.331-8.

Romeo, D., Skerlavaj, B., Bolognesi, M. and Gennaro, R. *J. Biol. Chem.* 1988, **263**, 9573-80.

Roseghini, M., Erspamer, W. and Endean, R. *Comp. Biochem. Physiol.* 1976, **54C**, 31-41.

Rothman, J.E. and Kennedy, E..P. *J. Mol. Biol.* 1977, **110**, 603-18.

Rozek, T., Waugh, R.J., Steinborner, S.T., Bowie, J.H., Tyler, M.J. and Wallace, J.C. *J. Peptide Sci.* 1998, **4**, 111-5.

Saberwal, G. and Nagaraj, R. *Biochim. Biophys. Acta.* 1994, **1197**, 109-31.

Saido-Sakanaka, H., Ishibashi, J., Sagisaka, A., Momotani, E. and Yamakawa, M. *Biochem. J.* 1999, **338**(Part 1), 29-33.

Sanders, C.C. and Sanders, W.E. *Clin. Infect. Dis.* 1992, **15**, 824-39.

Sanders II, C.R. and Prestegard, J.H. *Biophys. J.* 1990, **58**, 447-60.

Sanders II, C.R., Hare, B.J., Howard, K.P. and Prestegard, J.H. *Prog. NMR Spectro.* 1994, **26**, 421-44.

References

Schiffer, M. and Edmundson, A.B. *Biophys. J.* 1967, **7**, 121-35.

Schulz, G.E. and Schirmer, R.H. in *Principles of Protein Structure*. Springer-Verlag, Berlin. 1979.

Schumann, M., Dathe, M., Wieprecht, T., Beyermann, M. and Bienert, M. *Biochemistry*. 1997, **36**, 4345-51.

Seelig, J. and Niederberger, W. *J. Am. Chem. Soc.* 1973, **96**, 7, 2069-72.

Segrest, J.P., Loof, H.D., Dohlman, J.G., Brouillette, C.G. and Anantharamaiah, G.M. *Proteins*. 1990, **8**, 103-17.

Sekharam, K.M., Bradrick, T.D. and Georghiou, S. *Biochim. Biophys. Acta*. 1991, **1063**, 171-9.

Selsted, M.E., Novotny, M.J., Morris, W.L., Tang, Y.Q., Smith, W. and Cullor, J.S. *J. Biol. Chem.* 1992, **267**, 4292-9.

Separovic, F, Gehrmann, J., Milne, T.J., Cornell, B.A., Lins, S.Y. and Smith, R. *Biophys. J.* 1994, **67**, 1495-500.

Shafer W.M. in "Antibacterial peptide protocols". *Methods in Molecular Biology*. Vol. 78. Humana Press, Totowa. 1997.

Shai, Y. *Toxicology*. 1994, **87**, 109-29.

Shai, Y. *Trends. Biochem. Sci.* 1995, **20**, 460-4.

Shai, Y. in "Mode of action of antibacterial peptides". *Molecular Mechansims and Immune Responses of Insects*. Chapman and Hall, London. 1998. p.111-134.

References

Shai, Y. *Biochim. Biophys. Acta*. 1999, **1462**, 55-70.

Shemyakin, M.M., Ovchinnikov, Y.A. and Ivanov, V.T. *Angew. Chem. Int. Ed. Engl.* 1969, **8**, 492-9.

Shin, S.Y., Lee, M.K., Kim, K.L. and Hahm, K.S. *J. Pept. Res.* 1997, **50**, 279-85.

Shin, S.Y., Kang, J.H. and Hahm, K.S. *J. Pept. Res.* 1999, **53**, 82-90.

Shiraki, K., Nishikawa, K. and Goto, Y. *J. Mol. Biol.* 1995, **245**, 180-94.

Silberstein, A., Mirzabekov, T., Anderson, W,F. and Rozenberg, Y. *Biochim. Biophys. Acta*. 1999, **1461**, 1, 103-12.

Simmaco, M., Barra, D., Chiarini, F., Noviello, L., Melchiori, P., Kreil, G. and Richter, K. *Eur. J. Biochem*. 1991, **199**, 217-22.

Simmaco, M., Mignogna, G. and Barra, D. *Biopolymers*. 1998, **47**, 435-50.

Singer, S.J. and Nicolson, G.L. *Science*. 1972, **175**, 720-31.

Sitaram, N and Nagaraj, R. *Biochim. Biophys. Acta*. 1999, **1462**, 29-54.

Skerlavaj, B., Romeo, D. and Gennaro, R. *Infect. Immun*. 1990, **58**, 11, 3724-30.

Skurmik, M., Venho, R., Bengoechea, J.A. and Moriyon, I. *Mol. Microbiol*. 1999, **311**, 1443-62.

Smith, R., Thomas, D.E., Atkins, A.R., Separovic, F. and Cornell, B.A. *J. Mol. Biol.* 1990, **1026**, 161-6.

References

Smith, R., Separovic, F., Milne, T.J., Whittaker, A., Bennet, F.M., Cornell, B.A. and Makriyannis, A. *J. Mol. Biol.* 1994, **241**, 456-66.

Sokolov, Y., Mirzabekov, T., Martin, D.W., Lehrer, R.I. and Kagan, B.L. *Biochim. Biophys. Acta.* 1999, **1420**, 23-9.

Sönnichsen, F.D., Van Eyk, J.E., Hodges, R.S. and Sykes, B.D. *Biochemistry.* 1992, **31**, 8790-8.

Soravia, E., Martini, G. and Zasloff, M. *FEBS Lett.* 1988, **228**, 337-40.

Stanislawski, B. and Rüterjans, H. *Eur. Biophys. J.* 1987, **15**, 1-12.

Sternberg, M.J.E. in *Protein Structure Prediction.* IRL Press, Oxford. 1996. p. 236-8.

Steinborner, S.T., Wabnitz, P.A., Waugh, R.J., Bowie, J.H., Gai, C., Tyler, M.J. and Wallace, J.C. *Aust. J. Chem.* 1996, **49**, 955-63.

Steinborner, S.T., Bowie, J.H., Tyler, M.J. and Wallace, J.C. *Aust. J. Chem.* 1997a, **50**, 889-894.

Steinborner, S.T., Waugh, R.J., Bowie, J.H., Wallace J.C., Tyler, M.J. and Ramsay, S.L *J. Pep. Sci.* 1997b, **3**, 181-185.

Steinborner, S.T., Currie, G.T., Bowie, J.H., Wallace, J.C. and Tyler, M.J. *J. Pep. Res.* 1998, **51**, 121-126.

Steiner, H., Andreu, D. and Merrifield, R.B. *Biochim. Biophys. Acta.* 1988, **939**, 260-6.

References

Stone, D.J.M., Bowie, J.H., Wallace, J.C. and Tyler, M.J. *J. Chem. Soc. Chem. Commun.* 1992a, 1224-5.

Stone, D.J.M., Waugh, R.J., Bowie, J.H., Wallace, J.C. and Tyler, M.J. *J. Chem. Soc. Perkin Trans 1*. 1992b, 3173-8.

Stone, D.J.M., Waugh, R.J., Bowie, J.H., Wallace, J.C. and Tyler, M.J. *J. Chem. Res.* 1993, **S**, 138; **M**, 910-36.

Storrs, R.W., Truckses, D. and Wemmer, D.E. *Biopolymers*. 1992, **32**, 1695-1702.

Strahilevitz,J., Mor, A, Nicolas, P. and Shai, Y. *Biochemistry*. 1994, **33**, 10951-60.

Strom, R., Podo, F., Crifo, C., Berthet, C., Zulauf, M and Zaccai, G. *Biopolymers*. 1983, **22**, 391-7.

Subbalakshmi, C., Naqaraj, R and Sitaram, N. *FEBS. Lett.* 1999, **448**, 1, 62-6.

Sutcliffe, M.J. and Dobson, C.M. *Proteins*. 1991, **10**, 117-29.

Suzuki, S., Ohe, Y, Okubo, T., Kakegawa, T. and Tatemoto, K. *Biochem. Biophys. Res. Comm.* 1995, **212**, 1, 249-53.

Szilagyi, L. and Jardetzky, O. *J. Mag. Reson.* 1989, **83**, 441-9.

Tappin, M.J., Pastore, A., Norton, R.S., Freer. J.H. and Campbell, I.D. *Biochemistry*. 1988, **27**, 1643-7.

Teng, Q and Cross, T. *J. Mag. Reson.* 1989, **85**, 439-47.

References

Terry, A.S., Poulter, L., Williams, D.H., Nutkins, J.C. and Giovannini, M.G. *J. Biol. Chem.* 1988, **263**, 12, 5745-51.

Thomas, W.E. and Ellar, D.J. *J. Cell. Sci.* 1983, **60**, 181-97.

Tian, F. and Cross, T.A. *J. Mol. Biol.* 1999, **285**, 1993-2003.

Tieleman, D.P., Sansom, M.S.P. and Berendsen, H.J.C. *Biophys. J.* 1999, **76**, 40-9.

Tortora, G.J., Funke, B.R. and Case, C.L. in *Microbiology: An Introduction.* Benjamin-Cummings Publishing Co. Inc., California. 1982. p. 462-70.

Tossi, A., Chiara, T. and Romeo, D. *Eur. J. Biochem.* 1997, **250**, 549-58.

Tosteson, M.T. and Tosteson, D.C. *Biophys. J.* 1984, **45**, 112-9.

Turner, J.D. and Rouser, G. *Anal. Biochem.* 1970, **38**, 423-36.

Tyler, M.J. in *Toxic Plants and Animals: A Guide for Australia.* Queensland Museum, Brisbane. 1987. p.329-38.

Tyler, M.J. *Alytes.* 1991a, **9**, 43.

Tyler, M.J. in *Australian Frogs.* Viking O'Neil, Melbourne. 1991b.

Tyler, M.J. in *Encyclopaedia of Australian Animals.* Harper Collins, London. 1992. p.3-42.

Tyler, M.J., Stone, D.J.M. and Bowie, J.H. *J. Pharm. Toxicol. Methods.* 1992, **28**, 199-200.

References

Tytler, E.M., Anantharamaiah, G.M., Walker, D.E., Mishra, V.K., Palgunachari, M.N. and Segrest, J.P. *Biochemistry.* 1995, **34**, 4393-4401.

Urry, D.W. in *Spectroscopy of Biological Molecules.* (Sanddorfy, C. and Theophanides, T. Eds.) Reidel, Dordrecht. 1984. p.487-510.

Utsugi, T., Schroit, A.J., Conner, J., Bucana, C. and Fidler, I.J. *Cancer Res.* 1991, **51**, 3062-6.

Vallera, D.A., Ash, R.C., Zanjani, E.D., Kersey, J.H., LeBien, T.W., Neville, T.M. and Youle, R.J. *Science.* 1983, **222**, 512-5.

Vanhoof, G., Goossens, F., Meester, I., Hendriks, D. and Scharpe, S. *FASEB. J.* 1995, **9**, 736-44.

Vaz Gomes, A., de Waal, A., Berden, J.A. and Westerhoff, H.V. *Biochemistry.* 1993, **32**, 5365-72.

Verkleij, A.J., Zwaal, R.F., Roelofsen, B., Comfurius, P., Kastelijn, D. and Van Deenen, L.L.M. *Biochim. Biophys. Acta.* 1973, **323**, 178-93.

Voelker, D. in *Biochemistry of Lipids and Membranes.* Benjamin Press, Menlo Park, California. 1985. p.475-502.

Vogel, C. W., Wilkie, S.D. and Morgan, A.C. in *Modern Trends in Human Leukaemia.* Spinger-Verlag, Berlin. 1985. p.514-7.

Vogel, H. *Biochemistry.*1987, 26, 14, 4565-71.

Vold, R.R., Prosser, R.S. and Deese, A.J. *J. Biomol. NMR.* 1997, **9**, 329-35.

References

Vunnam, S., Juvvadi, P. and Merrifield, R.B. *J. Pep. Res.* 1997, **49**, 59-66.

Wabnitz, P.A., Bowie, J.H., Wallace, J.C. and Tyler, M.J. *Aust. J. Chem.* 1999, In Press.

Wade, D., Boman, A., Wahlin, B., Drain, C.M., Andreu, D., Boman, H.G. and Merrifield, R.B. *Proc. Natl. Acad. Sci. USA.* 1990, **87**, 4761-5.

Wade, D., Andreu, D., Mitchell, S.A., Silveira, A.M.V., Boman, A., Boman, H.G. and Merrifield, R.B. *Int. J. Pept. Prot. Res.* 1992, **40**, 429-36.

Wagner, G. and Wüthrich, K. *J. Mag. Reson.* 1979, **33**, 675-9.

Walz, T. and Grigorieff, N J. *Struct. Biol.* 1998, **121**, 142-61.

Waugh, R.J., Stone, D.J.M., Bowie, J.H., Wallace, J.C. and Tyler, M.J. *J. Chem. Res.* 1993, **S**, 139: **M**, 937-61.

Waugh, R.J., Steinborner, S.T., Bowie, J.H., Wallace, J.C. and Tyler, M.J., Hu, P. and Gross, M.L. *Aust. J. Chem.* 1995, **48**, 1981-7.

Weber, P.L., Morrison, R. and Hare, D. *J. Mol. Biol.* 1988, **204**, 483-7.

Wegener, K.L., Wabnitz, P.A., Carver, J.A., Bowie, J.H., Chia, B.C.S., Wallace, J.C. and Tyler, M.J. *Eur. J. Biochem.* 1999, **265**, 627-37.

Wegener, K.L., Wabnitz, P.A., Carver, J.A., Bowie, J.H., Wallace, J.C. and Tyler, M.J. *Eur. J. Biochem.* 2000. In Press.

Westerhoff, H.V., Juretic, D., Hendler, R.W. and Zasloff, M. *Proc. Natl. Acad. Sci. USA.* 1989, **86**, 6597-601.

References

Williams. R.W. *J. Mol. Biol.* 1983, **166**, 581-603.

Williams, R.W., Starman, R., Taylor, K.M.P., Gable, K., Beeler, T., Zasloff, M. and Covell, D. *Biochemistry.* 1990, **29**, 4490-6.

Wishart, D.S., Sykes, B.D. and Richards, F.M. *J. Mol. Biol.* 1991, **222**, 311-33.

Wishart, D.S., Sykes, B.D. and Richards, F.M. *Biochemistry.* 1992, **31**, 1647-1651.

Wishart, D.S., Bigam. C.G., Holm, A., Hodges, R.S. and Sykes, B.D. *J. Biomol. NMR.* 1995a, **5**, 67-81.

Wishart D.S., Bigam, C.G., Yao, J., Dyson, H.J., Oldfield, E., Markley, J.L., Sykes, B.D. *J. Biomol. NMR.* 1995b, **6**, 135-40.

Wong, H., Bowie, J.H. and Carver, J.A. *Eur. J. Biochem.* 1997, **247**, 545-57.

Woolfson, D.N. and Williams, D.H. *FEBS. Lett.* 1990, **277**, 185-188.

Wright, P.E. *Trends Biochem. Sci.* 1989, **14**, 255-60.

Wu, Y., He, K., Ludtke, S.J. and Huang, H.W. *Biophys. J.* 1995, **68**, 2361-9.

Wu, C.H., Ramamoorthy, A. and Gierasch, L.M. and Opella, S.J. *J. Amer. Chem. Soc.* 1995, **117**, 6148-57.

Wüthrich, K., Billeter, M. and Braun, W. *J. Mol. Biol.* 1984, **180**, 715-40.

Wüthrich, K. in *NMR of Proteins and Nucleic Acids.* Wiley, New York. 1986.

219

References

Wüthrich, K. *Acc. Chem. Res.* 1989a, **22**, 36-44.

Wüthrich, K. *Science.* 1989b, **243**, 45-50.

Wüthrich, K. *Nature Struct.Biol.* 1998, **5**, Supplement, 492-5.

Wüthrich, K., Billeter, M. and Braun, W. *J. Mol. Biol.* 1983, **169**, 949-61.

Xu, R.X., Word, J.M., Davis, D.G., Rink, M.J., Willard, D.H. and Gampe, R.T. *Biochemistry.* 1995, **34**, 2107-21.

Yang, L., Weiss, T.M., Harroun, T.A., Heller, W.T. and Huang, H.W. *Biophys. J.* 1999, 77, 5, 2648-56.

Yi, G.-S., Park, C.B., Kim, S.C. and Cheong, C. *FEBS. Lett.* 1996, **398**, 87-90.

Zadina, J.E. *Nature.* 1997, **386**, 499-501.

Zasloff, M. *Proc. Natl. Acad. Sci. USA.* 1987, **84**, 5449-53.

Zasloff, M., Martin, B. and Chen, H.C. *Proc. Natl. Acad. Sci. USA.* 1988, **85**, 910-3.

Zhou, N.E., Mant, C.T. and Hodges, R.S. *J. Peptide Res.* 1990, **3**, 8-20.

Zhou, N.E., Zhu, B.Y., Sykes, B.D. and Hodges, R.S. *J. Am. Chem. Soc.* 1992, **114**, 11, 4320-6.

Zubay, G. in *Biochemistry.* Addison-Wesley Publishing Co., Massachusetts. 1986. p.84-5.

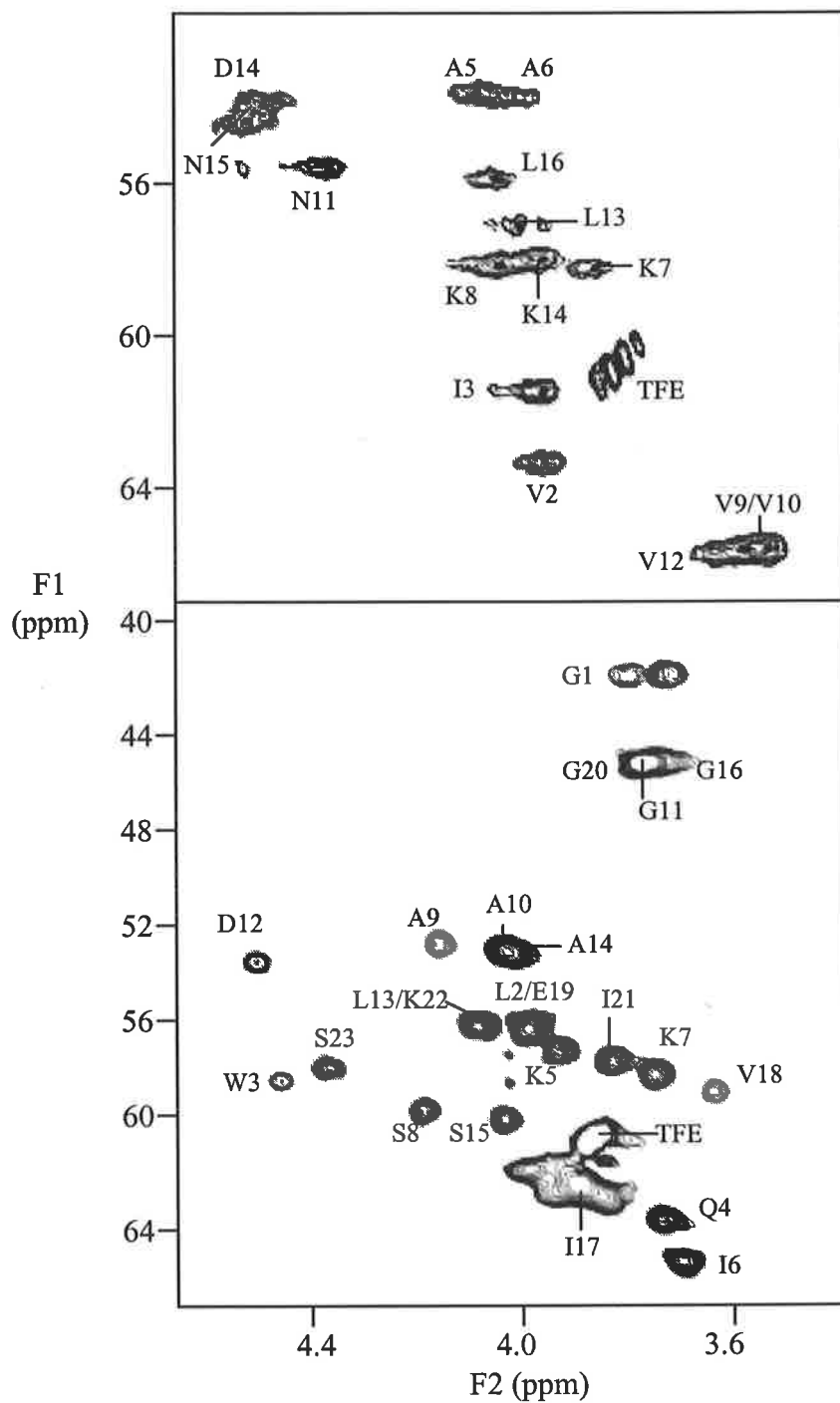Appendix
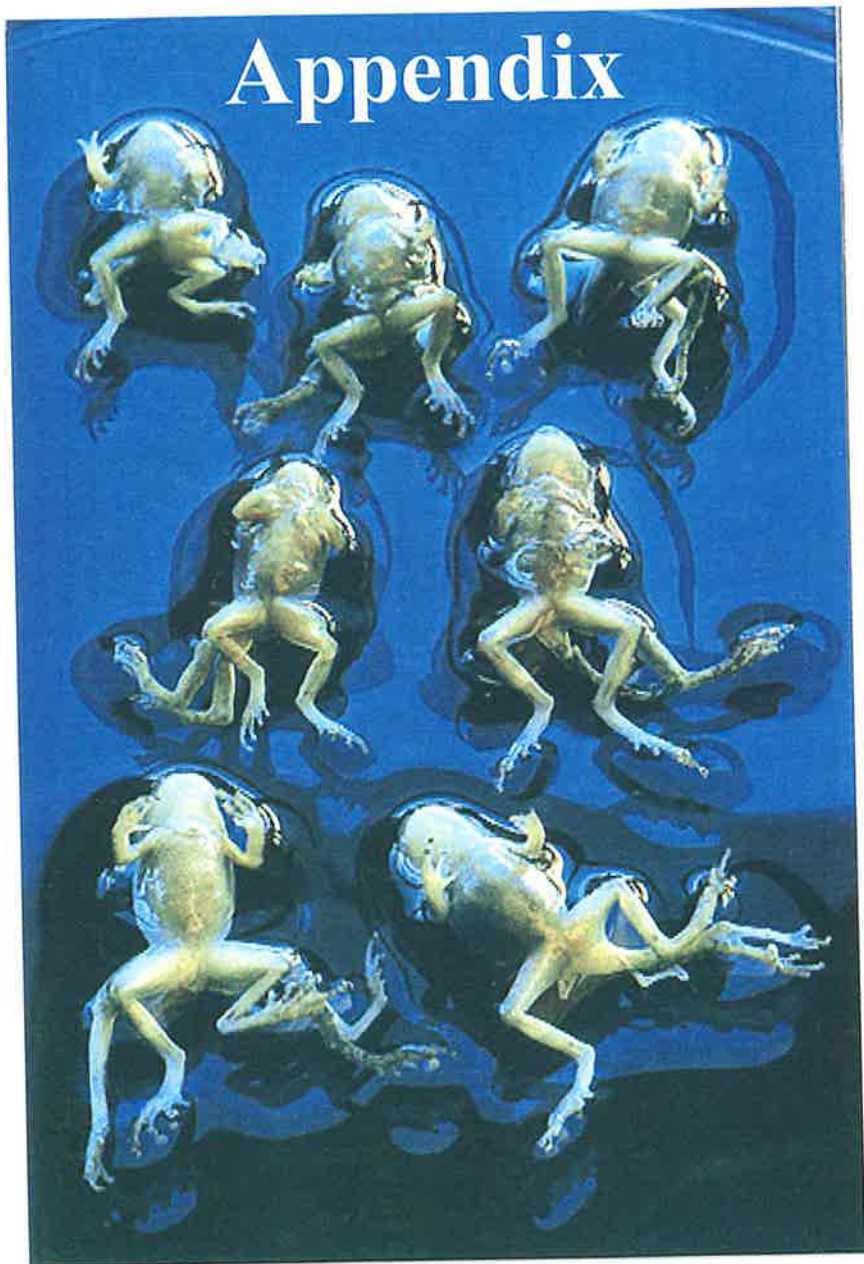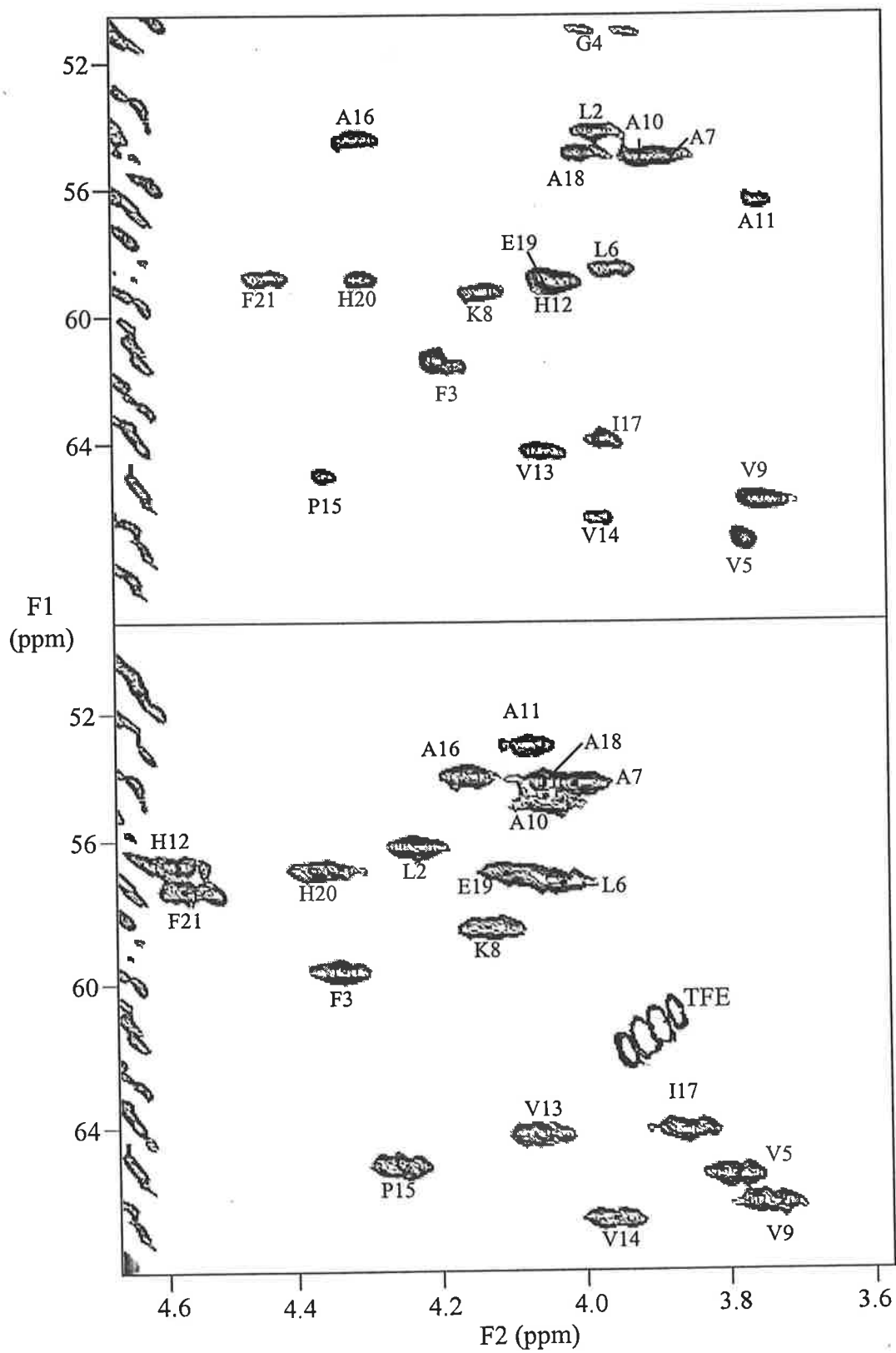
Top: HSQC of maculatin 1.1 in DPC/water pH 7.0, 37°C.

Bottom: HSQC of maculatin 1.1 in d_3-TFE/water (1:1 by vol.) pH 2.5, 25°C.
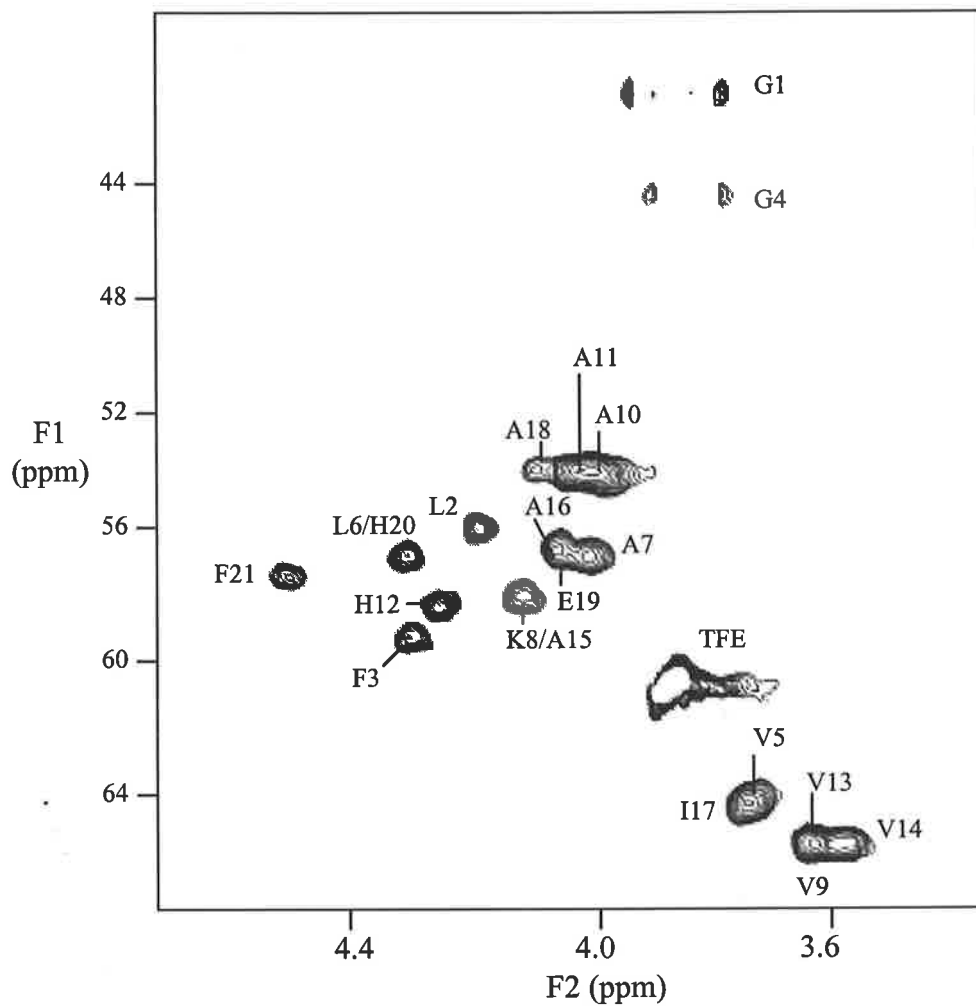
HSQC of Ala15 maculatin 1.1 analogue in d_3-TFE/water (1:1 by vol.) pH 2.5, 25°C.

Top: HSQC of uperin 3.6 in d_3-TFE/water (1:1 by vol.) pH 2.4, 25°C.

Bottom: HSQC of caerin 4.1 in d_3-TFE/water (1:1 by vol.) pH 2.8, 25°C.

Publications

1998 - 2000

List of Publications

1. Bowie, J.H., Tyler, M.J., Chia, B.C.S., Carver, J.A. and Wallace, J.C. The peptide arsenals of Australian Tree Frogs of the genus *Litoria*. *Chemistry in Australia*. 1998, **65**, 8, 45-8.

2. Bowie, J.H., Chia, B.C.S. and Tyler, M.J. Host defense peptides of Australian amphibians : A powerful chemical arsenal. *Pharmaceutical News*. 1998, **5**, 6, 16-21.

3. Bowie, J.H., Wegener, K.L., Wabnitz, P.A., Chia, B.C.S., Carver, J.A., Wallace, J.C and Tyler, M.J. Host defense antibacterial peptides from the skin secretions of Australian amphibians. The relationship between structure and activity. *Protein and Peptide Letters*. 1999, **6**, 259-69.

4. Chia, B.C.S., Carver, J.A., Mulhern, T.D. and Bowie, J.H. The solution structure and activity of Uperin 3.6, an antimicrobial peptide from the granular dorsal glands of the Australian toadlet *Uperoleia mjobergii*. *Journal of Peptide Research*. 1999, **54**, 137-45.

5. Wegener, K.L., Wabnitz, P.A., Carver, J.A., Bowie, J.H., Chia, B.C.S. and Tyler, M.J. Host defence peptides from the skin glands of the Australian Blue Mountains tree-frog *Litoria citropa*. The solution structure of citropin 1.1. *European Journal of Biochemistry*. 1999, **265**, 627-37.

6. Chia, B.C.S., Carver, J.A., Mulhern, T.D. and Bowie, J.H. Maculatin 1.1, an anti-microbial peptide from the Australian tree frog, *Litoria genimaculata*: Solution structure and biological activity. *European Journal of Biochemistry*. 2000. In press.

7. Chia, B.C.S., Carver, J.A., Bowie, J.H., Lie, W. and Wong, H. The solution structure and activity of Caerin 4.1, an antibiotic peptide from the skin glands of the Australian tree frog *Litoria caerulea*. *Australian Journal of Chemistry*. 2000. In press.

8. Chia, B.C.S., Lam, Y.-H., Separovic, F. and Bowie, J.H. Interaction of the antimicrobial peptide maculatin 1.1 with bicelles and phospholipid bilayers: an orientation study using solid-state NMR. Submitted to the *Journal of Biomolecular NMR*.

Bowie, J.H., Chia, C.S.B., Tyler, M.J., Carver, J.A. & Wallace, J.C. (1998) The peptide chemical arsenals of Australian tree frogs of the genus *Litoria*.
Chemistry in Australia, v. 65(8), pp. 45-48

Bowie, J.H., Chia, C.S.B. & Tyler, M.J. (1998) Host defense peptides from the skin glands of Australian amphibians: a powerful chemical arsenal.
Pharmaceutical news, v. 5(6), pp. 16-21

Bowie, J.H., Wegener, K.L., Chia, C.S.B., Wabnitz, P.A., Carver, J.A., Tyler, M.J. & Wallace, J.C. (1999) Host defence antibacterial peptides from skin secretions of Australian amphibians. The relationship between structure and activity.
Protein and Peptide Letters, v. 6(5), pp. 259-269

Chia, C.S.B., Carver, J.A., Mulhern, T.D. & Bowie, J.H. (1998) The solution structure of uperin 3.6 an antibiotic peptide from the granular dorsal glands of the Australian toadlet, *Uperoleia mjobergii*. *Journal of Peptide Research, v. 54(2), pp. 137-145*